Characterisation of a Novel Family of Eukaryotic Ammonium Transport Proteins

A thesis submitted for the Degree of the Doctor of Philosophy

at

The University of Adelaide

Faculty of Sciences

School of Agriculture, Food and Wine

Submitted by

Danielle Mazurkiewicz

December 2013

Table of Contents

I. List of Figures

II. List of Tables

III. Abbreviations

3′	Three prime of nucleic acid sequence
5′	Five prime of nucleic acid sequence
~	Approximately
±	plus and minus
β	Beta
µM	Micromolar
ADP	Adenosine diphosphate
AGRF	Australian Genome Research Facility
AMF1	Ammonium Major Facilitator 1
AMP	Ampicillin
AMT	Ammonium Transporter
ATP	Adenosine triphosphate
bp	Base pairs
bHLH	basic Helix-Loop-Helix
BLAST	Basic Local Alignment Search Tool
BSA	Bovine Serum Albumin
CARB	Carbenicillin
CaMV 35S	Cauliflower Mosaic Virus Constitutive Promoter
cDNA	Complementary deoxyribonucleic acid
CDS	Coding DNA sequence
CFP	Cyan Fluorescent Protein
Ct	Threshold cycle
C-terminal	Carboxyl terminal

DEPC	Diethyl pyrocarbonate
DNA	Deoxyribonucleic acid
cRNA	Capped RNA
EDTA	Ethylene Diamine Tetracetic Acid
EMS	Ethylene Methane Sulfonate
EMSA	Electromobility Shift Assay
g	Grams
Gal	Galactose
Gal1	Galactose inducible promoter 1
GFP	Green Fluorescent Protein
Glu	Glucose
GmSAT1	*Glycine max* Symbiotic Ammonium Transporter 1
h	Hour(s)
I/V	Current as a function of voltage
Kb	Kilo base(s)
kD	Kilo dalton(s)
LB	Luria broth
LiAc	Lithium acetate
M	Molar
MA	Methylammonium
MBS	Modified Barth's Solution
MEP	Methylammonium permease
MES	2- (N-Morpholino) ethanesulfonic acid, 4-morpholineethanesulfonic acid
MF	Major Facilitator
MFS	Major Facilitator Superfamily

Min	Minute(s)
mM	Millimolar
mRNA	messenger RNA
N	Nitrogen
NCBI	National Centre for Biotechnology Information
ng	Nanogram(s)
nl	Nanolitre(s)
nm	Nanometer(s)
N-terminal	Amine terminal
OD	Optical Density
P	Phosphate
PCR	Polymerase chain reaction
PEG	Polyethylene Glycol
PBS	Peribacteroid space
P_i	Inorganic phosphate
PAGE	Polyacrylamide Gel Electrophoresis
Pro	L-proline
PBS	Peribacteroid space
PEG	Polyethylene Glycol
PM	Plasma Membrane
Pro	L-proline
qPCR	quantitative PCR
Rh	Rhesus protein
RNA	Ribonucleic acid
RNase	Ribonuclease

RNAi	RNA Interference
s	Second(s)
SDS	Sodium Dodecyl Sulfate
SE	Standard Error
SM	Symbiosome Membrane
SPEC	Spectomycin
TAIR	The *Arabidopsis* Information Resource
TCA	Trichloroacetic acid
TEVC	Two-Electrode Voltage Clamp
TF	Transcription factor
Tris	Tris(hydroxymethyl)aminomethane
UTR	Untranslated region
v/v	volume/volume
w/v	weight/volume
YFP	Yellow Fluorescent Protein
YPD	Yeast extract peptone dextrose medium
YNB	Yeast Nitrogen Base

IV. Abstract

Species from the family *Leguminosae* are able to survive in nitrogen (N) limiting conditions via a symbiotic relationship with soil-borne N_2-fixing bacteria collectively known as *Rhizobium*. The symbiosis results in the development of the root nodule where invaded bacteria (bacteroids) reside within a plant derived membrane vesicle (symbiosome) located within the cytoplasm of infected nodule cortical cells. Bacterial nitrogenase activity converts atmospheric N_2 to ammonium (NH_4^+), which is delivered to the plant in exchange for photosynthetically derived carbon for bacterial consumption. The mechanism regulating the transfer of NH_4^+ to the plant across the symbiosome membrane is currently unknown. GmSAT1 (*Glycine max* Symbiotic Ammonium Transporter 1), a symbiosome membrane bound basic Helix-Loop-Helix (bHLH) transcription factor has previously been identified in soybean by its ability to enhance NH_4^+ and MA transport in the NH_4^+ transport deficient yeast strain 26972c (Kaiser et al., 1998). In this study, we have revisited microarray analysis of 26972c cells expressing *GmSAT1* to identify differentially regulated yeast genes with putative roles in NH_4^+/MA transport.

Central to this study is the identification of ScAMF1 (*Saccharomyces cerevisiae* Ammonium Major Facilitator 1), a previously uncharacterised major facilitator transport protein, which was upregulated 56.5-fold in response to GmSAT1 activity. ScAMF1 and GmAMF1;3, a representative AMF1 from soybean, were functionally analysed with respect to putative NH_4^+ transport using a combination of yeast and *Xenopus laevis* oocyte expression systems. Both AMF1 proteins enhanced ^{14}C-MA uptake and established a related sensitivity phenotype in 26972c and 31019b, an alternative NH_4^+ transport mutant strain. In the presence of low (1 mM) NH_4^+, *ScAMF1* overexpression partially rescued growth of 26972c but was unable to establish a similar phenotype in 31019b. The role of

ScAMF1 in NH_4^+ transport was less clear. However, this study reaffirmed endogenous high-affinity NH_4^+ transporters called MEPs (Methylammonium Permeases) play an important role in GmSAT1-mediated NH_4^+ complementation. Heterologous expression in *X. laevis* oocytes suggest that ScAMF1 and GmAMF1;3 behave as non-selective cation channels capable of low-affinity NH_4^+ transport, revealing NH_4^+ current activation by P_i or a product of P-metabolism and potential Ca^{2+}-gating. This study also provided a preliminary electrophysiological profile of the *Arabidopsis* AMF1 homologs with respect to NH_4^+ transport for future studies to explore in detail.

V. Declaration

I certify that this work contains no material which has been accepted for the award of any other degree or diploma in any university or other tertiary institution and, to the best of my knowledge and belief, contains no material previously published or written by another person, except where due reference has been made in the text. In addition, I certify that no part of this work will, in the future, be used in a submission for any other degree or diploma in any university or other tertiary institution without the prior approval of The University of Adelaide and where applicable, any partner institution responsible for the joint-award of this degree.

I give consent to this copy of my thesis when deposited in the University Library, being made available for loan and photocopying, subject to the provisions of the Copyright Act 1968.

I also give permission for the digital version of my thesis to be made available on the web, via the University's digital research repository, the Library catalogue and also through web search engines, unless permission has been granted by the University to restrict access for a period of time.

…….. ……..

Danielle Mazurkiewicz Date

VI. Acknowledgments

First and foremost, I would like to thank my supervisors, Prof. Brent Kaiser, Dr. Mamoru Okamoto and Prof. Steve Tyerman, for all of their help and encouragement throughout my PhD experience. In particular, I would like to express my gratitude to Brent, who supervised my Honours year and was still willing to encourage my research pursuits as a PhD candidate. I have really valued his patience and guidance throughout my time in the Kaiser group. I am also grateful for his help securing a University of Adelaide Faculty of Sciences Divisional Postgraduate Scholarship and an ARC short-term scholarship that have made this thesis possible. I am also very appreciative to Mamoru for all of his invaluable research and professional advice. Thank you to Steve, who has been a great source of knowledge and suggestion, especially in electrophysiology.

I would like to thank Sunita Ramesh and Wendy Sullivan for performing *Xenopus laevis* oocyte surgeries. Discussions with Sunita about electrophysiology techniques have greatly aided the progress of my research. I would also like to recognise Nenah McKenzie, who always had time to assist with yeast flux experiments, never minding the long hours. I really enjoyed your company. I must also acknowledge David Chiasson for cloning the *GmAMF1;3* CDS and assessing the localisation of GmAMF1;3 in onion epidermal cells.

I know I shall think fondly on my time in the Kaiser group, and would like to acknowledge both past and present members, all of whom have contributed immensely to my growth as a scientist. Many thanks to Karen Francis, Manijeh Mohammadidehcheshmeh, Allen Wen, Evgenia Ovchinnikova, Julie Dechorgnat, Jon Wignes, Apriadi Situmorang and Nenah MacKenzie for all of your assistance.

Thank you to Jorge for all the times you have let me prattle on about science, whilst reminding me to enjoy life outside of the lab. I am so grateful for your friendship. Suz Zhao, thanks for befriending me and wondering the beautiful walking trails around the Waite campus with me. It has been great sharing the ups and downs of a PhD project with you.

Last but not least, I would like to sincerely thank my family. I cannot express the gratitude I feel towards my parents for entertaining my scientific curiosity as a child and providing endless support and encouragement during my time at university. Thank you to my Nana Doreen, who believed I would be a scientist before I knew. My siblings, Symone and Stephen, have also weathered the long journey to completing this thesis with me. This thesis would not exist without you.

Chapter 1 Literature Review

1.1 Reduced nitrogen sources available for plant consumption

Nitrogen (N) is a key macronutrient for healthy plant development, growth, metabolism and reproduction. N is essential to most cellular structures and processes (Miller and Cramer, 2005). It is a fundamental component of nucleic acids, proteins, vitamins and other N-containing compounds, such as chlorophyll, a pigment central to photosynthesis. N is also required for intracellular energy transfer compounds, such as adenosine triphosphate (ATP), and is vital for metabolic and physiological mechanisms.

Plant roots predominately take up reduced N in the forms of ammonium (NH_4^+) and nitrate (NO_3^-) from the soil by the coordinated effort of low and high-affinity transport mechanisms (Glass et al., 2001). Organic N, such as urea and amino acids in the soil solution can also be utilised by plants (Näsholm et al., 2009). Plants acquire NH_4^+ through the activity of high-affinity transport system (HATS) mediated by Ammonium Transporter (AMT) proteins (Ninnemann et al., 1994), and a poorly understood low-affinity transport system (LATS) (Wang et al., 1993; Kronzucker, 1996). AMT proteins are active at external NH_4^+ concentrations up to 5 mM, following a Michaelis-Menten saturable uptake kinetics profile (Yuan et al., 2007). Homologs of AMT proteins account for HATS flux in yeast and vertebrates, and belong to the MEP/AMT/Rh transport superfamily (Marini et al., 1994; Ninnemann et al., 1994; Marini et al., 2000a). The growth rate and biomass of crop species is highly correlated to the availability of reduced N in the soil (Lawlor et al.,

2009). The availability of N is therefore important in the productivity of economically important agricultural crop species and to general food production worldwide. Unfortunately, the availability of sufficient levels of reduced N for plant consumption is influenced by many abiotic and biotic factors, which leads to considerable variation in plant growth between seasons and soil types (Angus, 2001). In high-input monoculture agricultural soils, N availability is often inadequate, calling for the application of alternative N inputs. Although the Haber-Bosch process, by which N_2 is converted to ammonia (NH_3) by an iron catalyst, provides a profuse N supply suitable for use in agriculture, there are significant economic and environmental costs associated with its synthesis and potential environmental footprint once used in the field (Ramos, 1996; Stulen, 1998; Beman et al., 2005).

1.2. Legume-rhizobia N_2-fixing symbiosis: An alternative nitrogen resource

Despite being the most abundant gas in the atmosphere (~ 79% v/v N_2, 21% v/v O_2), dinitrogen (N_2) is inert and cannot be directly used as a source of N for most plants. The N_2-fixation symbiosis is a phenomenon that occurs between species from the *Leguminosae* (legume) family and soil-borne N-fixing bacteria collectively known as rhizobia from the genera *Rhizobium*. Bacteria from the *Frankia* genera are also able to establish N_2-fixing symbiosis with actinorhizal plants (Masson-Boivin et al., 2009). The symbiotic bacteria reduce atmospheric N_2 to ammonia (NH_3^+) by the enzymatic activity of nitrogenase, a bacterium encoded enzyme, using the following reaction:

$$N_2 + 8H^+ + 8e^- + 16ATP \longrightarrow 2NH_3 + H_2 + 16ADP + 16P_i$$

The fixed N is supplied to the host legume in exchange for photosynthetically reduced carbon (Udvardi and Day, 1997). The *Rhizobium* symbiotic relationship allows the host legume to access atmospheric N_2 in conditions where reduced N resources are scarce (Udvardi and Day, 1997; Edvardo et al., 2002). Symbiotic N_2-fixation has the potential to offer an alternative sustainable supply of reduced N to agriculture, reducing the dependence on N fertilizers.

1.3. Nodulation: The rhizobial infection of legumes

Rhizobium infection leads to the development of specialised organs called nodules on the roots of the host legume (Cohn et al., 1998). Within the root, symbiotic bacteria reside within infected cortical cells of the nodule and are surrounded by a plant derived SM (symbiotic membrane). The infection process giving rise to root nodules, is established through the exchange of chemical signals between legumes and compatible *Rhizobium* (Denarie et al., 1996). In general, *Rhizobium* infection of legumes species is specific for the strain of bacterium (Stougaard, 2001). Legumes excrete flavonoids compounds into the surrounding soil to attract complementary *Rhizobium* to the roots (Coronado et al., 1995). Molecular recognition of the flavonoids stimulates the bacterial expression of *nodulation* (*NOD*) genes, which are involved in the synthesis and export of NOD factors (Denarie et al., 1996). NOD factors are lipochitooligosaccharides, which contain specific chemical modifications depending on the stain of bacteria (Lerouge et al., 1990; Ardourel et al., 1994; Denarie et al., 1996). In turn, compatible NOD factors are recognised by specific entry-LysM receptors (NFP) on the surface of legume epidermal root hair cells. Binding of NOD factor to the LysM receptor triggers a signal transduction event including root hair cell membrane depolarisation, intracellular Ca^{2+} oscillation, and differentiation of inner root cortex cells (precursors of nodule cells) (Cardenas et al., 2000). The Ca^{2+} signalling

cascade is involved in stimulating the root hair to curl around the rhizobia, which proceeds to transverse the cell wall via a channel-like structure referred to as the infection thread (Oldroyd et al., 2004; Gage et al., 2004). The Ca^{2+} oscillations lead to an alteration of *ENOD* (*early nodulation*) gene expression (Riely et al., 2006). The infection thread, filled with multiplying bacteria, continues to grow to the dividing cortical cells of the developing nodule (Oldroyd et al., 2004; Gage et al., 2004). The infection thread fuses with the plasma membrane (PM) of nodule cortical cells, releasing the bacteria in membrane vesicles into the plant (Oldroyd et al., 2004; Gage et al., 2004). The maturing nodule protrudes from the surface of the root.

1.4. Symbiosome: The basic unit of N_2-fixation

The rhizobia residing in the nodules are differentiated (now referred to as bacteroids), equipped with specialised functions for the maintenance of the symbiotic association (Oldroyd et al., 2004; Gage et al., 2004). Upon release from the infection thread, the bacteroids are enveloped in a plant derived symbiosome membrane (SM), suspended in the acidic peribacteroid space (PBS) (Whitehead and Day, 1997; Oldroyd et al., 2004; Gage et al., 2004). The structure of the symbiosome membrane partitions the bacteria from the cytosol of the infected root nodule cortical cell.

1.5. Nutrients exchange between the symbionts is coordinated by the symbiosome membrane

The symbiotic partnership is beneficial to both symbionts (Udvardi and Day, 1997). The host legume receives a sustainable supply of NH_4^+ in exchange for malate, a reduced photosynthetic carbon source derived from the host plant. Malate is essential in bacterial respiration to produce ATP, which is used to harness energy for nitrogenase activity.

Biogenesis of the SM, a selectively permeable barrier, coincides with the elevation in the activity of plant encoded *nodulin* genes, which encode an array of SM associated proteins, including enzymes and transport proteins that maintain the obligate relationship between the bacteroids and the host legume (Whitehead and Day, 1997). To date, a number of SM transport proteins have been identified and characterised, which include a number of transporter proteins mediating the movement of H^+ (Blumwald et al., 1985), dicarboxylates (Udvardi et al., 1988), zinc (Moreau et al., 2002), iron (Kaiser et al., 2003), sulfate (Krusell et al., 2005) and nitrate (Vincill et al., 2005). In the nodule, approximately 1354 genes have been shown differentially activated, 473 of which are nodule specific (Benito et al., 2008), suggesting that a number of essential genes have yet to identified. Thus far, the host plant encodes all of the identified SM-associated transport proteins.

1.6. An H^+-ATPase associated with the SM drives the secondary transport of nutrients between the symbionts

The activity of an H^+-ATPase, a primary-active transporter, is fundamental to the exchange of nutrients across the SM. The transport of nutrients into the symbiosome takes advantage of the membrane potential across the symbiotic interface generated by the ATPase (Blumwald et al., 1985, Udvardi et al., 1991, Fedorova et al., 1999). The H^+-ATPase extrudes H^+ into the PBS, establishing an electrochemical potential gradient across the membrane interface that drives the activity of secondary transporters.

1.7. Evidence of an ammonium channel in the SM

Atmospheric N_2 passively diffuses into the PBS where it is enzymatically reduced to NH_3 by the bacterial enzyme nitrogenase. Generated NH_3 diffuses into the acidic PBS and is rapidly protonated, forming NH_4^+ (Blumwald et al., 1985; Udvardi and Day, 1997;

Fedorova et al., 1999). The NH_4^+ is then translocated across the SM to the cytosol of the host plant for assimilation by glutamine synthase into biologically important compounds, such as nucleic and amino acids (Day et al., 2001). The mechanism coordinating the delivery of NH_4^+ across the SM to the plant is presently unknown.

The current activity of a non-selective voltage-gated channel permeable to NH_4^+, K_M = 37.5 mM, and gated by divalent cations was detected in soybean SM by patch-clamp analysis of symbiosomes (Tyerman et al., 1995; Whitehead et al., 1998; Kaiser et al., 1998; Obermeyer and Tymerman, 2005). Similar currents were detected in the SM of *Lotus japonicus* and in *Pisum sativum* (pea) (Mouritzen and Rosendahl, 1997; Roberts and Tyerman, 2002). Genetic identification and functional characterisation of the mechanism regulating the transfer of NH_4^+ from the endosymbiont bacteria to the legume is of great interest, as this will provide the key to understanding the mechanisms regulating N delivery to the host plant.

GmSAT1 (*Glycine max* Symbiotic Ammonium Transporter 1), a soybean SM basic Helix-Loop-Helix (bHLH) transcription factor (TF), has been implicated in the development of effective N_2-fixating nodules (P. Loughlin, 2007). GmSAT1 was originally identified in a complementation screen with the 26972c NH_4^+ transport mutant yeast strain, promoting growth on low ammonium (1 mM), as well as enhancing uptake of a toxic NH_4^+ analog, methylammonium (MA), and activating a low-affinity NH_4^+ current with non-selective cation properties comparable to the SM NH_4^+ channel (Kaiser et al., 1998). Marini et al., (2000b), suggested that GmSAT1 complements the disrupted MEP 1, 2 and 3 high-affinity NH_4^+ system (Methylammonium Permeases) of 26972c by elevating *MEP3* transcript or protein levels to overcome transinhibtion by a mutant version of MEP1 (mep1-1).

1.8. Aim, significance and contribution of the project to the discipline

The aim of this study was to investigate the means by which GmSAT1 restores defective NH_4^+ transport and enhances MA accumulation and related sensitivity in the 26972c mutant yeast strain. Although GmSAT1 is essential for N_2-fixation (Kaiser et al., 1998; Loughlin, 2007), the role of this protein in yeast and *in planta* remains elusive. Here, we hypothesised that GmSAT1 regulates the activity of a putative NH_4^+ transport protein in yeast that shares a degree of molecular identity with the symbiotic NH_4^+ transporter in soybean. Described in this thesis is the identification and characterisation of a new class of NH_4^+ transport protein called AMF1 (Ammonium Major Facilitator 1), which was identified in yeast through a direct interaction with GmSAT1. ScAMF1 transport properties with respect to NH_4^+ were characterised using a combination of yeast and *Xenopus laevis* oocyte expression systems. In turn, characterisation of ScAMF1 has led to the identification of similar proteins in plants. Subsequent functional analysis of soybean and *Arabidopsis* AMF1 homologs has increased our general understanding of poorly understood low-affinity NH_4^+ acquisition in agriculturally important crop species, which may ultimately eliminate considerable reliance on N fertilizers.

Chapter 2 Functional analysis of ScAMF1, a novel cation transport protein in yeast

2.1 Introduction

2.1.1 Legume symbiotic N_2-fixation

Nitrogen (N) is an essential component of many biological compounds such as nucleic acids and proteins. Plants acquire N mainly in the form of NO_3^- and NH_4^+ from the soil by means of low and high-affinity transport mechanisms operating in root systems (Glass et al., 2001). Plants are unable to utilise atmospheric N (N_2). However, many species of legumes have evolved a symbiotic relationship with N_2-fixing bacteria from the genus *Rhizobium*, thereby enabling the host legume to make use of the generally inaccessible atmospheric resource. Plant encoded transport proteins embedded in the symbiosome membrane (SM) are responsible for translocating bacterially fixed N from the symbiosome to the cytosol of the host-legume, and the exchange of other essential nutrients between the symbionts (Udvardi and Day, 1997). This chapter presents the characterisation of the putative MA and NH_4^+ yeast transporter ScAMF1, first identified as a result of enhanced expression by the soybean TF, GmSAT1. The identification of and characterisation of ScAMF1 introduces a previously unknown mechanism by which yeast cells can manage NH_4^+ transport.

2.1.2 The MEP/AMT/Rh superfamily of NH_4^+ transport proteins

In yeast, PM proteins, MEP1, MEP2 and MEP3, mediate high and low-affinity NH_4^+ transport, possessing K_M values for NH_4^+ of 5-10 μM, 1-2 μM and 1.4-2.1 mM, respectively (Marini et al., 1994; Marini et al., 1997). Mutant yeast strains with a single functional MEP are able to grow as wild-type in the presence of < 1 mM concentrations of NH_4^+ (Dubois and Grenson, 1979). The functional redundancy is considered due to the structural similarities between MEP proteins: MEP3 shares 79% similarity with MEP1, whilst MEP2 shares 40%. Using yeast strains where MEP(1-3) activity is not active has allowed multiple opportunities to study the NH_4^+ transport systems of a wide range of organisms in a simple expression system. These include identifying the vertebrate Rh proteins associated with the Rhesus-blood group (Marini et al., 2000a) and AMT proteins from *Arabidopsis* (Ninnemann et al., 1994). Related AmtB NH_4^+ transport proteins have also been identified in bacteria including *Escherichia coli* (Khademi et al., 2004; Zheng et al., 2004; Javelle et al., 2005). Consequently, numerous high-affinity NH_4^+ transporters of the AMT/MEP/Rh family have been identified across bacteria, archaea and eukarya generally all involving functional screens in yeast (von Wirén and Merrick, 2004).

2.1.3 Genetic basis of the NH_4^+ transport deficiency in the 26972c yeast strain

The NH_4^+ transport mutant *Saccharomyces cerevisiae* strain 26972c was used in the initial identification of AMT/MEP/Rh proteins. The strain was created by treatment with mutagen ethyl methane sulphonate (EMS), and selected by lack of sensitivity to high concentrations (0.1 M) of MA, a toxic NH_4^+ analog (Dubois and Grenson, 1979). The NH_4^+ transport defect of 26972c, which cannot grow on media containing less than 1 mM NH_4^+ as the sole N source, is the result of a single EMS dependent conversion of glycine 413 residue to aspartate (G413D) in the C-terminus of MEP1 (mep1-1) (Marini et al.,

1997). The *MEP2* locus was also found to be absent in this strain, most likely the result of mutations over generations of propagation in the laboratory prior to EMS mutagenesis (Marini et al., 1997). Functional studies revealed that mep1-1 physically interacts with MEP3, interfering the activity of (trans-inhibits) of the protein (Dubois and Grenson, 1979; Marini et al., 1997; Marini et al., 2000b). A subsequent NH_4^+ transport mutant strain, 31019b (MATa*::ura3 mep1Δ mep2Δ::LEU2 mep3::kanMX2*), has also been employed in the characterisation of putative NH_4^+ transport proteins. This strain was created by physical deletion of all three *MEP* loci by homologous recombination (Marini et al., 1997). Both mutants are isogenic to the ∑1278b haploid wild-type strain (Dubois and Grenson, 1979).

2.1.4 Initial characterisation of GmSAT1 in yeast

Although the soybean SM NH_4^+ transporter has not been identified, GmSAT1, a SM bound TF has been implicated in promoting effective bacterial N_2-fixation in soybean nodules (P. Loughlin, 2007). The 26972c mutant yeast strain was used in a functional complementation screen to isolate *GmSAT1* from a soybean nodule cDNA library. GmSAT1 restored the ability of the mutant strain to grow on low NH_4^+ (1 mM) and significantly enhanced the accumulation of ^{14}C-MA, routinely used to investigate NH_4^+ transport properties in yeast (Kaiser et al., 1998). GmSAT1, a mainly hydrophillic protein, was observed anchored to PM of yeast and the soybean SM (P. Loughlin, 2007). Subsequently, GmSAT1 was classified as a SM NH_4^+ transporter.

However, the initial classification of GmSAT1 as an NH_4^+ transporter was challenged and shown to be incorrect as GmSAT1 activity could not restore the disrupted NH_4^+ transport of the 31019b strain, suggesting that a functional MEP3 is required to establish NH_4^+ complementation (Marini et al., 1997, Marini et al., 2000b). However, GmSAT1 activity was still able to enhance the accumulation of ^{14}C-MA and cause MA

toxicity in the 31019b strain (P. Loughlin, 2007). It was, therefore, apparent that GmSAT1 could not be responsible for facilitating the direct movement of NH_4^+ (Marini et al., 2000b). A subsequent structural assessment of GmSAT1 showed that it has an atypical structure for a transporter, not sharing homology with any known NH_4^+ transport protein (Howitt and Udvardi, 2000). SAT1 proteins are common in plants consisting of 28-42 kDa in size and contain a single C-terminal transmembrane anchor and an N-terminal bHLH DNA binding domain. The bHLH domain is homologous to a ubiquitous family of regulatory proteins involved in a wide range of cellular pathways (Atchley and Fitch, 1997). There exists 1363 documented bHLH binding locations identified across the yeast genome (Teixeira et al., 2006). *SAT1* homologs are not represented in the *S. cerevisiae* genome or that of prokaryotes but are identified widely across both dicot and monocot plant species often as members of multi-gene families. Marini et al., (2000b) alluded that GmSAT1 might influence NH_4^+ transport by transcriptionally elevating the expression of *MEP3* to overcome the trans-inhibition of mep1-1. Functional studies performed by P. Loughlin (2007) and D. Chiasson (2012) have established that GmSAT1 is a bonafide TF based on its nuclear localisation in yeast and soybean, perturbed activity as a result of disrupted bHLH domain integrity and affinity for putative promoter regions.

2.1.5 *In planta* assessment of GmSAT1 activity

GmSAT1 is predominantly expressed in soybean root nodules formed when the soybean plant is infected with symbiotic *Rhizobium* bacterium (Kaiser et al., 1998). *GmSAT1* is also expressed in both infected and uninfected roots but at a significantly lower level than that of nodules (Kaiser et al., 1998; D. Chiasson, 2012). GmSAT1 activity is regarded to be indispensable for soybean symbiosome biogenesis as determined through RNA interference (RNAi) (P. Loughlin, 2007). Abnormal infection development was observed

in *GmSAT1*-silenced soybean nodules where the architecture of infected cortical cells was underdeveloped, highly vacuolated and contained a reduced number of bacteroids (P. Loughlin, 2007). The poorly developed nodules lead to impaired plant growth most likely as a result of the ineffective N_2-fixing nodules. The growth of the plant was restored with application of N fertiliser (P. Loughlin, 2007). These observations suggest that *GmSAT1* is an important gene controlling soybean symbiotic processes. Immunogold labeling has shown that GmSAT1 is sequestered in the SM by a C-terminal transmembrane anchor (P. Loughlin, 2007). Immunogold labeling also detected GmSAT1 in the nucleus, suggesting that the N-terminal portion of the protein containing the bHLH domain is cleaved by some unidentified signal (P. Loughlin, 2007). However, the mechanisms through which GmSAT1 achieves this are still unclear. As GmSAT1 possesses a bHLH DNA-binding domain, it is therefore useful to observe the genes regulated by GmSAT1 in a simple model organism like yeast. The transcriptional regulation of genes encoding transporters, or transcriptional regulators of other genes, could give insight into the role of GmSAT1 in the legume N_2-fixing symbiotic processes.

2.1.6 Global genetic events regulated by GmSAT1 activity in yeast

The genetic events regulated by GmSAT1, resulting in the restoration of the NH_4^+ transport system of 26972c yeast, have been assessed by Affymetrix microarray analysis (D. Mazurkiewicz, 2008). GmSAT1 activity in yeast under low (1 mM) NH_4^+ conditions was found to both positively and negatively influence transcriptional activity across the yeast genome. Microarray results also revealed that GmSAT1 enhanced the transcription of genes encoding components of the yeast phosphate (P) metabolic (PHO) system, *PHO84* (~35-fold), *PHO3*, *PHO5*, *PHO11* and *PHO12* (~2-fold), implicating GmSAT1 in the regulation of P homeostasis in yeast (D. Mazurkiewicz 2008). Inspection of the

regulatory ‘promoter’ sequences of these genes revealed the presence of multiple putative and real endogenous yeast bHLH binding sites called ‘E-box elements’ with a general consensus sequence of CANNTG (Atchley and Finch, 1997; Massari et al., 2000). Sequence analysis of the bHLH domain of GmSAT1 identifies an H-E-R amino acid motif at positions 5, 9 and 13 of the basic region, which are major determinant in the recognition of the CACGTG promoter E-box variant sequence (Atchley and Finch, 1997).

Described in this chapter is a series of yeast-based experiments, which provide the basis for the characterisation of GmSAT1 as an established MA and NH_4^+ transport regulator in yeast. Central to the study is the characterisation of the endogenous ScAMF1, a novel transport protein. Here, we show that ScAMF1, which has limited sequence similarity to members of the DHA2 family of drug:H^+ antiporters belonging to the MFS transporters, is a PM protein capable of mediating low-affinity MA transport in both 26972 and 31019b yeast cells, while disruption of *AMF1* (Δ*amf1*) in 26972c, eliminated GmSAT1-dependent MA transport/toxicity and partially reduced its NH_4^+ complementation capacity.

2.2 Methods and Materials

2.2.1 Cloning *ScAMF1* from the *BG1805* yeast expression vector

The complete sequence of *ScAMF1* was cloned from the *BG1805* yeast expression vector (Open Biosystems Yeast ORF Collection, Thermo Scientific) with FwScAMF1seq and FwScAMF1seq primers (Table 2.1) using High Fidelity Platinum DNA polymerase (Invitrogen) and the following PCR conditions: 94°C for 1 min, 30 cycles of 94°C for 30 s, 55°C for 30 s, 68°C for 1.5 min, followed by 68°C for 5 min.

2.2.2 The synthesis of the m*GFP5::ScAMF1* and *ScAMF1*::m*GFP5* fusion constructs

The *mGFP5::ScAMF1* (N-terminus of ScAMF1 tagged with mGFP5) and *ScAMF1::mGFP5* (C-terminus of ScAMF1 tagged with mGFP5) fusion constructs were synthesised by means of a 2-step PCR based strategy. The *mGFP5* and *ScAMF1* sequences were amplified in separate PCR reactions with Phire Hot Start DNA polymerase (Finnzymes, Finland). The N-terminal fusion construct was synthesised by amplifying the *mGFP5* sequence without the stop codon from the *pCAMBIA1302* vector (www.cambia.org), using BeginningGFPFw and N-termGFPScAMF1Rv primers (Table 2.1), while the complete *ScAMF1* sequence was amplified from the yeast expression vector *BG1805-ScAMF1* (Open BioSystems Yeast ORF Collection, Thermo Scientific), using the N-termGFPScAMF1Fw and ScAMF1Rv primers (Table 2.1). The C-terminal fusion construct was synthesised by amplifying the complete *mGFP5* sequence using the C-

termScAMF1GFPFw and EndGFPRv primers (Table 2.1), while the *ScAMF1* sequence was amplified without the stop codon using the ScAMF1Fw and C-termScAMF1GFPRv primers (Table 2.1). The primers were designed to amplify *mGFP5* and *ScAMF1* with overlapping 3' and 5' sequences (44 nucleotides in length), which would allow the separate PCR products to anneal in a subsequent PCR to create the fusion construct. Initial PCR conditions were as follows: 98°C for 30 s, 30 cycles of 98°C for 10 s, 55°C for 10 s and 72°C for 30 s, followed by 72°C for 5 min. The amplified *mGFP5* and *ScAMF1* products were combined in a second PCR to amplify m*GFP5::ScAMF1* and *ScAMF1::*m*GFP5* (BeginningGFPFw + RvScAMF1 and ScAMF1Fw + EndGFPRv, respectively) with High Fidelity (HIFI) 5 Prime PCR Extender DNA polymerase (5 Prime, USA). PCR cycle conditions were as follows: 94°C for 2 min, 25 cycles of 94°C for 20 s, 55°C for 20 s and 72°C for 2 min, followed by 72°C for 5 min. The HIFI 5 Prime PCR Extender DNA polymerase added 3' adenine overhangs to the PCR products, which is required for subsequent cloning into the Gateway© *pCR8/GW/TOPO* entry vector (Invitrogen). The complete *mGFP5* sequence was amplified (BeginningGFPFw + EndGFPRv primers) as a negative control using HIFI 5 Prime PCR Extender DNA polymerase (5 Prime) as before with an extension time of 40 s.

2.2.3 Gateway© cloning

Amplified gene or fusion products were inserted into the *pCR8/GW/TOPO* entry vector using Gateway© cloning kit (Invitrogen). Inserts were then recombined into the *pYES3*-destination (*pYES3-DEST*) vector (Figure 2.1) by means of *LR Clonase*™ II (Invitrogen).

2.2.4 Selection of recombinant plasmids

The recombinant plasmids were transformed by heat-shock (Sambrook et al., 1989) into

the XL-Blue (Stratagene) or TOP10 (Invitrogen) *E. coli* strains. Selection was carried out on solid reduced salt LB (1% (w/v) NaCl, 2% (w/v) Bacto-tryptone (Difco), 1% (w/v) yeast extract (Difco) and 2% (w/v) agar) supplemented with 50 μg ml^{-1} spectinomycin (*pCR8/GW/TOPO*) or 100 μg ml^{-1} carbenicillin (*pYES3-DEST*) after 2-3 days incubation at 28°C. Plasmid DNA was isolated from mid-log phase cultures by GenElute Plasmid MiniPrep kit according to the manufacturers protocol (Sigma-Aldrich). Plasmids with inserts in the correct orientation were identified by restriction enzyme analysis and then sequenced to confirm the absence of mutations.

2.2.5 DNA sequencing

The selected plasmids were sequenced with primers provided with the Gateway© *pCR8/GW/TOPO* cloning kit (Invitrogen) or specific to the *T7 promoter* (T7-Fw primer) and *Cyclic 1 terminator* (Cyc1-Rv primer) of *pYES3-DEST* (Table 2.1), in conjunction with the BigDye® Terminator v3.1 Cycle Sequencing Kit (Applied Biosystems) following the manufactures protocols. Capillary separation of sequencing products were analysed by the AGRF sequencing facility (Waite Campus, South Australia). Sequences were analysed using MacVector version 12.7.0 (Eastman Kodak, USA) and compared to those on NCBI gene and protein databases using BLAST programs.

2.2.6 Modified lithium acetate yeast transformation

The *S. cerevisiae* strain 26972c (MAT**a***::ura3 mep1-1*, *mep2Δ*, *mep3*) and its derivative strain 31019b (MATa::*ura3 mep1Δ mep2Δ::LEU2 mep3::kanMX2*) were used in the homologous analysis of ScAMF1 activity. Expression plasmids were introduced into the yeast strains using the transformation method described by Gietz et al., (1995) with modifications. Starter cultures of 100 ml YPD (1% (w/v) Bacto yeast extract, 2% (w/v)

Bacto peptone and 2% (w/v) D-glucose (Glu)) were inoculated and aerobically grown in sterile 250 ml glass conical flasks. Inoculants were incubated for approximately 16 h at 28°C with shaking at 200 rpm, reaching mid-log growth phase (OD_{600nm} of 0.7-1.0). The cultures were collected in 50 ml sterile polypropylene centrifuge tubes (Sarstedt, Germany) at 14,000 x *g* for 2 min. Cells were washed with 50 ml of sterile Milli-Q H_2O before being transferred to a 1.5 ml polypropylene microcentrifuge tube (Axygen, USA). The cell pellets were then washed twice in 750 µl of lithium acetate wash solution (10 mM Tris-HCl, 1 mM EDTA, 0.1 M LiAc, pH 7.5), before 50 µl aliquots were resuspended in 300 µl of PEG/lithium acetate transformation solution (35% (w/v) PEG 4000, 10 mM Tris-HCl, 1 mM EDTA, 0.1 M LiAc, pH 7.5), 25 µl of 2 mg ml^{-1} sterile salmon sperm DNA and approximately 500 ng of plasmid DNA. Cells were briefly vortexed, then incubated at 28°C for 1 h followed by incubation in a 42°C H_2O bath for 45 min. After the incubation period, the cells were washed twice with 1 ml of sterile Milli-Q H_2O. Transformations were selected on solid YNB (6.7% (w/v) Difco-Yeast Nitrogen Base without amino acids, 2% (w/v) agar) supplemented with 2% (w/v) Glu. Cells transformed with the *pYES3-DEST* plasmid are auxotrophic for uracil as the plasmid carries a functional *URA3* gene. Transformed yeast colonies, which appeared after 3-4 days of incubation at 28°C were re-streaked out onto fresh solid YNB Glu media for transformation confirmation.

2.2.7 Yeast starter culture preparation

Starter transformed yeast cultures were grown in 20 ml of liquid modified minimal yeast media (Grenson, 1966) or Difco-YNB (without amino acids or N source) supplemented with 2% (w/v) Glu and 0.1% (w/v) L-proline (Pro) in sterile 100 ml glass conical flasks with aluminium capped cotton stoppers. Cultures were incubated to mid-log phase at 28°C

and shaken at 200 rpm. Expression of *GmSAT1* was induced in the presence of 2% (w/v) galactose (Gal).

2.2.8 Yeast phenotypic analysis

To assess the functionality of ScAMF1, a yeast complementation screen was carried out. Yeast starter cultures were harvested by centrifugation at 4,000 rpm and washed twice in 50 ml of sterile Milli-Q H_2O. The yeast solutions were resuspended to a uniform OD_{600nm} of 0.6. A 10-fold dilution series was carried out for each yeast transformation and spotted out in 5 µl aliquots onto solid (2% (w/v) agar) minimal yeast media (Grenson, 1966) with 2% (w/v) Glu or Gal. Preliminary functional growth analysis was carried out on Grenson's selective media supplemented with 0.1% (w/v) Pro or 0.1% (w/v) Pro with 0.1 M MA or 1 mM NH_4Cl. The effect of external pH on MA sensitivity of 31019b cells overexpressing *ScAMF1* was also assessed on solid Difco-YNB supplemented with 25 mM, 50 mM, 100 mM and 200 mM MA buffered with MES/Tris at pH 5.0, 6.0, 7.0 and 8.0. Yeast plates were incubated for 5 d at 28°C.

2.2.9 Visualisation of ScAMF1 GFP fusions in yeast

Starter cultures were diluted to an OD_{600nm} of 0.4 and expression of *mGFP5* or fusions were induced in 26972c cells for 16 h in the presence of 2% (w/v) Gal and 0.1% (w/v) Pro in Difco-YNB with 40 µg ml^{-1}tryptophan, 20 µg ml^{-1} histidine and 60 µg ml^{-1} leucine. mGFP5 was detected using an excitation 488 nm argon laser, and light emission detected at 505-503 nm, with a LSM 5 Pascal Laser Scanning microscope (Zeiss, Oberkochen, Germany). Images were captured and further analysed using the LSM Pascal 5.0 software suite (Zeiss, Oberkochen, Germany).

2.2.10 Generation of the 26972c:Δ*amf1* mutant yeast strain

The *ScAMF1* locus was replaced with the kanamycin resistance gene (*kanMX4*) in the 26972c strain through homologous recombination, creating 26972c:Δ*amf1* (MAT**a**::ura3 mep1-1, *mep2Δ, mep3,* Δ*amf1::kanMX4*). The *kanMX4* gene was amplified by two rounds of PCR from the *pFA6a* plasmid (Wach et al., 1994) using forward and reverse primers (YOR378wF-KanMx4 and YOR378wR-KanMx4; Table 2.1) designed with overhangs specific to 15 nucleotides immediately upstream and downstream of the *ScAMF1* locus (Figure 2.14). High Fidelity Phusion DNA polymerase (Finnzymes, Finland) was used to amplify *kanMX4* with the following PCR conditions: 95°C for 3 min, 25 cycles of 95°C for 30 s, 55°C for 30 s, 72°C for 1 min and 30 s, followed by 72°C for 5 min. The PCR product was used in a subsequent PCR with primers (F-UP and R-DN; Table 2.1) to extend the genomic flanking regions to 40 nucleotides. The amplified *kanMX4* product was transformed into the 26972c yeast strain. After heat treatment, cells were spun down, and resuspended in 40 ml YPD and incubated at 28°C with shaking at 200 rpm over night before plating on 2xYPD supplemented with 200 µg ml^{-1} geneticin (Sigma-Aldrich). Colonies that appeared after 2-3 days of incubation at 28°C were re-streaked on 2 x YPD geneticin (Sigma-Aldrich) medium to verify resistance to geneticin. Deletion of *ScAMF1* was determined by PCR using primers (Table 2.1) internal to *kanMX4* (kanB and kanC) and to the genomic sequence up and downstream of the *ScAMF1* locus (FwYOR378wKO and RvYOR378wKO) in the following combination: FwYOR378wKO and kanB, RvYOR378wKO and kanC (Figure 2.15 B).

2.2.11 GmSAT1 binding to the predicted promoter region of *ScAMF1*

2.2.11.1 Expression and purification of GmSAT1

A truncated version of GmSAT1 (128-270 amino acids) was amplified (GmSAT1 pMAL F and GmSAT1 pMAL R primers) with Phusion DNA polymerase (Finnzymes, Finland) and inserted into *CloneJET* plasmid (Fermentas). The fragment was then excised with *Nde* I and *Bam* HI and ligated into the *pMAL-c5X* plasmid (New England Biolabs, USA) to create a N-terminal fusion to the maltose-binding protein (MBP). The fusion was sequenced using primers pMAL Forward Seq and pMAL Reverse Seq (Table 2.1). The maltose binding protein was expressed by using the empty *pMAL-c5X* plasmid. The plasmids were transformed into the *E. coli* strain NEB Express (NEB, USA). MBP-GmSAT1 and MBP alone were expressed and purified according to the manufacturers instructions using amylose resin (NEB, USA).

2.2.11.2 Electro Mobility Shift Assay

The *ScAMF1* putative promoter (-284 to 0) was amplified (*YOR378w* Promoter 3F + 1R primers) and ligated into *pGEM-T Easy* (Promega). The promoter fragment was then excised with *Not* I and end-filled with ^{32}P dCTP (3000 ci/mmol, Easytide 5' Triphosphate-^{32}P, PerkinElmer) using the Klenow fragment (3'->5' exonuclease, New England Biolabs) in a 50 µl reaction (1 µl ^{32}P-dCTP, 1 µl 1 mM dGTP, 1 µl Klenow, 400 ng promoter fragment). Labeled probe was desalted with S-200 HR Microspin Columns (GE Healthcare) prior to incubation with 1 µg of MBP-GmSAT1 or MBP alone in a 20 µl reaction at room temperature for 25 min. The reaction contained 15 % (v/v) glycerol, 20 mM Tris pH 8.0, 175 mM NaCl, 5 mM EDTA, 50 mM KCl, 0.5 mM DTT, 0.5 µl Poly [d(I-C)] (1 µg µl^{-1}) and 4 µl of probe. The reaction was then loaded on a 6% (w/v) native

Tris-glycine polyacrylamide gel containing 10% (v/v) glycerol. After separation, the gel was vacuum dried and exposed to film for 24 h at -20°C.

2.2.12 Transcriptional analysis of 26972c yeast overexpressing *GmSAT1* mutants

2.2.12.1 Yeast growth conditions for quantitative PCR analysis

Uniform starter cultures (48 h) of 26972c cells harbouring the *pYES3-GmSAT1* (wild type or mutant *GmSAT1*) or the *pYES3-DEST* empty vector were diluted 1 in 20, and expression of *GmSAT1* was induced for 12 h in the presence of 0.5 mM $(NH_4)_2SO_4$ and 2% (w/v) Gal. Cell cultures were harvested and cell pellets were transferred to 1.5 ml microcentrifuge tubes (Sarstedt) with 1 ml of sterile Milli-Q H_2O, mixed and centrifuged at 1,4000 x *g*. Supernatant was aspirated off and the cell pellets snap frozen in liquid nitrogen for 30 s. Frozen cell pellets were stored at -80°C until RNA extraction was required.

2.2.12.2 Hot acid-phenol RNA extraction from yeast cultures

Total RNA was extracted using hot acidified phenol according to Collart et al., (2001). Frozen cell pellets were resuspended in 400 µl of TES solution (10 mM EDTA, 10 mM Tris-Cl, pH 7.5 and 0.5% (w/v) SDS) and 400 µl of acidified phenol buffered at pH 5.0 with Tris-HCl (Sigma-Aldrich). The cell solution was vortexed for 10 s and then incubated in a 65°C H_2O bath for 60 min with intermitting light vortexing every 15 min. The cell solution was placed on ice for 5 min before centrifugation at 14,000 x *g* at 4°C for 5 min. The centrifugation resulted in the separation of organic and aqueous phases. The aqueous phase, containing the RNA, was collected and re-extracted with 400 µl of new acid phenol. The solution was vortexed for 10 s and kept on ice for another 5 min. After the incubation period the solution was centrifuged for 5 min at maximum speed at 4°C. The aqueous

phase was once again collected into a new twice-autoclaved 1.5 ml microcentrifuge (Sarstedt). The aqueous phase was re-extracted with 400 µl of chloroform, which was then vortexed and centrifuged for 5 min at maximum speed at 4°C.

2.2.12.3 RNA clean up

The RNA was precipitated with 40 µl of 3 M sodium acetate (pH 5.3) and 1 ml of ice-cold 100% (v/v) ethanol. The samples were incubated at -80°C for 30 min before maximum speed centrifugation at 4°C for 5 min. The supernatant was carefully removed from the RNA pellet, which was then washed in 250 µl of 70% (v/v) ice-cold ethanol. The RNA pellet was resuspended in 50 µl of ice-cold 0.1% (v/v) diethyl pyrocarbonate (DEPC) treated Milli-Q H_2O and heated at 65°C for approximately 10 min to dissolve the RNA entirely. The RNA was snap frozen in liquid nitrogen for 30 s and stored at -80°C. The concentration and purity of the RNA samples was determined by analysing 2 µl aliquots with a NanoDrop ND-1000 spectrophotometer (NanoDrop Technologies, USA).

2.2.12.4 Assessment of qPCR primer efficiency

The efficiency of each primer pair was assessed in a preliminary qPCR prior to the extensive transcriptional analysis to ensure sufficient amplification. A representative cDNA sample was subjected to a 5-fold dilution series and qPCR was carried out as previously described. The Ct values of three technical replicates were averaged and plotted as a function of template dilution, and the efficiency was calculated from the standard curve using the $E = (10^{(1/slope)})-1$ equation (Peirson et al., 2003). Primers with efficiencies between 0.8 and 1.15 were deemed acceptable and used in subsequent qPCR analyses.

2.2.12.5 Quantitative PCR analysis

The extracted total RNA (2 µg) was treated with TURBO DNase to remove residual genomic DNA contamination prior to cDNA synthesis according to the TURBO DNA-free™ kit protocol (Ambion) in a 20 µl reaction. The DNase-treated total RNA (11 µl) was converted to cDNA using the SuperScript™ III Reverse Transcriptase kit (Invitrogen) with oligo(dT)$_{50}$ and a quarter of the recommended enzyme per reaction. The cDNA was diluted 10-fold with sterile Milli-Q H_2O and stored at -20°C. The qPCR with performed using iQ SYBR Green Supermix reagent (BioRad) in conjunction with 0.50 µM forward and reverse qPCR primers (Table 2.1) and 2 µl of diluted cDNA in a 20 µl reaction volume. The cycling conditions were 2 min at 95°C, 40 cycles of 95°C for 30 s, 55°C for 30 s and 72°C for 1 min, followed by 1 cycle of 95°C for 1 min and 80 cycles at 55°C with 0.5°C increment rise in temperature.

The expression of *ScAMF1*, *MEP1*, *MEP3* or other gene of interest was calculated with respect to *pYES3-DEST* controls from the mean Ct values obtained form a number of biological replicates (n =3 or 9, each consisting of three technical replicates), normalised to *TUB1* or *TUB1* and *ALG9* housekeeping genes (Teste et al., 2009; Yui et al., 2008) by means of the $2^{-\Delta CT}$ equation (Livak and Schmittgen, 2011).

2.2.13 ^{14}C-Methylammonium yeast flux experiments

Overnight starter cultures of 26972c cells harbouring the *pYES3-GmSAT1, pYES3-ScAMF1* or the *pYES3-DEST* empty vector were diluted to an OD_{600nm} of 0.2. The expression of *GmSAT1* and *ScAMF1* was induced for 16 h in the presence of 1 mM NH_4Cl and 2% (w/v) Gal. The cells were harvested at an approximate OD_{600nm} 1.0, and washed twice with 50 ml of sterile Milli-Q H_2O before being resuspended in room temperature KPO_4 buffer (20 mM

K_2HPO_4/KH_2PO_4 buffer (pH 6.2) supplemented with 2% (w/v) Gal) to a uniform OD_{600nm} 4.0. The flux experiment consisted of 6 replicate reactions of 100 µl of cells incubated in 100 µl of MA KPO_4 reaction buffer spiked with ^{14}C-MA (Perkin-Elmer) in 1.5 ml microcentrifuge tubes (Sarstedt, Germany). After 5 min, the aliquots of cells were collected by vacuum filtration on to 0.45 µM nitrocellulose filter (Millipore, USA) and washed twice with 5 ml of ice-cold KPO_4 buffer to prevent further ^{14}C-MA uptake. The filters were carefully placed into scintillation vials (Sarstedt) with 4ml of scintillation fluid (StarScint-Perkin-Elmer). The radioactivity of the samples was determined with a liquid scintillation counter (Tri-Carb 2100, Beckmann or Packard). Counts were converted to equivalent amounts of MA and samples were normalised against total protein according to a modified Lowry method (Peterson, 1977).

2.2.14 Stopped flow spectrophotometry

To gain further insight into the NH_4^+ transport capacity of ScAMF1, the osmotic response of yeast spheroplasts overexpressing *ScAMF1* was observed. Overnight starter cultures were diluted to an OD_{600nm} of 0.2 and the expression of *GmSAT1* was induced for 16 h in the presence of 2% (w/v) Gal and 0.5 mM $(NH_4)_2SO_4$. The cultures were harvested at an OD_{600nm} 0.8-1.0, and the cell pellets were washed with 50 ml of 5 mM KH_2PO_4 (pH 7.5), resuspending the cells to an OD_{600nm} of 1.0 in 10 ml of 5 mM KH_2PO_4 (pH 7.5) solution supplemented with 20 µl of ß-mercaptoethanol (98% (v/v)). The cells were incubated at 28°C with shaking at 200 rpm for 30 min. The cells were then centrifuged at 14,000 x *g* for 2 min, the supernatant decanted, and the cells were resuspended in a buffer containing 2.4 M sorbitol, 5 mM KH_2PO_4 and 600 units of lyticase (Sigma-Aldrich). The cells were incubated for 45 min at 28°C, and then centrifuged at 4,000 rpm for 5 min. The supernatant was carefully aspirated and the spheroplasts were washed once and resuspended in 1 ml of

resuspension buffer (10 mM trisodium citrate, 1 mM EDTA and 0.5 M sorbitol and 0.4 M K_2SO_4, pH adjusted to 6.0 with MES) and then diluted to a uniform OD_{475nm} 1.0. The spheroplast suspensions and an equal volume of resuspension solution plus supplements were mixed in a fast kinetics instrument (SFM-300, BioLogic) equipped with a spectrofluorometer (MOS-250, BioLogic). Volume changes in response to uptake of supplements were recorded at 16°C as light scattering at an angle 90° and 475 nm. The kinetics presented are the averages of 6-9 trace recordings over a period of 6 s.

2.3 Results

The yeast heterologous expression system has been a powerful tool for the preliminary characterisation of GmSAT1 regulation of NH_4^+/MA transport proteins, leading to the identification of a GmSAT1 induced MF transport protein, ScAMF1. Sequence based *in silico* analysis has thus identified *AMF1* homologs in plants, including soybean, *Medicago*, maize and *Arabidopsis* (D. Chiasson, 2012). In this chapter, the characterisation of ScAMF1 in yeast is presented.

2.3.1 Identification of ScAMF1 as a transcriptional target of the soybean symbiosome bHLH transcription factor GmSAT1

Transcriptional analysis obtained as part of my Honours project was revisited in this study to identify a candidate for the NH_4^+ transporter transcriptionally targeted by GmSAT1 (D. Mazurkiewicz, 2008). The previous microarray analysis was carried out on 26972c yeast transformed with *pYES3-GmSAT1* and *pYES3-DEST*, and expression of *GmSAT1* was induced for 12 h in the presence of low (1 mM) NH_4^+. Multiple yeast genes were differentially regulated in response to GmSAT1 activity. The 20 most significant ($p<0.05$) upregulated genes with expression changes greater than 4-fold with respect to *pYES3-DEST* controls were inspected to identify a potential candidate encoding a putative transport protein (Figure 2.2). The expression fold-changes of the 5-most transcriptionally enhanced genes in descending order were *ScAMF1* (YOR378w; ~56-fold), *YML132c* (~38-fold), *YDR046c* (~18-fold), *YHL024w* (~15-fold) and *YDR281c* (~14-fold), validated with qPCR analysis using the pools of RNA prepared for the array (Figure 2.3 A-E). Although

the fold-changes detected by qPCR analysis are different to those obtained from the array, the qPCR data are consistent across the independent experiments presented in this chapter.

2.3.2 GmSAT1 regulates the expression of a novel major facilitator protein in yeast

One gene in particular, *YOR378w* (here on referred to as *ScAMF1* for *Saccharomyces cerevisiae Ammonium Facilitator 1*) was upregulated 56.5-fold ($P = 8.6E^{-14}$) compared to that of the *pYES3-DEST* transformed controls (Figure 2.3 A) (D. Mazurkiewicz, 2008). The enhanced regulation of *ScAMF1*, in particular, proved to be intriguing as eight predicted E-box bHLH DNA binding sites were identified in the putative promoter region 1.5 kb upstream of the *ScAMF1* locus start codon (Figure 2.4). D. Chiasson (2012) demonstrated that a truncated version of GmSAT1 containing the bHLH domain was able to bind a 284 bp segment of the *ScAMF1* promoter in an Electromobility Shift Assay (EMSA) (Figure 2.5). The cloned *ScAMF1* CDS was 1548 bp in length and is predicted to encode 515 amino acids (Figure 2.6). Furthermore, topology analysis using the Kyte/Doolittle hydrophilicity protocol (MacVector 12.7.0, Eastman Kodak, USA) predicted ScAMF1 to be a 56.11 kDa hydrophobic protein with 14 transmembrane spanning regions (Figure 2.7). ScAMF1 displays limited sequence similarity to ScART1 (YML116w, 38.7 % residue identity) and ScART2 (YMR279c, 26.5% residue identity) transport proteins involved in boron efflux and tolerance, respectively (Kaya et a., 2009; Bozdag et al., 2011) (Figure 2.8). These proteins belong to the DHA2 drug:H^+ antiporter subfamily of the Major Facilitator Superfamily (MFS), which are typically arranged symmetrically about a central pore through which substrates transverse membranes (Pao et al., 1998; Gbelska et al., 2006). The amino acid sequence of ScAMF1 is unrelated to the NH_4^+ transporters of the MEP/AMT/Rh family, representing a novel mechanism for NH_4^+ transport.

2.3.2.1 Preliminary analysis of ScAMF1 activity in the yeast mutant yeast strains 26972c and 31019b

Initial characterisation of ScAMF1 was conducted by overexpressing the putative transporter in the 26972c yeast strain. *ScAMF1* (Figure 2.6) was cloned into the *pYES3-DEST* yeast expression vector under the control of the *Galactose Inducible 1* (*Gal1*) promoter (Figure 2.1). Cells overexpressing *ScAMF1* exhibited MA sensitivity comparable to GmSAT1 heterologous activity in yeast when grown on medium supplemented with elevated MA (0.1 M) concentrations (Figure 2.9). MA sensitivity was also exhibited by a null *MEP* mutant yeast strain, 31019b, overexpressing *ScAMF1* under the same conditions (Figure 2.10). The 31019b yeast strain is not subject to potential MEP3 mediated NH_4^+/MA flux unlike the 26972c strain, which may be subject to wild-type like reversion of mep1-1 activity (loss of C-terminal point mutation). Further to this, when supplied with 1 mM ^{14}C-MA, *ScAMF1* overexpression in both yeast strains allowed for ^{14}C-MA accumulation at equivalent rates to *GmSAT1* expressing cells both of which were significantly ($p<0.05$) higher than cells harbouring the corresponding *pYES3-DEST* empty vector controls (Figure 2.11). The rate of ^{14}C-MA uptake of 31019b-ScAMF1 cells was mostly linear between 0.025 - 1 mM MA, and was significantly ($p<0.05$) higher than the *pYES3-DEST* empty vector controls from 0.1 mM MA and above (Figure 2.12). As the concentration of MA was elevated in the minimal media, MA sensitivity was further exacerbated relative to *pYES3-DEST* empty vector cells (Figure 2.13). We found that external pH also influenced ScAMF1 induced MA toxicity. At pH 7.0, 31019b cells transformed with *pYES3-DEST* empty vector control or *ScAMF1* became highly sensitive to MA, while at pH 6.0 and below, control cells remained resistant to MA but cells expressing *ScAMF1* continued to show toxicity responses (Figure 2.13). To further investigate the transport properties of ScAMF1 we used stopped-flow spectrometry, an

assay measuring the osmotic-induced changes in 26972c spheroplast size through a process of light diffraction at 475 nm as spheroplasts are rapidly mixed with differing buffers (Bienert et al., 1997). The spheroplasts swell in response to a substrate moving into the cell, resulting in a proportional decrease in diffracted light. We found that when 31019b-spheroplasts were mixed in a buffer containing 0.5 mM MA, ScAMF1 induced rapid swelling of spheroplasts, while those harbouring the empty vector *pYES3-DEST* exhibited slight shrinking (Figure 2.16 B).

In the presence of NH_4^+, *ScAMF1* overexpression partially rescued the growth on 26972c yeast on low (1 mM) NH_4^+ containing media (Figure 2.15). However, expression analysis in the 31019b cells presented a different growth phenotype under similar NH_4^+ concentrations. Although growth was prevented when 31019b-ScAMF1 cells were grown on 0.1 M MA, NH_4^+ complementation was not observed (Figure 2.15). In the presence of 5 mM NH_4^+, swelling was also observed in 26972c spheroplasts overexpressing *ScAMF1* relative to the empty vector controls (Figure 2.16 A). The specific ^{14}C-MA accumulation rates of 31019b-ScAMF1 competed with an equimolar concentration of an anion in its chloride salt form was calculated by subtracting the corresponding rates of 31019b-*pYES3-DEST* controls (Figure 2.17). In the presence of equimolar concentrations of NH_4^+, ^{14}C-MA uptake was reduced, although not significantly ($p>0.05$) at this concentration. However ^{14}C-MA uptake did not change in the presence of Na^+, and surprisingly increased significantly ($p<0.05$) in the presence of K^+, Ca^{2+} and Mg^{2+}. This result is opposite to that previously observed with GmSAT1 in 26972c, where both Ca^{2+} and Mg^{2+} reduced MA transport (Kaiser et al., 1998).

2.3.3 Expression of *MEP* genes in response to GmSAT1 heterologous activity in yeast

It has been suggested that GmSAT1 negatively regulates the mep1-1 trans-inactivation of MEP3 either through a direct protein interaction at the membrane or through an indirect manner that ultimately influences enhanced MEP3 protein delivery to the membrane fraction (Marini et al., 2000b). Given the TF-like properties of GmSAT1, we first examined whether GmSAT1 induced changes in transcript abundance of either *mep1-1* or *MEP3* in 26972c cells. Although, inspection of the putative promoter regions of *MEP1* and *MEP3* revealed a number of endogenous yeast E-Box bHLH-binding motifs (*MEP1* has three E-box motifs, and *MEP3* has five E-box motifs), the CACGTG variant capable of facilitating the binding of GmSAT1 was absent (Figure 2.18 A & B). However, *MEP3* transcript levels were significantly ($p<0.05$) enhanced approximately 2.0-fold in response to GmSAT1 activity in both array and qPCR analysis (Figure 2.19 B & D). Although *mep1-1* expression in the array was enhanced significantly ($p<0.05$), qPCR analysis failed to reveal a significant effect ($p>0.05$) (Figure 2.19 A & C). This result is consistent with previous observations indicating either elevated expression of *MEP3* in 26972c or elimination of mep1-1 transinhibtion (Δ*mep1-1*) of MEP3-NH_4^+ transport activity (Marini et al., 2000b).

Previously, *MEP1* expression was shown to be negatively regulated by increasing concentrations of external NH_4^+ and reduced N compounds (Marini et al., 1994). As our data show that overexpression of *ScAMF1* does enhance NH_4^+ permeability across the yeast PM, we investigated the possibility that ScAMF1 might have an influence on *MEP* expression, which might account for the partial NH_4^+ complementation phenotype initiated by ScAMF1 activity in 26972c cells. Transcriptional analysis of *ScAMF1* overexpression in the presence of 1 mM NH_4^+ for 12 h demonstrated that transcription of *mep1-1* (Figure

2.20 B) and *MEP3* (Figure 2.20 B) were significantly ($p<0.05$) enhanced relative to *pYES3-DEST* controls.

2.3.4 Methylammonium phenotypes established by GmSAT1 activity in yeast are dependent on *ScAMF1* expression

In a prior study, the ability of GmSAT1 to enhance ^{14}C-MA transport and MA sensitivity in yeast strain 26972c was abolished by the introduction of selected mutations in the predicted DNA binding (R180K – a region involved in hydrogen bonding with phosphate in the DNA backbone) or dimerisation domains (L191V and L207V – two regions important for homo- and/or hetero-dimerisation of bHLH proteins to bind DNA) (P. Loughlin, 2007). The mutagenesis was revisited in this study by qPCR analysis. It was found that the expression of *ScAMF1* was significantly ($p<0.05$) reduced in cells expressing bHLH mutant GmSAT1 under low NH_4^+ conditions for 12 h relative to wild-type GmSAT1-cells (Figure 2.14 A). P. Loughlin (2008) also found that the mutations affected the ability of GmSAT1 to restore NH_4^+ complementation of 26972c cells. Here, no significant ($p>0.05$) change was found in the level of *mep1-1* or *MEP3* transcripts relative to *pYES3-DEST* controls (Figure 2.14 B & C).

2.3.5 Reverse genetics reveals that ScAMF1 is responsible for methylammonium phenotypes.

In order to further verify that *ScAMF1* was the genetic target of GmSAT1 and the protein responsible for the MA related phenotypes, a reverse genetics approach was employed. The kanamycin resistance gene (*kanMX4*) was amplified from the *pFA6a* plasmid (Wach et al., 1997) with primers that created a product with flanking regions homologous to the genomic sequence immediately flanking the start and stop codons of the *ScAMF1* locus,

which were extended in a subsequent round of PCR (Figure 2.21). The *ScAMF1* locus was removed from the 26972c genome by replacing it with the *kanMX4* using homologous recombination. The deletion was confirmed by amplification of products with primers flanking the *ScAMF1* locus coupled with primers homologous to the introduced *kanMX4* gene (Figure 2.22). Phenotypic analysis of the 26972c:Δ*amf1* mutants expressing *GmSAT1* or harboring the *pYES3-DEST* empty vector showed that loss of ScAMF1 activity eliminated the ability of GmSAT1 to instate a MA sensitivity phenotype (Figure 2.23) or significantly enhance the accumulation ^{14}C-MA (Figure 2.24). Interestingly though, loss of *ScAMF1* activity partially restored the cells' ability to grow on low concentrations of NH_4^+ (Figure 2.23). This phenotype does not appear to involve *mep1-1* as its expression was not influenced by the loss of *ScAMF1* (Figure 2.25 A). GmSAT1 was also unable to significantly ($p>0.05$) enhance the expression of *MEP3* in the absence of *ScAMF1* (Figure 2.25 B).

2.3.6 ScAMF1 is localised to the plasma membrane in yeast

Protein localisation is indicative of putative cellular function. Structural predictions suggest that ScAMF1 is predominately hydrophobic and most likely involved in membrane transport. In light of the transport activities observed with ScAMF1 in yeast, it was predicted that ScAMF1 is most likely localised to the yeast PM. In order to assess the localisation of ScAMF1, an overlapping PCR strategy was employed to create mGFP5::fusion constructs (Figure 2.27), which were sub-cloned into the *pYES3-DEST* yeast expression vector. Fluorescence confocal microscopy was performed on 26972c yeast expressing *mGFP5*, *mGFP5::ScAMF1* (mGFP5 fused to the N-terminus of ScAMF1) or *ScAMF1::mGFP5* (mGFP5 fused to the C-terminus of ScAMF1) in the presence of 2% (w/v) Gal and 0.1% (w/v) Pro. Untagged mGFP5 protein was observed throughout the

yeast cytoplasm (Figure 2.27 A), whilst mGFP5 fused to the N-terminus of ScAMF1 was observed specifically localised to the PM (Figure 2.27 B). The mGFP5::ScAMF1 fusion protein was functional and able to establish MA toxicity in the 26972c yeast strain in the presence of high (0.1 M) MA, whist cells expressing *mGFP5* did not present a toxicity phenotype (Figure 2.27 C). This indicates that mGFP5 is not toxic to the cell, and that fusion of mGFP5 to the N-terminus of ScAMF1 does not interfere with the targeting of ScAMF1 protein. When mGFP5 was fused to the C-terminus of ScAMF1, I was unable to detect mGFP5 using fluorescence confocal microscopy (data not presented).

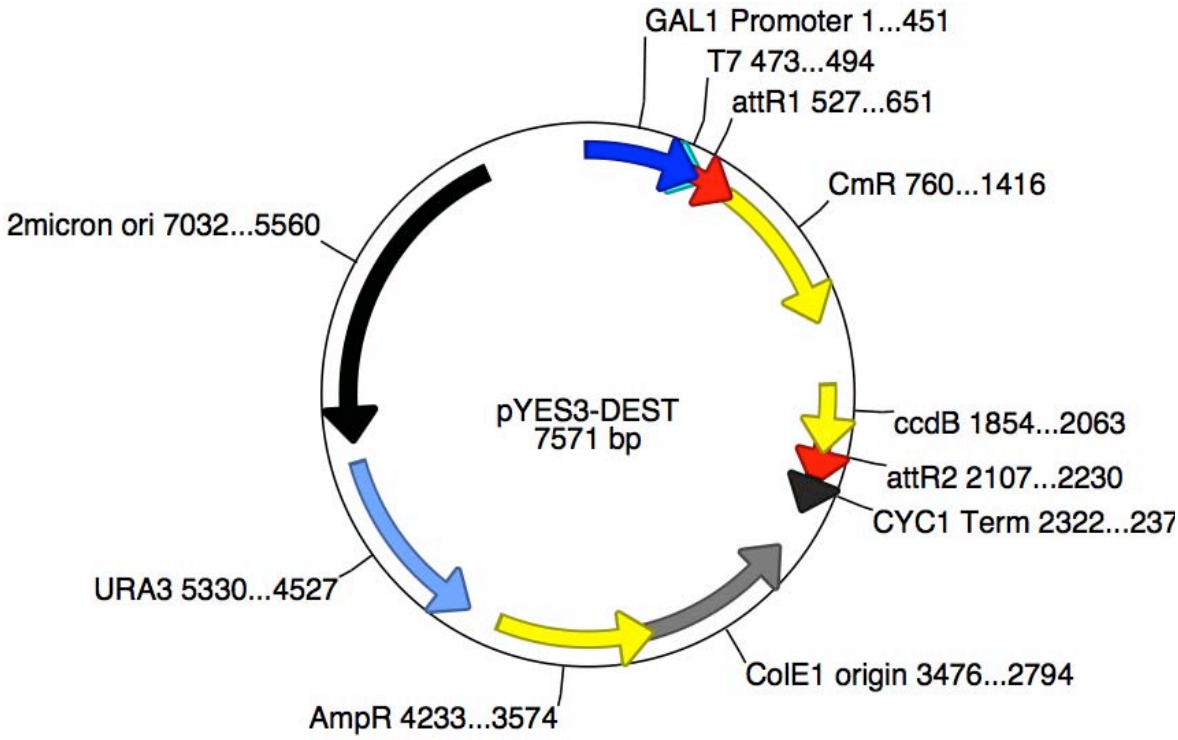

Figure 2.1 Vector map of *pYES3-destination*

The *pYES3* yeast expression vector was converted to a Gateway© destination vector (*pYES3-DEST*) by ligating the Gateway Conversion reading frame cassette A into the *Bam* H1 restriction sites (M. Shelden, unpublished).

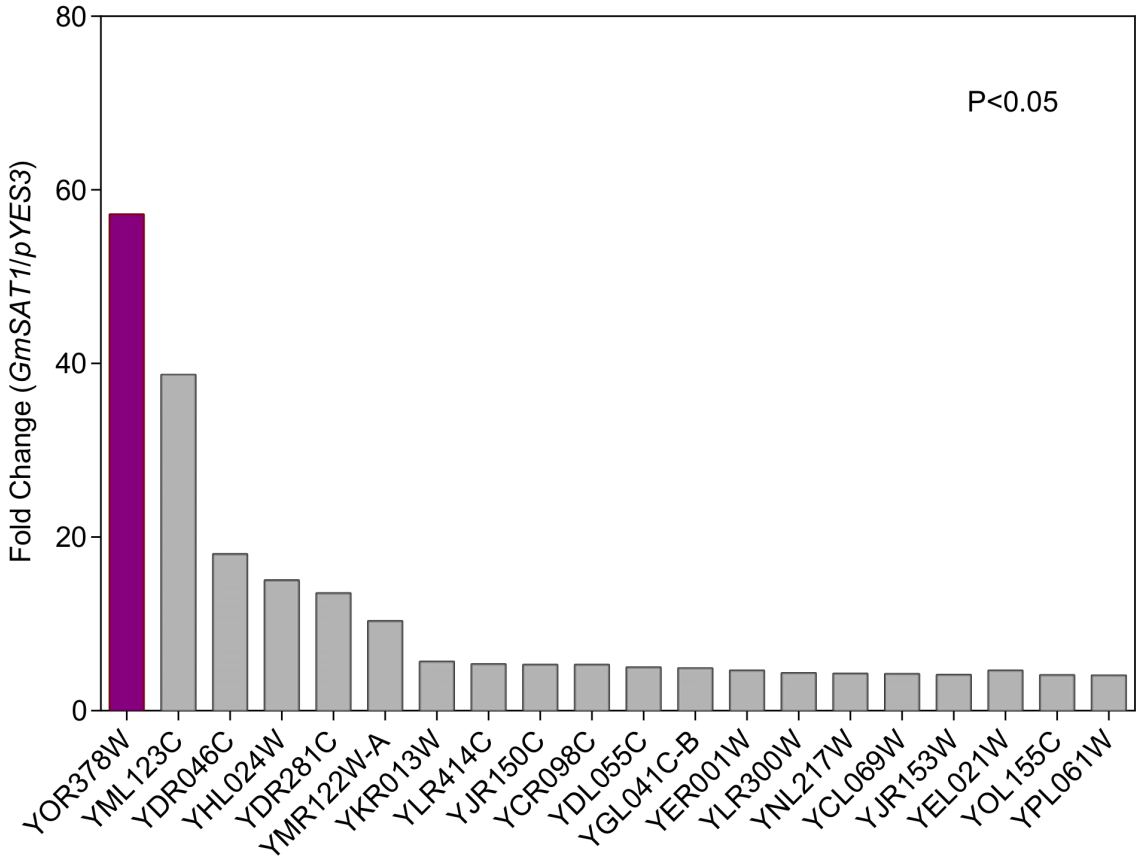

Figure 2.2: Expression profile of selected genes across the genome of 26972c yeast in response to GmSAT1 activity

26972c cells transformed with *pYES3-GmSAT1* (experiment) or *pYES3-DEST* (control) were prepared for microarray analysis. The treatment was applied to all samples and consisted of a 12 h 2% (w/v) galactose and 1 mM NH_4^+ induction. Total RNA samples were converted to cDNA, fluorescently labelled and hybridised to Yeast Genome 2.0 Arrays (3 technical replicates) by the Ramaciotti Centre (The University of New South Wales). The data are presented as the mean (n = 3) fold-change in expression in the GmSAT1 experiment with respect to *pYES3-DEST* control cells. *YOR378w* is from here on referred to as *ScAMF1*.

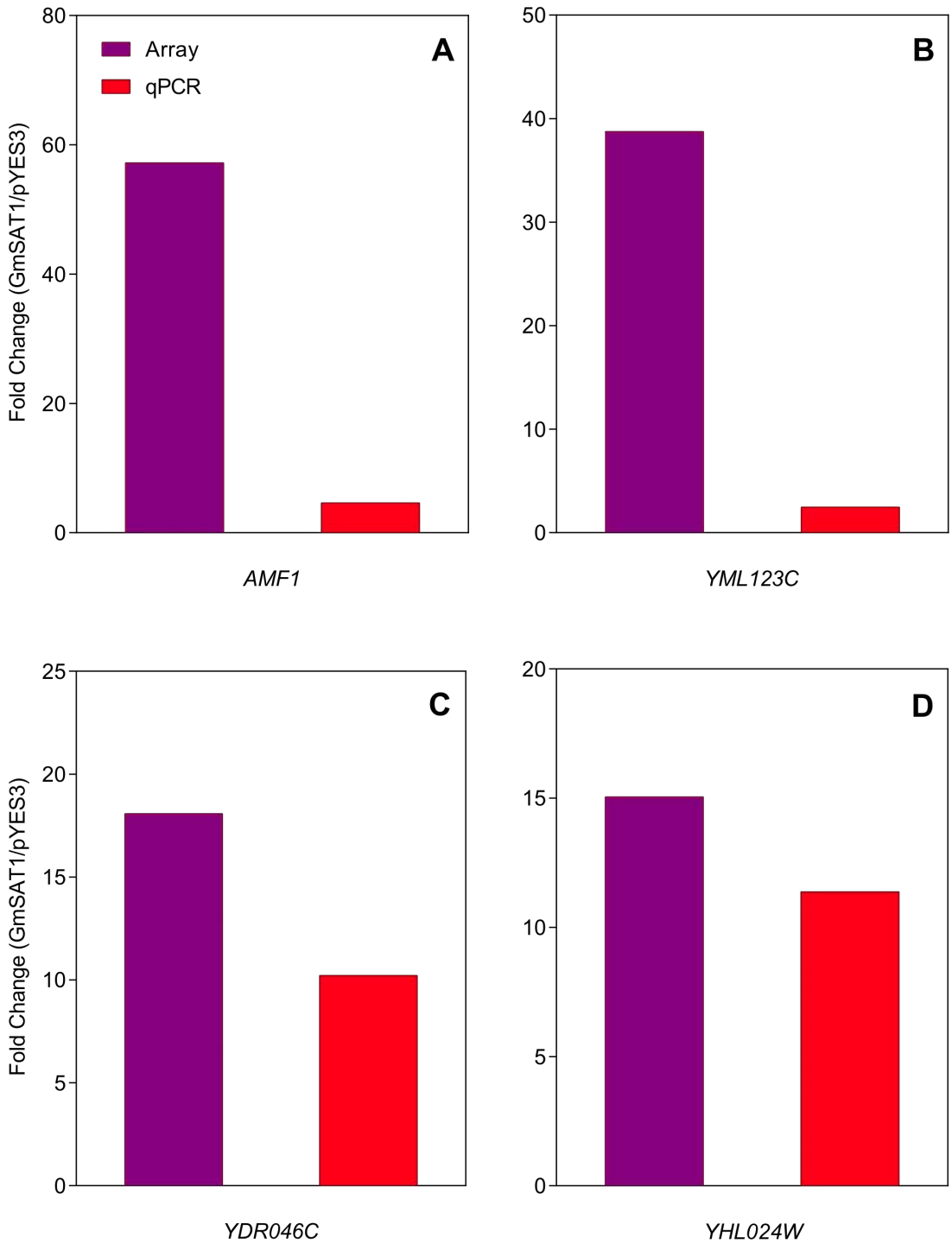
A
Array
qPCR
Fold Change (GmSAT1/pYES3)
80
60
40
20
0
AMF1
B
50
40
30
20
10
0
YML123C
C
25
20
15
10
5
0
YDR046C
D
20
15
10
5
0
YHL024W

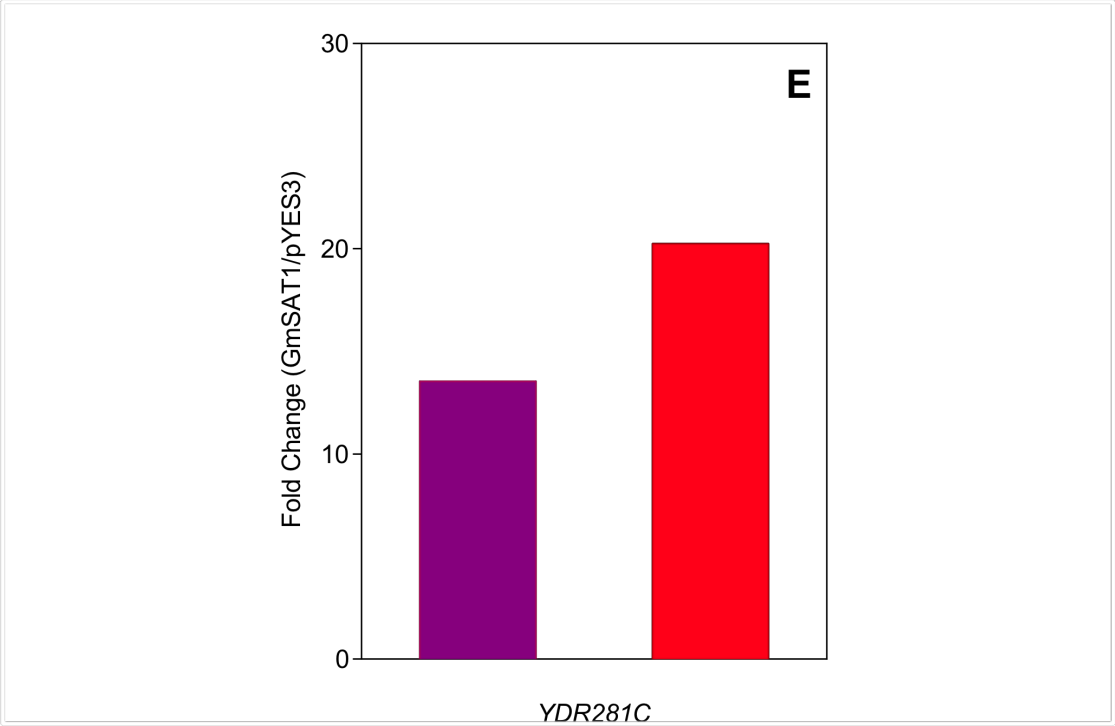

Figure 2.3: Quantitative PCR verification of the 5-most transcriptionally enhanced genes in microarray analysis

26972c cells transformed with *pYES3-GmSAT1* (experiment) or *pYES3-DEST* (control) were incubated for 12 h in the presence of 2% (w/v) galactose and 1 mM NH_4^+. Total RNA was converted to cDNA and processed for expression analyses. Affymetrix microarray analysis (n = 3) was carried out as described in Figure 2.2. RT-PCR was carried out with iQ SYBR Green Supermix reagent (BioRad) and qPCR primers listed in Table 2.1. The Ct values obtained for 3 technical replicates were normalised to *TUB1* housekeeping gene by means of the $2^{-\Delta CT}$ equation (Livak and Schmittgen, 2011). The data are presented as a fold-change in expression in the GmSAT1 experiments with respect to *pYES3-DEST* control cells.

CGAAGTAAATAACGTGCAGAACATTG**CATATG**ATAGATAACAACCTATAGTATATATTTCAAAATCGCGAC
AAATCTGAAATATTAATTGATTTGATTAGCTGCAGAGATCTTCTCGATGTAAGGAGCTATTTAAATAGAAAG
GGTCAGAATCGTCGTCCTGTGGGAGCTGGTATATACTAAATTGATGAACAACTAAAATAGCACTCTCATTGT
CATTTTGGGTGTGAGACCTTAAGCAAGGAGAGATATTTTTAATGGATGTATTAGCGCAGCCGTTGCTTACGG
TATTCCTTGGCATATTGTCCCTGAAAAAAAACCGTTGTACACTCGGATACGCATTTTTCGGACTTCTCCCACC
CAAGAAACGCAACTTTTGAAGGGCGCCTACACCACTAGACCAACAAGGCCAATGCAAAGCTACAAA**CAAA**
TGCGTGGGCGCATGGGCATAAGGAGGTGTAAAAAGCTTTTTTTTTTTATGTGAGGAATTACAGGCGGAAGA
TACTCAAATAAAGCACTGATTTGATGTTACCGAACTTTTCCCCAGGCATAAAATTTTATTTTCATATTTCATC
AATTCGATATTATTGATATCGCACCTAATGTAGTCATTTCCTTTCTCTCTTTGCTAGTAGATTTTAAAAAGGT
TTCTTGCTGTATTTTTTTATACTTTTATAGACGCCGCTTTCCAAAGTTCATCTAAAATAAGTCGCTACAATGA
TTTGATCTTGATTCGGTGCTTCAGGAGCCTGCTTGCTTCTTTGCAGCTTCGGCAATTTGGAACCTTGTGTGCA
TATCCTCGTTTGTAAGCCCAGAAGCACACAGACATCGATCACATCTATAATAGGAGCATGCTATCATAAAAG
ATTCACAGTATTCGTATAATTACATGGCAGACTTTTTGAAAAGAATGGTATGGAAC**CAAGTG**AGCGCCTAG
AAAAAAAGCTGAAAAGCTGAAATCTTAATTGGATAAGAAACTTCAATAACATTTTTCACGCGTTTCTTTTTC
AACTAGATTAGCCTTAACAAACGACAATCATCGAGTACCCACGCTCATTACGCTGAACGTG**CAAATG**TAAC
GGGGTGGAAACCTAAAACGTTGAATGAACTAGCCAGAACGATGA**CAATTG**CGGCAAGCTTTCCATACGTGT
TCTGTTGTTGCGGCTTAGAGTGGTAGGTAACCGCGCCAAGCAAAATTACCTACCACTTTAAGCCCAAAAAGG
TGATGTGTAGCTATTGCGGCTGTGGCGGCTATTGCGGTTGTCGCCACGCTTGTCGCCA**GGGTTGTCGCTAC**
GAATGTTTCAGCTTTTTTTTCAATGGGCCACTCTTTTCACGTG**AAGCGCTCCACGAAATGTGCGGATA**
TTGCGGAAGCTCTCAATGATGAGCTATCGGTAGGGATTAAAATAAACGAGATTTGGCAGCAGTTTTAA
ATACCAAGGGAGTAGTATATCTAGCCTCCAATAACTTCATTTG**TGGAAACTTACTTCTATCTCACTCTC**
TACCTGAAAAGAAAACAAATATTGTACATTCATCAATTG**CTGGAACATAAAGAACATAAAATCAAT**AT
G

Figure 2.4: Overview of *ScAMF1* promoter sequence

In the predicted promoter region (1500 bp upstream) of the *ScAMF1* locus there is a number of putative 'E-box' box motifs (CANNTG) that may facilitate the binding of bHLH transcription factors highlighted blue. GmSAT1 has the sequence H-E-R at positions 5-9-13 of the basic region, which are major determinants for the recognition of CACGTG E-box variant sequence highlighted green (Atchley and Fitch, 1997). The start codon of *ScAMF1* is highlighted red. Bold and underlined sequences indicate the cloned fragments used for *ScAMF1* EMSA analysis performed by D. Chiasson (2012).

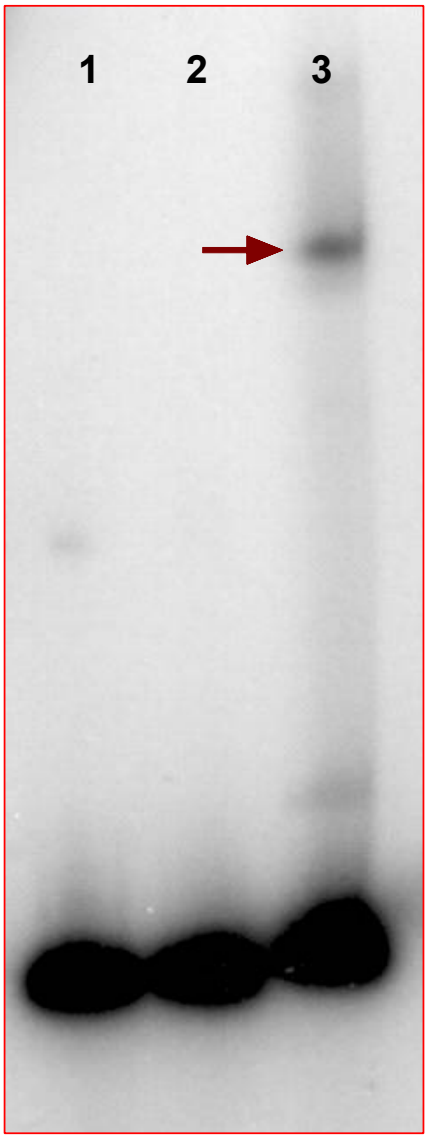

Figure 2.5: GmSAT1 binds to *ScAMF1* promoter *in vitro*.

Electromobility shift assay (EMSA) was carried out with purified MBP::GmSAT1 and *ScAMF1* (288 bp – see Figure 2.4) promoter fragments labeled with ^{32}P. Samples were incubated at room temperature for 25 min, separated by 6% (w/v) native-PAGE, dried, and exposed to film. Probe alone (lane 1), empty MBP + probe (lane 2), MBP::GmSAT1 + probe (lane 3). Arrows indicated shifts in mobility of the respective probes. Note: David Chiasson conducted protein purification and EMSA experiment (D. Chiasson, 2012).

```
   1 ATGTCAACTAGCTCCTCCGTAACGCAGAAAAACTTGGATACAAACGCGGAAGCCTTGAAA 60
   1  M  S  T  S  S  S  V  T  Q  K  N  L  D  T  N  A  E  A  L  K  20

  61 AAGGAGGATAAAGTATTATCAGAGTTTGATATTCAGGATGAGAGGCCTAAATCCCTTTTA 120
  21  K  E  D  K  V  L  S  E  F  D  I  Q  D  E  R  P  K  S  L  L  40

 121 TGGGAGAGTGCCTTTGTCGGAGTGCTGTGCTCTGCCCAACTAATGACTCAGGCAGGACTT 180
  41  W  E  S  A  F  V  G  V  L  C  S  A  Q  L  M  T  Q  A  G  L  60

 181 GGACAATCATTAGCGCCGCTTCACATCATCGGTAACAGTTTTGGAACAACGAATGCTGGA 240
  61  G  Q  S  L  A  P  L  H  I  I  G  N  S  F  G  T  T  N  A  G  80

 241 CAACTTAGTTGGTTTGCTTCCGCATATTCGCTAACTGTTGGTACATTCATTTTAATTGCT 300
  81  Q  L  S  W  F  A  S  A  Y  S  L  T  V  G  T  F  I  L  I  A  100

 301 GGAAGACTCGGAGATATCTTCGGACACAAGAAATTCTTTGTCCTTGGCTTCTTTTGGTAC 360
 101  G  R  L  G  D  I  F  G  H  K  K  F  F  V  L  G  F  F  W  Y  120

 361 GCACTTTGGTCCTTACTTGCTGGGTTTAGCGTCTACTCTAATCAGATTTTTTTTGACTGC 420
 121  A  L  W  S  L  L  A  G  F  S  V  Y  S  N  Q  I  F  F  D  C  140

 421 TGTCGTGCATTTCAAGGCATGGGTCCGGCCTTTTTGTTGCCAAATGCCATTGCGATTCTC 480
 141  C  R  A  F  Q  G  M  G  P  A  F  L  L  P  N  A  I  A  I  L  160

 481 GGACGCACATATAAGCCAGGAAGAAGAAAAAACATGGTCTTTAGTCTGTTTGGTGCTTCA 540
 161  G  R  T  Y  K  P  G  R  R  K  N  M  V  F  S  L  F  G  A  S  180

 541 GCACCTGGTGGCTTCTTCCTTGGGGCTGTTTTCTCATCCATGTTGGGTCAACTGGCGTGG 600
 181  A  P  G  G  F  F  L  G  A  V  F  S  S  M  L  G  Q  L  A  W  200

 601 TGGCCATGGGCTTACTGGATAATGGGTATTGCATGCTTTGTTTTAGCTGTAGCAGGTTAC 660
 201  W  P  W  A  Y  W  I  M  G  I  A  C  F  V  L  A  V  A  G  Y  220

 661 TTTGTAATCCCTCACACCCCCATGCCAAGCCGCGATGCCTCATCTTTCAAGTTGTTGGAA 720
 221  F  V  I  P  H  T  P  M  P  S  R  D  A  S  S  F  K  L  L  E  240

 721 CGAATCGATTTTGCAGGGTCAGTTACCGGCGTTGTTGGATTAATTCTCTTTAATTTCGCT 780
 241  R  I  D  F  A  G  S  V  T  G  V  V  G  L  I  L  F  N  F  A  260

 781 TGGAACCAAGGCCCCGTTGTGGGTTGGCAAACTCCATACACATACGCTCTTTTGATAGTT 840
 261  W  N  Q  G  P  V  V  G  W  Q  T  P  Y  T  Y  A  L  L  I  V  280

 841 GGTACCTTTTTCTTGGTTATTTTTGCATATATCGAGTCCCGAGCAGCTTTCCCTCTGCTA 900
 281  G  T  F  F  L  V  I  F  A  Y  I  E  S  R  A  A  F  P  L  L  300

 901 CCATTTGCTGCTCTTTCTAGTGATACTGCTTTTGTACTTAGCTGCATAGCTGCGGGATGG 960
 301  P  F  A  A  L  S  S  D  T  A  F  V  L  S  C  I  A  A  G  W  320

 961 GCCAGCTTTGGTATTTGGATATTCTATACATGGCAGTTCATGGAAGACTCAAGGGGCCAA 1020
 321  A  S  F  G  I  W  I  F  Y  T  W  Q  F  M  E  D  S  R  G  Q  340

1021 ACCCCCCTTCTTTCTAGTGCACAGTTTTCACCTGTAGCAATCAGTGGATTTTGTGCAGCC 1080
 341  T  P  L  L  S  S  A  Q  F  S  P  V  A  I  S  G  F  C  A  A  360

1081 GTGACGACAGGTTTCCTTCTAAGCCATACACCCCCAAGCACAGTTATGCTTTTTGCGATG 1140
 361  V  T  T  G  F  L  L  S  H  T  P  P  S  T  V  M  L  F  A  M  380

1141 ACAGCTTTCACAGTCGGAACTATATTGATTGCTACGGCCCCCGTTCACCAAACGTATTGG 1200
 381  T  A  F  T  V  G  T  I  L  I  A  T  A  P  V  H  Q  T  Y  W  400
```

```
1201 GCTCAAACGTTTGTGTCAATCATTGTTATGCCTTGGGGAATGGACATGTCCTTTCCGGCC 126
 401  A  Q  T  F  V  S  I  I  V  M  P  W  G  M  D  M  S  F  P  A  420

1261 GCTACAATAATGCTTAGTGACTCGATGCCACACGAACATCAAGGTCTTGCAGCCTCTTTG 132
 421  A  T  I  M  L  S  D  S  M  P  H  E  H  Q  G  L  A  A  S  L  440

1321 GTTAATACGGTGGTAAACTATTCGATATCGATAGGTTTGGGTATTGCAGGTACAATTGAA 138
 441  V  N  T  V  V  N  Y  S  I  S  I  G  L  G  I  A  G  T  I  E  460

1381 TCTAGAGTAAATGACGGAGGTGCCAAGCCTTTGAAAGGATATCGTTGTTCGTGGTACATG 144
 461  S  R  V  N  D  G  G  A  K  P  L  K  G  Y  R  C  S  W  Y  M  480

1441 GGCATCGGGTTGAGCGGACTTGGCATTTTTGTCGCAGCAACGTATGCATGGAGCACTTTT 150
 481  G  I  G  L  S  G  L  G  I  F  V  A  A  T  Y  A  W  S  T  F  500

1501 ATGAAGTCTAAAAAAAGGATCTCCGAAAAGCAGCATTTTATAGAATAA 1548
 501  M  K  S  K  K  R  I  S  E  K  Q  H  F  I  E  *  516
```

Figure 2.6: Cloned *ScAMF1* CDS and translation

The coding sequence (CDS) and protein translation of *ScAMF1* was retrieved from the *Saccharomyces cerevisiae* genome database (www.yeastgenome.org).

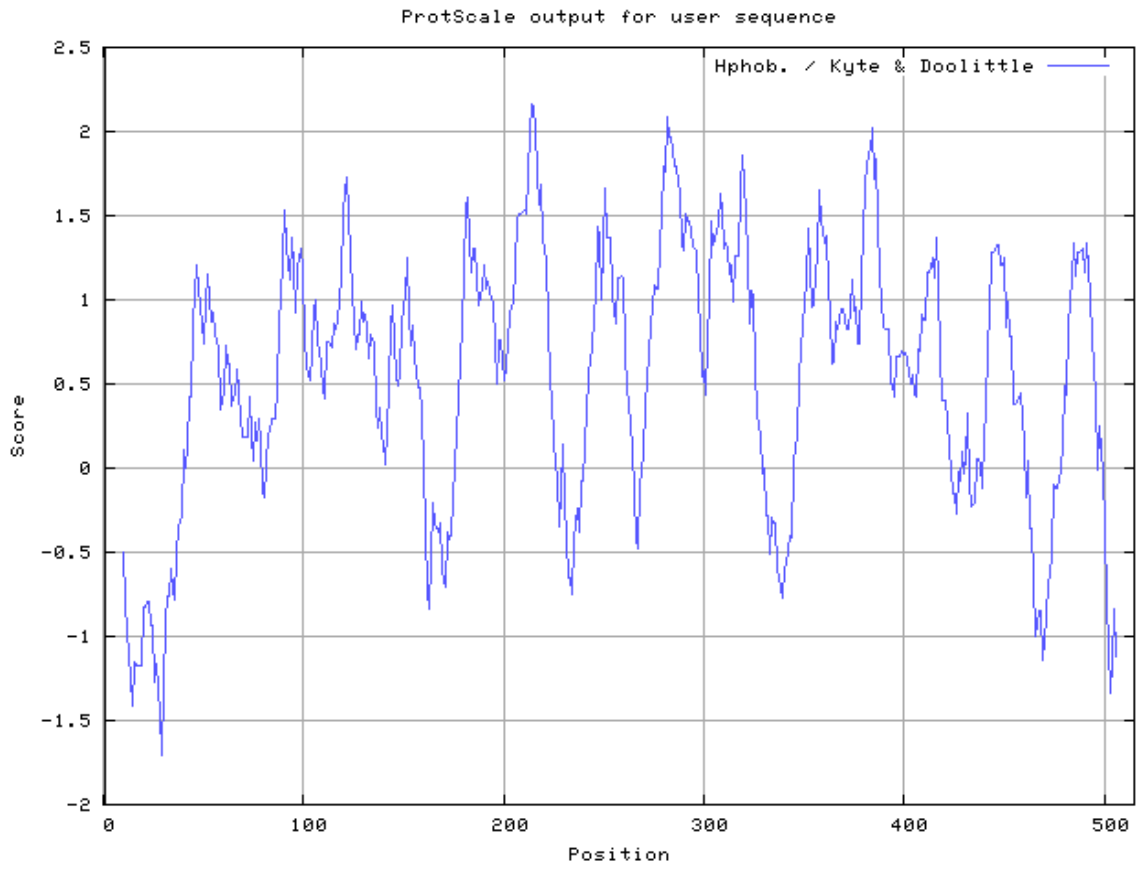

Figure 2.7: ScAMF1 predicted topology

The hydrophobicity plot was generated using MacVector version 12.7.0 (MacVector Inc., NC, USA) using the Kyte / Doolittle protocol with an amino acid window size of 19. The hydrophobic regions are indicated by positive hydrophilicity values.

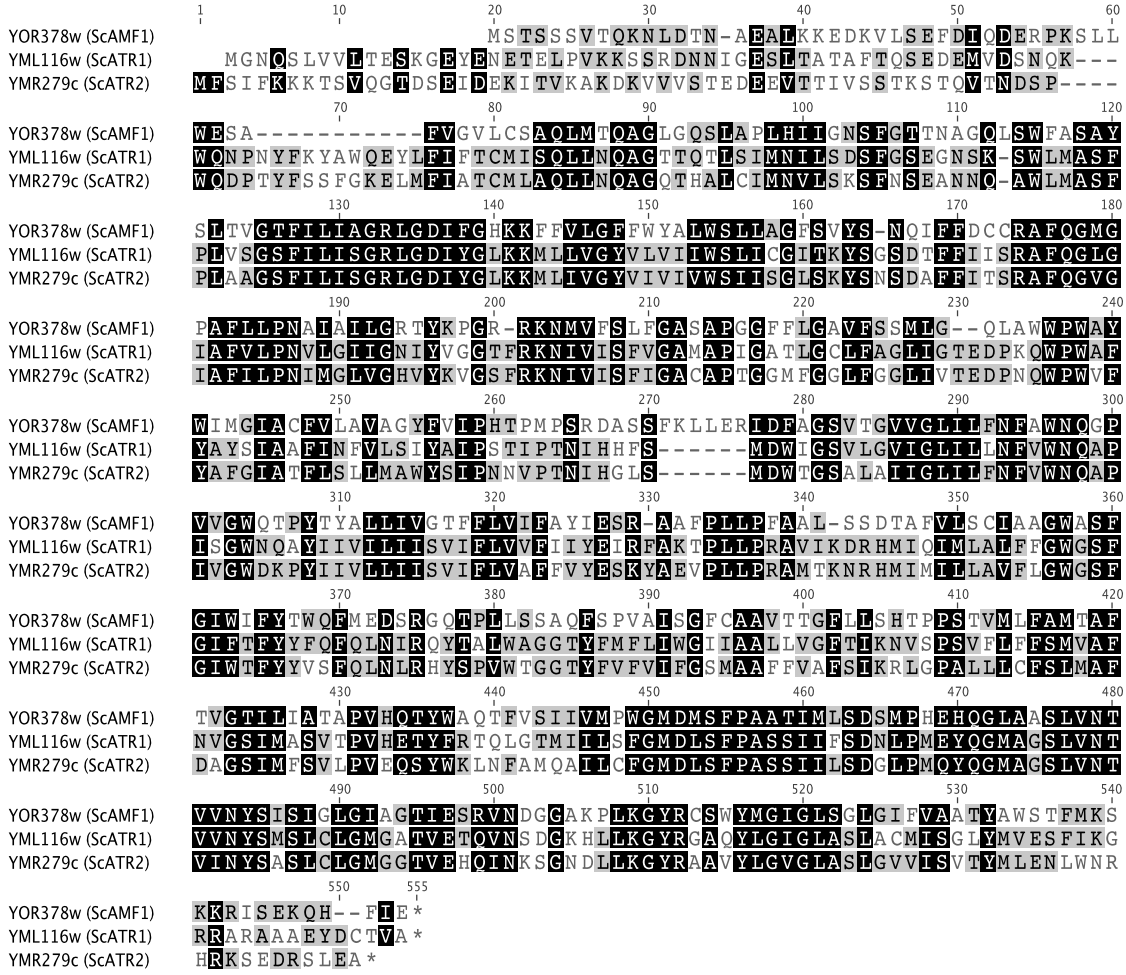

Figure 2.8: Alignment of ScAMF1 with ScATR1 and ScATR2

Multiple MUSCLE alignment of the ScAMF1, ScATR1 and ScATR2 amino acid sequences as generated with Geneious® V 5.6 software.

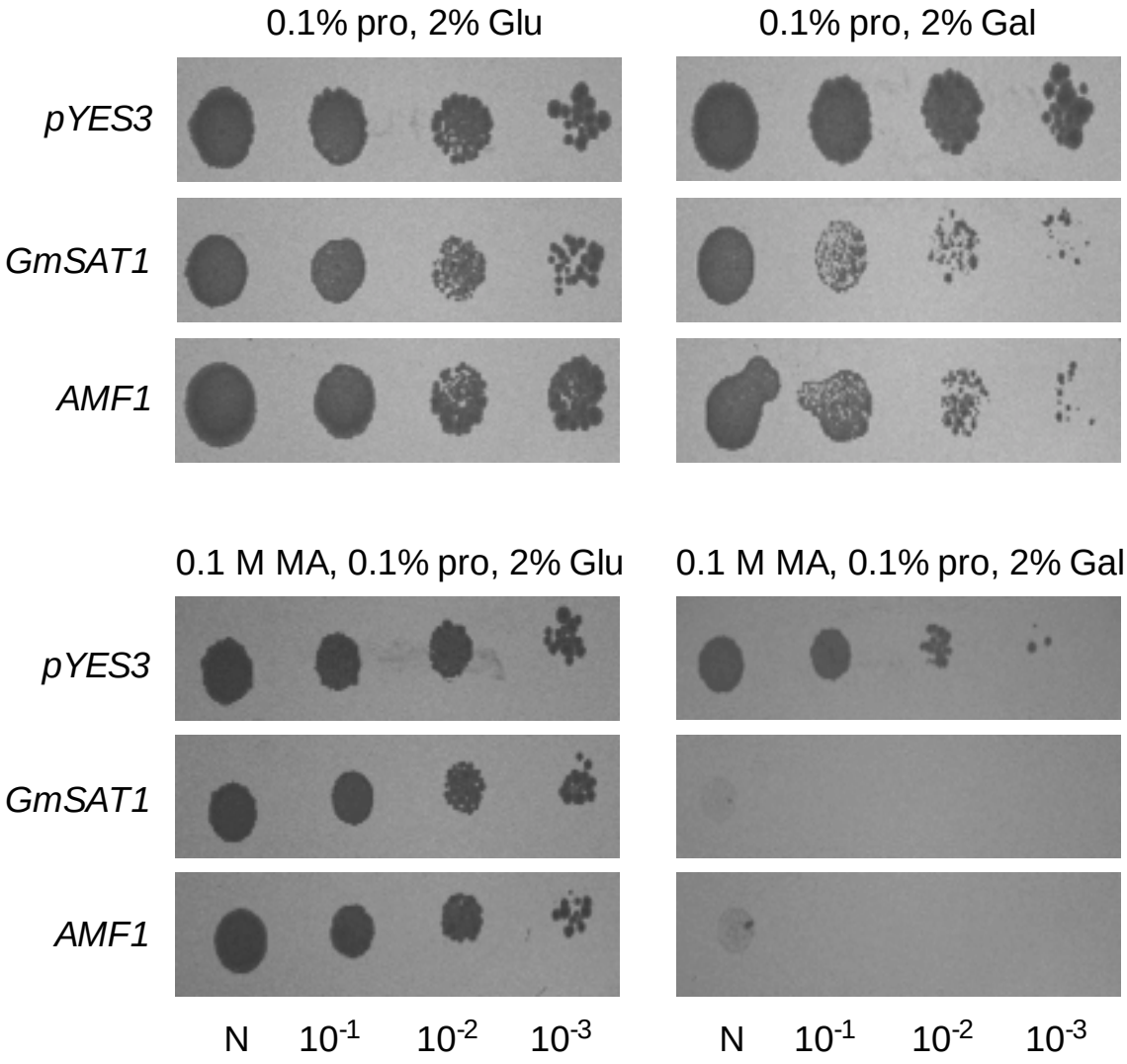

Figure 2.9: Growth of 26972c NH_4^+ transport deficient yeast strain expressing *GmSAT1* or *ScAMF1* in the presence of methylammonium

The 26972c yeast strain was transformed with *pYES3-DEST* (control), *pYES3-GmSAT1* or *pYES3-ScAMF1*. Cells were grown to mid-log phase and diluted to a uniform OD_{600nm} 0.5. The cells were then subjected to 1 in 10 serial dilution. Aliquots (5 µl) of cells were spotted onto yeast minimal media (Grenson, 1966) supplemented with 0.1% (w/v) L-proline (pro) and 2% (w/v) glucose (Glu) or galactose (Gal) with or without 0.1 M MA where indicated. The yeast plates were incubated for 6 d at 28°C. Data presented are representative of 3 independent biological replicates.

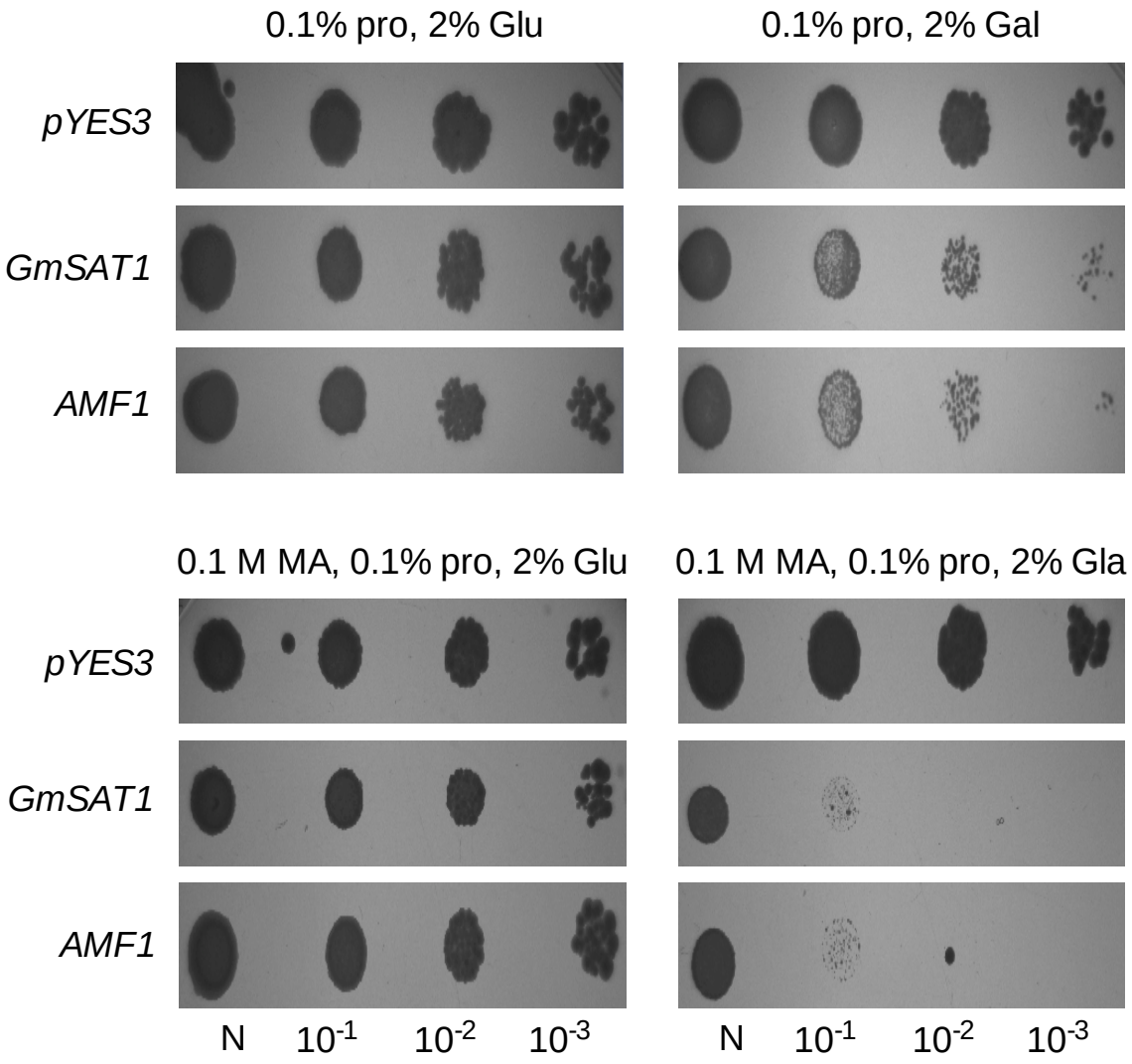

Figure 2.10: Growth of 31019b NH_4^+ transport deficient yeast strain expressing *GmSAT1* or *ScAMF1* in the presence of methylammonium

The 31019b yeast strain was transformed with *pYES3-DEST* (control), *pYES3-GmSAT1* or *pYES3-ScAMF1*. Cells were grown to mid-log phase and then serially diluted as described in Figure 2.9. Diluted cells were spotted onto yeast minimal media (Grenson, 1966) supplemented with 0.1% (w/v) L-proline (pro) and 2% (w/v) glucose (Glu) or galactose (Gal) with or without 0.1 M MA where indicated. The yeast plates were incubated for 6 d at 28°C. Data presented are representative of 3 independent biological replicates.

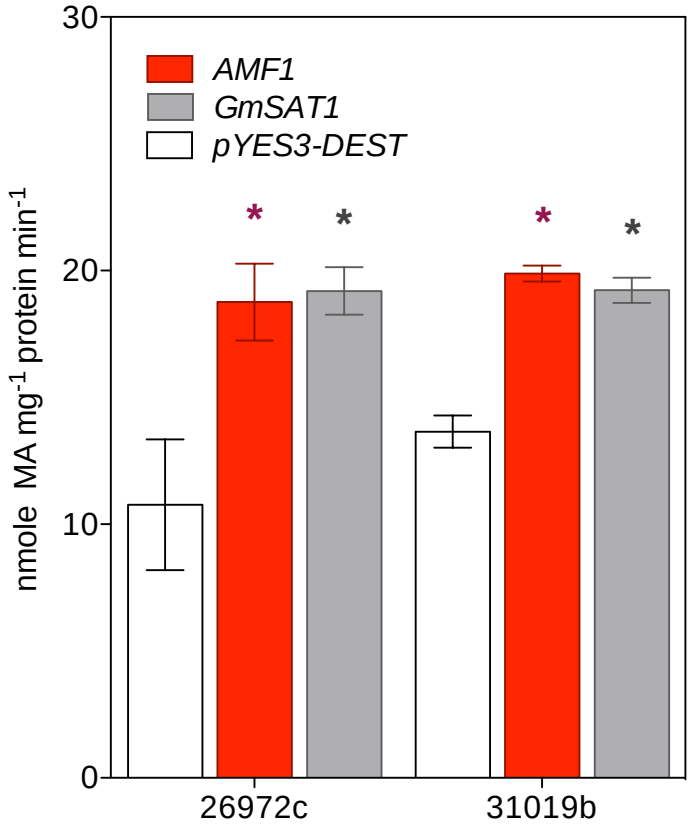

Figure 2.11: Rate of ^{14}C-MA influx into yeast cells over-expressing *GmSAT1* or *ScAMF1* relative to the empty *pYES3-DEST* vector

26972c and 31019b yeast strains were transformed with *pYES3-DEST* (control), *pYES3-GmSAT1* or *pYES3-ScAMF1* and grown for 16 h using liquid yeast minimal media without uracil (Grenson, 1966) supplemented with 2% (w/v) galactose and 1 mM NH_4^+. Uptake of 1 mM ^{14}C-MA in a 2% (w/v) galactose KPO_4 buffer (pH 6.2) was measured over 5 min. Accumulated ^{14}C-MA was quantified by measuring the β-decay using a scintillation counter. Data presented are mean rate of MA uptake (n = 6) ± SE. The data are representative of at least 5 independent biological experiments. Where indicated data are significant ($p<0.05$) from the empty vector controls denoted by an astrix (*).

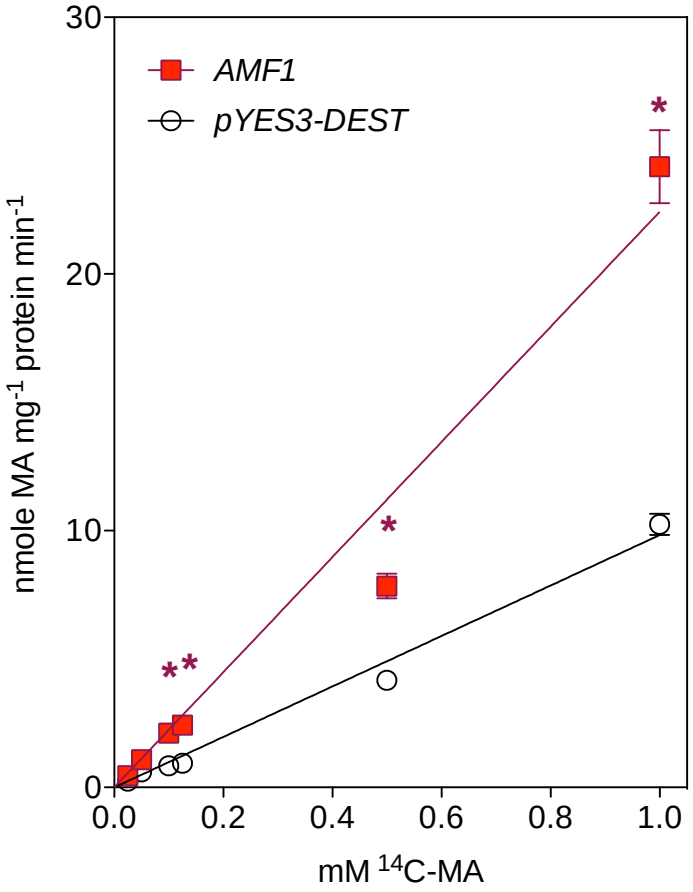

Figure 2.12: Concentration dependent uptake of ^{14}C-MA in 31019b cells transformed with *pYES3-DEST* or *pYES3-ScAMF1*

The triple MEP mutant yeast strain 31019b was transformed with *pYES3-DEST* (control) or *pYES3-ScAMF1* and grown for 16 h using liquid yeast minimal media without uracil (Grenson, 1966) supplemented with 2% (w/v) galactose and 1 mM NH_4^+. Uptake of ^{14}C-MA was performed over a 5-min period and normalised against total cellular protein. Accumulated ^{14}C-MA was quantified by measuring the β-decay using a scintillation counter. Data presented are mean rate of MA uptake (n = 6) ± SE. Where indicated data are significantly different ($p<0.05$) from the empty vector controls denoted by an astrix (*). The data are representative of 2 independent biological experiments.

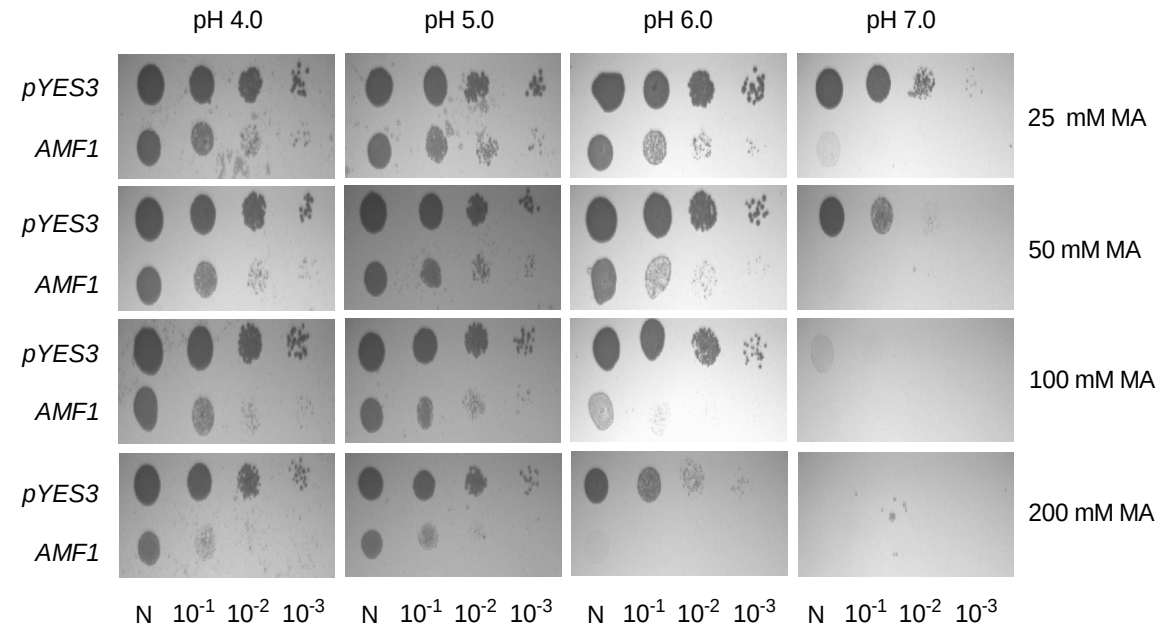

Figure 2.13: Influence of external pH on the sensitivity to MA of 31019b cells expressing *pYES3-DEST* or *pYES3-ScAMF1*

31019b yeast strains were transformed with *pYES3-DEST* (control) or *pYES3-ScAMF1*. Cells were grown to mid-log phase and then serially as diluted described in Figure 2.9. Diluted cells were spotted and spotted onto solid yeast minimal media (Difco-YNB) without amino acids or nitrogen source supplemented with 2% (w/v) galactose and 0.1% (w/v) L-proline with increasing MA (25, 50, 100 or 200 mM) buffered with 50 mM MES/Tris at pH 4.0, 5.0, 6.0 or 7.0. The yeast plates were incubated for 6 d at 28°C. Data presented are representative of 3 independent biological replicates.

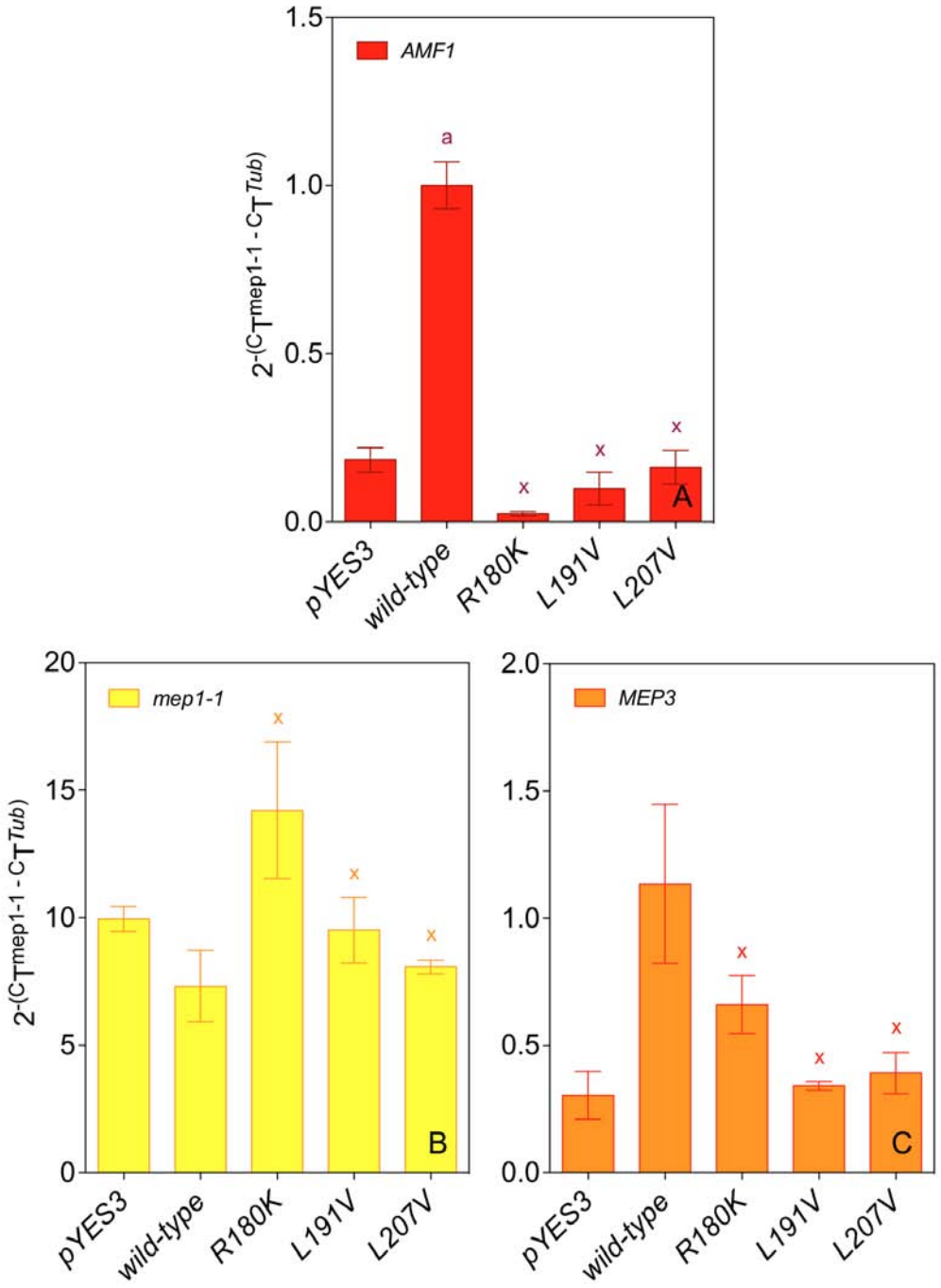

Figure 2.14: Influence of mutant GmSAT1 proteins on *ScAMF1, mep1-1 and MEP3* expression

Total RNA was extracted from 26972c transformed with *pYES3-GmSAT1* (wild-type), selected

pYES3-GmSAT1 mutants (R180K, L191V, L207V) (experiment) or *pYES3-DEST* (control) incubated for 12 h in the presence of 2% (w/v) galactose and 1 mM NH_4^+. RT-PCR was performed as described in Figure 2.2, normalised to TUB1 housekeeping gene. Data presented are mean 3 biological replicates (each with 3 technical replicates) (n = 9) ± SE. Lack of significance ($p<0.05$) with respect to *pYES3-DEST* controls and is denoted by 'x', and determined by Two-way ANOVA analysis.

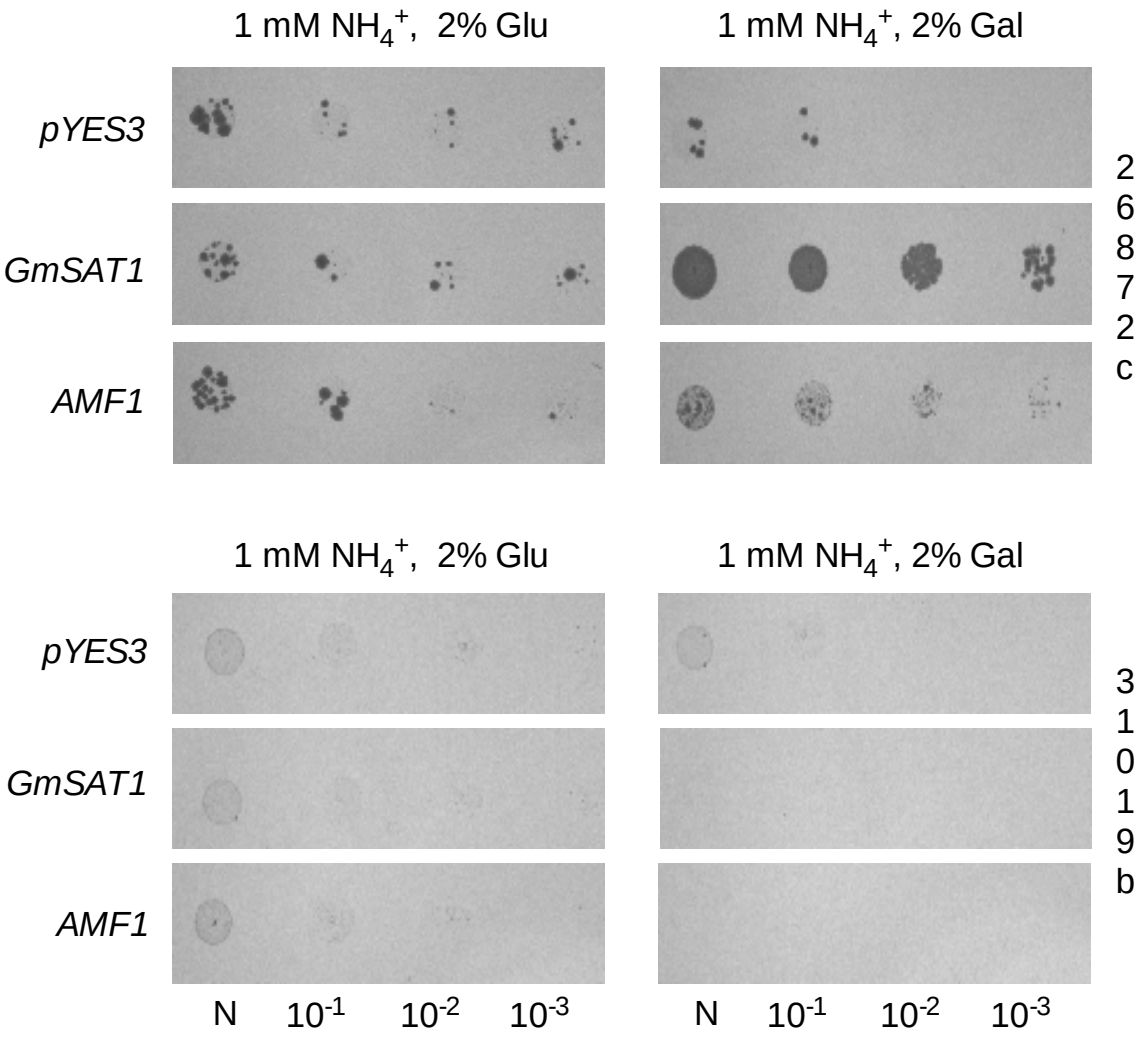

Figure 2.15: Complementation of NH_4^+ transport mutant yeast strains on NH_4^+ containing media

26972c and 31019b yeast strains were transformed with *pYES3-DEST* (control), *pYES3-GmSAT1* or *pYES3-ScAMF1*. Cells were grown to mid-log phase and then serially diluted as described in Figure 2.9. Diluted cells were spotted and spotted onto yeast minimal media (Grenson, 1966) supplemented with 2% (w/v) glucose (Glu) or 2% (w/v) galactose (Gal) and 1 mM NH_4^+. The yeast plates were incubated for 6 d at 28°C. Data presented are representative of 3 independent biological replicates.

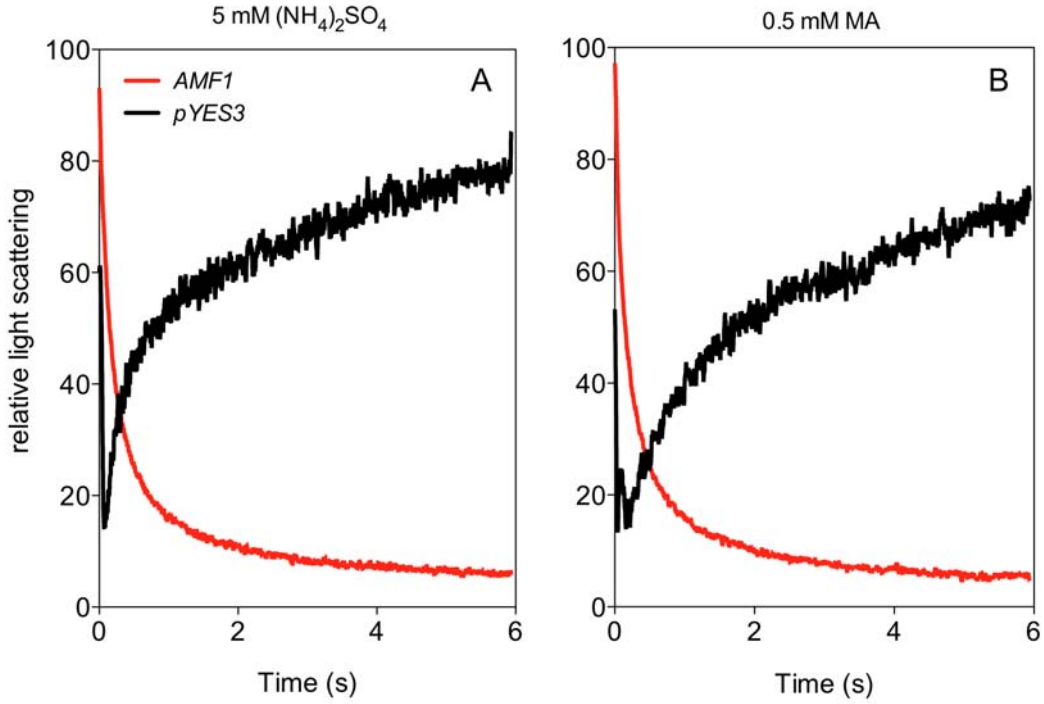

Figure 2.16: The swelling profile of 26972c spheroplasts expressing *ScAMF1* in response to NH_4^+ and MA

Spheroplasts were made from 26972c yeast cells transformed with *pYES3-ScAMF1* or *pYES3-DEST* as a control. Spheroplasts were resuspended in 0.5 M sorbitol plus 0.4 M potassium sulfate base buffer to a uniform OD_{475nm} of 1.0 and mixed with an equal volume of base buffer supplemented with (**A**) 10 mM $(NH_4)_2SO_4$ or (**B**) 1 mM MA in a fast kinetics SFM-300, Biologic instrument. Volume changes were recorded at 16°C as light scattering at an angle 90° and light wavelength of 475 nm. The swelling kinetics presented are the means of 6-9 spheroplast trace recordings each collected over a period of 6 s, which were normalised and smoothed to 21 neighbours.

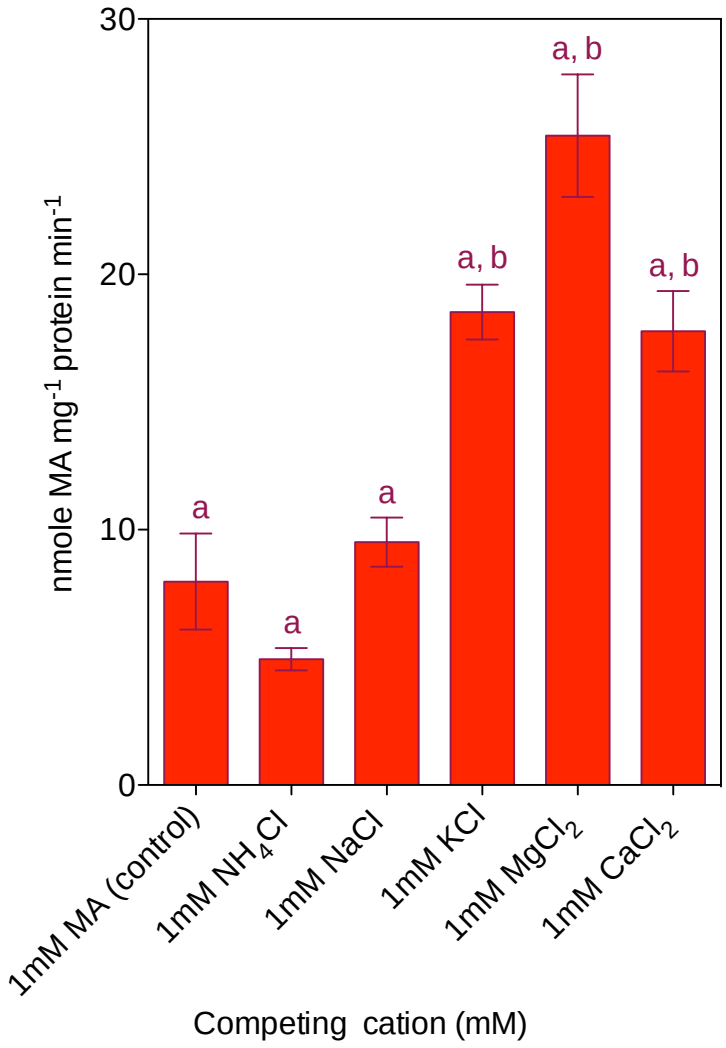

Figure 2.17: Competition of ^{14}C-MA influx into 31019b yeast over-expressing *ScAMF1* or *pYES3-DEST* vector

The uptake of 1 mM ^{14}C-MA was competed with an equimolar concentration of a chloride salt (1 mM NH_4Cl, NaCl, KCl, $CaCl_2$ or $MgCl_2$) in a 20 mM phosphate reaction buffer supplemented with 2% (w/v) galactose, pH 6.2. After 10 min of uptake, cells were collected and washed, and accumulated ^{14}C-MA was quantified by measuring the β-decay using a scintillation counter. The accumulated ^{14}C-MA was normalised against total protein extracted and specific rates were calculated by subtracting the corresponding *pYES3-DEST* control uptake rates. Data presented are the mean (n = 6) ± SE. Data are significant from the empty vector controls at 'a' and MA accumulation at 'b' ($p>0.05$).

GTTGTTGCAG**CAATTG**AAACTCTAATGATAGCTGATTAAGGACGTTGAGAACCTGCATCTTTTGGCAATCAT
TAGCTGTGTTTATTTGAAAATTCTTTCCAAGAAAGCAGATTAAGCCTAGACCTCTCTTTAGATAGGTCCCGC
TTGTTGTCCATAAGTTATTTGACGCTTGTGAAGATTCATAAGCTCTGTACAATGTTTCAATACCGATGTCTTG
ATAAAATACGGCAACATTGATTAACGCAATCGCTATCTCCTCTTCAATGAGAGCGGCGTCATTATTAGCTTC
GTACCTGTGGGTTAACAAACCCTCTGTGTATTTTAGCCACGTATCTATACATGTAATGCTGTCAGCTTTGGA
CGAGGAACTGTTCAGTGAATTTATGCAATTATTTCGCAGTATGATTAAATCATTAGGTATGGAAGTTGTTAT
TTTGCTGCTGCCAGATAATTTATAGGGAAGTTTCTTTGTAGACATTGCATTCTCACGCATGATTTATTTTGTT
AGAGCTACTTTTCACTTTAAAGTTCAACCTTTGAATAACCAGTTCTCGATTATACGTTTTTTCTTACAGCCGG
TTTACGTCAGCGCAGGAAAATTGAAAACTATACTATTCAATACATAGAACGTAACACAATGGCGTCCCCTC
AAAAGTGTACACTTCTTCAAGATGTTACTGCGGCTACATGCAACACCCCTAGAGCTATTTGTAAGGGAAGA
CAAGATCT**CAAGTG**TTACCACAGCCCGTAATTGAGTTCGGCACTATTCGAGCGCACAAAAAATCCCGTACT
GTTTTTTTTCAGATAAGAAAGACTGAGCCTATATAAACACTACCTGAACCATTTTTAAGATAAAAGTTATAT
ACGATAGAGTTATCCCCTCTTAATAATTGATCAAGAACCTCTGAAGCACAAAAGGGAGCATAAGAGCACTT
AGGGACAAACGTATTTCTTTCCCCCACTCCCCTTTTTCCCTTTGCGATGCACATCCATAACTTGTACTTGTGT
CTTGACATTCTTCAAAATCAACATGGCGATGCTCTTCTACGGTTGTCCTTTGCCACGAACTTTGTTTTGCGCC
TCCCCTCCCTTTGTCAGGCTGAGTGCAAAAGAAAAGGCCCTGGTTGCTTATCTCTGCGGACACGCGCCCCTC
TTATTGGATGAGACATCTCAGAGATTGCGATAACGATAAGATTCA**CAATTG**CTACAGACACCCTTGTGTGA
CATCTTATGGCTATGTAAGCACAGAAGAGAAGAAGAAAGAAATGACAAAGTATTGATGGAAGATGTTTTTC
CTGAAAAAAAAAAAAAAAAAAAATCGGAAAAGTGGTGTAGGCTTCTATAGCACCTTCTGCTTACCAGTCGA
TAATGCAGTTCCAGAATAAGATACTTAAAAGGTAGTTTATTTATATAGGCGCTCTTGTAACTTGTTTAGGCT
TATGATCAGAGAATTATTTTAGTAAACATAACTGCAGTACGGATTCTTATACTGTAGAAACT**ATG**

A

ATCCTAGGGGTGAAAACCATTATAATGCTACCATTGATTATGCTGTACCTTCTAACTGGCCAGAACAACTTA
CTGGGTTTGATATTGAAGTTTACATT**CAGTTG**GAAAGAGGAAATTACCGTGCAAGGAATCAAGAAACGTGA
CGTAAGGAAATCCAAGCATTATCCACAGAAGGGCAAGCTTTATATTTGTACCTCACCTTTAGATGCTTTTTC
AGTGGTGTTATTAGCTCAAGGGCCTGTTACGTTGTTGGTCCCATCCAATGACATTGTATACAAAGTTTCCAT
AAGAGAATTCATCAACTTCATCCTCGCCGGTGGGTTAGATATAAAACTCTATGGCCACGAGGTAGCAGAGC
TATCT**CAATTG**GGCAATACCGTGAATTTTATGTTTGCTGAGGGTACCTCATGTAATGGTAAAAGCGTCTTAC
CGTTTAGTATAACCGGGAAAAAACTTAAAGAATTCATAGACCCTTCAATAACCACAATGAACCCCGCAATG
GCCAAAACTAAAAAATTTGAATTGCAGACCATCCAAATCAAAACTAATAAAACTGCCATCACCACATTGCC
CATCTCCAATATGGAGTATTTATCTAGATTTCTGAACAAGGGCATTAATGTTAAATGCAAGATCAACGAGCC
ACAAGTACTCTCGGATAATTTAGAGGAATTACGCGTTGCATTAAACGGTGGCGACAAATATAAACTAGTCT
CACGGAAGTTAGATGTTGAATCTAAGAGGAATTTTGTGAAGGAATATATCAGCGATCAACGTAAAAAGAGG
AAGTAGAAATACTTATGAAGGCATGCATGCATGCATACATATTTATATATATATGTCTTTAGGAGTATGTAT
TGCATTTAATCGAAACAAACAAGAAAAAGAAGAGTAGATGTGCCCGTTTCTGTCACTCCTATTTACTGACA
CTTTCTTGACCTACCTCAAACCAGTTCCAGTTCCGGCAAAAAGTGCCGCGCGGCGGAGAAACATCTCCACCT
TATCTCGGCGCCAAATCCTTATCTCTCGTAGCTGGTTTGCCCGCGATAAGGCGGGCGAGTTATTTTGAAGTT
TTCCATAAACTGGTTTTCCATCTCGAGGTTTTTCCTCGCTTTCCACGCTATGACCCTTTTTAGTTAAGGTACC
CGATGGCATACTTTATATATTATATATATATGTTAAGTTAATATGTTTTAGCAGATTTGATATGCTGATATGC
AGCACGGACTTTCCCTCTCCTTGTCTTATCGCATCTTATCGCAACAATTTGATAGATATCTTCTCCCTTTCCT
ATCTTGTAGAATAAGGTTGTGTGCTTTGAGTCTGATAGCCGTCTTCTTTCGGTCGCTTCTTCTCTCTTTTGGTT
CTTTGATTGTCTATTACAATCAATGCAGGCTAGTTAAGGGTCCAATCACTTTTGAAATTGTTTTGTAAAAAG
CGAAGGCATTTTTTTTTTAGAAGATA**CAATTG**AAAACATATAGATTTAGAGTT**CACATG**GCTCGGGGTGAC
GGACATCTATGGACAGAGA**CATATG**ATAGTTCCAC**AGT**

B

Figure 2.18: Overview of *MEP* loci putative promoter sequences

In the predicted promoter region (1500 bp upstream) of (**A**) *MEP1* and (**B**) *MEP3* loci, putative E-box motifs (CANNTG) are present that may facilitate the binding of bHLH transcription factors highlighted blue. GmSAT1 has the sequence H-E-R at positions 5-9-13 of the basic region, which are major determinants for the recognition of CACGTG E-box variant (Atchley and Fitch, 1997),

which do not exist in the sequence upstream of the *MEP* loci. Start codons are highlighted red.

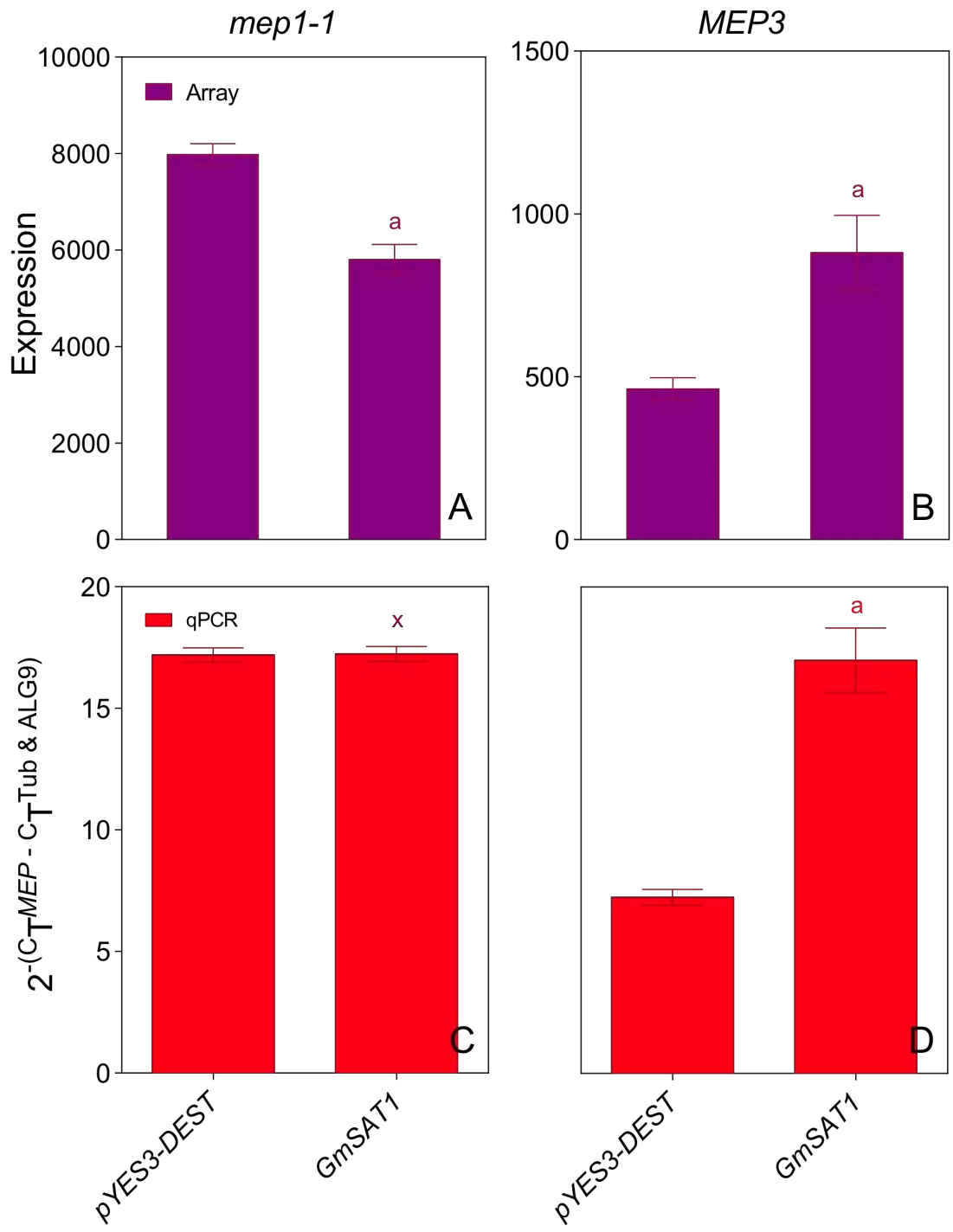

Figure 2.19: Transcriptional verification of GmSAT1 induced changes in *mep1-1* and *MEP3* expression in 26972c cells

Total RNA was extracted from 26972c transformed with *pYES3-GmSAT1* (experiment) or *pYES3-*

DEST (control) incubated for 12 h in the presence of 2% (w/v) galactose and 1 mM NH_4^+. The total RNA was converted to cDNA and processed for (**A** & **B**) Affymetrix microarray and (**C** & **D**) RT-PCR analyses as described in Figure 2.2. The Ct values obtained for 9 technical replicates were normalised to *TUB1* and *ALG9* housekeeping genes by means of the $2^{-\Delta CT}$ equation (Livak and Schmittgen, 2011). The RT-PCR data presented as mean (n = 9) ± SE. Two-way ANOVA analysis show that although there is a significant ($p>0.05$) response in the *mep1-1* response to SAT1, there is no significance ($p<0.05$) in the RT-PCR (denoted by 'x'). The response of *MEP3* is significant (denoted by 'a') in both the array and RT-PCR.

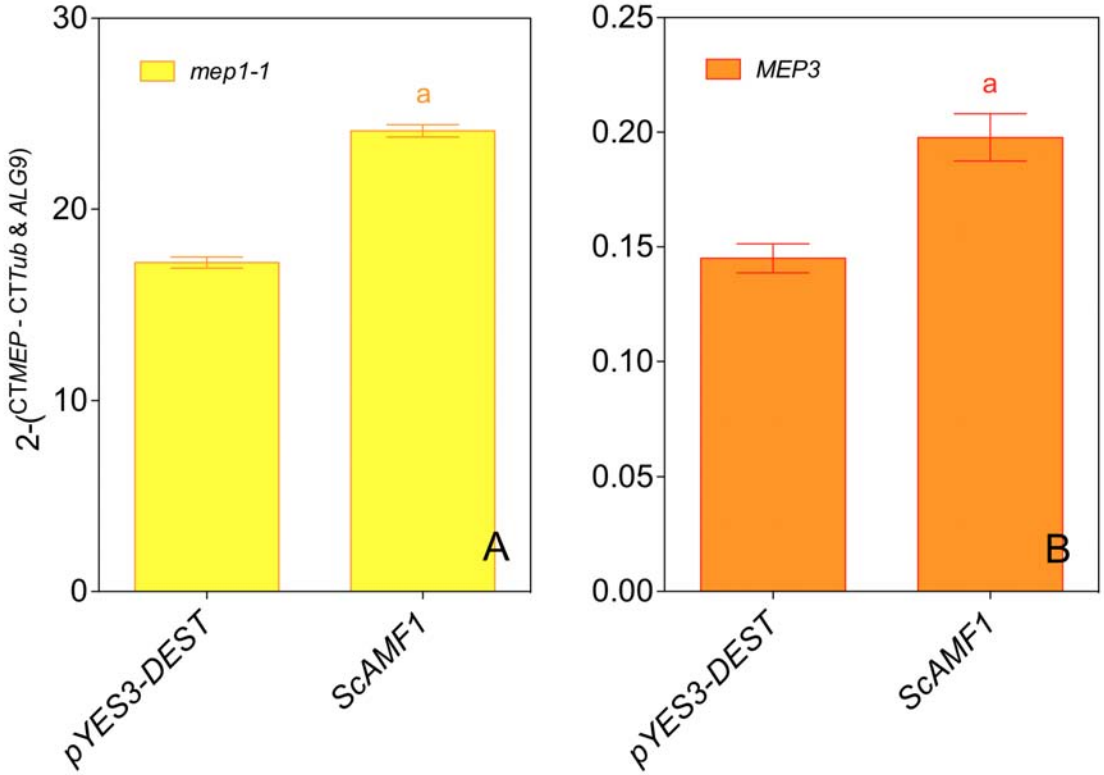

Figure 2.20: Transcriptional analysis of ScAMF1 induced changes in *mep1-1* and *MEP3* expression in 26972c cells

RT-PCR (see Figure 2.2) was performed on the same pools of cDNA as Figure 2.18. The Ct values obtained for 9 technical replicates were normalised to *TUB1* and *ALG9* housekeeping genes by means of the $2^{-\Delta CT}$ equation (Livak and Schmittgen, 2011). Data presented as the mean (n = 9) ± SE. The expression of *mep1-1* and *MEP3* were increased in cells overexpressing *ScAMF1*. Two-way ANOVA analysis shows that the *mep1-1* and *MEP3* responses to ScAMF1 were significant (denoted by 'a').

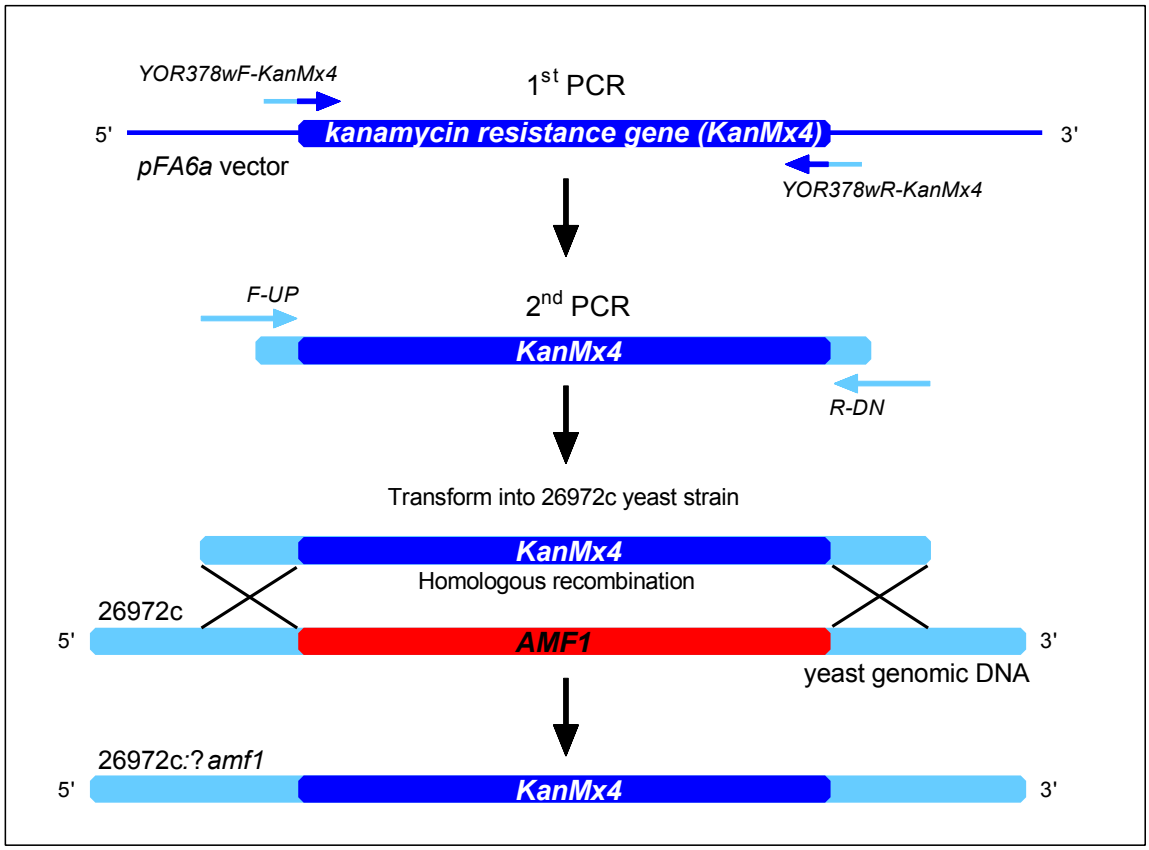

Figure 2.21: *ScAMF1* locus replacement with *kanMX4*

The *kanMX4* sequence was cloned from the *pFA6a* plasmid (Wach et al., 1994) with primers designed to create a product with flanking regions homologous to the yeast genome upstream and downstream of the *ScAMF1* locus. The flanking sequences were extended in a subsequent PCR. The *kanMX4* was introduced into the yeast genome by homologous recombination, replacing the *ScAMF1* locus.

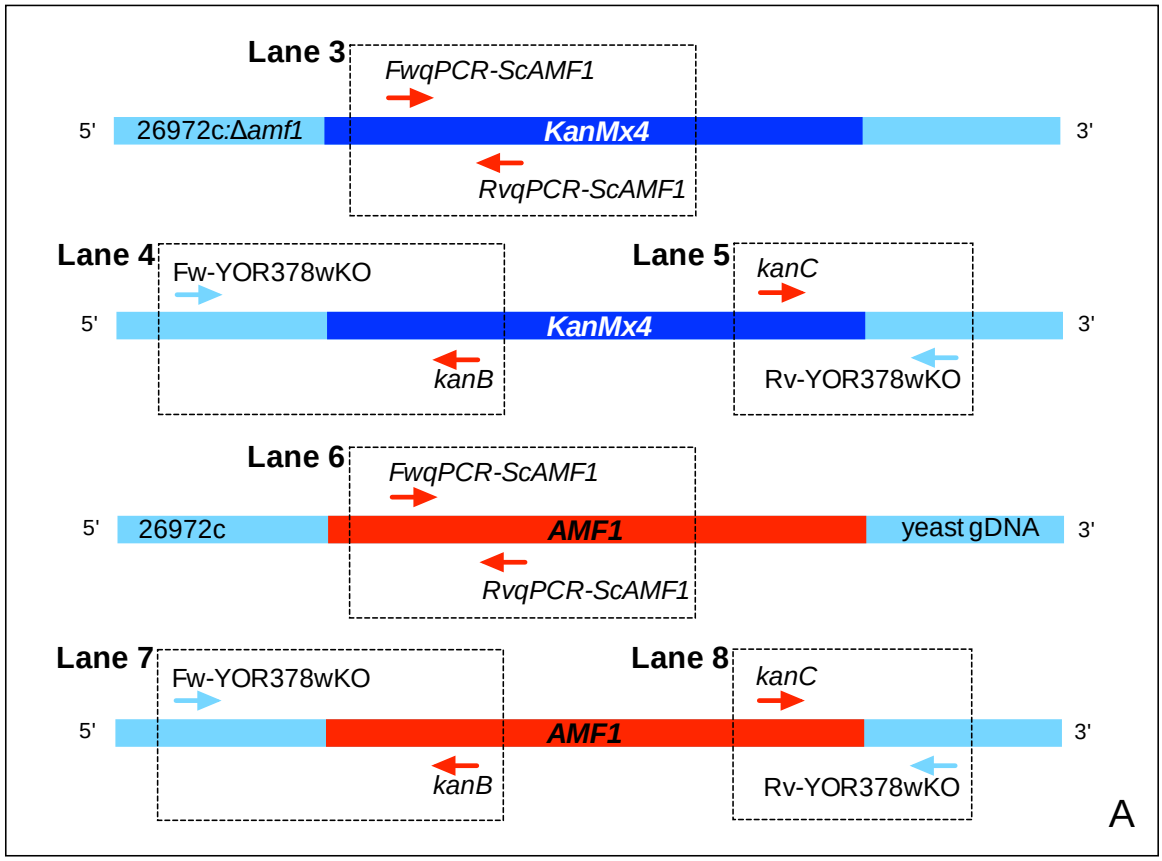
Lane 3
FwqPCR-ScAMF1
5'
26972c:Δamf1
KanMx4
3'
RvqPCR-ScAMF1
Lane 4
Fw-YOR378wKO
Lane 5
kanC
5'
KanMx4
3'
kanB
Rv-YOR378wKO
Lane 6
FwqPCR-ScAMF1
5'
26972c
AMF1
yeast gDNA
3'
RvqPCR-ScAMF1
Lane 7
Fw-YOR378wKO
Lane 8
kanC
5'
AMF1
3'
kanB
Rv-YOR378wKO
A

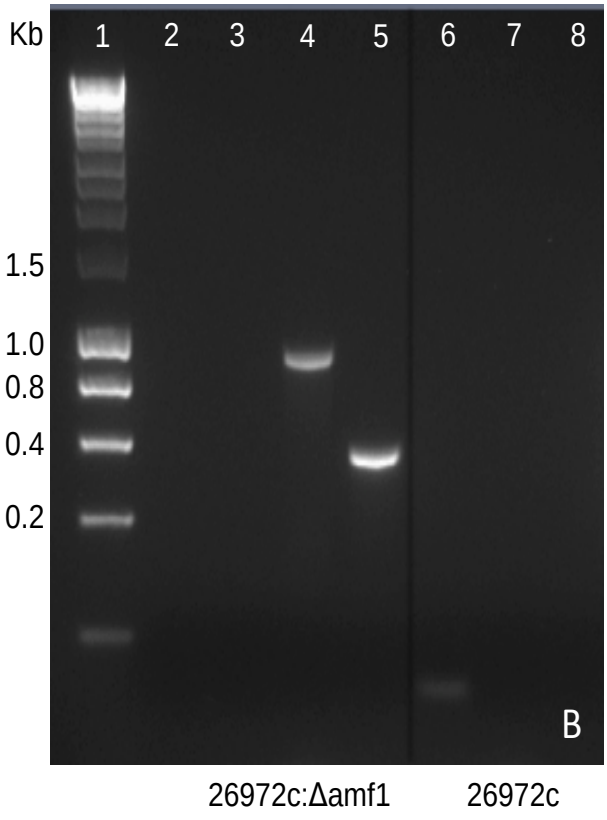
Kb
1
2
3
4
5
6
7
8
1.5
1.0
0.8
0.4
0.2
B
26972c:Δamf1
26972c

Figure 2.22: PCR verification of *ScAMF1* locus replacement with *kanMX4*

(**A**) Replacement of the *ScAMF1* locus with *kanMX4* was confirmed by the amplification of *kanMX4* segments in conjunction with primers homologous to the *kanMX4* locus and genomic sequences flanking the *ScAMF1* locus (listed in Table 2.1). (**B**) Gel electrophoresis of PCR verification. Lane 3 - 5 presents the PCR amplification with 26972c:Δ*amf1* genomic DNA template, while lanes 6 - 8 presents the complementary 26972c PCR amplification. In Lane 1: 5 µl *HyperLadder I* (Bioline, USA), lanes 3 & 6: FwqPCRAMF1 and RvqPCRAMF1 (~100bp), lane 4 & 7: Fw-YOR378wKO and kanB (~1000 bp), and lane 5 & 8: Rv-YOR378wKO and kanC (~350 bp). The absence of the *AMF1* locus is verified by the absence of *AMF1* product in lane 3 and the presence of *KanMx4* products in lanes 4 and 5, respectively.

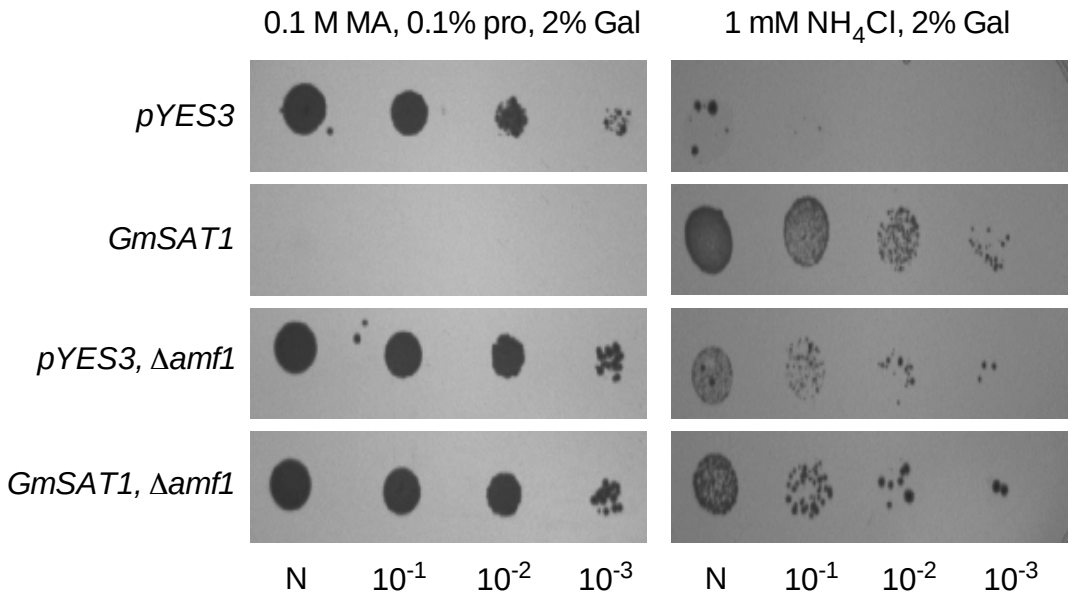

Figure 2.23: Growth analysis of 26972c yeast with or without the *ScAMF1* locus

26972c and 26972c:Δ*amf1* knock-out yeast strains were transformed with *pYES3-DEST* or *pYES3-GmSAT1*. Cells were grown to mid-log phase and then serially diluted as described in Figure 2.9. Diluted cells were spotted onto yeast minimal media (Grenson, 1966) supplemented with 0.1% (w/v) L-proline (pro) and 2% (w/v) glucose (Glu) or galactose (Gal) with 0.1 M MA or 1 mM NH_4Cl where indicated. The yeast plates were incubated for 6 d at 28°C.

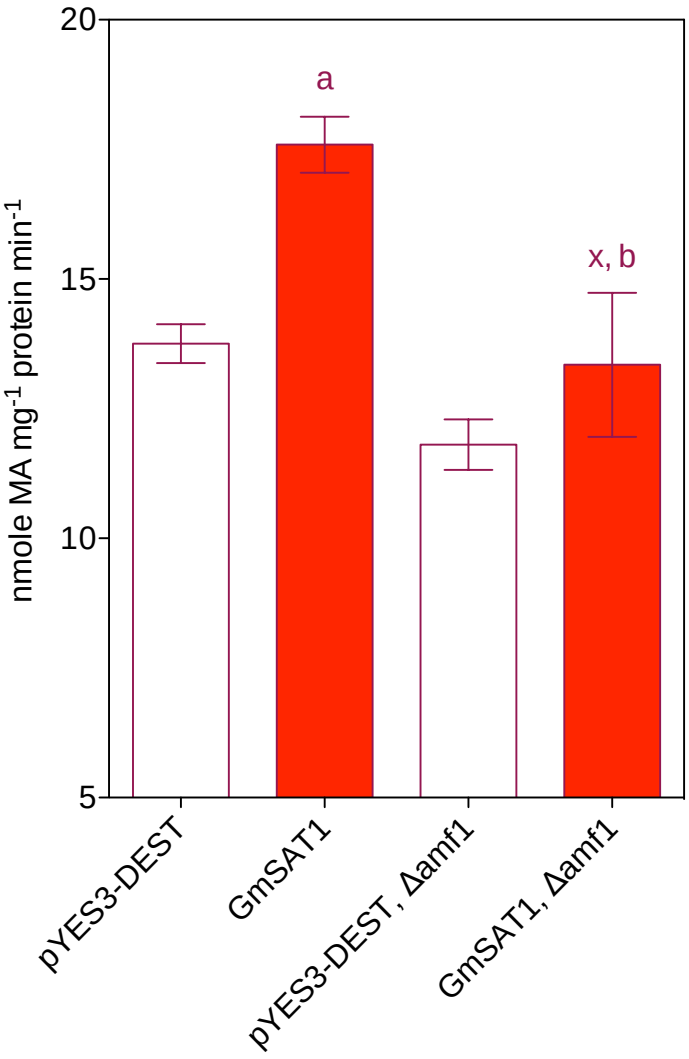

Figure 2.24: Growth analysis of 26972c yeast with or without the *ScAMF1* locus

Yeast cultures were grown for 16 h using liquid yeast minimal media without uracil (Grenson, 1966) supplemented with 2% (w/v) galactose and 1 mM NH_4^+. Uptake of ^{14}C-MA was performed over a 5-min period and normalised against total cellular protein. Accumulated ^{14}C-MA was quantified by measuring the β-decay using a scintillation counter. Data presented as mean (n = 3) rate of MA uptake ± SE. Significance ($p>0.05$) with respect to ^{14}C-MA uptake rate of corresponding *pYES3-DEST* controls determined by Two-way ANOVA analysis is denoted by 'a', whilst lack of significance ($p<0.05$) is denoted by 'x', and significance with respect to GmSAT1 response is denoted by 'b'.

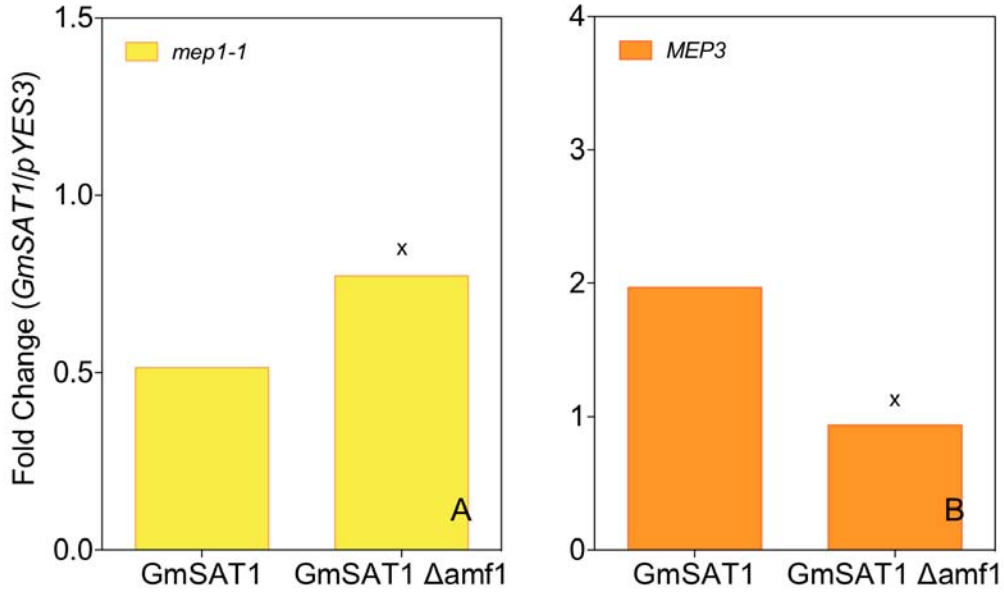

Figure 2.25: Relationship between GmSAT1 and ScAMF1 on *mep1-1* and *MEP3* gene expression

Total RNA was extracted from 26972c (control) and 26972c:Δ*amf1* yeast transformed with either *pYES3-DEST* or *pYES3-GmSAT1* after 12 h induction in the presence of 2% (w/v) galactose and 1 mM NH_4^+. RT-PCR was performed described in Figure 2.2. The Ct values obtained for 3 technical replicates were normalised to *TUB1* housekeeping gene by means of the $2^{-\Delta CT}$ equation (Livak and Schmittgen, 2011), and a fold-change (n = 3) was calculated with respect to *pYES3-DEST* controls. MEP transcription with respect to GmSAT1-fold change in Δ*amf1* background is not significant ($p<0.05$) as determined by Two-way ANOVA analysis is denoted by 'a', whilst lack of significance ($p<0.05$) is denoted by 'x'.

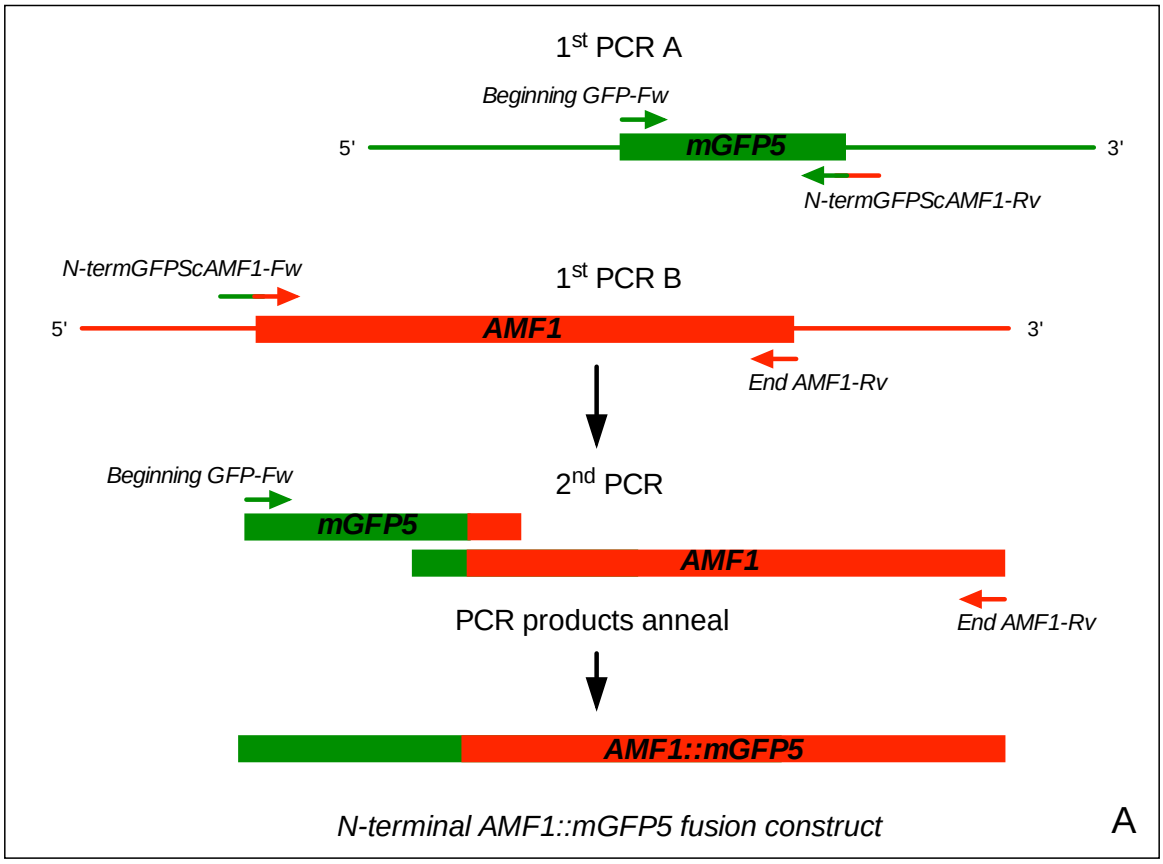
1st PCR A
Beginning GFP-Fw
5'
mGFP5
3'
N-termGFPScAMF1-Rv
N-termGFPScAMF1-Fw
1st PCR B
5'
AMF1
3'
End AMF1-Rv
Beginning GFP-Fw
2nd PCR
mGFP5
AMF1
PCR products anneal
End AMF1-Rv
AMF1::mGFP5
N-terminal AMF1::mGFP5 fusion construct
A

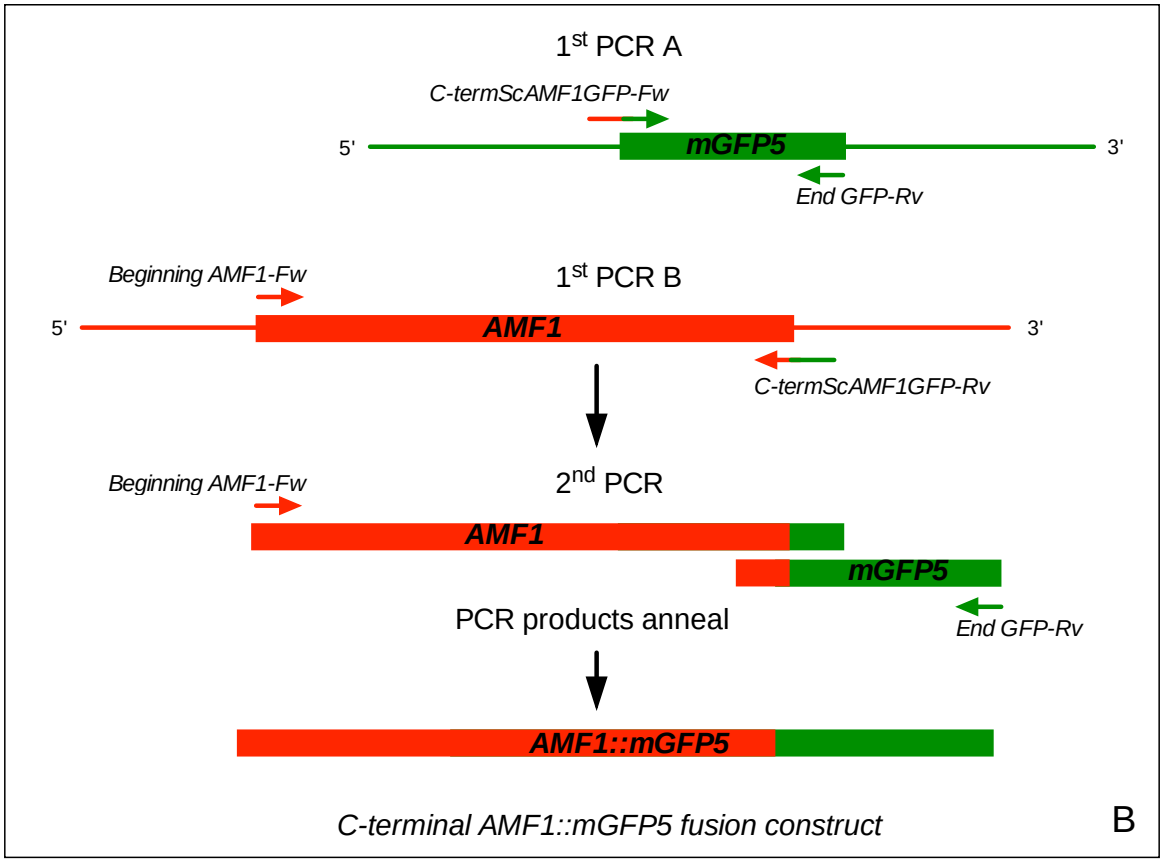
1st PCR A
C-termScAMF1GFP-Fw
5'
mGFP5
3'
End GFP-Rv
Beginning AMF1-Fw
1st PCR B
5'
AMF1
3'
C-termScAMF1GFP-Rv
Beginning AMF1-Fw
2nd PCR
AMF1
mGFP5
PCR products anneal
End GFP-Rv
AMF1::mGFP5
C-terminal AMF1::mGFP5 fusion construct
B

Figure 2.26: Synthesis of ScAMF1 fused with GFP constructs

The ScAMF1 protein was tagged (**A**) N-terminally or (**B**) C-terminally with Green Fluorescent Protein (GFP) by means of a 2-step PCR based strategy. The *mGFP5* and *ScAMF1* sequences were amplified in separate reactions with primers designed to create overlapping sequences (44 nucleotides in length) to assist in annealing in a subsequent PCR. Stop codons were omitted from the design of the primers to amplify *mGFP5* and *AMF1* for the N-terminal and C-terminal fusions, respectively. The initial PCR products were combined in a second PCR with High Fidelity (HIFI) 5 Prime PCR Extender DNA polymerase (5 Prime, USA), which added 3' adenine overhangs to the final PCR product, required for the subsequent Gateway© (Invitrogen) cloning into the *pYES3-DEST* vector (Figure 2.1).

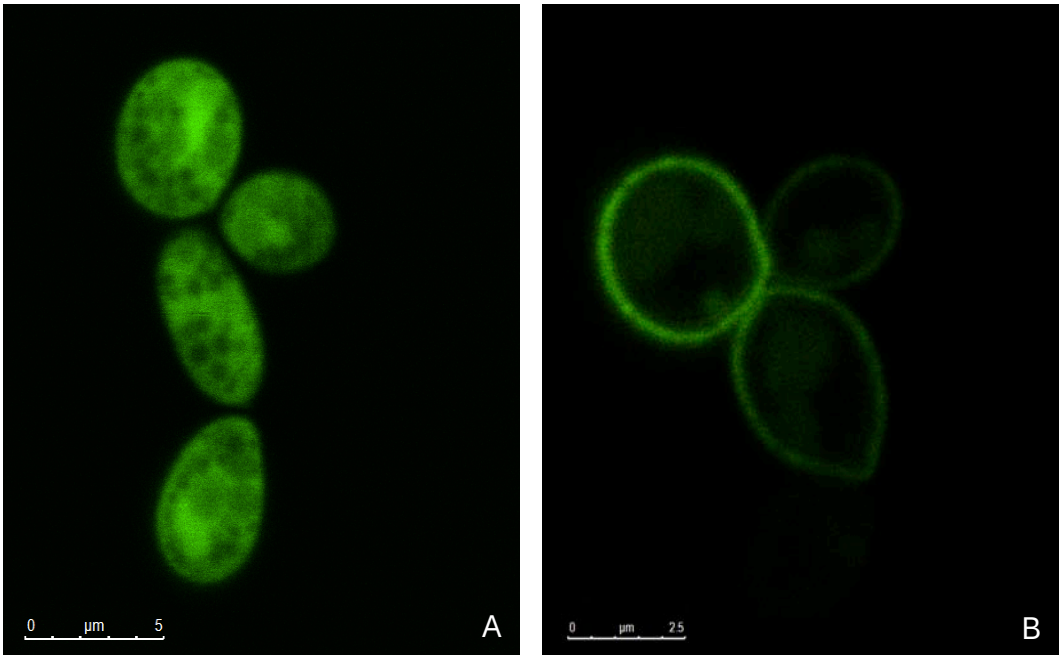

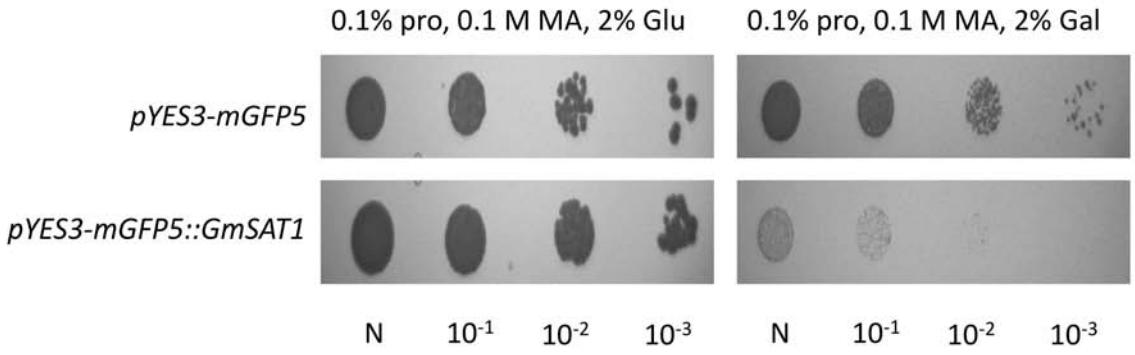

C

Figure 2.27: Localisation of mGFP5 alone or fused to the N-terminus of ScAMF1 in yeast cells

26972c cells were transformed with (**A**) *pYES3*-m*GFP5* or (**B**) *pYES3-mGFP5::ScAMF1*. Expression of *mGFP5* or *mGFP5::ScAMF1* was induced for 16 h in the presence of 2% (w/v) galactose and 0.1% (w/v) L-proline in Difco-YNB with tryptone, histidine and leucine. mGFP5 was detected using an excitation 488nm argon laser, and light emission detected at 505-503 nm, with a LSM 5 Pascal Laser Scanning microscope (Zeiss, Oberkochen, Germany). (**C**) To provide a

indication of correct protein targeting, 26972c cells harbouring *pYES3-mGFP5* or *pYES3-mGFP5::ScAMF1* were grown to mid-log phase and then serially diluted as described in Figure 2.9. Diluted cells were spotted onto yeast minimal media (Grenson, 1966) supplemented with 0.1% (w/v) L-proline (pro), 0.1 M MA and 2% (w/v) glucose (Glu) or galactose (Gal). The yeast plates were incubated for 6 d at 28°C.

Table 2.1: List of primers used in Chapter 2.

All primers were ordered from GeneWorks (Adelaide, South Australia).

Primer Name	Final primer sequence (5'-3')
FwScAMF1seq	ATGTCAACTAGCTCCTCCGTAA
RvScAMF1seq	TTCTATAAAATGCTGCTTTTCG
FWqPCR-ScAMF1	TGTGCTCTGCCCAAC TAATG
RVqPCR-ScAMF1	GCGGAAGCAAACCAACTAAG
FwqPCR-MEP1	GCGATGCTCTTCTACGGTTGTC
RvqPCR-MEP1	CGTGTCCGCAGAGATAAGCAAC
FwqPCR-MEP3	GGTGGTTGGTTGACGCATAAC
FwqPCR-MEP3	CGGCTTCCTCAGTGACTCTTAG
FWqPCR-ScTUB1	AGGAGGACGCGGCTAATAAT
RVqPCR-ScTUB1	AACCCATCACATTGGTCTGC
YOR378wF-KanMx4	GAACATAAAATCAATATGCGTACGCTGCAGGTCGAC
YOR378wR-KanMx4	CTCTATATATGAACTTAATCGATGAATTCGAGCTCG
F-UP	TACATTCATCAATTGCTGGAACATAAAGAACATAAAATCAATATG
R-DN	TTGGGTTATATACCACGATGAAGTATTTCTCTATATATGAACTTA
Fw-YOR378wKO	GGGTTGTCGCTACGAATGTT
kanB	CTGCAGCGAGGAGCCGTAAT
Rv-YOR378wKO	TTTCGGACTCTTTGTCGCTT
kanC	TGATTTTGATGACGAGCGTAAT
Beginning GFP-Fw	ATGGTAGATCTGACTAGTAAAG
C-termScAMF1GFP-Fw	CAGCATTTTATAGAAATGGTAGATCTGACT
C-termScAMF1GFP-Rv	AGTCAGATCTACCATTTCTATAAAATGCTG
N-termScAMF1GFP-Fw	GAACTATACAAAGCTATGTCAACTAGCTCC
N-termScAMF1GFP-Rv	GGAGCTAGTTGACATAGCTTTGTATAGTTC
End GFP-Rv	AGCTTTGTATAGTTCATCCATG
GmSAT1 pMAL F	CATATGCCTAAAATTGACAACAATGCTCTTG
GmSAT1 pMAL R	GATCCTTATCTTGCTTCAATTTCAGGTAGTG
pMAL Forward Seq	GGTCGTCAGACTGTCGA TGAAGCC
pMAL Reverse Seq	TGTCCT ACTCAGGAGAGCGTTCAC
YOR378w Promoter 3F	GGGTTGTCGCTACGAATGTT
YOR378W Promoter 1R	ATTGATTTTATGTTCTTTATGTTCCAG
T7 Fw	TAATACGACTCACTATAGGG
M13 Fw	TGTAAAACGACGGCCAGT
Cyc1 Rv	GCGTGAATGTAAGCGTGAC
GW1	GTTGCAACAAATTGATGAGCAATGC
GW2	GTTGCAACAAATTGATGAGCAATTA

2.4 Discussion

The genetic identity of the soybean SM transporter facilitating the movement of bacterially fixed N_2 (NH_4^+) from the symbiosome to the cytosol of the host legume has not been identified. However, a soybean SM associated bHLH TF, GmSAT1, is purported to be essential in the poorly understood cellular signalling mechanism that regulates nodulation in soybean. Mutant yeast strains with defective NH_4^+ transport systems, which were originally used to isolate GmSAT1, have been made use of in this thesis for the search for analogous mechanisms regulated by GmSAT1 activity. Here, it was reasoned that the genetic events regulated by GmSAT1 in yeast might reflect aspects of events occurring in soybean.

2.4.1 Transcriptional studies of GmSAT1 activity in yeast has lead to the identification of a new class of NH_4^+ transport protein

Yeast expression systems have proved to be an invaluable tool for the discovery of homologous and heterologous genes encoding novel transport proteins. Functional complementation of disrupted transport systems and toxicity assays are common yeast screening techniques to isolate and assess the function of putative transport proteins. P. Loughlin (2007) and D. Chiasson (2012) demonstrated that GmSAT1 is a bonafide TF by localisation, selective mutagenesis and *in vitro* DNA binding assays. The studies indicate that GmSAT1 is sequestered in the yeast PM by a C-terminal transmembrane anchor and cleaved upon an unidentified signal, releasing the N-terminal portion of the protein containing the bHLH DNA binding domain. The truncated GmSAT1 was then shown to be

transported into the nucleus where it bound to the promoter region of *ScAMF1*. Using both microarray and quantitative RT-PCR experiments, the data clearly show that GmSAT1 elevates the expression of *ScAMF1*. ScAMF1 was of particular interest as a number of topology programs have predicted that ScAMF1 has 14-transmembrane spanning domains and is most likely a membrane-localised protein, belonging to the DHA2 drug efflux subfamily of MF proteins. The direct transcriptional relationship between GmSAT1 and *ScAMF1* is also supported by experiments where substitutions introduced within the DNA binding region of the GmSAT1 bHLH motif compromised the MA sensitivity phenotype (P. Loughlin, 2007) and caused a reduction in *ScAMF1* expression.

2.4.2 The Major Facilitator Superfamily

Major Facilitator (MF) proteins are present in all domains of life, acting as secondary active transporters (Pao et al., 1998), and are conserved amongst yeast species, including *Ashbya gossypii*, *Candida glabrata*, *Kluyveromyces lactis*, *Kluyveromyces waltii* and *S. cerevisiae* (Gbelska et al., 2006). In yeast, DHA2 proteins have been implicated in ion homeostasis (Pao et al., 1988), while seven members are yet to be characterised (Sa-Correia et al., 2009). ScAMF1 shows limited sequence similarity to ATR1 (38.7% residue identity) and ATR2 (36.5% residue identity) involved in yeast boron efflux and tolerance, respectively, but is not involved in either pathway (Kaya et al., 2009; Bozdag et al., 2011). Enhanced expression in response to GmSAT1 activity combined with the mGFP5 fusion experiments, which localised ScAMF1 to the yeast PM, gave weight to the postulation that ScAMF1 is the previous unidentified MA/NH_4^+ transporter targeted by GmSAT1 in yeast.

2.4.3 ScAMF1 mediates the low-affinity transport of MA

Prior to this study, the most characterised proteins involved in NH_4^+ transport in plants have been members of the high-affinity MEP/AMT/Rh superfamily. The NH_4^+ transport capabilities of ScAMF1 were investigated using a number of yeast-based approaches, which included growth studies on media supplemented with NH_4^+ and MA, ^{14}C-labelled MA flux analyses and swelling assays of yeast spheroplasts in the presence of these cations. Here, it was shown that ScAMF1 activity in yeast is capable of mediating the low-affinity transport of MA, an analogous NH_4^+ compound. MA is routinely used in the characterisation of NH_4^+ transporters and therefore can be used to correlate ScAMF1 activity with NH_4^+ transport. Reverse genetics showed that *ScAMF1* is targeted by GmSAT1 to instate enhanced MA accumulation and MA sensitivity. Physical loss of the *ScAMF1* allele from the yeast genome eliminated GmSAT1 induced MA transport and sensitivity phenotype in 26972c cells.

2.4.4 ScAMF1 mediates the low-affinity transport of NH_4^+

Many high-affinity NH_4^+ transporters, including MEP and AMT proteins, are capable of rescuing the growth of the 26972c yeast strain on low (1 mM) NH_4^+. ScAMF1 behaved differently, presenting partial or no complementation of 26972c growth on low NH_4^+. This may indicate ScAMF1's capacity to take up NH_4^+ at low concentrations is not sufficient relative to high-affinity NH_4^+ transport proteins. Disruption of *ScAMF1* in the 26972c genome also partially reduced the ability of GmSAT1 to complement the NH_4^+ transport system. Additionally, NH_4^+ transport of 31019b was not restored by the overexpression of *ScAMF1*. Together, the growth analyses suggest ScAMF1 might be involved in NH_4^+ transport but is not the sole means by which GmSAT1 establishes NH_4^+ transport in yeast. This also suggests that ScAMF1 has an activity more suited to higher NH_4^+ concentrations.

In yeast, native low-affinity NH_4^+ transporters may operate at high external NH_4^+ concentrations potentially masking ScAMF1 mediated NH_4^+ transport. However, as the genetic identity of low-affinity NH_4^+ transport in yeast is unknown, mutant yeast strains cannot be created to assess the activity of ScAMF1 at higher NH_4^+ concentrations. *X. laevis* oocytes offer an alternative simple expression system for exploring the extent of ScAMF1 NH_4^+/MA transport properties, pairing chemical and electrical analyses to support putative movement of NH_4^+, where currents can be defined and differentiated from endogenous transport systems (Sobczak et al., 2010; Grewer et al., 2013).

2.4.3 GmSAT1 influences the MEP system to complement NH_4^+ transport in yeast by an unidentified mechanism

To help explain how GmSAT1 complemented 26972c, I tested its influence on *mep1-1* or *MEP3* expression. Here, GmSAT1 activity in 26972c was shown to lead to a modest but significant increase in *MEP3* transcripts, while *mep1-1* transcripts remained unchanged relative to the empty vector controls. This result supports a previous finding that elevated expression of *MEP3* or elimination of *mep1-1* inhibition (*mep1-1*Δ) can restore MEP3 activity (i.e. NH_4^+ complementation) in 26972c (Marini et al., 2000b). However, since the putative promoter region of *MEP3* does not present E-box motifs capable of binding GmSAT1, the enhanced expression by GmSAT1 may be indirect. The GmSAT1 bHLH domain may mediate heterodimerisation with native yeast bHLH TFs, which could recognise the other E-box motifs regulate *MEP3* expression. My data show that overexpression of *ScAMF1* does enhance NH_4^+ permeability across the yeast PM, a phenotype that may ultimately account for the *MEP* expression response. Interestingly, data show that overexpression of *ScAMF1* results in a modest but significant increase in both *mep1-1* and *MEP3* expression although significantly less than observed in the

presence of GmSAT1 activity. This relationship between the high-affinity MEP and low-affinity ScAMF1 NH_4^+ transport pathways in yeast remains to be determined. However, it is possible that changes in *mep1-1* and/or *MEP3* expression may also result from a nutrient based-signal as *MEP1* expression has previously been shown to be negatively regulated by increasing concentrations of external NH_4^+ and reduced N compounds (Marini et al., 1994).

2.4.4 ScAMF1 may facilitate the transport of multiple substrates

Thus far, preliminary data suggests that ScAMF1 is a putative MA/NH_4^+ transport protein. In plants, low-affinity NH_4^+ transport has been implicated in non-selective cation fluxes (Tyerman et al., 1995; Demidchik, 2002a). As MF proteins mediate the movement of a diverse range of substrates, it is feasible to hypothesise that ScAMF1 may also be capable of mediating the movement of multiple substrates differing in specificity, particularly if it is operating as a non-selective cation channel. Indeed, Na^+ reduced ScAMF1 mediated ^{14}C-MA transport into yeast cells, while K^+, Ca^{2+} or Mg^{2+} increased ^{14}C-MA uptake. ScAMF1 mediated uptake of ^{14}C-MA is unchanged by NH_4^+. It is unclear why Ca^{2+} or Mg^{2+} influenced ScAMF1 activity but it may signal a form of regulatory control. It is now possible to conclude that ScAMF1 activity account or at least contribute to the apparent non-selective cation current detected by Kaiser et al., (1998) in yeast spheroplasts expressing *GmSAT1*. GmSAT1 was found to influence the activity of a number of metabolic and transport pathways (D. Mazurkiewicz, 2008), which may account for the differences between ScAMF1 mediated ^{14}C-MA uptake and the results obtained by Kaiser et al., (1998). In future experiments, a range of competing cation concentrations should also be investigated to gain a better understanding of ScAMF1 transport. It also is a possibility that ScAMF1 fortuitously or opportunistically mediates the transport of

NH_4^+/MA and a possible range of ions and compounds as a result of its enhanced expression by GmSAT1. In yeast, ScAMF1 might have a role in N detoxification, mediating the efflux of NH_4^+ from the yeast cells as a result of enhanced NH_4^+ uptake. Interestingly, ScAMF1 also shares significant homology with the vertebrate SPINSTER-like proteins (SPIN1) predicted to be involved in sugar transport (Figure 4.4; Rong et al., 2011). ScAMF1 is a MF protein, and therefore may operate as a co-transporter or exchanger. ScAMF1 mediated MA sensitivity was enhanced with increase in pH, suggestive of H^+ co-transport. However, the nature of ScAMF1 remains unclear, requiring further experiments to investigate the nature of ScAMF1.

2.4.5 Homologs of ScAMF1 exists in soybean.

I hypothesised that GmSAT1 activity in yeast may be reminiscent of its native function *in planta*. However, the global genetic events influenced by *GmSAT1* induction in yeast, may or may not reflect the genetic events in soybean as GmSAT1 could bind opportunistically to native yeast E-box motifs. The interactions of GmSAT1 with DNA remain to be explored in soybean. Sequence comparison was employed in an effort to identify soybean AMF1 homologs with the aim of isolating the endogenous transcriptional targets of GmSAT1 (D. Chiasson, 2012). A soybean protein predicted to share homology with ScAMF1 was identified and labelled GmAMF1;3. The soybean homolog is expressed in N_2-fixing legume root nodules (D. Chiasson, 2012). Homologs of AMF1 have also been identified in *Arabidopsis thaliana* but have yet to be functionally characterised.

Chapter 3 Functional analysis of ScAMF1 in the *Xenopus laevis* oocyte expression system

3.1 Introduction

3.1.1 Heterologous expression of transmembrane transport proteins in the *Xenopus laevis* oocyte expression system

Xenopus laevis oocytes offer an excellent opportunity to study the functional activities of exogenous transport proteins in a simple system with relatively quiet native currents that is unavailable in many other expression systems (Sobczak et al., 2010; Grewer et al., 2013). Electrophysiology studies using *X. laevis* oocytes have defined the molecular selectivity and affinity for numerous membrane transport systems derived from animal or plant tissues, including active and passive transporters, receptors and a whole plethora of other membrane proteins, providing an invaluable insight into the specific roles that may exist in vivo. Injected 5' capped RNA (cRNA) is translated by endogenous protein synthesis machinery, and the processed mature protein is effectively targeted to the oocyte PM (Gurdon et al., 1971).

3.1.2 Electrical signatures of GmSAT1 activated NH_4^+ channel(s) in yeast

Previously, patch-clamp analysis has been useful in assessing the electrical signatures of GmSAT1-activated transport pathways in 26972c spheroplasts. Spheroplasts expressing *GmSAT1* exhibited electrochemical properties characteristic of a non-selective channel(s) (Kaiser et al., 1998). GmSAT1-activated channel(s) were previously shown to be permeable to Na^+ and K^+. However, in the previous Chapter (Figure 2.17) K^+ increased ^{14}C-MA uptake and Na^+ had no effect. Currents were regulated by divalent cations, Mg^{2+} and Ca^{2+}, dictating the unidirectional transport of NH_4^+ (Kaiser et al., 1998). Cation transport kinetics were comparable to the NH_4^+ channel previously detected in the SM of soybean, *Lotus japonicus* (lotus) and *Pisum sativum* (pea) (Tyerman et al., 1995; Mouritzen and Rosendahl, 1997; Kaiser et al., 1998; Roberts and Tyerman, 2002).

3.1.3 Detection of NH_4^+ channel activity in legume SM

Although the genetic identity of the soybean symbiotic NH_4^+ transport protein remains to be determined, patch-clamp analysis of soybean symbiosomes detected a voltage-gated channel selectively permeable to NH_4^+ (K_M 37.50 mM) (Tyerman et al., 1995; Obermeyer and Tyerman, 2005). The channel was also found to possess non-selective properties, although more permeable to NH_4^+ at the apparent K_M of the channel (Tyerman et al., 1995). The presence of divalent cations, Mg^{2+} and Ca^{2+}, regulates the transport of NH_4^+ across the symbiosome membrane to the host cytosol (Whitehead et al., 1998). The presence of a similar current was detected in the symbiosome membrane of *Lotus japonicus* and *Pisum sativum* (pea) (Mouritzen and Rosendahl, 1997; Roberts and Tyerman, 2002). Homologs of ScAMF1 have been identified in most sequenced dicots (D. Chiasson, 2012). In soybean nodules, GmSAT1 may have a role in regulating a protein

similar to ScAMF1, which might be the elusive symbiotic NH_4^+ channel or operate in other unidentified low-affinity NH_4^+ transport systems.

3.1.4 ScAMF1 activity and GmSAT1 regulated NH_4^+ transport

The functional characterisation presented in this thesis indicates that ScAMF1 is responsible for the involvement of GmSAT1 in both MA uptake and MA sensitivity in NH_4^+ transport defective yeast strain. While it is apparent that MEP proteins are required for growth on low NH_4^+ (Marini et al., 1997), the mechanism(s) by which GmSAT1 complements NH_4^+ transport is less clear. GmSAT1 might indirectly enhance NH_4^+ permeability in yeast through regulation of ScAMF1, which may ultimately influence *mep1-1* expression and its possible negative interactions with MEP3. Changes in *mep1-1* and/or *MEP3* expression may also result from ScAMF1 activity influencing intracellular N homeostasis.

Unlike high-affinity MEP/AMT/Rh proteins, ScAMF1 demonstrated limited ability to restore growth of 26972c or 31019b cells on low NH_4^+, suggestive of activity more suited to higher NH_4^+ concentration ranges. As endogenous low-affinity NH_4^+ systems may be activated, the characterisation of putative ScAMF1 low-affinity NH_4^+ transport in yeast was difficult. The *X. la*evis oocyte is an appropriate alternative expression system to study the low-affinity NH_4^+ transport properties of ScAMF1 as heterologously NH_4^+-stimulated currents can be assessed at concentrations up to 5 mM NH_4^+ before native currents are induced (Burckhardt and Burckhardt, 1997). *X. laevis* oocytes have been used to characterise NH_4^+ transport properties of Rhesus glycoproteins (Bakouh et al., 2004; Nakhoul et al., 2004), AMT proteins (Ludwig et al., 2002; Ludwig et al., 2003) and aquaporins (Holm et al., 2005).

3.1.5 Multi-drug efflux proteins and NH_4^+ transport in yeast

ScAMF1 is designated as a drug:H^+ antiporter belonging to the DHA2 subfamily of the MF proteins that comprise the multi-drug efflux mechanism, which operates in most organisms, conferring resistance to a diverse range of structurally and functionally distinct cytotoxic substrates (Pao et al., 1998; Gbelska et al., 2006). In addition to physiological specific substrates, such proteins are thought to fortuitously or opportunistically mediate the transport of a range of ions. In yeast, MF proteins have been directly or indirectly implicated in influencing intracellular homeostasis and metabolism. Under NH_4^+ limitation, *ScQDR2* encoding a drug-efflux protein is upregulated and implicated in K^+ influx independent of major K^+ transport pathways, and amino acid homeostasis (Vargas et al., 2007). Overexpression of *ScAQR1*, an orthologous DHA2 protein, enhanced excretion of amino acids that may be deleterious to cell physiology in parallel with elevated amino acid permease activity, apparently in response to NH_4^+ toxicity (Hess et al., 2006). Homology suggests ScAQR1 couples K^+ uptake with the export of surplus amino acids (Velasco et al., 2004).

Described in this chapter is Two-Electrode Voltage Clamping (TEVC) analysis of ScAMF1 activity in *X. laevis* oocytes, which was employed to substantiate its NH_4^+ transport capacity in a heterologous system. Electrophysiological analysis of ScAMF1 activity in oocytes has the potential to shine light on the likely roles of related plant proteins. The results presented in this chapter strongly suggest that ScAMF1 facilitates the low-affinity influx of NH_4^+ into *X. laevis* oocytes, an activity, which may be linked to P metabolism. The electrophysical data collected also indicates that ScAMF1 possesses transport properties reminiscent of non-selective cation channels, providing preliminary data suggestive of Na^+ and K^+ transport capabilities.

3.2 Methods and Materials

3.2.1 Cloning of *ScAMF1* into *X. laevis* oocyte expression vector *pGEMHE-DEST*

The *pCR8/GW/TOPO-ScAMF1* was recombined into the *pGEMHE-destination* (*pGEMHE-DEST*) vector (Shelden, 2009; Figure 3.1). The *pGEMHE-ScAMF1* plasmids were transformed in XL-Blue *E.coli* (Stratagene) and selected on solid reduced salt LB (5 g L^{-1} NaCl) solid media supplemented with 100 µg ml^{-1} carbenicillin after 2-3 days of incubation at 28°C. Recombinant plasmid DNA was isolated from the mid-log phase cultures by GenElute Plasmid MiniPrep kit according to the manufacturers protocol (Sigma-Aldrich). Plasmids with inserts in the correct orientation were identified by *Sph* I (NEB, USA) restriction analysis and then sequenced with *T7* promoter forward and *M13* reverse primers (Table 2.1) as described in Chapter 2.

3.2.2 Synthesis of cRNA and injection into *X. laevis* oocytes

The *pGEMHE-ScAMF1* plasmid was prepared for cRNA synthesis by linearisation with *Nhe* I (NEB, USA) for 1 h at 37°C, followed by heat inactivation at 65°C for 25 min. Potential RNase contaminates were then eliminated by incubating the digestions with 1 µl of proteinase K (20 mg ml^{-1}) (Invitrogen) in the presence of 0.5% (w/v) SDS for 1 h at 50°C. The linearised *pGEMHE-ScAMF1* plasmid was then extracted with 1 volume of phenol/chloroform/isoamyl-alcohol, followed by ethanol precipitation with 0.1 volume of 5 M ammonium acetate (pH 5.6). After 15 min incubation at -80°C, cRNA was pelleted by

microcentrifugation at maximum speed at room temperature for 15 min. The cRNA synthesis was carried out according to the mMESSAGE mMACHINE® T7 Kit (Ambion) protocol. The remaining plasmid template was digested with 1 µl of TURBO DNase (Ambion) at 37°C for 15 min. The cRNA was precipitated by adding 30 µl of LiCl precipitation solution (Ambion) and then chilled at -80°C for 1 h. The cRNA was pelleted at 4°C for 15 min at maximum speed. The cRNA pellet was washed three times with 100 µl of 70% (v/v) ethanol. The quality of the cRNA was observed by electrophoresis with TBE (9 mM Trizma-base, 9 mM H_3BO_3, 0.2 mM EDTA) denaturing gel at 90 V for 1 h. The concentration of cRNA was calculated for 0.2 µl using a VersaFluor Fluorometer (BioRad) according to the Quant-iT RiboGreen RNA assay kit (Invitrogen) protocol. The cRNA was diluted to a uniform concentration of 500 ng μl^{-1} and stored at -80°C until required for injection into oocytes.

3.2.3 Preparing injection pipettes and electrodes

Pipettes for the injection of oocytes were prepared from glass capillaries (3.5" Drummond #3-000-203-9/x, AdeLab) using a pipette puller PP-83 (Narishige, Japan) with heater 1 set at 11.5 and heater 2 at 10.0. The tips of the pipettes were ground to 4-6 µM using a microgrinder (Narishige, Japan). Pipettes were filled with silicon oil and attached to a Drummond 'Nanoinject II' automatic nanolitre injector for injecting oocytes with cRNA or RNase-free H_2O (Drummon Scientific Company). Electrodes were prepared from borosilicate glass capillaries (GC150F-10, Harvard Apparatus, UK) with pipette puller heater 1 & 2 settings at 11.83 & 9.03, respectively.

3.2.4 Harvesting oocytes for electrophysiology

Healthy stage IV and V oocytes were harvested from *X. laevis* (NASCO Biology)

according to the protocol described by Hill et al., (2005). Following the harvest, oocytes were transferred to fresh Calcium-Frog Ringers solution (96 mM NaCl, 2 mM KCl, 5 mM $MgCl_2$, 0.6 mM $CaCl_2$, 5 mM HEPES, pH 7.6) supplemented with 8% (w/v) horse serum, 100 µg ml^{-1} tetracycline, 1000 U ml^{-1} penicillin and 100 µg ml^{-1} streptomycin (Hill et al., 2005). The oocytes were kept at 18°C until required. The Calcium-Frog Ringers solution was changed on a daily basis.

3.2.5 *X. laevis* Two-Electrode Voltage Clamp analysis

Individual healthy oocytes were injected with 46 nl (23 ng) of cRNA into the animal pole (brown hemisphere). Additional oocytes were similarly injected with 46 nl of nuclease-free Milli-Q H_2O to serve as negative controls. Injected oocytes were pre-incubated for 1-2 days at 18°C in Calcium-Frog Ringers solution or ND10 buffer (10 mM NaCl, 200 mM mannitol, 2 mM KCl, 1.8 mM $CaCl_2$, 1 mM $MgCl_2$, 10 mM HEPES, with or without 10 mM PO_4^{3-} (as 10 mM KH_2PO_4 or 10 mM NaH_2PO_4 instead of 10 mM NaCl) and pH 7.5 adjusted with Trisma-base) supplemented with 8% (w/v) horse serum, 100 µg ml^{-1} tetracycline, 1000 U ml^{-1} penicillin and 100 µg ml^{-1} streptomycin. TEVC experiments were performed at room temperature in either Modified Barth's Solution (MBS; 96 mM NaCl, 2 mM KCl, 2 mM $CaCl_2$, 1 mM $MgCl_2$, 5 mM MES, pH adjusted to 6.5 with NaOH) or ND10 buffer with modifications plus supplements (See Figures for details of modifications and supplements analysed). Healthy oocytes were impaled with electrodes filled with 0.22 µM filtered 3 M KCl, and signals were amplified using a GeneClamp500 voltage clamp amplifier (Axon Instruments, USA) and displayed using Clampex8 (Axon Instruments, USA). Oocytes that were clamped at stable resting potentials negative of -10 mV were considered satisfactory provided that the membrane conductance was not large. The voltage clamp protocol measured current at 20 mV increments from -140 mV to +60 mV

for 1.5 s (Figure 3.15). I/V curves (current as a function of voltage) were generated from current recorded 1.2 to 1.3 s into the voltage clamp.

3.2.6 Electrophysiology data analysis

Mean currents were graphed with standard errors (± SE) using Prism GraphPad Version 5.0d (GraphPad inc.). The degree of significance with respect to NH_4^+ activated currents (denoted a), corresponding H_2O-injected controls (denoted b) and P_i-preincubation or Ca^{2+} concentration (denoted c) was assessed using Two-way ANOVA analysis where P-values less than 0.05 ($p<0.05$) were considered significant.

3.2.7 *X. laevis* oocyte ^{14}C-MA uptake analysis

Prior to ^{14}C-MA uptake analysis, oocytes were incubated in MBS buffer for 20 min. Single oocytes were incubated at 18°C in 180 µl of MBS supplemented with 0.025 mM, 0.05 mM, 0.15 mM, 0.30 mM, 0.60 mM or 1 mM MA labeled with ^{14}C-MA (Perkin Elmer). After an incubation period of 16 h, the oocytes were washed twice in 5 ml of ice-cold MBS buffer with unlabeled MA in place of ^{14}C-MA. Individual oocytes were pipetted into scintillation vials with 50 µl of dilute HNO_3 and dissolved for 2 h before adding 4 ml of IRGA-Safe Plus scintillation fluid (Perkin Elmer). The β-decay was measured using a liquid scintillation counter (Tri-Carb 2100TR, Packard). Significance was assessed using Two-way ANOVA analysis (Prism GraphPad Version 5.0d) where P-values less than 0.05 ($p<0.05$) were considered significant.

3.3 Results

ScAMF1 was subcloned into the *pGEMHE-DEST* vector downstream of the *T7* promoter and flanked by *X. laevis ß-globin* gene 5' and 3' UTRs (Shelden et al., 2009; Figure 3.1), which was used as a template for cRNA synthesis. The quality of the synthesised *ScAMF1* cRNA and positive control *X. laevis elongation factor 1α* cRNA was assessed by electrophoresis (Figure 3.2), and 23 ng (46 nl) of *ScAMF1* cRNA was injected into the animal pole of healthy Stage IV and V oocytes. Control oocytes were injected with an equal volume of RNase-free H_2O.

3.3.1 ^{14}C-MA accumulation was enhanced in *X. laevis* oocytes injected with *ScAMF1* cRNA

When oocytes were bathed in MBS, the concentration dependence of ^{14}C-MA accumulation into *ScAMF1*-injected oocytes relative to H_2O-injected controls increased significantly ($p<0.05$) from 0.15 mM to 1 mM MA over a 16 h period (Figure 3.3). The rate of ^{14}C-MA tracer accumulation was linear across both high (< 250 μM) and low (> 250 μM) affinity ranges, suggestive of low-affinity transport capacity.

3.3.2 Development of an electrophysiological screen to assess the putative NH_4^+ current activity of *X. laevis* oocytes expressing *ScAMF1* cRNA

ScAMF1 activity in *X. laevis* oocytes resulted in outward currents (at positive membrane potentials) when oocytes were voltage clamped in MBS buffer, whilst inward currents

(negative membrane potentials) were comparable to H_2O-injected controls (Figures 3.4 A). The outward current exhibited by ScAMF1-ooctytes suggests that ScAMF1 facilitates the efflux of a positively charged ion from the oocyte or the influx of a negative charged ion under these conditions. When 0.2 mM and 0.5 mM NH_4Cl was applied to the voltage-clamping buffer, there was no significant difference in currents observed. The high concentration of Na^+ in the voltage-clamping buffer may have masked the ability of ScAMF1 to mediate the transport of the NH_4^+ and MA across the oocyte PM by stimulating endogenous cation currents.

3.3.2.1 Inward currents catalysed by ScAMF1 activity in *X. laevis* oocytes were inhibited by the presence of NH_4^+ and MA in the voltage-clamping buffer

Large currents were detected in *ScAMF1*-injected oocytes when ND10, which contains 10 mM NaCl compared to MBS with 100 mM NaCl, was used as the voltage-clamping buffer in comparison to H_2O-injected control oocytes (Figure 3.4 B). When oocytes were voltage-clamped in the presence of NH_4Cl, the inward currents were significantly ($p<0.05$) reduced from voltages negative of -80 mV, suggesting that NH_4^+ is influencing the current in some way, but it is not clear at this stage that the current is carried by NH_4^+. The change in current could also suggest that NH_4^+ acts as an antagonist to the current carried by the influx of some other cation or efflux of an anion.

3.3.2.2 Effect of Na^+ and K^+ on the current activity of *X. laevis* oocytes injected with *ScAMF1* cRNA

In an attempt to resolve the putative NH_4^+ and MA transport, oocytes expressing *ScAMF1* cRNA were voltage clamped in a series of modified ND10 voltage-clamping buffers differing in monovalent cations. The electrophysiological profiles thus far suggest that

ScAMF1 might mediate the influx of Na^+ or K^+ into the oocyte, accounting for the observed inward currents. The Na^+ and K^+ cations are the dominant monovalent species in the ND10 voltage-clamping buffer. The electrophysiology profile of oocytes expressing *ScAMF1* cRNA was assessed in another modified ND10 buffer without Na^+ (Figure 3.4 C). However, eliminating the presence of Na^+ in the voltage-clamping buffer did not reduce the currents. Once again, the inward currents were inhibited with increasing concentrations of NH_4^+. Currents were significantly ($p<0.05$) reduced at voltages negative of -120 mV by the application of 1 mM NH_4Cl. Large currents were also recorded in H_2O-injected controls.

3.3.2.3 ScAMF1 mediated NH_4^+ currents and anion coupling

In the absence of the monovalent cation species, Na^+ and K^+, ScAMF1-oocytes produced a significant increase in inward currents in response to 1 mM NH_4Cl when voltage-clamped at membrane potentials negative of -120 mV. Oocytes were also pre-incubated with 10 mM P_i prior to TEVC analysis as this appeared to improve health after 1-2 days incubation. Under these conditions, reversal potentials (the voltage at which the current is 0 nA) shifted slightly towards positive voltages (Figure 3.5). The affect of the accompanying anion on NH_4^+ -dependent currents was also analysed. ScAMF1-oocytes were voltage-clamped in the presence of 0.5 mM $(NH_4)_2SO_4$ and 1 mM $NH_4H_2PO_4$. When NH_4^+ was supplied as the SO_4^{2-} salt, inward currents were slightly increased, although not significantly ($p>0.05$), whilst with HPO_4^{2-} there was no noticeable change. There were no noticeable changes in reversal potential between SO_4^{2-} and HPO_4^{2-} and ND10 control currents. It is important to note that the voltage-clamping buffer also contained reduced (0.2 mM) Ca^{2+} to circumvent potential Ca^{2+} flux through ScAMF1.

3.3.2.4 Relationship between P_i and NH_4^+ flux mediated by ScAMF1-oocytes

3.3.2.4.1 Effect of P_i on the mortality of *X. laevis* oocytes expressing *ScAMF1* cRNA

The mortality rate of oocytes expressing *ScAMF1* was greater relative to H_2O-injected controls when incubated in MBS. Pre-incubation of ScAMF1-oocytes with 1 mM or 10 mM P_i was shown to enhance the rate of survival for oocytes expressing *ScAMF1* cRNA (Figure 3.6). In the presence of monovalent cation-free ND10 buffer, endogenous outward and inward currents were reduced by pre-incubation with ND10 supplemented with 10 mM P_i coupled to K^+ or Na^+, but were lowest with NaH_2PO_4 (Figure 3.7). Therefore, subsequent experiments were carried out with oocytes pre-incubated with or without 10 mM NaH_2PO_4 in place of 10 mM NaCl.

3.3.3 Electrophysical profile of NH_4^+ currents facilitated by ScAMF1

Possibly competing Na^+ and K^+, and divalent cations were omitted from the voltage-clamping buffers for all subsequent analyses in order to observe NH_4^+ currents facilitated by ScAMF1. The NH_4^+ carried currents mediated by ScAMF1 in the presence of low Ca^{2+} (0.2 mM $CaCl_2$) were activated at increasingly negative voltages pulses, although currents observed were not significant (Figure 3.8 A). As the NH_4^+ concentration was increased, the reversal potential shifted more positive indicating that the current is carried by the influx of cations (NH_4^+) as opposed to the efflux of anions (Cl^-). In the presence of low Ca^{2+}, currents elicited by ScAMF1-oocytes were not significant with respect to corresponding H_2O-injected controls, for which large endogenous currents were observed with or without P_i-preincubation When ScAMF1-oocytes were pre-incubated with 10 mM NaH_2PO_4 (*from here on referred to as* P_i) prior to TEVC, currents carried by NH_4^+ became significant with 1 mM and 5 mM NH_4^+ at voltages negative of -140 mM and -100 mV, respectively (Figure

3.8 B).

3.3.3.1 Effect of Ca^{2+} on ScAMF1 mediated NH_4^+ currents

The influence of elevated Ca^{2+} (1.8 mM $CaCl_2$) relative to low Ca^{2+} concentration on NH_4^+ flux catalysed by ScAMF1 activity in oocytes was assessed (Figure 3.9). Here, the oocytes were pre-incubated with 10 mM P_i prior to TEVC. Under both Ca^{2+} concentrations, NH_4^+-stimulated currents at more-hyperpolarized voltages negative of -100 mV were significant with respect to corresponding H_2O-injected controls and currents induced without NH_4^+. It was anticipated that increasing the external Ca^{2+} (from 0.2 mM to 1.8 mM Ca^{2+}) concentration in the voltage-clamping buffer would have an inhibitory effect on ScAMF1 activity thereby reducing the current elicited by NH_4^+. However, high Ca^{2+} (1.8 mM) in the voltage-clamping buffer resulted in an increased conductance, significantly ($p<0.05$) enhancing the amplitude of NH_4^+ inward current negative of -140 mV relative to similar currents elicited in the presence of low Ca^{2+}. Reversal potential shifted towards negative voltages when external Ca^{2+} was high, and shifted further positive with the application of NH_4Cl. No significant changes in current were observed in H_2O-injected control oocytes as a result of Ca^{2+} concentrations.

3.3.3.2 Effect of P_i gradient across the oocyte plasma membrane on ScAMF1 catalysed NH_4^+ currents

To further examine the effect of altering the gradient of P_i across the PM on the ScAMF1 induced currents, ScAMF1-oocytes and control H_2O-oocytes were incubated in ND10 buffer supplemented with 0 mM or 10 mM P_i prior to TEVC in the presence of minus Na^+ and K^+ modified ND10 buffer with or without P_i. *X. laevis* oocytes have been used for characterization of various P_i transporters including mammalian sodium (Na^+)-P_i co-

transporters and low-affinity P_i MF transporters of the PHT1 subfamily from rice and barely (Bacconi et al., 2005; Ai et al., 2009; Preuss et al., 2010). ScAMF1-oocytes analysed with low Ca^{2+} buffer presented a shift in reversal potential towards positive voltages, which was greater with P_i-preincubation (Figure 3.10 A). However, the H_2O-injected control oocytes demonstrated substantial change in current under identical conditions. Under high Ca^{2+}, inward currents at negative voltages were greater when ScAMF1-injected oocytes were pre-incubated with P_i, and current changes were absent in corresponding H_2O-injected controls. The 5 mM NH_4^+ induced current mediated by ScAMF1 activity was significant at membrane potentials negative of -100 mV when similar oocytes were voltage-clamped in the presence of high Ca^{2+} compared to low Ca^{2+} (Figure 3.10 B). Again, the NH_4^+ driven current at -140 mV elicited by P_i-preincubated ScAMF1-oocytes was significant with respect to ScAMF1-oocytes without P_i-pre-incubation. There was no shift in reversal potential for ScAMF1-oocytes voltage clamped in the presence of high external Ca^{2+} with or without the P_i pre-treatment. Without P_i-preincubation, H_2O-injected control oocytes produced large currents when voltage clamped with high Ca^{2+} in comparison to low Ca^{2+} although the difference was not significant, while preincubation with P_i reduced the observed current in H_2O-injected controls.

ScAMF1 mediated current as a function of time (ms) revealed activation by NH_4^+ was not time-dependent. Changing Ca^{2+} concentration in the voltage-clamping buffer did not alter the lack of time-dependence (Figure 3.12). Activation of NH_4^+ currents elicited by 10 mM P_i pre-incubated ScAMF1-oocytes was also independent of time (Figure 3.13), and was not effected by Ca^{2+} concentration. Currents were comparable to H_2O-injected oocytes voltage-clamped under the same conditions. Note that data are derived from same set of oocyte experiments as Figure 3.10, and a representative trace (n = 1) is displayed for each

oocyte injection and voltage-clamp buffer analysed, which serves to provide evidence of a trend.

3.3.3.3 Conductance of ScAMF1 mediated currents in *X. laevis* oocytes as a function of NH_4^+ concentration

In order to analyse the movement of NH_4^+ across the oocyte PM mediated by ScAMF1 , the conductance over a range of NH_4^+ concentrations (0 mM, 0.5 mM, 1 mM and 5 mM NH_4^+) was calculated, from which the conductance of corresponding H_2O-injected oocytes was subtracted. Under low Ca^{2+} conditions, the conductance of ScAMF1 increased with elevated NH_4^+ concentration and was greater for oocytes subjected to incubation with P_i prior to TEVC analysis (Figure 3.11 A). Without P_i pre-incubation, the conductance was negative at 0.5 mM NH_4^+, meaning that the H_2O controls had greater conductance than ScAMF1. In the presence of high Ca^{2+}, the conductance of ScAMF1 for the range NH_4^+ concentrations analysed was also negative, while the conductance of P_i pre-incubated oocytes was positive and increased linearly with increasing NH_4^+ concentration (Figure 3.11 B). This confirms that the slope conductance were significantly ($p<0.05$) larger than controls when oocytes were pre-incubated with P_i, suggesting that P_i or a product of P_i metabolism is required to activate the current. The conductance of ScAMF1 was greater under these conditions relative to low Ca^{2+} conditions with P_i-preincubation.

3.3.4 Assessment of carbohydrate catalysed electrochemical signatures in *ScAMF1* cRNA injected into *X. laevis* oocytes

As described previously, oocytes expressing *ScAMF1* cRNA produced greater currents in response to the basal buffer when compared to H_2O-injected controls, suggesting that there is movement of some unknown substrate. As ScAMF1 shares a high degree of homology

with the DmSPIN1 (Rong et al., 2011) from the SPINSTER family of vertebrate major facilitator carbohydrate efflux proteins (Figure 4.4), the ability of ScAMF1 to facilitate the movement of different monosaccharides was also assessed using TEVC analysis. Despite the inability of sugar to ionise in solution, and therefore inability to produce a current if a electrical charge is applied, it was hypothesised that ScAMF1 might act to transport sugar in exchange for P_i or other ions, which could serve as a means to trace the transportation of sugar. The potential selectivity of ScAMF1-induced currents to different monosaccharides was investigated by measuring steady-state currents at -140 mV (Figure 3.14 A) and +60 mV (Figure 3.14 B). Oocytes were pre-treated with and without P_i prior to analysis. However, the steady-state currents recorded for sorbitol, galactose and glucose were not significantly ($p>0.05$) different from that observed for mannitol (the osmolyte used in previous electrophysiology experiments) regardless of P_i-preincubation. As a result the investigation was not continued and the electrical analysis was not verified with oocyte uptake of ^{14}C-labled sugars.

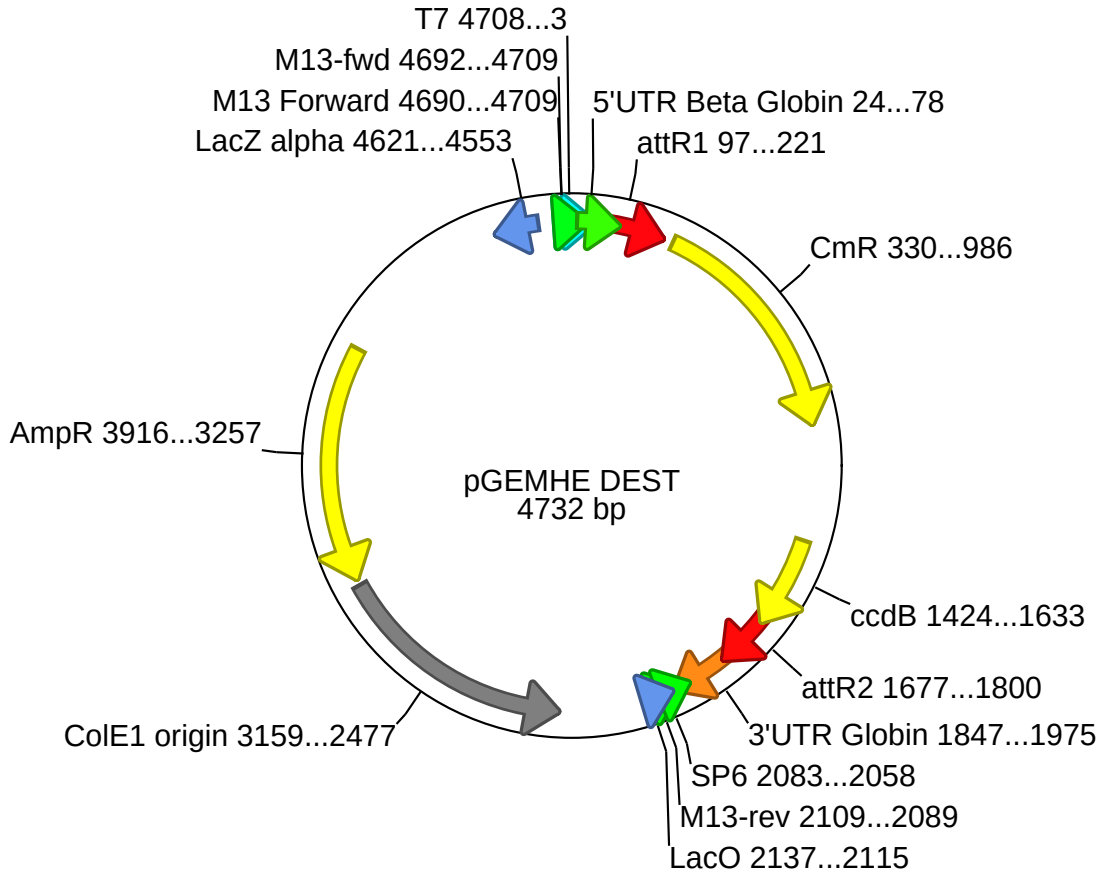

Figure 3.1: Vector map of *pGEMHE-destination*

The 5’ and 3’ UTRs from *X. laevis ß-globin* gene flanking a polylinker (Krieg and Milton, 1984) enabling the recombination of the reading frame cassette A containing the *ccdB* gene and chloramphenical resistance gene (M. Shelden, 2009).

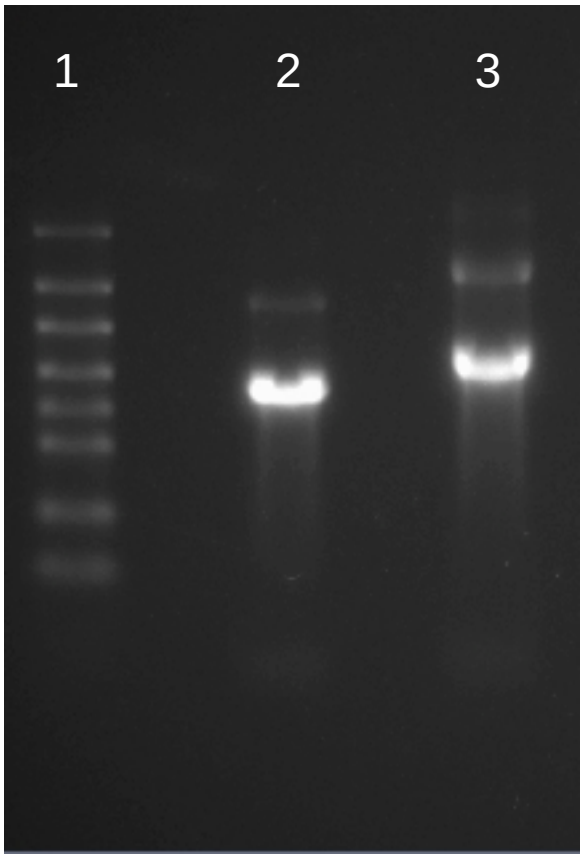

Figure 3. 2: Synthesised *ScAMF1* capped RNA

Gel electrophoresis of cRNA synthesised and used to inject *X. laevis* oocytes for Two-Electrode Voltage-Clamp physiology presented in this thesis. Lane 1. RNA ladder (NEB, USA); 2. *ScAMF1* cRNA; 3. *X. laevis elongation factor 1α* cRNA (positive control) synthesised from the linearised TRIPLEscript plasmid *pTRI-Xef* provided with the *T7* mMessage mMachine kit.

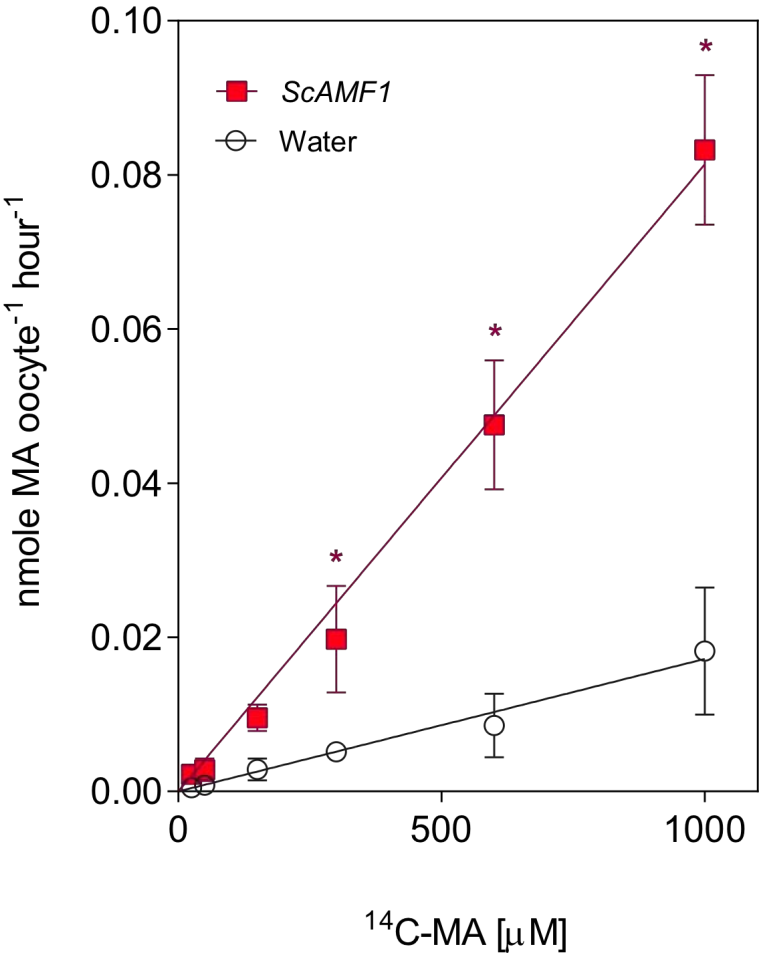

Figure 3.3: Concentration-dependence of ^{14}C-MA uptake into *X. laevis* oocytes expressing *ScAMF1*

X. laevis oocytes expressing *ScAMF1* (red solid squares) or injected with RNase-free H_2O (black open circles) were bathed in Frog Ringers with Calcium solution plus horse serum and antibiotics for 48 h prior to analysis. Single oocytes were incubated at 18°C in 180 µl of MBS buffer with MA at 0.025 mM, 0.05 mM, 0.15 mM, 0.3 mM, 0.6 mM and 1 mM plus ^{14}C-labeled MA (Perkin Elmer) for 16 h. Individual oocytes were pipetted into scintillation vials containing 4 ml of IRGA-Safe Plus scintillation fluid (Perkin Elmer). The β-decay was measured using a liquid scintillation counter (Tri-Carb 2100TR, Packard). Data points in each experiment represent mean (n = 10-12) ± SE, and asterisks denote significance (*P<0.05) using Two-way ANOVA analysis.

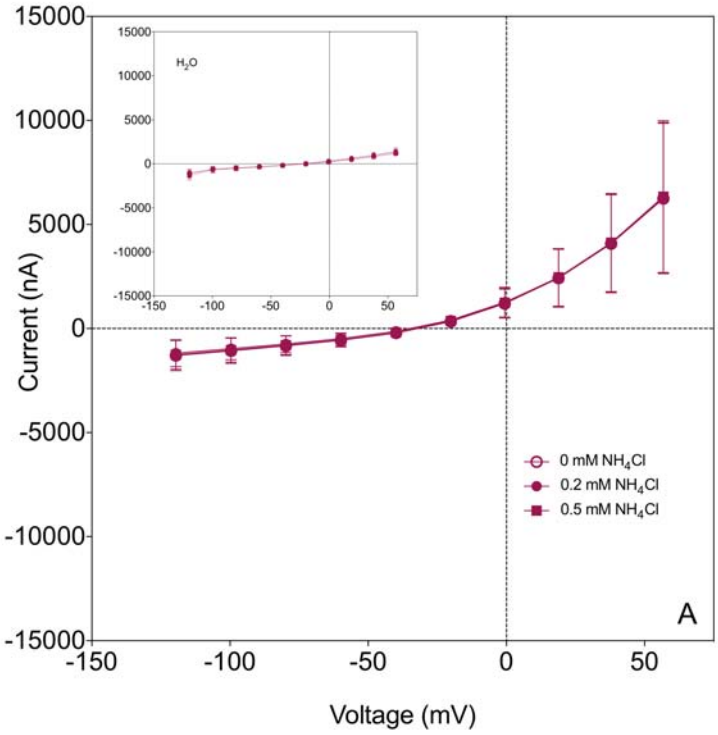
15000
10000
5000
0
-5000
-10000
-15000
Current (nA)
-150
-100
-50
0
50
Voltage (mV)
H2O
0 mM NH4Cl
0.2 mM NH4Cl
0.5 mM NH4Cl
A

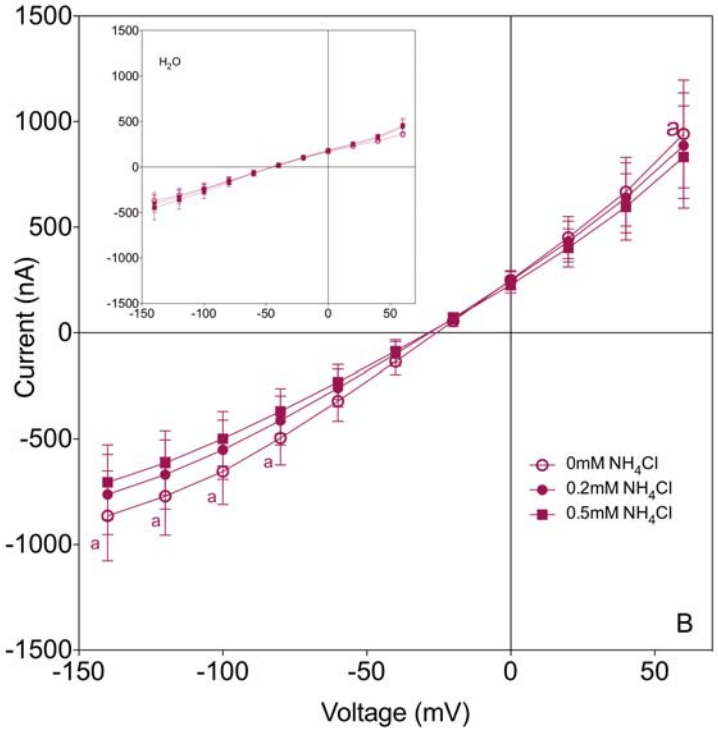
1500
1000
500
0
-500
-1000
-1500
Current (nA)
-150
-100
-50
0
50
Voltage (mV)
H2O
a
0mM NH4Cl
0.2mM NH4Cl
0.5mM NH4Cl
B

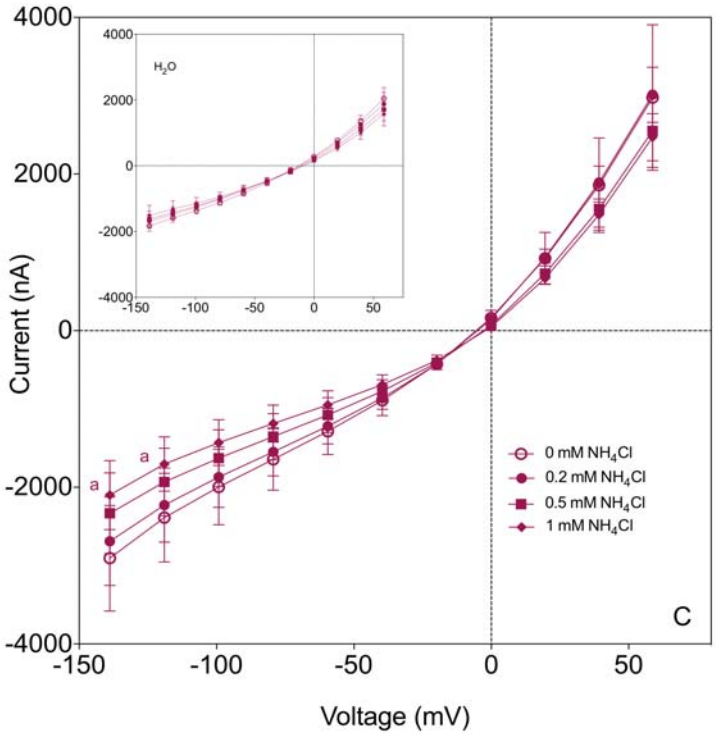

Figure 3.4: The current / voltage relationship of *X. laevis* oocytes expressing *ScAMF1* cRNA in the presence of Modified Barth Solution

X. laevis oocytes expressing *ScAMF1* cRNA or injected with an equal volume of RNase-free H_2O (inset) and incubated in (**A**) Frog Ringers plus calcium or (**B** & **C**) ND10 bathing buffer for 48 h prior to Two-Electrode Voltage Clamp analysis. Oocytes were voltage clamped at room temperature in (**A**) MBS (96 mM NaCl, 2 mM KCl, 2 mM $CaCl_2$, 1 mM $MgCl_2$, 5 mM MES, pH adjusted to 6.5 with NaOH), (**B**) ND10 (10 mM NaCl, 2 mM KCl, 1.8 mM $CaCl_2$, 1 mM $MgCl_2$, 10 mM HEPES, 200 mM mannitol, pH adjusted to 7.5 with Trisma-base) (n = 3), or (**C**) modified ND10 minus NaCl (H_2O -injected n = 11, *ScAMF1*-injected n = 5). Error bars indicate ± SE, and data points represent the means. Data are significantly different from corresponding 0 mM NH_4^+ currents using Two-way ANOVA analysis.

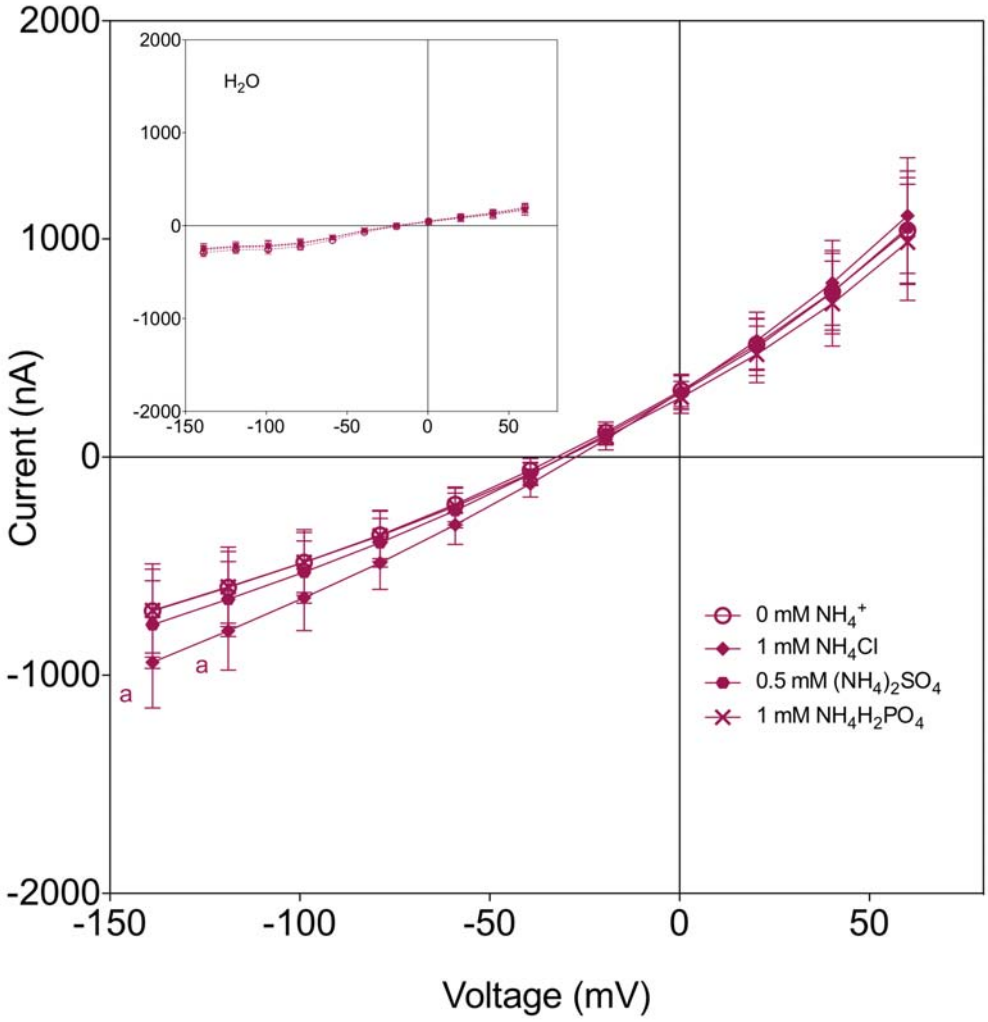

Figure 3.5: The current / voltage relationships of *X. laevis* oocytes expressing *ScAMF1* cRNA as a function of external anions coupled with NH_4^+

X. laevis oocytes expressing *ScAMF1* cRNA or injected with an equal volume of RNase-free H_2O (inset) were preincubated ND10 buffer plus 10 mM KH_2PO_4 prior to Two-Electrode Voltage Clamp analysis in modified ND10 (minus NaCl or KCl) plus with 0 mM NH_4^+, 0.5 mM $(NH_4)_2SO_4$, 1 mM $NH_4H_2PO_4$ or 1 mM NH_4Cl. Data points in each experiment represent mean (n = 3) ± SE, and asterisks denote significance (*P<0.05) using Two-way ANOVA analysis. There is no significant difference between H_2O-injected control oocytes.

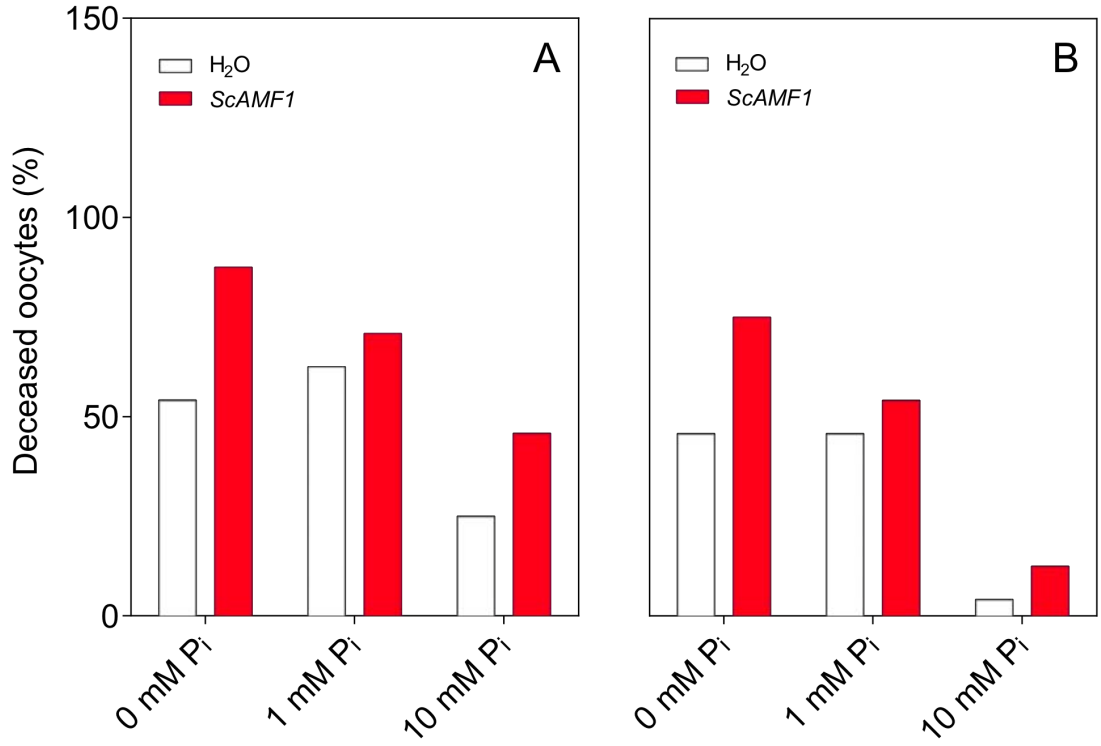

Figure 3.6: Mortality of *X. laevis* oocytes expressing *ScAMF1* cRNA in different pre-incubation buffers

X. laevis oocytes injected with *ScAMF1* cRNA (red) or injected with an equal volume of RNase-free H_2O (white) were incubated in ND10 buffer or Calcium Frog Ringers supplemented with 0 mM, 1 mM or 10 mM P_i for 48 h at 18°C before the health of oocytes were visually assessed. Data points in each experiment represent percentage of (n = 10-12) deceased after the incubation period and is the average percentage of deceased oocytes in 2 independent experiments. Two-way ANOVA analysis showed that the data were not significantly different from corresponding controls.

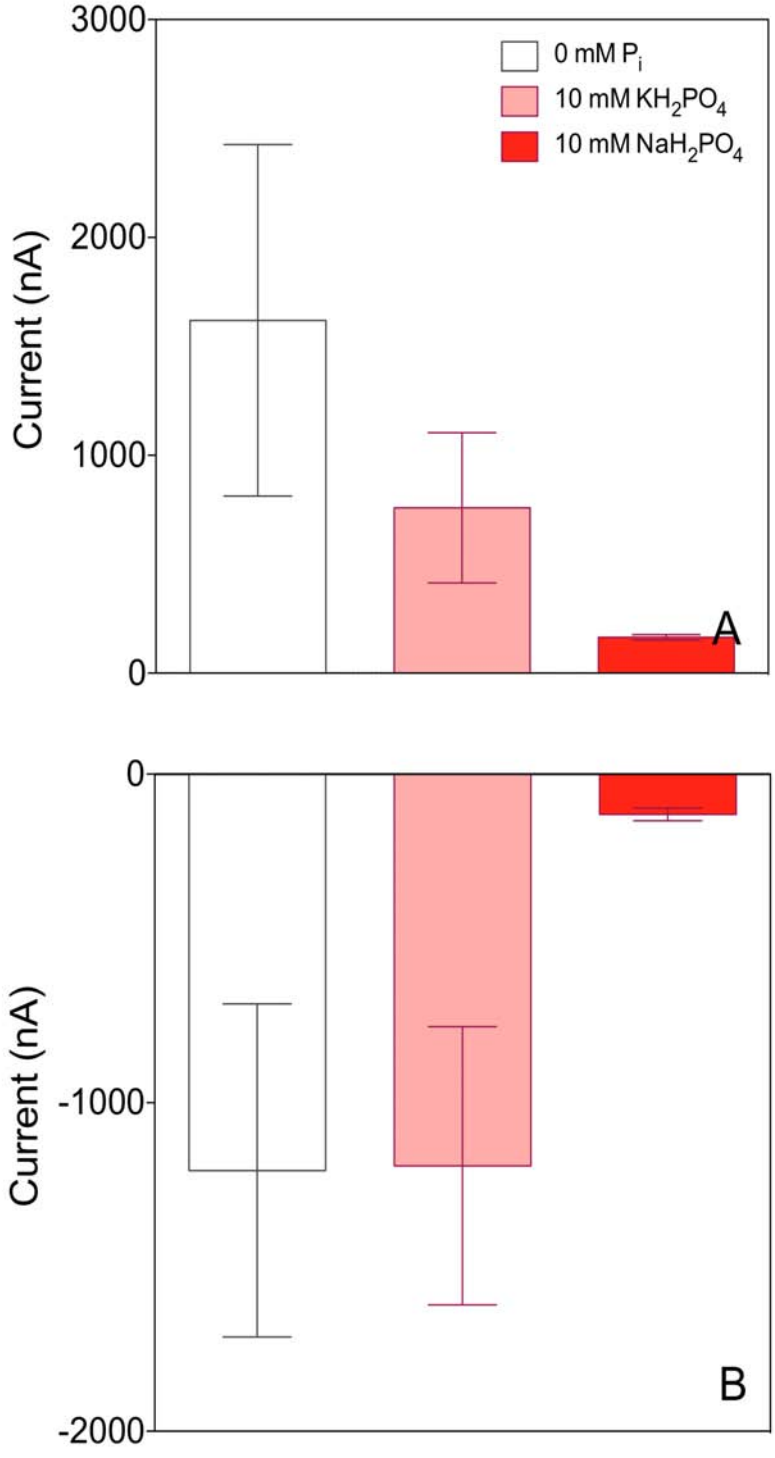
3000
2000
1000
0
Current (nA)
0 mM P_i
10 mM KH_2PO_4
10 mM NaH_2PO_4
A
0
-1000
-2000
Current (nA)
B

Figure 3.7: Effect of P_i preincubation on endogenous currents elicited in H_2O-injected *X. laevis* oocytes

X. laevis oocytes injected with RNase-free H_2O were preincubated in ND10 buffer supplemented with 0 mM P_i**,** 10 mM KH_2PO_4 or 10 mM NaH_2PO_4 for a day prior Two-Electrode Voltage Clamp analysis in ND10 buffer minus monovalent cations. Data points in each experiment represent mean (n = 3 - 6) ± SE.

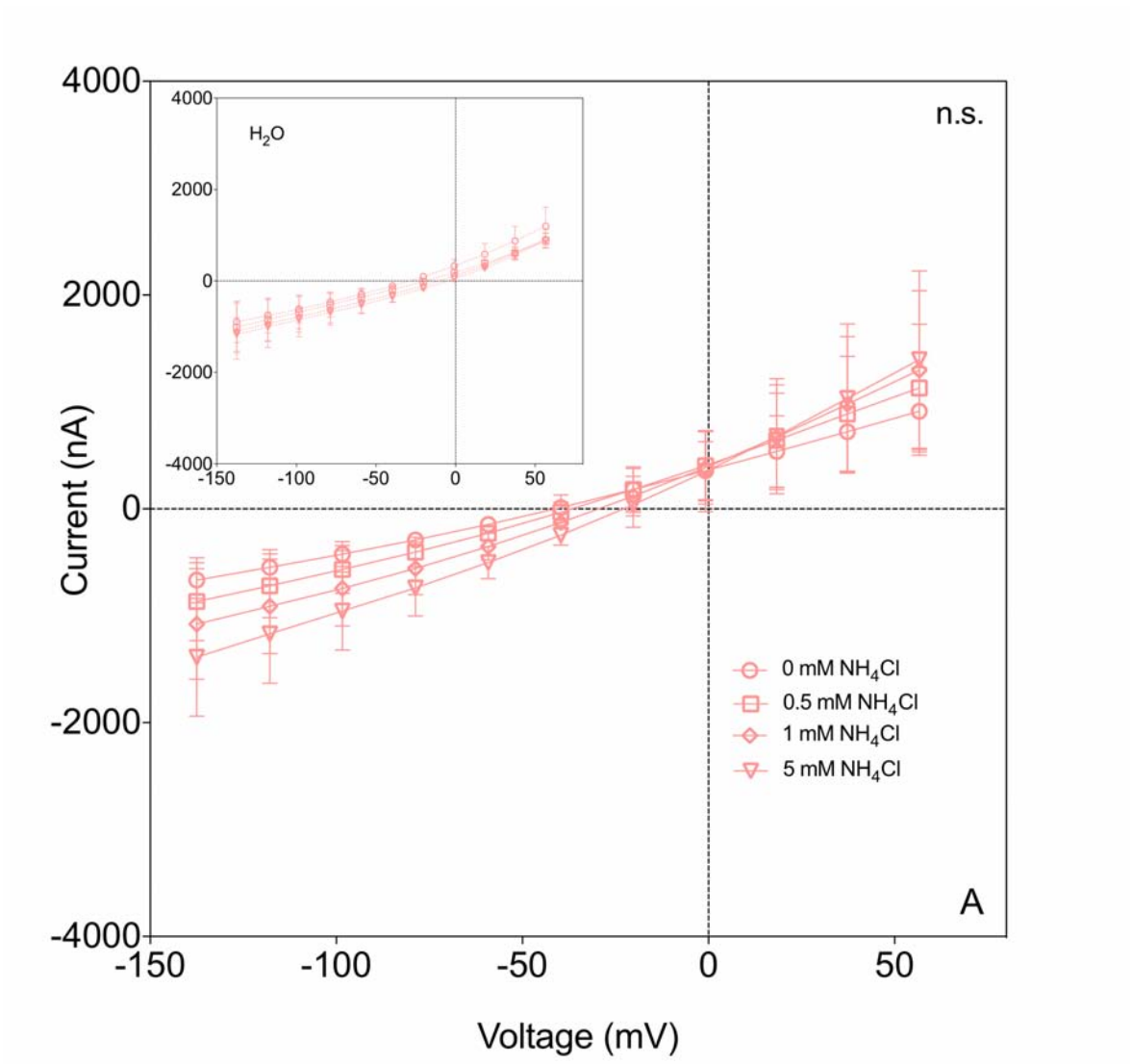
4000
2000
0
-2000
-4000
Current (nA)
-150
-100
-50
0
50
Voltage (mV)
n.s.
A
H2O
0 mM NH4Cl
0.5 mM NH4Cl
1 mM NH4Cl
5 mM NH4Cl

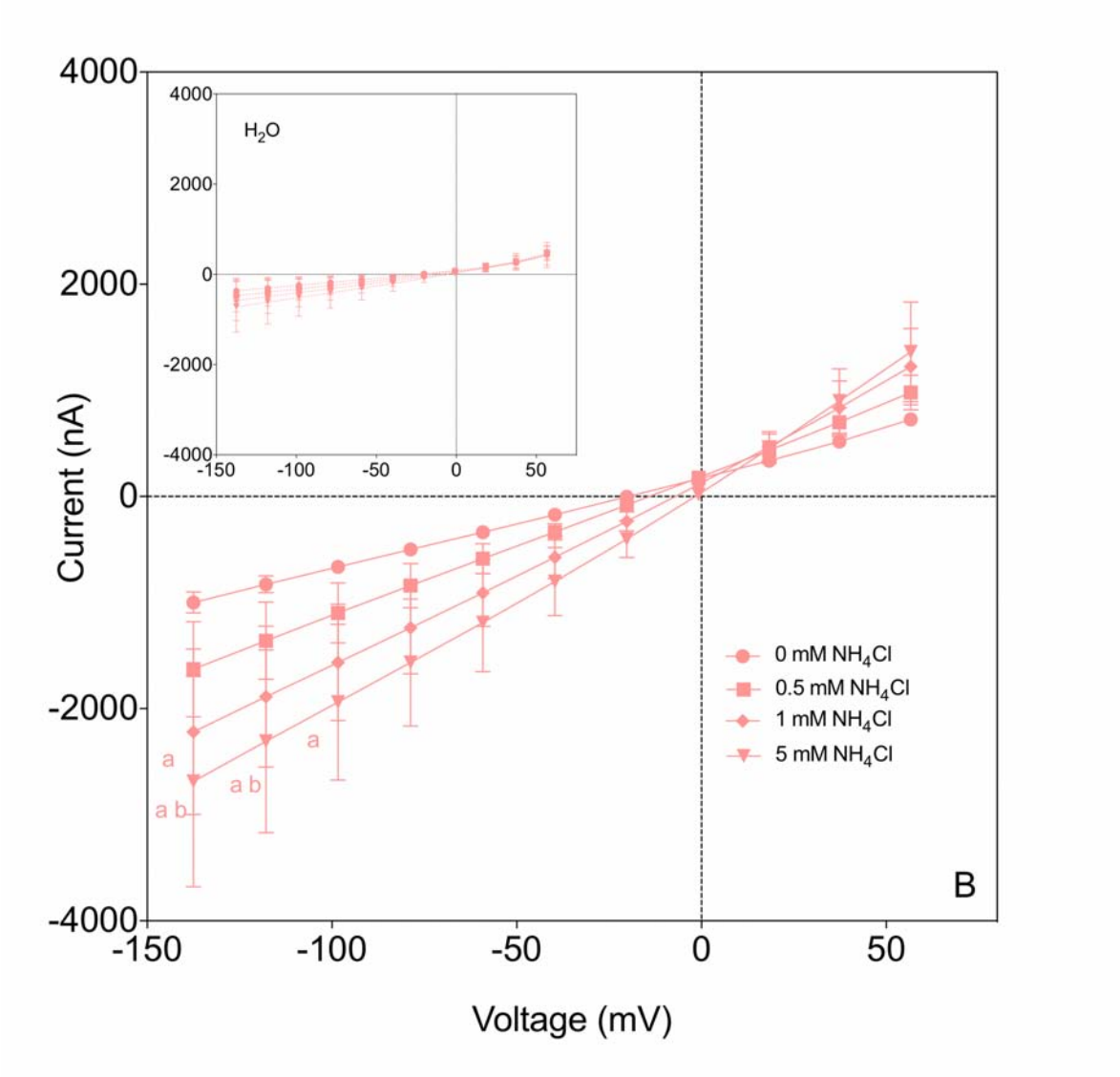

Figure 3.8: The NH_4^+ elicited current through *X. laevis* oocytes expressing *ScAMF1* cRNA in the absence of monovalent cations and low $CaCl_2$

X. laevis oocytes expressing *ScAMF1* cRNA or injected with an equal volume of RNase-free H_2O (inset) were preincubated in ND10 buffer with (**A**) 0 mM NaH_2PO_4 or (**B**) 10 mM NaH_2PO_4 prior Two-Electrode Voltage Clamp analysis in modified ND10 buffer (minus monovalent cations plus 0.2 mM $CaCl_2$) plus 0 mM, 0.5 mM, 1 mM or 5 mM NH_4Cl. Data points in each experiment represent mean (n = 3) ± SE. Significance with respect to NH_4^+ activated currents (denoted a) or corresponding H_2O-injected controls (denoted b) was assessed using Two-way ANOVA analysis where P-values less than 0.05 were considered significantly different from corresponding controls.

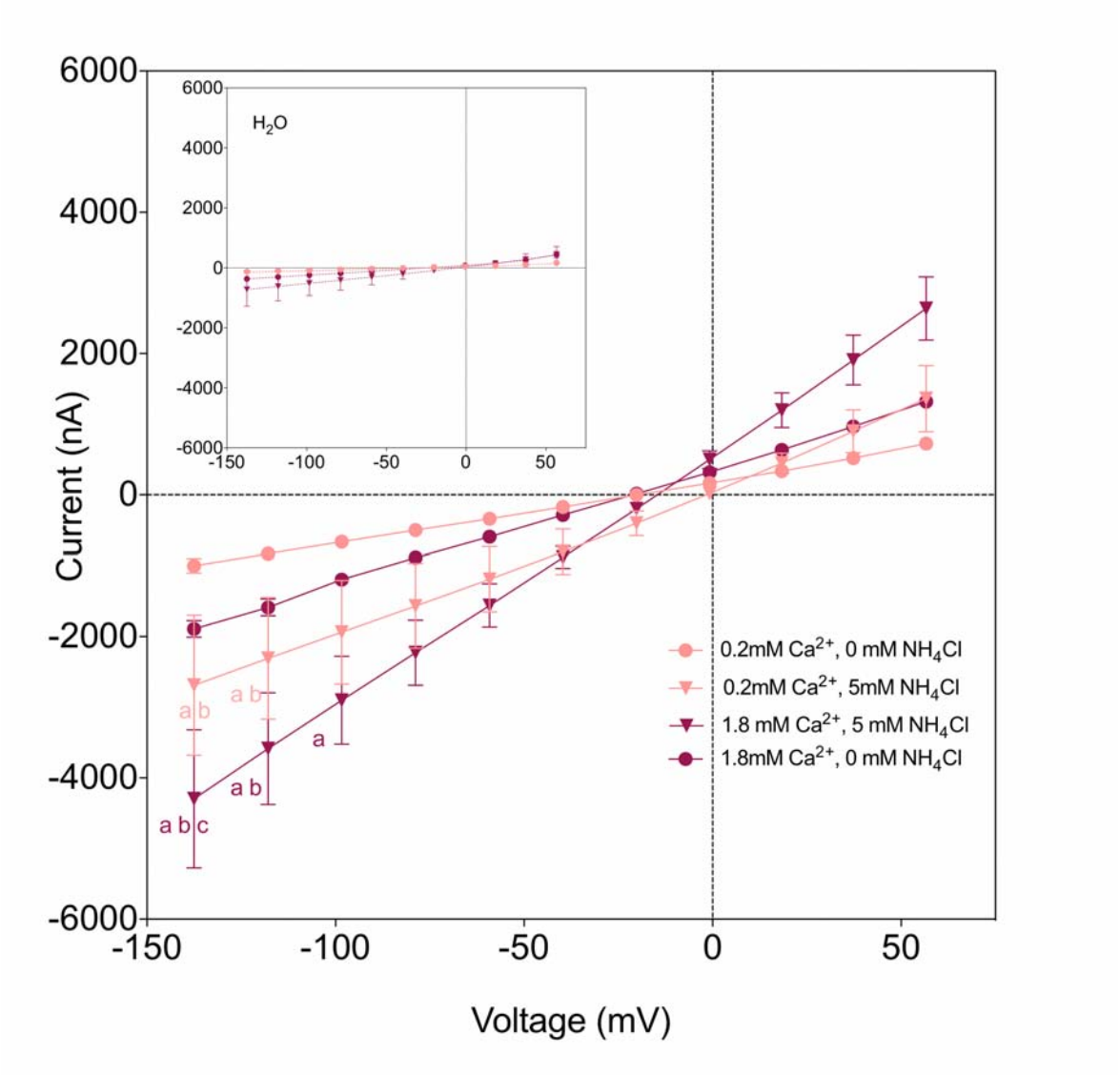

Figure 3.9: Effect of calcium on NH_4^+ elicited currents through *X. laevis* oocytes expressing *ScAMF1* cRNA

X. laevis oocytes expressing *ScAMF1* cRNA or injected with an equal volume of RNase-free H_2O (inset) were preincubated in ND10 buffer with 10 mM NaH_2PO_4 prior to Two-Electrode Voltage Clamp analysis in modified ND10 buffer (minus monovalent cations plus 0.2 mM $CaCl_2$) with 0.2 mM $CaCl_2$ or 1.8 mM $CaCl_2$ plus 0 mM or 5 mM NH_4Cl. Data points in each experiment represent mean (n = 3) ± SE. The degree of significance with respect to NH_4^+ activated currents (denoted a),

corresponding H_2O-injected controls (denoted b) or Ca^{2+} concentration (denoted c) was assessed using Two-way ANOVA analysis where P-values less than 0.05 were considered significantly different.

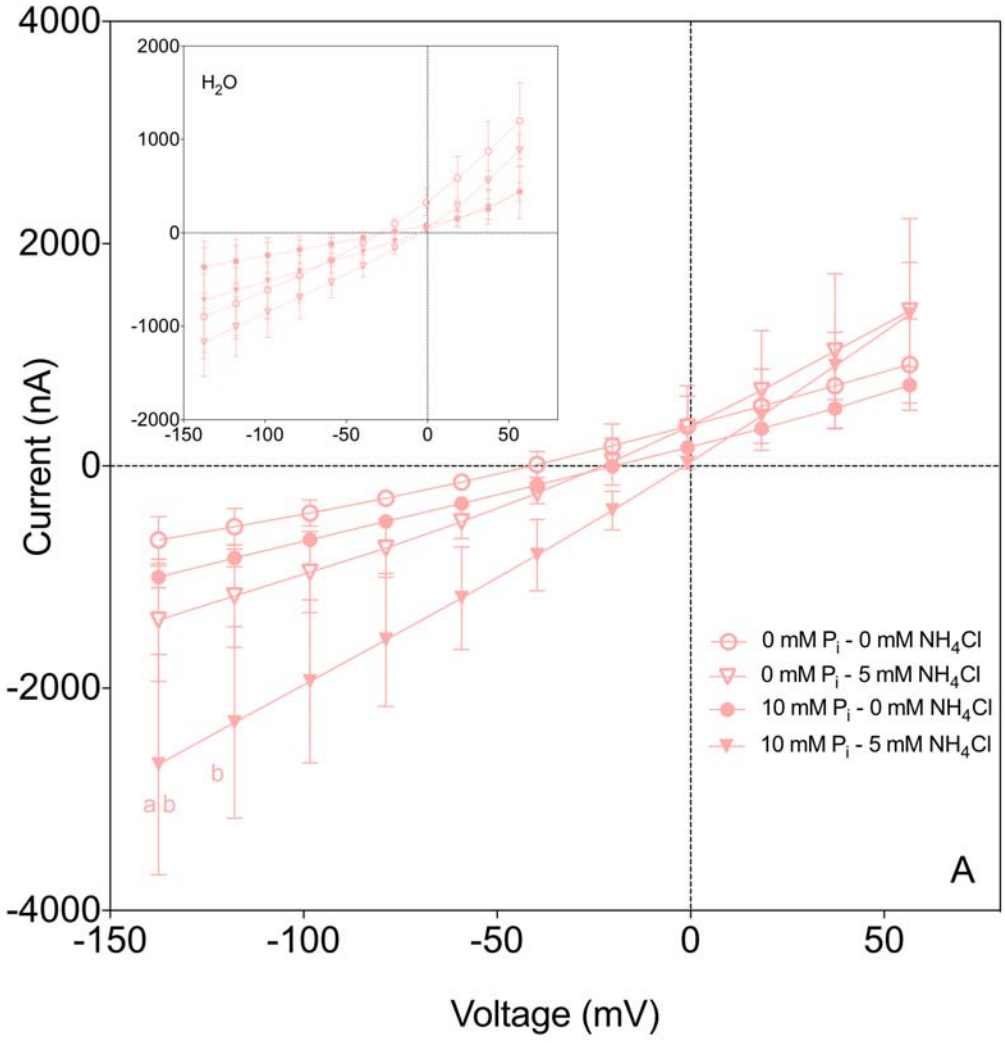
4000
2000
0
-2000
-4000
Current (nA)
-150
-100
-50
0
50
Voltage (mV)
2000
1000
0
-1000
-2000
H2O
-150
-100
-50
0
50
a
b
b
0 mM Pi - 0 mM NH4Cl
0 mM Pi - 5 mM NH4Cl
10 mM Pi - 0 mM NH4Cl
10 mM Pi - 5 mM NH4Cl
A

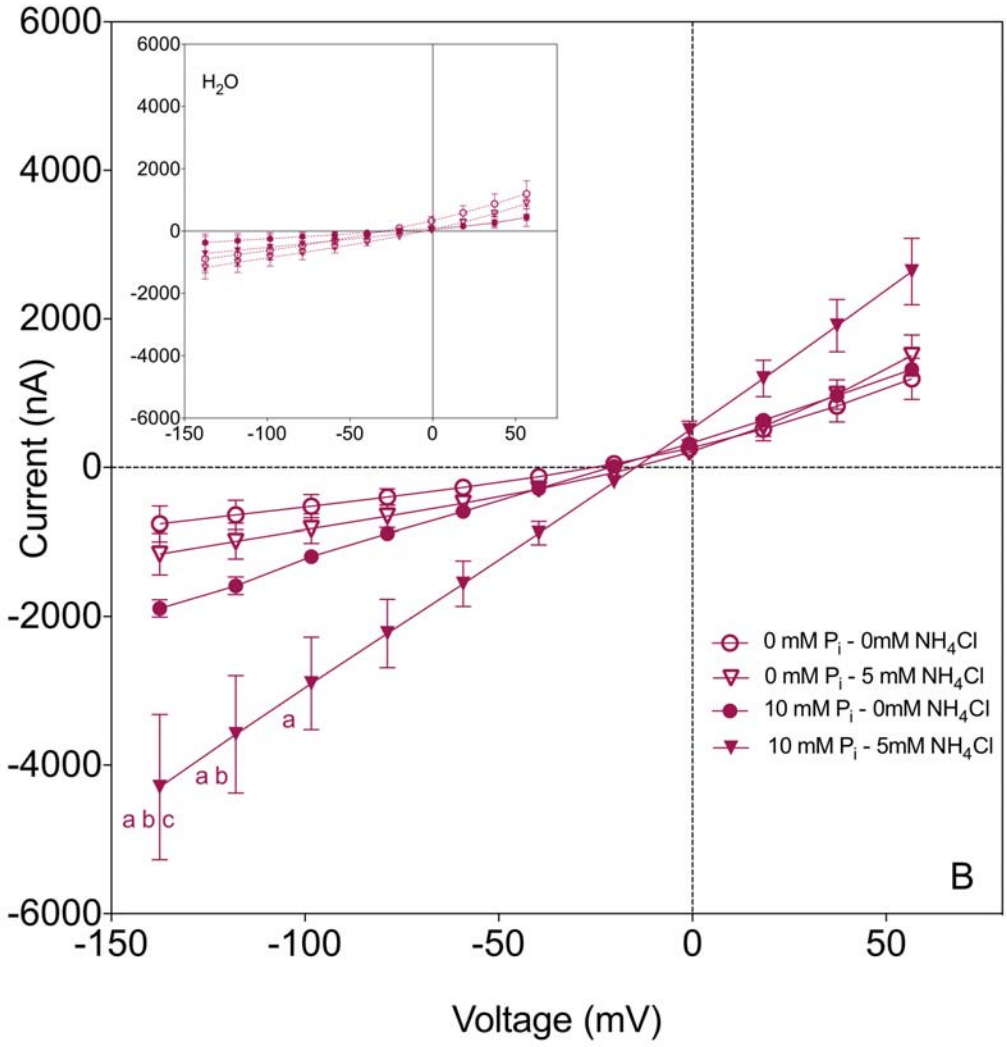

Figure 3.10: Influence of P_i preincubation on the NH_4^+ current elicited by *X. laevis* oocytes expressing *ScAMF1* cRNA

X. laevis oocytes expressing *ScAMF1* cRNA or H_2O (inset) were pre-incubated with 0 mM NaH_2PO_4 (open symbols) or 10 mM NaH_2PO_4 (solid symbols) prior to Two-Electrode Voltage Clamp in modified ND10 buffer (minus monovalent cations) with (**A**) 0.2 mM $CaCl_2$ or (**B**) 1.8 mM $CaCl_2$ plus 0 mM or 5mM NH_4Cl. Data points in each experiment represent mean (n = 3) ± SE. The degree of significance with respect to NH_4^+ activated currents (denoted a), corresponding H_2O-injeced controls (denoted b) or P_i-preincubation was assessed using Two-way ANOVA

analysis where P-values less than 0.05 were considered significantly different.

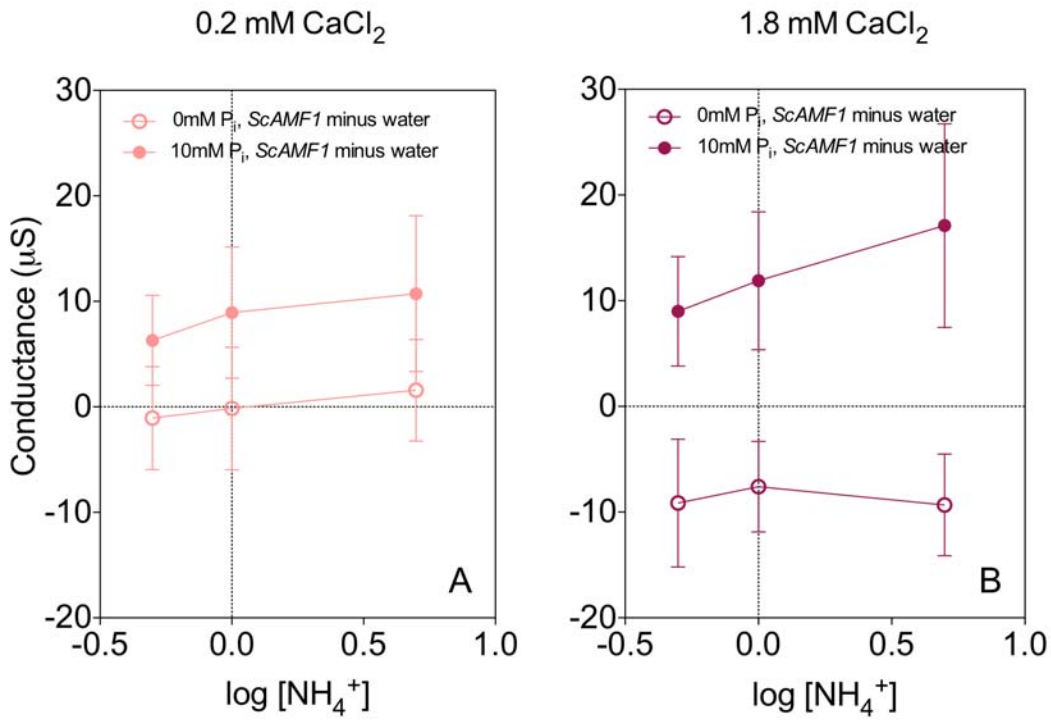

Figure 3.11: The influence of P_i-preincubation and Ca^{2+} concentration on the conductance of NH_4^+ activated ScAMF1 currents

The data presented here has been derived from Figure 3.10, with additional 0.5 mM and 1.0 mM NH_4Cl treatments. At potential of-140 mV, the conductance of *X. laevis* oocytes injected with H_2O (controls) was subtracted from the conductance of corresponding oocytes expressing *ScAMF1* cRNA. Oocytes were pre-incubated with 0 mM NaH_2PO_4 (open symbols) or 10 mM NaH_2PO_4 (solid symbols) prior to Two-Electrode Voltage Clamp analysis in modified ND10 with (**A**) 0.2 mM $CaCl_2$ (light blue) or (**B**) 1.8 mM $CaCl_2$ (dark blue) plus 0 mM, 0.5 mM, 1 mM or 5 mM NH_4Cl.

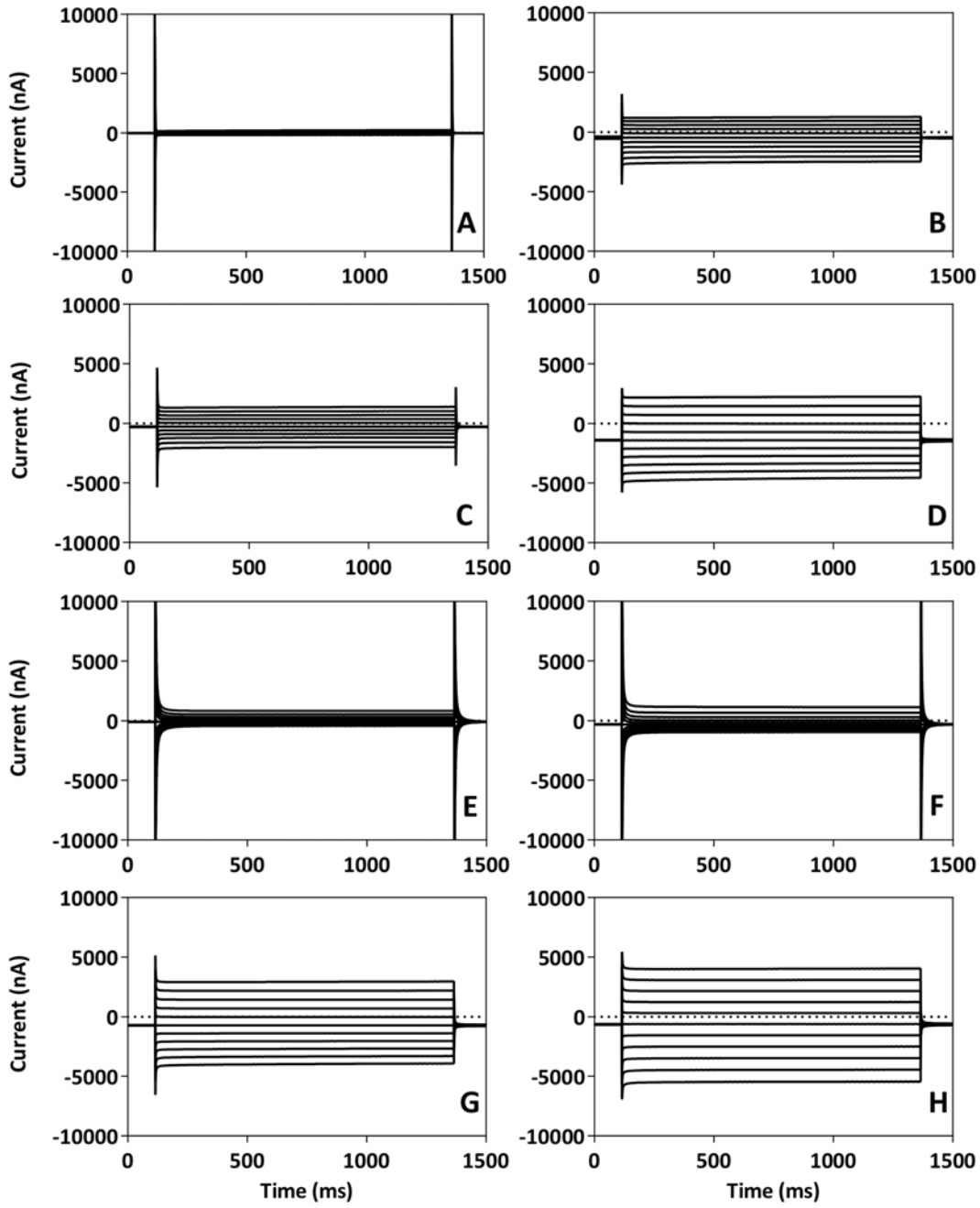

Figure 3.12: Representative currents elicited by *X. laevis* oocytes expressing *ScAMF1* cRNA or injected with H_2O in the presence of varied Ca^{2+} concentrations

Representative time dependant current profiles of oocytes (n = 1) injected with *ScAMF1* cRNA (**C, D, G, H**) or H_2O (**A, B, E, F**). Oocytes were prepared as described in Figure 3.10. Oocytes were

voltage-clamped in modified ND10 buffer (minus NaCl or KCl) with 0.2 mM $CaCl_2$ (**A, B, E. F**) or 1.8 mM $CaCl_2$ (**C, D, G, H**) plus 0 mM NH_4Cl (**A, C, E, G**) or 5 mM NH_4Cl (**B, D, F, H**).

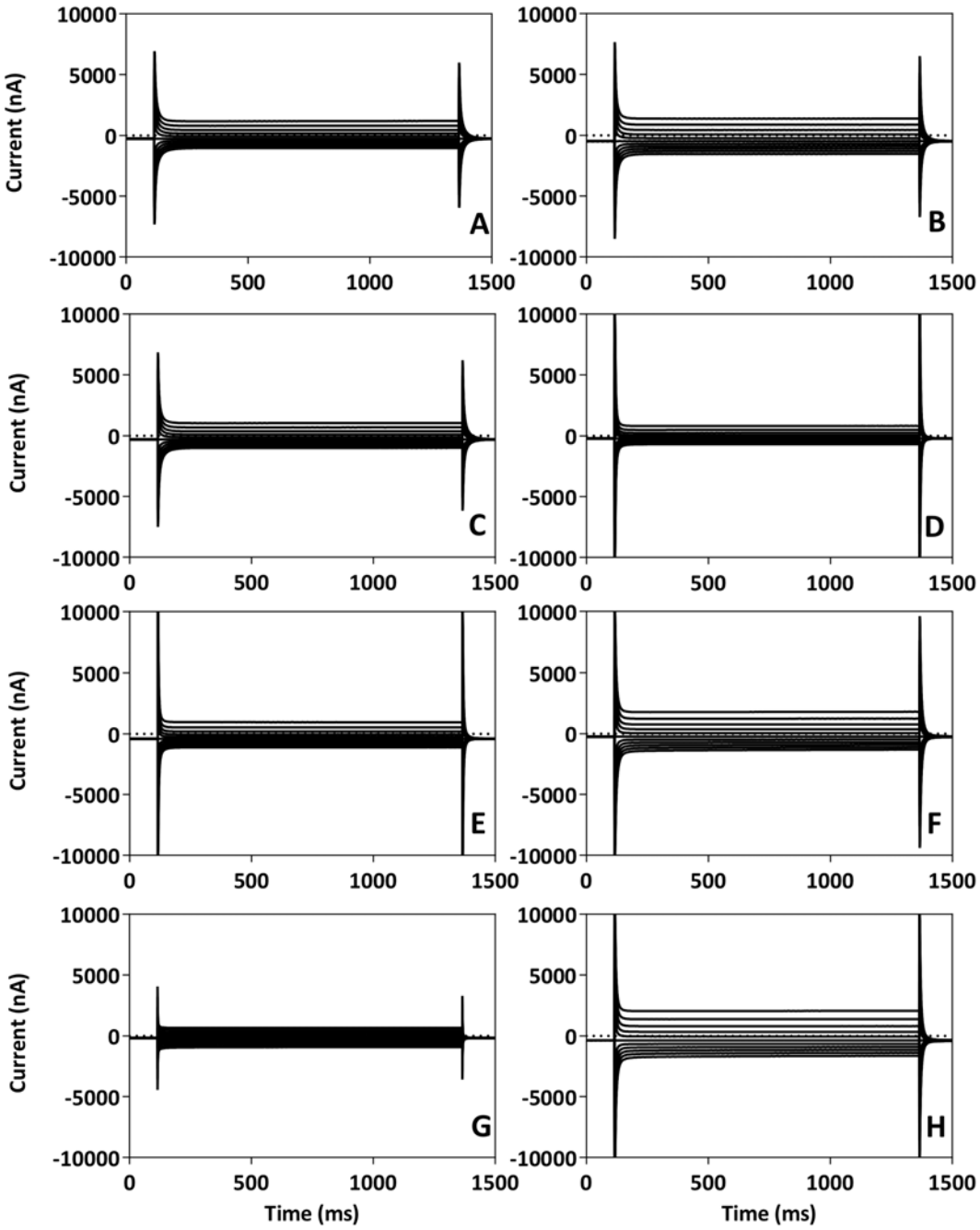

Figure 3.13: Representative currents elicited by *X. laevis* oocytes expressing *ScAMF1* or injected with H_2O in the presence of varied Ca^{2+} concentrations after P_i-preincubation

Representative time dependant current profiles of oocytes (n = 1) injected with *ScAMF1* cRNA (**C, D, G, H**) or H_2O (**A, B, E, F**). Oocytes were prepared as described in Figure 3.10 with 10 mM NaH_2PO_4 preincubation. Oocytes were voltage-clamped in modified ND10 buffer (minus NaCl or KCl) with 0.2 mM $CaCl_2$ (**A, B, E. F**) or 1.8 mM $CaCl_2$ (**C, D, G, H**) plus 0 mM NH_4Cl (**A, C, E, G**) or 5 mM NH_4Cl (**B, D, F, H**).

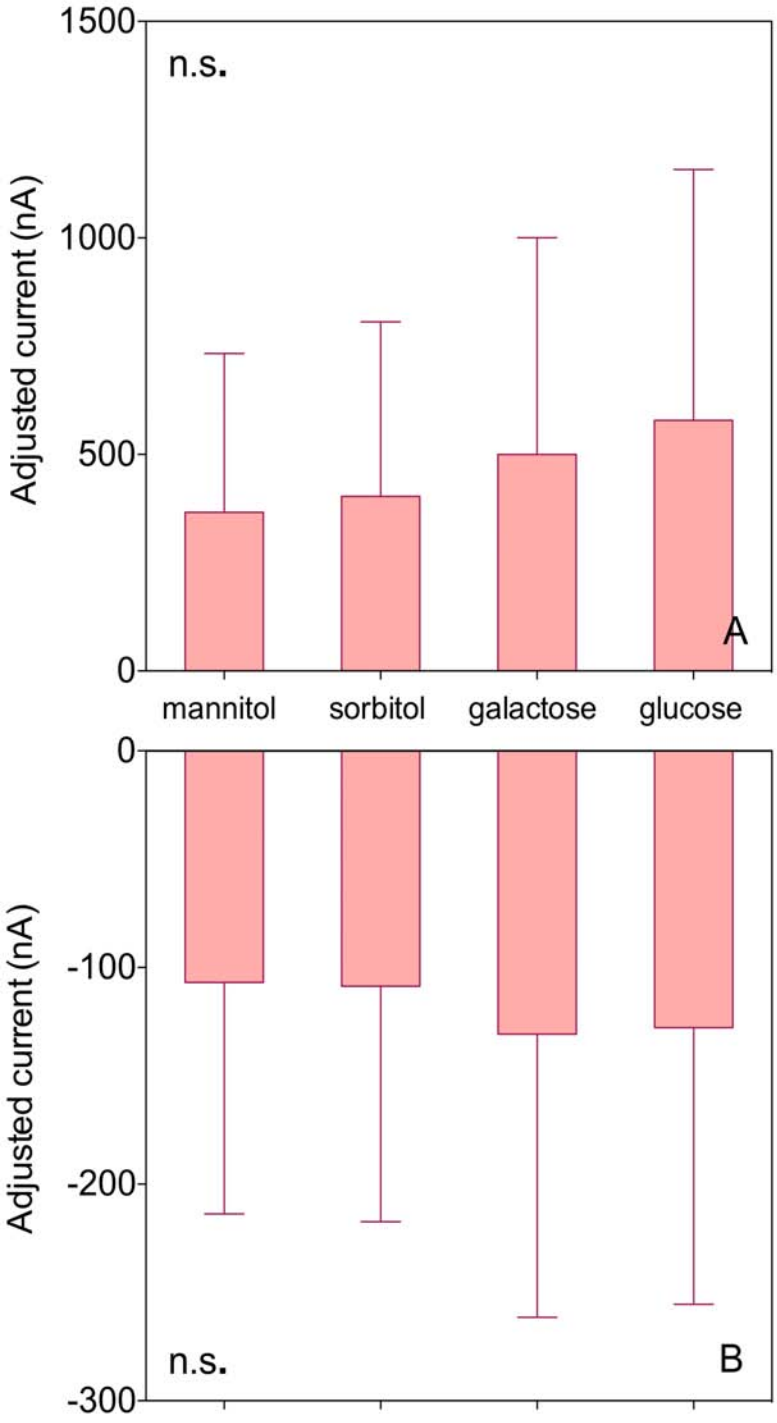

Figure 3.14: Steady state currents of *X. laevis* oocytes expressing the *ScAMF1* cRNA at -140 and +60 mV in response to different monosaccharides

X. laevis oocytes expressing *ScAMF1* or injected with an equal volume of RNase-free H_2O were

preincubated ND10 buffer for 16 h prior to Two-Electrode Voltage Clamp analysis. Analysis was carried out at room temperature in modified ND10 (1.8 mM $CaCl_2$, 1 mM $MgCl_2$, 10 mM HEPES with pH adjusted to 7.5 with Tris-base) supplemented with 200 mM mannitol, sorbitol, galactose or glucose. Data points in each experiment represent means of 4 (n = 4) oocytes ± SE. The data presented are the ScAMF1 current minus corresponding H_2O control currents taken at potentials of +60 mV and -140 mV. The adjusted currents are not significant different between sugars using the Two-way ANOVA statistical analysis ($p > 0.05$).

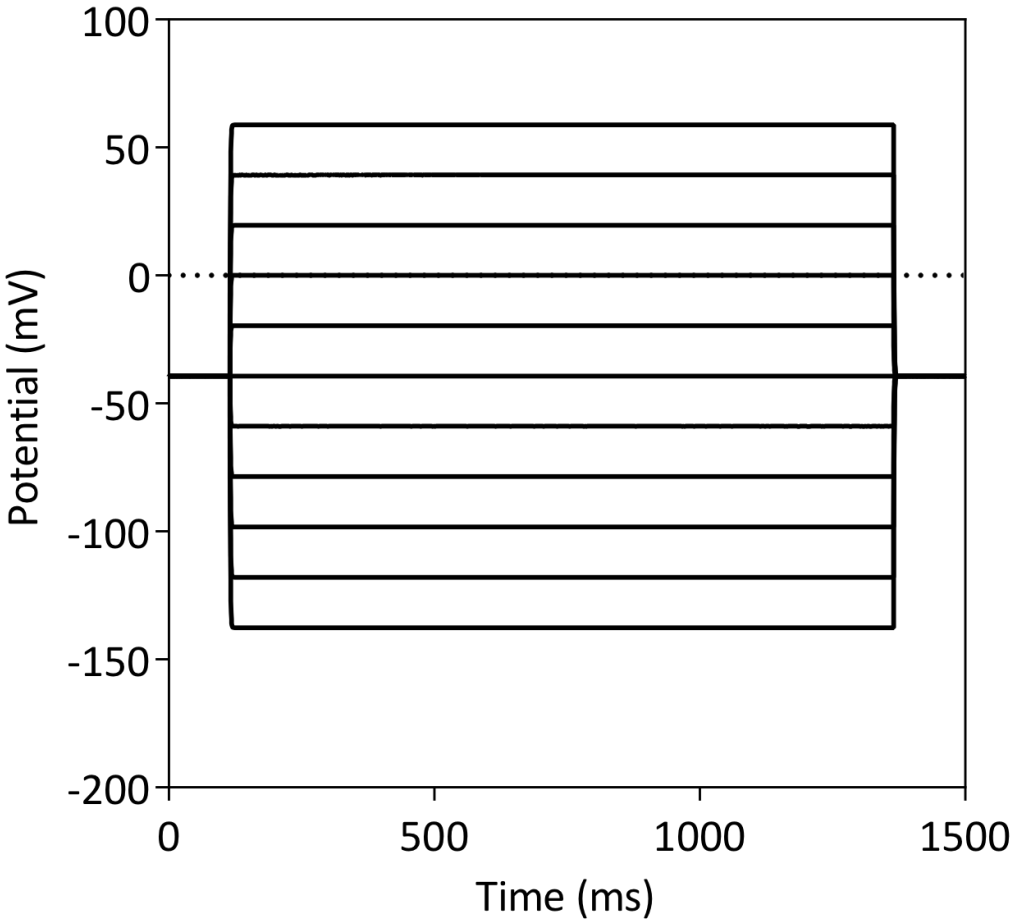

Figure 3.15: Voltage-clamp protocol

3.4 Discussion

3.4.1 ScAMF1 activity in *X. laevis* oocytes demonstrates monovalent cation non-selectivity

The chemical and electrical analysis described thus far for ScAMF1 activity in *X. laevis* oocytes has suggested the protein behaves as a NH_4^+ permeable transport protein, possessing low-affinity transport characteristics reminiscent of non-selective cation channels. ScAMF1 demonstrates increased current in response to Na^+ and K^+, which NH_4^+ decreased. This can be interpreted as ScAMF1 having a greater preference for NH_4^+ over other monovalent cations. Further in depth electrophysiological analyses are required to investigate the apparent lack of ScAMF1 monovalent cation selectivity and to define specific affinities.

3.4.2 ScAMF1 is a member of a novel class of transport proteins, capable of facilitating low-affinity NH_4^+ transport in *X. laevis* oocytes

Perfusion of ScAMF1-oocytes with a buffer with monovalent cations omitted resulted in the NH_4^+-induction of inward currents measured by TEVC recording. The transport activity is linear for NH_4^+-stimulated inward current over a concentration range of 0.5 mM to 5 mM. It is believed that the current is carried by NH_4^+ influx as the reversal potentials shift positive with increasing external NH_4^+ concentration. Like the non-selective NH_4^+ channel detected in yeast spheroplasts expressing *GmSAT1*, the amplitude of the NH_4^+

carried currents was influenced by the presence of Ca^{2+}. In this case, high Ca^{2+} did not reduce the NH_4^+ current facilitated by ScAMF1 activity in oocytes but rather enhanced transport. Again, the conductance of ScAMF1-oocytes was lower than corresponding H_2O-injected controls. The potential regulatory role of Mg^{2+} on the ScAMF1 mediated currents was not explored, as Mg^{2+} might be important for endogenous cation flux in oocytes. It is also a possibility that ScAMF1 may transport Ca^{2+} as non-selective cation channels have been reported to facilitate Ca^{2+} (Demidchik et al., 2002b). The electrical profile of ScAMF1 activity in oocytes is consistent with the NH_4^+ channel detected in the soybean SM, which does not discriminate between monovalent cations at high concentrations (Tyerman et al., 1995). However, ScAMF1 mediated NH_4^+ currents were not found to be time-dependent. As previously mentioned, the NH_4^+ channel detected in yeast spheroplasts (Kaiser et al., 1998) could be the result of multiple transport pathways influenced by GmSAT1.

3.4.3 The relationship between P_i and NH_4^+ transport through ScAMF1

As ScAMF1 is a member of the DHA2 drug efflux subfamily of MF transport proteins, it is a possibility that ScAMF1 drives the influx of NH_4^+ by coupling the transport with other ion species. A recent study using a *ScAMF1* knock-out mutant yeast strain has provided preliminary evidence that that ScAMF1 is involved in P regulation in GmSAT1-disrupted P homeostasis (Z. Holman, 2012), supporting the apparent correlation between ScAMF1-mediated NH_4^+ and inorganic phosphate (P_i) transport. Oocytes that were pre-incubated in buffers supplemented with P_i had better rates of survival. It was hypothesised that the expression of *ScAMF1* impairs the health of oocytes in ND10 buffer by facilitating the efflux of cytosolic P_i or another unknown ion. However, mortality rates were similar for H_2O-injected controls. The data suggests that pre-incubation with P_i stabilises the oocytes,

possibly through replenishment of depleted cytosolic P_i pools. Endogenous currents at negative and positive voltages were lowest when pre-incubated with NaH_2PO_4.

By changing the P_i concentration gradient across the PM of ScAMF1-oocytes, I have demonstrated that NH_4^+ driven currents are greater when the gradient favours P_i efflux (oocytes pre-incubated in 10 mM P_i and 0 mM P_i in voltage-clamping buffer), producing an even greater NH_4^+ carried current. The conductance of ScAMF1-oocytes exposed to various NH_4^+ concentrations was greater than H_2O-injected controls when oocytes were pre-incubated with P_i, suggestive of outward movement of P_i. The current previously observed in H_2O controls is absent with P_i pre-incubation. Furthermore, the conductance of ScAMF1 mediated NH_4^+ currents (minus corresponding H_2O-controls), was greater when oocytes were pre-incubated with 10 mM P_i compared to 0 mM P_i. In ScAMF1-oocytes, the current is not carried by P_i or by NH_4^+ when treated with external P_i, suggesting that such conditions do not favor the outward movement of P_i and that ScAMF1 operates as an exchanger, mediating the outward movement of P_i to drive the inward movement of NH_4^+ into oocytes. It is also a possibility the supplementation of P_i to the pre-incubation buffer improves the endogenous cytosolic ion homeostasis perturbed by ScAMF1 activity. Unfortunately, how P_i impacts these currents cannot be ascertained from the electrophysical data alone. As oocytes were pre-incubated and not directly injected with P_i prior to TEVC analysis, it cannot be assumed that oocytes expressing *ScAMF1* cRNA have accumulated P_i and that the efflux P_i accounts for the change in observed currents. Alternatively, P metabolism of ScAMF1-oocytes may have been influenced by external P. Products of P metabolism, such as ATP, ADP, AMP or pyrophosphate, may directly or indirectly attribute to the change in current. In subsequent research, ^{32}P flux analysis would need to be carried out to investigate potential P_i efflux from oocytes expressing *ScAMF1*.

3.4.4 Potential endogenous substrates of AMF1 proteins

ScAMF1 shares limited sequence identity with vertebrate SPINSTER-like (SPIN1) major facilitator efflux proteins, which have been implicated in monosaccharide transport. In *Drosophila melanogaster* (fruit fly), these proteins are predicted to be carbohydrate permeases integral to lysosomes (Rong et al., 2011). *In planta* analysis, performed in parallel to this study, provides preliminary evidence linking *Arabidopsis AMF1* homologs and carbon transport, where knock-outs of single *AMF1* genes results in enhanced total carbon accumulation (A. Situmorang, 2012). Central to the rhizobial symbiosis is the exchange of host-reduced carbon for reduced nitrogen (NH_4^+), to provide energy for the symbiont bacteria. However, *ScAMF1* expression in oocytes did not elicit any difference in current in response to the different monosaccharides analysed.

AMF1 homologs exist in many plants, and in particular a soybean homolog is highly expressed in symbiotic root nodules, implicating AMF1 in symbiotic transport processes (D. Chiasson, 2012). As ScAMF1 is a member of the MFS transport proteins, it is a possibility that *AMF1* homologs *in planta* also possess NH_4^+, K^+ and Na^+ transport characteristics, as such proteins have been shown to possess a functional overlap (Paulsen et al., 1996). It is also a possibility that ScAMF1 activity reflects a direct role for AMF1 homolgs to *in planta* P homeostasis. The PHT, a P_i MF transport protein, operating in plants shares homology with the yeast PHS symporters (Paulsen et al., 1996; Nagy et al., 2005; Bucher, 2007).

Chapter 4 Functional analysis of soybean and *Arabidopsis* AMF1 homologs in yeast and *Xenopus laevis* oocyte expression systems

4.1 Introduction

4.1.1 Detection of NH_4^+ channel activity in the legume symbiotic membrane

Although the genetic identity of the soybean symbiosome NH_4^+ transport protein remains to be determined, patch-clamp analysis of soybean symbiosomes has detected a voltage-gated non-selective cation channel selectively permeable to NH_4^+ (K_M 37.50 mM) (Tyerman et al., 1995; Obermeyer and Tyerman, 2005). Similar currents were detected in the SM of *Pisum sativum* (pea) and *Lotus japonicus* (Mouritzen and Rosendahl, 1997; Roberts and Tyerman, 2002). Homologs of ScAMF1 have been identified in most sequenced dicots (D. Chiasson, 2012). In soybean nodules, GmSAT1 may have a role in regulating a protein similar to ScAMF1, which may transport NH_4^+ across the symbiosome. It is also possible that AMF1 proteins have a role in low-affinity NH_4^+ transport in plants.

4.1.2 Legume major facilitator proteins involved in the transport of nutrients between symbionts

The channel(s) elicited by the heterologous expression of *GmSAT1* in yeast, show electrophysiological similarities to the NH_4^+ channel detected in the endogenous SM (Kaiser et al., 1998). The research described in Chapters 2 & 3, reveals that GmSAT1 enhances the transcription of ScAMF1, a novel MF protein, which mediates the low-affinity transport of NH_4^+ and MA across the PM of yeast and *X. laevis* oocytes, respectively. To date, putative MF proteins have been identified in legume nodules, which include LjN70 and GmN70 (Szczyglowski et al., 1998; Vincill et al., 2005). These transporters are believed capable of mediating the flux of anions into the symbiosome with a preference for nitrate. It has been suggested that these transport proteins might have roles in the regulation of ion and pH gradients in response to nitrate levels in the soil, and in osmoregulation and cytosolic ion homeostasis (Vincill et al., 2005).

4.1.3 Soybean AMF1 orthologs

Analysis of the recently sequenced soybean genome revealed 978 transporters, with 278 being classified as MFS members (D. Chiasson, 2012). Phylogenetic analysis has identified homologs of *ScAMF1* amongst the identified soybean MF transporters. These MFS proteins have 20-30% similarity to ScAMF1 and are present in most sequenced dicots and monocot species, including *Medicago*, lotus, grapevine, maize, rice and poplar (D. Chiasson, 2012). A representative member from soybean, *GmAMF1;3* (*Glyma08g06880*), was cloned in an attempt to clarify a potential role of AMF1 proteins in symbiotic or other cellular NH_4^+ transport pathways (D. Chiasson, 2012). *GmAMF1;3* shows elevated expression in N-fixing root nodules compared to other tissues including roots, leaves and stems (D. Chiasson, 2012). As MF proteins have been shown to facilitate

the movement of a range of biological substrates differing by specificity (Paulsen et al., 1996), a functional analysis of GmAMF1;3 was undertaken, with the aim to shed light on its potential NH_4^+ transport properties and its relationship to previously described symbiosome membrane NH_4^+ channels (Tyerman et al., 1995; Obermeyer and Tyerman, 2005; Roberts and Tyerman, 2002).

It is critical that the genetic identity of the symbiotic NH_4^+ transport protein is established in order to advance our understanding of the complex nutrient exchange between symbiont bacteria and legume hosts. The characterisation of ScAMF1, as described in Chapter 3, serves as a starting point for the characterisation of homologous proteins that have been identified in plant species. The analysis of ScAMF1 activity in the *X. laevis* oocyte expression system showed that ScAMF1 catalyses low-affinity NH_4^+ transport. Given the similarities between native and heterologous GmSAT1-elicited current activity, and the NH_4^+ transport capability of ScAMF1, it is possible that ScAMF1 shares functionality with homologous soybean proteins.

4.1.4 *Arabidopsis* AMF1 orthologs

Arabidopsis thaliana, a member of the mustard (*Brassicaceae*) family, is a common used model for molecular and physiological plant research. In the context of NH_4^+ transport processes, *Arabidopsis* has been used extensively for the *in planta* characterisation of the high-affinity NH_4^+ transporter family, AMT. With this in mind a project was developed to explore the transport properties of putative *Arabidopsis* AMF1 proteins and to use *Arabidopsis* as a tool to define functional relevance of the channel to plant growth and development. The availability of the entire *Arabidopsis* genome sequence has allowed for the *in silico* identification of 137 predicted genes encoding putative MF proteins (D. Chiasson, 2012). To date, the transport properties of 25 putative *Arabidopsis* MF proteins

have been partially characterised. These include a TMT-tonoplast monosaccharide transporter (Wormit et al., 2006), AtPMT-polyol/monosaccharide transporter (Klepek et al., 2005; Reinders et al., 2005), AtSUC-sucrose:H^+ symporter (Srivastava et al., 2008) and STP-sugar transporter (Sauer et al., 1990). In *Arabidopsis*, three proteins At5g64500, At5g65687 and At2g22730 (here on referred to as AtAMF1;1, AtAMF1;2 and AtAMF1;3, respectively), were found to have high sequence similarity with the yeast and soybean AMF1 homologs (D. Chiasson, 2012).

4.1.5 NH_4^+ transport mechanisms operating in plants

Physiological analyses have discovered two distinct NH_4^+ transport mechanisms operating in higher plants. In *Arabidopsis*, high-affinity NH_4^+ transport (HATS) is mediated by a coordinated effort of AMT transport proteins (*AtAMT1;1*, *AtAMT1;2*, *AtAMT1;3* and *AtAMT2;1*) that are active at external NH_4^+ concentrations 0.5 mM and less (Yuan et al., 2007). At high external NH_4^+ concentrations, a low-affinity transport system (LATS) is the prevailing means of NH_4^+ uptake, presenting unsaturable kinetics (Wang et al., 1993; Kronzucker, 1996; Glass et al., 2002). However, the genetic basis for LATS flux has not been identified. As ScAMF1 has been shown to have a low affinity for NH_4^+ in yeast and *X. laevis* oocytes, the AMF1 proteins may have a role in the low-affinity flux of NH_4^+ across biological membranes in plants. We hypothesize that *Arabidopsis* AMF1 homologs are also capable of facilitating the transport of NH_4^+. These proteins may have a role in the low-affinity flux of NH_4^+ across biological membranes in plants, which may have a role in NH_4^+ uptake into root cells or remobilization or recovery of NH_4^+.

Described in this chapter are preliminary experiments investigating NH_4^+ and MA transport activities of the soybean and *Arabidopsis* AMF1 homologs by heterologous expression in NH_4^+ transport mutant yeast strains and *X. laevis* oocytes. The putative

Arabidopsis AMF1 homologs, *AtAMF1;1 and AtAMF1;2,* were cloned. Using an electrophysiological profile generated for yeast AMF1 activity in oocytes, the putative NH_4^+ transport activities of GmAMF1;3, AtAMF1;1 and AtAMF1;2 homologs were defined by Two-Electrode Voltage Clamp analysis. This provided a preliminary electrophysiological profile of the *Arabidopsis* and soybean AMF1 homologs with respect to NH_4^+ transport that future studies can explore in further detail. The results suggest that GmAMF1;3 behaves as a non-selective cation channel capable of low-affinity NH_4^+ transport, concurrent with the functional analysis of the yeast homolog in these systems.

4.2 Methods and Materials

4.2.1 Functional analysis of GmAMF1;3

4.2.1.1 Soybean growth and cDNA library synthesis

Soybeans were planted in Waikerie sand (ten seeds per 10 cm diameter pot) and inoculated with *Bradyrhizobium japonicum* USDA110 on the day of planting and again the following day (100 ml of a 1/10 dilution of a late log phase culture). Plants were grown in a glasshouse and watered daily, substituting N-free Herridge's nutrient solution (Herridge, 1982) three times per week. Nodules were collected from roots and frozen in liquid nitrogen. Total RNA was extracted from nodules with the RNeasy kit (Qiagen) according to the manufacturers protocol, and cDNA was synthesized from 1.25 μg of total RNA using Superscript III Reverse Transcriptase (Invitrogen).

4.2.1.2 Cloning *GmAMF1;3* CDS

The *GmAMF1;3* CDS was cloned from a 28 day-old N-fixing soybean nodule cDNA library. Initially, primers (GmAMF1;3 CDS F and R; Table 4.1) were designed to clone *GmAMF1;3* based on the Phytozome genome prediction method (http://www.phytozome.net). However, the primer set was unsuccessful in amplifying a product. Based on sequence alignments, it was found that an exon was potentially missing in the online genome annotation. Therefore, the GmAMF1;3 CDS R3 primer (Table 41.)

was synthesized, which in conjunction with the GmAMF1;3 CDS F primer, successfully amplified a full-length product with Platinum Taq High Fidelity (Invitrogen). The PCR conditions were as follows: 35 cycles of 94°C for 30 s, 55°C for 30 s and 68°C for 1.5 min, followed by a final extension at 68°C for 5 min. The full-length product was then inserted into the *pCR8/GW/TOPO* donor vector as described in Chapter 2, but upon transformation into the TOP10 *E. coli* strain (Invitrogen) few colonies were observed after 16 h at 37°C. Sequencing of isolated plasmids showed that mutations had occurred in the *GmAMF1;3* CDS. Therefore, the *pCR8/GW/TOPO* reaction was transformed into the XL1-Blue *E. coli* strain (Stratagene) and grown at room temperature on LB media containing a reduced concentration of NaCl (5 g L^{-1}). After 4 days growth, numerous colonies appeared. Plasmids were isolated from multiple colonies and sequenced to ensure mutation-free inserts.

4.2.2 Functional analysis of AtAMF1;1 and AtAMF1;2

4.2.2.1 *Arabidopsis thaliana* growth and cDNA library synthesis

Arabidopsis thaliana (ecotype Columbia *gl1*) seeds were scattered on the surface of soil (1 part vermiculite, 1 part peat moss and 2 parts soil) in 10 cm diameter pots. Seeds were vernalised at 4°C for 6 days under a plastic wrap to create a humid environment. The pots were transferred to a growth chamber. After 3-4 days, the plastic covering was pierced to reduce the humidity, and another 2 days later the plastic was removed. Plants were grown under a day/night regime (11 h light / 13 h dark) under fluorescent lights (230 $\mu mole.m^{-2}.s^{-1}$) and at 25°C/22°C day/night temperatures. Plants were grown for approximately 4 weeks before harvesting (roots and shoots separately) and freezing in liquid nitrogen for RNA extraction at a later date.

Total RNA was extracted from 200 mg of root tissue collected from four combined *Arabidopsis* plants by adding 1 ml of Trizol® (Life Technologies, USA) reagent and vortexing for 1 min at room temperature, followed by a 5 min incubation period. The aqueous phase containing the RNA was separated by centrifugation for 5 min at 14,000 *g* at 4°C. The aqueous phase was re-separated with another 1 ml of Trizol® reagent. The aqueous phase was then re-extracted twice with 500 µl of chloroform, vortexed briefly and centrifuged for 5 min at 14,000 *g* at 4°C. Total RNA was precipitated with ethanol and 3 M sodium acetate (pH 5.3), and incubated at -80°C for 30 min before centrifugation for 5 min at 14,000 *g* at 4°C. The RNA pellet was washed with 1 ml of 70% (v/v) ice-cold ethanol and resuspended in 50 µl of ice-cold 0.1% (v/v) DEPC treated Milli-Q H_2O. The extracted total RNA (2 µg) was treated with TURBO DNase to remove residual genomic DNA contamination according to the TURBO DNA-free™ kit protocol (Ambion). Total RNA (1 µg) was converted to cDNA using Superscript III Reverse Transcriptase (Invitrogen).

4.2.2.2 Cloning *Arabidopsis AMF1* homologs

The TAIR database (www.arabidopsis.org) was used to design primers (Table 4.1) to amplify the predicted complete coding sequences of *At5g64500* (*AtAMF1;1*), *At5g65687* (*AtAMF1;2*) and *At2g22730* (*AtAMF1;3*). The genes were cloned from whole plant cDNA using High Fidelity Phusion DNA polymerase (Finnzymes, Finland) and the following PCR conditions: 35 cycles of 94°C for 30 s, 55°C for 30 s and 68°C for 1.5 min, followed by a final extension at 68°C for 5 min. The amplified *Arabidopsis AMF1* CDS were inserted into the *pCR8/GW/TOPO* donor vector and transformed into XL-Blue (Stratagene) or TOP10 (Invitrogen) *E. coli* strains, which were propagated as described for *GmAMF1;3* to avoid potential mutations.

4.2.3 Functional characterisation of soybean and *Arabidopsis* AMF1 homologs in yeast

4.2.3.1 Subcloning *AMF1* homologs into *pYES3-DEST* yeast expression vector

The *GmAMF1;3*, *AtAMF1;1* and *AtAMF1;2* inserts were recombined into the *pYES3-DEST* by *LR Clonase* II according to manufacturer's protocol (Invitrogen), and positive clones in the correct orientation were selected by restriction enzyme analysis and sequenced as described in Chapter 2.

4.2.3.2 Transformation of *pYES3-GmAMF1;3, pYES3-AtAMF1;1* and *pYES3-AtAMF1;2* into yeast

The *pYES3-DEST* yeast expression plasmids harbouring *GmAMF1;3*, *AtAMF1;1* and *AtAMF1;2* were introduced into the NH_4^+ mutant yeast strains using the transformation method described in Chapter 2.

4.2.3.3 Phenotypic analysis of AMF1 homologs in yeast

Cultures for spot plates were prepared as described in Chapter 2. Washed yeast solutions were diluted to an OD_{600nm} of 0.6, and a 10-fold dilution series was spotted out in 5 µl aliquots onto solid basal growth media (Grenson, 1966) supplemented with 2% (w/v) Glu or Gal plus 0.1 M MA or 1 mM NH_4Cl.

4.2.3.4 ^{14}C-methylammonium yeast flux experiments

As described in Chapter 2, ^{14}C-MA uptake experiments were carried on cultures of 26972c or 31019b cells harbouring the *pYES3-DEST* empty vector, *pYES3-GmSAT1* or *pYES3-GmAMF1;3*, *pYES3-AtAMF1;1* or *pYES3-AtAMF1;2*.

4.2.3.5 Stopped flow spectrophotometry

To gain further insight into the NH_4^+ transport capacity of plant AMF1 homologs, the osmotic response of yeast spheroplasts overexpressing *GmAMF1;3*, *AtAMF1;1* or *AtAMF1;2* was observed. The expression of plant *AMF1* homologs were induced and spheroplasts were prepared as described in Chapter 2. The spheroplasts were resuspended in osmotic buffer to a uniform $OD_{475\ nm}$ 0.5 (*AtAMF1;1* and *AtAMF1;2* spheroplasts) or 1.0 (*GmAMF1;3* spheroplasts). As the osmotic response was great for the soybean AMF1 homolog, diluted suspensions of AtAMF1 spheroplasts were analysed. The spheroplasts suspensions were mixed in a fast kinetics stopped flow spectrophotometer (SFM-300, Biologic) with an equal volume of resuspension solution. Volume changes were recorded at 16°C as light scattering at an angle 90° and 475 nm. The kinetics presented are the averages of 6-9 trace recordings each over a period of 3 s.

4.2.4 *In planta* analysis

4.2.4.1 Localisation of GmAMF1;3 in onion epidermal cells

The *pCR8/GW/TOPO-GmAMF1;3* was recombined into the *pYFP-attr* plasmid (Figure 4.6 A) by *LR Clonase* II (Invitrogen), transformed into XL-Blue *E. coli* (Stratagene), and positive clones were selected as previously described. The plasmid drives

the expression of N-terminal *YFP::GmAMF1;3* fusion under the control of the cauliflower mosaic virus (CaMV) *35S* promoter. The *pCD3-1007* plasmid, which drives the expression of C-terminal mCherry AtPIP2;1 (known PM marker) fusion, was created by digesting *PM-RK CD3-1007* (Nelson et al., 2007) with *Sac* I and *Eco* RI and inserting the fragment into *pBluescript* plasmid (Figure 4.6 B). The *pYFP-GmAMF1;3* and *pCD3-1007* plasmids were co-precipitated (total 5 μg in 10 μl) onto 1.5 mg of 0.6 μm gold macrocarriers (Bio-Rad) in a 50% glycerol suspension. Onion epidermal peels were bombarded with gold particles using a PDS-1000/He particle delivery system (Bio-Rad) with a 1100 psi Rupture Disc. Epidermal peels were maintained on Murashige and Skoog basal medium with vitamins (Austratec, Australia) supplemented with 120 g L^{-1} sucrose, 500 mg L^{-1} tryptone and 9 g L^{-1} tissue culture grade agar (Austratec, Australia). After bombardment, the peels were incubated in the dark for 24 h at room temperature before viewing. Images were obtained using a Zeiss LSM 5 Pascal confocal microscope (Zeiss, Oberkochen, Germany). The YFP fluorescence was monitored by excitation at 515 nm with an argon laser combined with a 535-580 nm bandpass filter, while the mCherry fluorescence was obtained by excitation at 543 nm with a helium/neon laser combined with 615 nm longpass filter. Images were captured and further analysed using the LSM Pascal 5.0 software suite (Zeiss, Oberkochen, Germany).

4.2.2.2 Localisation of AtAMF1;1 and AtAMF1;2 in onion epidermis

4.2.4.2.1 Ligation of *AtAMF1;1* and *AtAMF1;2* into the *pAVA554* plasmid

Primers were designed to amplify *AtAMF1;1* and *AtAMF1;2* (both genes are approximately 1.5 kb) from 4-week old *Arabidopsis* root cDNA with Phusion polymerase (Finnzymes, Finland) and the following cycling conditions were 35 cycles of 98°C for 10 s,

55°C for 10 s, and 72°C for 30 s, followed by a final extension at 72°C for 5 min. PCR fragments were purified using the GenElute PCR Clean-up kit (Sigma-Aldrich) according to manufactures protocol. The fragments were ligated into the *pAVA554* plasmid downstream of a *35S* promoter to drive C-terminal e*YFP::AtAMF1* expression. The PCR fragments and *pAVA554* plasmid (Figure 4.19) were digested with *Nco* I restriction enzyme. The *pAVA554* plasmid was subsequently treated with *calf intestinal alkaline phosphates* (NEB, USA) to remove 5' phosphate groups, which could promote re-circularisation of the linearised plasmid. Again, PCR fragments and plasmid were purified as before. Each PCR fragment was ligated with the linearised plasmid with *T4* ligase (2:1 ratio of insert (1.5 kb) to plasmid ratio (4.79 kb)). The ligase reactions were incubated at room temperature for approximately 20 min, before transformation into XL-Blue *E. coli* (Stratagene), which were propagated on reduced salt LB media supplemented with 100 μg ml^{-1} ampicillin at 28°C for 2-3 days. Positive clones in the correct orientation were selected by restriction enzyme analysis and sequenced as described in Chapter 2.

As described previously, *pAVA554-AtAMF1;1* or *pAVA554-AtAMF1;2* plasmid was co-precipitated with *AtRop11::eCFP* plasmid, a known PM marker, onto gold macrocarriers (Bio-Rad) and bombarded into onion (*Allum cepa*) epidermal cells as previously described. After bombardment, the peels were transferred to Murashige and Skoog basal medium with vitamins (*Phyto*Technology, USA), and supplemented with 30 g L^{-1} sucrose, 500 mg L^{-1} tryptone and 4 g L^{-1} GelRite agar (*Phyto*Technology, USA), pH adjusted to 5.85, to aide recovery. Bombarded cells were incubated in the dark for 24 h at room temperature before viewing. Images were obtained using a Zeiss LSM 5 Pascal confocal microscope (Zeiss, Oberkochen, Germany). The eYFP fluorescence was monitored as previously described, while the eCFP fluorescence was obtained by excitation at 405 nm with an argon laser combined with 450-490 nm bandpass filter.

Images were captured and further analysed using the LSM Pascal 5.0 software suite (Zeiss, Oberkochen, Germany).

4.2.3 *X. laevis* oocyte experiments

4.2.3.1 Subcloning *GmAMF1;3, AtAMF1;1* and *AtAMF1;2* into the *X. laevis* oocyte expression vector *pGEMHE-DEST*

The *GmAMF1;3*, *AtAMF1;1* or *AtAMF1;2* inserts in the *pCR8/GW/TOPO* plasmids were recombined into the *pGEMHE-DEST* by *LR Clonase* II according to manufacturer's protocol (Invitrogen), and positive clones in the correct orientation were selected by restriction enzyme analysis and sequenced as described in Chapter 3.

4.2.3.2 Synthesis of *GmAMF1;3, AtAMF1;1* and *AtAMF1;2* cRNA and injection into *X. laevis* oocytes

The *pGEMHE-GmAMF1;3*, *pGEMHE-AtAMF1;1* and *pGEMHE-AtAMF1;2* plasmids were linearised with *Nhe* I for 1 h at 37°C. The linearised template was prepared for cRNA synthesis as described in Chapter 3. The cRNA synthesis was carried out using the cleaned linearised plasmid as a template according to the mMESSAGE mMACHINE® *T7* Kit (Ambion) protocol. Quality and quantity of the synthesised cRNA was assessed by gel electrophoresis and Quant-iT RiboGreen RNA assay (Invitrogen) as described in Chapter 3, diluting the cRNA to a uniform concentration of 500 ng μl^{-1}. The cRNA aliquots were stored at -80°C until required for injection into oocytes.

4.2.3.3 *X. laevis* electrophysiology

Oocyte harvests, and preparation of injection pipettes and electrodes were performed as described in Chapter 3. Individual healthy oocytes were injected with 46 nl (23 ng) of cRNA or 46 nl of nuclease-free Milli-Q H_2O and incubated for 1 - 2 days at 18°C in ND10 solution with or without 10 mM PO_4^{3-} supplemented with 8% (w/v) horse serum, 100 µg ml^{-1} tetracycline, 1000 U ml^{-1} penicillin and 100 µg ml^{-1} streptomycin. Two-electrode voltage clamp experiments were performed at room temperature in modified ND10 voltage-clamping buffer (without horse serum or antibiotics) plus supplements (See Figure legends for details of modified voltage-clamping buffers and supplements analysed) as described in Chapter 3 (Figure 3.15).

4.2.4 Data Analysis

Mean currents were graphed with standard errors using Prism GraphPad Version 5.0d (GraphPad inc.). The degree of significance with respect to NH_4^+ activated currents (denoted a), corresponding H_2O-injected controls (denoted b) and P_i-preincubation or Ca^{2+} concentration (denoted c) was assessed using Two-way ANOVA analysis where P-values less than 0.05 were considered significantly different.

4.2.3.5 Bioinformatics

Phylogenetic analysis of soybean, and *Arabidopsis* MF transporter proteins sequences was performed with the neighbour-joining tree method, using the Jukes-Cantor distance model (Geneious® V 5.6 software Biomatters Ltd). Scale represents the number of amino acid substitutions per site.

Multiple amino acid sequence alignments were generated with MUSCLE algorithm using the neighbour joining clustering method (Geneious® V 5.6 software Biomatters Ltd). The hydropathy plot for ScAMF1 was calculated using the Kyte/Doolittle algorithm with a window size of 19 (web.espy.org/protscale/).

4.3 Results

4.3.1 Cloning of *GmAMF1;3*

Initially, a primer set was designed to clone *Glyma08g06880* (*GmAMF1;3*) based on the Phytozome (http://www.phytozome.net) genome prediction however a product could not be amplified. Based on sequence alignments to the other MFS members, it was found that there could be a missing exon in the genome annotation. Therefore, the downstream genomic sequence of *GmAMF1;3* was searched for potential exons. A candidate was found, and a new primer was created and used to successfully amplify a full-length product. The final sequence encodes for a protein of 537 amino acids with a predicted molecular weight of 58.30 kDa, and shares 10.5% identity with ScAMF1 (Figure 4.1).

4.3.2 Soybean and *Arabidopsis* AMF1 family

Comparative sequence analysis using the cloned *ScAMF1* CDS was conducted to identify related proteins in plants. This led to the identification of GmAMF1;3, which in turn revealed a novel group transporters belonging to the major facilitator superfamily. In legumes, the MF proteins sharing most similarity with GmAMF1;3 are GmAMF1;1 (Glyma13g32670), GmAMF1;2 (Glyma07g30370) and GmAMF1;4 (Glyma15g06660), ranging from 93.6% to 57.9% overall identity (Figure 4.2). Initially, *GmAMF1;5* (*Glyma09g33680*) was overlooked because of incorrect sequence prediction but was revisited after it was identified as being downregulated in *GmSAT1* RNAi microarray

experiments (D. Chiasson, 2012). Again, a BLAST search was conducted to find related proteins in *Arabidopsis* revealing three proteins (At2g22730, At5g64500, and At5g65687) having 16-14% or 65-53% amino acid identity with ScAMF1 (Figure 4.3). Further comparative analysis revealed that At5g64500 is most similar to legume proteins, while At2g22730 and At5g65687 share the most similarity (D. Chiasson, 2012). Subsequent BLAST analysis revealed that ScAMF1 and GmAMF1;3 proteins share 9-11% and 13-16% homology, respectively, with MF proteins belonging to the *Arabidopsis* PHT P_i transporter subfamily and vertebrate SPINSTER sugar transporters (Figure 4.4). After constructing a phylogenetic tree based on amino acid differences revealed a number of clusters. AtAMF1;1 and GmAMF1;5 formed a cluster with a subcluster comprised of GmAMF1;1, GmAMF1;4, and GmAMF1;2. A second cluster contained AtAMF1;3, and AtAMF1;2 with DmSPIN1, whilst representative AtPHT proteins and ScAMF1 forming a distinct branches (Figure 4.5).

4.3.3 Cellular localisation of GmAMF1;3 protein in onion epidermal cells

Based on the Kyte/Doolittle hydrophilicity protocol (web.espy.org/protscale/), GmAMF1;3 is predicted to contain 12 transmembrane domains (Figure 4.6). In a parallel study, D. Chiasson (2012) showed that GmAMF1;3 is localised in the PM of onion epidermal cells. In order to assess the localisation of GmAMF1;3, it was subcloned into the expression plasmid *pYFP-attr* (Subramanian et al., 2006). The *pYFP-attr* plasmid contains a double copy of the *35SCamV* (*2x35S*) promoter, driving a N-terminal YFP fusion to a protein of interest (Figure 4.7 A). The *pYFP::GmAMF1;3* plasmid was precipitated onto gold particles and bombarded into onion epidermal peels. After initial assessments of localization, the *pYFP-GmAMF1;3* plasmid was co-precipitated with the *pDC3-1007* plasmid, which contains a *2x35S* driven C-terminal mCherry fusion to the AtPIP2;1

(aquaporin) to serves as a known PM marker (Figure 4.7 B). After observing the co-bombarded tissues, it was found that GmAMF1;3 (Figure 4.8 A) co-localised with AtPIP2;1 (Figure 4.8 B) to the PM.

4.3.4 Preliminary analysis of NH_4^+ transport of GmAMF1;3 in yeast

Since ScAMF1 was shown to transport ^{14}C-MA into yeast and induce swelling of yeast spheroplasts in the presence of MA and NH_4^+, *GmAMF1;3* was subcloned into the yeast expression vector *pYES3-DEST* (D. Chiasson, 2012). In this study, overexpression of *GmAMF1;3* cells established a MA sensitivity phenotype in 26972c cells (Figure 4.9) and was unable to complement the disrupted high-affinity MEP transport system on 1 mM NH_4^+ (Figure 4.10). *GmAMF1;3* expression significantly ($p<0.05$) enhanced the ability of the NH_4^+ mutant yeast strains to accumulate 1 mM ^{14}C-MA relative to empty *pYES3-DEST* vector transformed control cells (Figure 4.11). Osmotic changes in GmAMF1;3 yeast spheroplasts, as a function of light scattering at 475 nm over time, indicated swelling in the presence of compatible buffer supplemented with 0.5 mM MA (Figure 4.12 A) or 5 mM NH_4^+ that was not observed for control spheroplasts harbouring *pYES3-DEST* (Figure 4.12 B).

4.3.5 Heterologous expression of *GmAMF1;3* in the *X. laevis* oocyte expression system

As there was no apparent NH_4^+ complementation phenotype associated with GmAMF1;3 activity in NH_4^+ defective yeast apart from transient swelling of GmAMF1;3-spheroplasts in the presence of 5 mM NH_4^+, putative low-affinity NH_4^+ transport capabilities were assessed in *X. laevis* oocytes by TEVC analysis. The electrophysiological profile of ScAMF1, presented in Chapter 3 has helped to serve as a guide for the preliminary characterisation of GmAMF1;3. Oocytes injected with *GmAMF1;3* cRNA were compared

to H_2O-injected controls for their ability to transport NH_4^+ in a series of different voltage-clamping buffers.

4.3.6 The NH_4^+-stimulated currents in *GmAMF1;3* cRNA injected oocytes

4.3.6.1 External Ca^{2+} and P_i on NH_4^+ currents in oocytes expressing *GmAMF1;3* cRNA

A non-selective NH_4^+ channel previously detected in soybean symbiosome membranes was gated by divalent cations including Ca^{2+} and Mg^{2+} (Tyerman et al., 1995). We tested for the impact of Ca^{2+} on GmAMF1;3 mediated currents in *X. laevis* oocytes. Currents were analysed without monovalent cations and with 5 mM NH_4^+. Like ScAMF1, (Figure 3.9), the amplitude of NH_4^+ currents of GmAMF1;3-oocytes increased when voltage clamped in the presence of high (1.8 mM) Ca^{2+} in comparison to low (0.2 mM) Ca^{2+} (Figure 4.13). However, the data can only be considered a trend, as the ScAMF1 mediated currents were not significantly ($p>0.05$) different from corresponding H_2O-injected controls. Reversal potential of NH_4^+ currents mediated by GmAMF1;3 in response to changes in external Ca^{2+} were similar to H_2O-control currents, shifting towards positive voltages as a result of elevated Ca^{2+}.

When oocytes were preincubated in 10 mM P_i prior to TEVC analysis currents of GmAMF1;3 oocytes increased in the basal voltage-clamp buffer, increasing the current carried by NH_4^+ when compared to oocytes that have not been subjected to the P_i pre-incubation (Figure 4.14 A). At low Ca^{2+}, NH_4^+ carried currents were only significant with respect to 0 mM NH_4^+ when P_i pre-incubated GmAMF1;3-oocytes were clamped at voltages negative of -120 mV. Interestingly, currents elicited by GmAMF1;3-oocytes in the presence of elevated Ca^{2+} were found to be even greater when oocytes were pre-

incubated with 10 mM P_i (Figure 4.14 B). P_i-preincubation significantly ($p<0.05$) elevated the currents elicited by GmAMF1;3-oocytes at voltages negative of -60 mV, which were also significantly ($p<0.05$) different to corresponding H_2O-injected controls at hyperpolarised membrane potentials. The NH_4^+ driven current of GmAMF1;3-oocytes was significant from the current elicited in basal buffer at -140 mV. Corresponding P_i-preincubated H_2O-injected control oocytes did not display large currents when voltage clamped under identical conditions.

Similarly to ScAMF1, GmAMF1;3 mediated current as a function of time (ms) revealed that activation by NH_4^+ was not time-dependent. Changing Ca^{2+} concentration in the voltage-clamping buffer did not alter the lack of time-dependence (Figure 4.15). Again, activation of NH_4^+ currents elicited by 10 mM P_i pre-incubated GmAMF1;3-oocytes was also independent of time (Figure 4.16), and was not effected by Ca^{2+} concentration. Currents were comparable to H_2O-injected oocytes voltage-clamped under the same conditions. Note that data are derived from the oocyte experiments, a representative trace (n = 1) is displayed for each oocyte injection and voltage-clamp buffer analysed, and serves to provide evidence of a trend.

As P_i pre-incubation had an effect on currents elicited by GmAMF1;3-oocytes voltage-clamped in the presence of NH_4^+, the effect of P_i in the voltage-clamping buffer was also analysed. The adjusted steady state current was calculated by subtracting the H_2O control current from GmAMF1;3-oocyte current (Figure 4.17). Without P_i-preincubation, NH_4^+ did not have a significant effect on the amplitude of adjusted steady state currents elicited by GmAMF1;3-oocytes. Again, currents were greater with P_i-preincubation. When NH_4^+ was coupled to PO_4^{3-} or Cl^- (5 mM $NH_4H_2PO_4$ or 5 mM NH_4Cl), the adjusted steady state currents recorded at -140 mV (Figure 4.17 A) and +59 mM (Figure 4.17 B) were

significantly ($p<0.05$) enhanced with respect to 0 mM NH_4^+. However, there was no significant difference when NH_4^+ coupled to PO_4^{3-} or Cl^-. H_2O-injected controls produced smaller steady state currents, which were not affected by NH_4Cl or $NH_4H_2PO_4$.

4.3.7 Identification and cloning of *Arabidopsis* AMF1 homologs

The *AtAMF1;1* (*At5g64500*) and *AtAMF1;2* (*At5g65687*) CDS were amplified by PCR from 4-week-old soil-grown wild-type *Arabidopsis* (Columbia *gl1*) root cDNA. Primers were designed to amplify the *Arabidopsis AMF1* homologs using the predicted CDS available in the TAIR database (www.arabidopsis.org). The cloning conditions of *Arabidopsis AMF1* homologs were as described for the *GmAMF1;3* CDS to avoid potential mutations arising during propagation in *E. coli*. The cloned *AtAMF1;1* and *AtAMF1;2* sequences were as predicted in the TAIR database. The *AtAMF1;1* translated sequence is 484 amino acids in length with a predicted molecular weight of 52.16 kDa, and AtAMF1;2 is 492 amino acids in length with a predicted molecular weight of 53.51 kDa, showing 15.5% and 17.4% identity with ScAMF1, respectively (Figure 4.4). The Kyte/Doolittle transmembrane prediction algorithm suggests that AtAMF1;1 has 12 transmembrane spanning regions (Figure 4.18 A), and that AtAMF1;2 has 11 transmembrane spanning regions (Figure 4.18 B).

Attempts were made to clone the *AtAMF1;3* (*At2g22730*) CDS from the same cDNA pool, using primers based on the TAIR database predicted sequence. However, *AtAMF1;3* was unable to be amplified. *AtAMF1;3* transcripts exists *in vivo* as a number of corresponding expressed sequences tags (EST) that were identified in the GenBank EST database (http://www.ncbi.nlm.nih.gov/dbEST/).

4.3.8 Cellular localisation of AtAMF1;1 and AtAMF1;2 C-terminal YFP fusion proteins

As the yeast expression system has been used in this study to provide evidence of AMF1 transport characteristics, the system was also used to investigate the localisation of the *Arabidopsis* AMF1 proteins. The *Arabidopsis AMF1* homologs were subcloned downstream of *eGFP* in the *pAG426-DEST* yeast expression vector and expressed in 26972c yeast cells. However, the localisation of eGFP::AtAMF1;1 or eGFP::AtAMF1;2 in yeast proved difficult (data not presented).

Subsequent attempts to determine the membrane localisation of AtAMF1;1::eYFP and AtAMF1;2::eYFP proteins were carried out in transient plant expression systems. The *AtAMF1;1* and *AtAMF1;2* were ligated into the *Nco* I restriction site of the *pAVA554* expression plasmid (Figure 4.19; Subramanian et al., 2006), downstream of a *35SCamV* promoter driving an C-terminal eYFP fusion of AtAMF1;1 or AtAMF1;2. The plasmids were individually transformed into *Arabidopsis* protoplasts and onion epidermal cells. The plasmids were transformed into protoplasts prepared from 4-5 week hydroponically grown *Arabidopsis* leaf by PEG/LiAC treatment. Again, localisation of AtAMF1;1::eYFP and AtAMF1;2::eYFP fusions in *Arabidopsis* protoplasts proved difficult (data not presented). Transformation efficiency was low, and only a few protoplasts were successfully transformed with *pAVA554* empty vector controls, which presented non-specific localisation of eYFP protein. Therefore, localisation studies were attempted in an alternative transient expression system. The *pAVA554-AtAMF1;1* and *pAVA554-AtAMF1;2* plasmids were co-precipitated with a C-terminal *AtRop11::eCFP* known PM GTPase (Molendijk et al., 2008) onto gold particles, which were bombarded into onion epidermal peels. After observing the co-bombarded tissues, it was found that both

AtAMF1;1::eYFP (Figure 4.20) and AtAMF1;2::eYFP (Figure 4.21) co-localised with AtRop11 under the control of the *35S* promoter.

4.3.9 Characterisation of *Arabidopsis* AMF1 homologs in yeast

Arabidopsis AMF1 homologs were recombined into the *pYES3-DEST* vector and transformed into NH_4^+ transport mutant yeast strains for preliminary transport analysis. Overexpression of *AtAMF1;1* in 26972c yeast cells increased sensitivity to elevated MA (0.1 M MA), whilst *AtAMF1;2*-cells did not (Figure 4.22). However, neither *Arabidopsis* AMF1 homolog was able to complement the growth of 26972c cells on low NH_4^+ (Figure 4.23). The expression of *AtAMF1;1* or *AtAMF1;2* in 26972c cells significantly ($p<0.05$) enhanced ^{14}C-MA accumulation with respect to *pYES3-DEST* control cells, and was comparable to that of GmSAT1 activity (Figure 4.24). As GmAMF1;3 presented an obvious osmotic response, AtAMF1-spheroplasts were diluted 2-fold prior to osmotic analysis. AtAMF1;1 and AtAMF1;2 activity also resulted in a decrease in light scattering relative to control spheroplasts harbouring the *pYES3-DEST* empty vector in response to 5 mM NH_4^+ (Figure 4.25 A & C) or 0.5 mM MA (Figure 4.25 B & D).

4.3.10 Heterologous expression of *AtAMF1;1* and *AtAMF1;2* homologs in the *X. laevis* oocyte expression system

The following sections detail a series of experiments in *X. laevis* oocytes that helped to define the functional activities of *AMF1* genes cloned from soybean and *Arabidopsis*. Again, the electrophysiological profile of ScAMF1, presented in Chapter 3 has helped to serve as a guide for the preliminary characterisation of plant AMF1 proteins. Oocytes injected with *AtAMF1;1* or *AtAMF1;2* cRNA were compared to H_2O-injected controls for their ability to transport NH_4^+ in a series of different voltage-clamping buffers.

4.3.11 Assessment of *Arabidopsis* AMF1 catalysed currents in the presence or absence of various monovalent cations

Individual oocytes expressing *AtAMF1;1* or *AtAMF1;1* cRNA, with GmAMF1;3 activity as a measure of functionality, were voltage-clamped in a basal ND10 buffer containing monovalent cations (10 mM NaCl, 2 mM KCl, 1 mM $MgCl_2$, 1.8 mM $CaCl_2$, 200 mM mannitol, 10 mM HEPES/Trizma-base, pH 7.5). GmAMF1;3 activity in oocytes resulted in inward and outward currents comparable to H_2O-injected control oocytes (Figure 4.26 A). Under the same conditions and performed in parallel, voltage-clamping *X. laevis* oocytes, expressing either *AtAMF1;1* or *AtAMF1;2* at negative and positive membrane potentials, elicited similar large currents that were greater than the H_2O-injected control oocytes. The application of 0.2 mM or 0.5 mM NH_4Cl to the voltage-clamping buffer did not affect the amplitude of inward or outward currents elicited by AtAMF1;1 (Figure 4.26 B) or AtAMF1;2 (Figure 4.26 C). Although there appeared to some response to the plant *AMF1* cRNA, the precise nature of these currents is not clear. As these sets of experiments were being conducted we observed that H_2O-injected control oocytes benefited from a pre-incubation period in a buffer contained 10 mM P_i with NaH_2PO_4 (in place of 10 mM NaCl) eliciting the quietest endogenous currents (Figure 3.7). The oocytes appeared healthier, and when presented with 5 mM NH_4^+ were capable of inducing an inward current distinct from the H_2O-injected controls. Consequently, all subsequent experiments were conducted with a P_i pre-incubation stage.

4.3.12 Are other cations influencing *Arabidopsis* AMF1 NH_4^+ inducible currents?

In this study, we tested for NH_4^+ inducible currents in oocytes injected with cRNA from *AtAMF1;1* or *AtAMF1;2* when incubated in a Na^+-free ND10 voltage-clamping buffer. Once again, both H_2O-injected oocytes and those with *GmAMF1;3* cRNA activated large

currents at both positive and negative membrane-potentials, which were comparable to each other (Figure 4.27 A). In contrast, AtAMF1;1 activity in oocytes produced currents that were relatively smaller than H_2O-injected controls (Figure 4.27 B). Under the same conditions, AtAMF1;2 activity in oocytes led to larger inward and outward currents that were greater than H_2O-injected controls (Figure 4.27 C). The current response of AtAMF1;2 was more similar to GmAMF1;3 than AtAMF1;1. The application of 0.2, 0.5 or 1 mM NH_4Cl resulted in a sequential decrease in current, where 1 mM NH_4^+ significantly ($p<0.05$) reduced the current at -140 mV. AtAMF1;2 showed a loss of linearity when voltage clamped at membrane potentials negative of -80mV relative to the current response elicited in H_2O-injected control oocytes. The currents elicited by AtAMF1;1 activity were linear across the range of potentials investigated when 0.2 mM, 0.5 mM or 1 mM NH_4Cl was applied to the basal voltage-clamping buffer, becoming increasingly reduced and saturating at 0.5 mM NH_4Cl. Again, the currents elicited by AtAMF1;1 were not significantly ($p>0.05$) different.

The Na-free ND10 buffer described above still contained other monovalent cations including K^+. It was therefore decided to remove other potential competing cations from the ND10 buffer. In the absence of monovalent cations, an NH_4^+ (1 mM NH_4Cl) inducible current began to develop at increasingly negative voltage pulses in AMF1 containing oocytes, which was not present in H_2O-injected (Figure 4.28 A). Currents were also analysed in the presence of 0.5 mM $(NH_4)_2SO_4$ and 1 mM $NH_4H_2PO_4$ to determine if specific anion coupling has an affect. The inward currents elicited by AtAMF1;1 were reduced relative to the basal buffer when NH_4^+ was coupled to SO_4^{2-} or HPO_4^{2-}, while outward currents were not significantly ($p>0.05$) different and presented no noticeable shift in reversal potential (Figure 4.28 B). The amplitude of the AtAMF1;2 elicited inward current increased with the application of NH_4^+ to the basal buffer, but then was slightly

reduced when NH_4^+ was coupled to SO_4^{2-} or HPO_4^{2-} (Figure 4.28 C). There was no obvious difference between outward currents. Reversal potentials of currents carried by NH_4^+ in the absence of other monovalent cations shifted towards positive voltages when coupled to SO_4^{2-} and slightly further with Cl^- and PO_4^{3-}. The currents observed for H_2O-injected controls voltage-clamped under identical conditions were comparably smaller with no significant change.

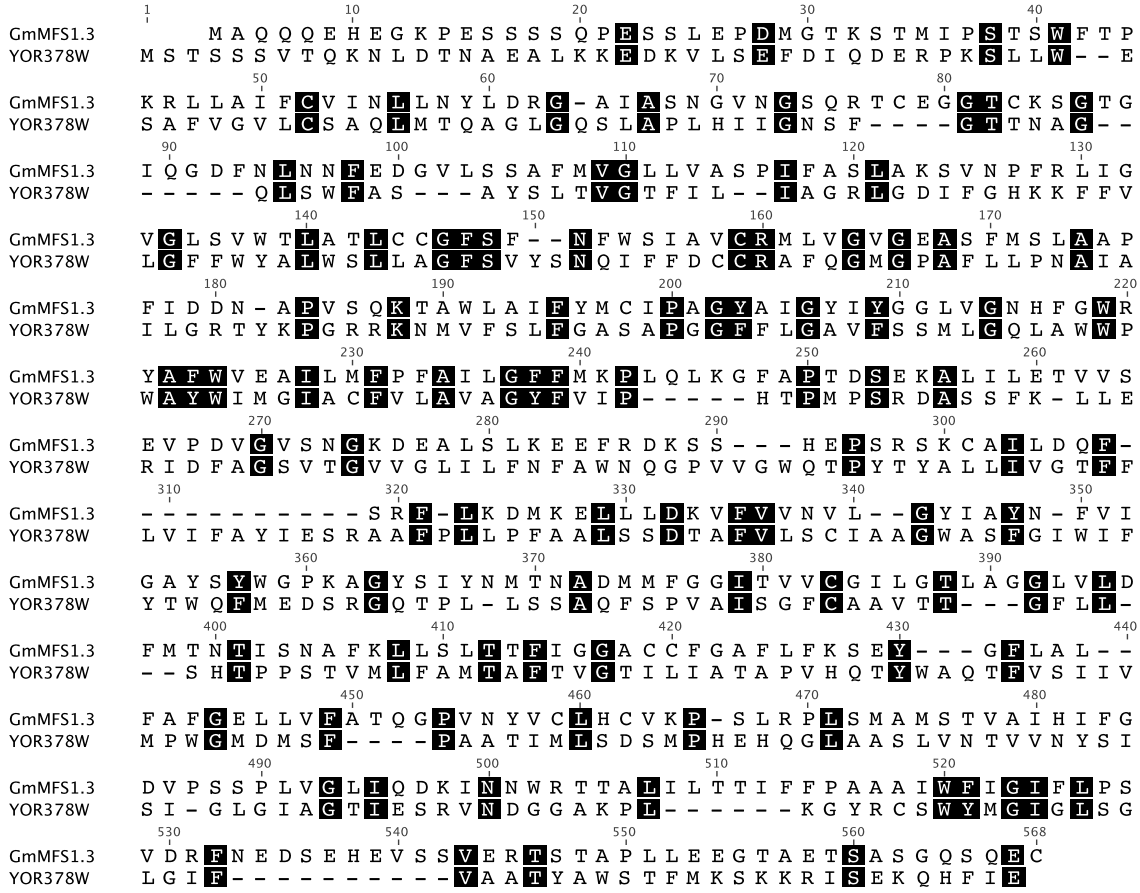

4.1 Comparison of GmAMF1;3 and ScAMF1 amino acid sequence

Pairwise MUSCLE alignment of ScAMF1 (YOR378W) and GmAMF1;3 (GmMFS1.3) amino acid sequences generated with Geneious® V 5.6 software. The GmAMF1;3 amino acid sequence was translated from the CDS cloned by D. Chiasson (2012).

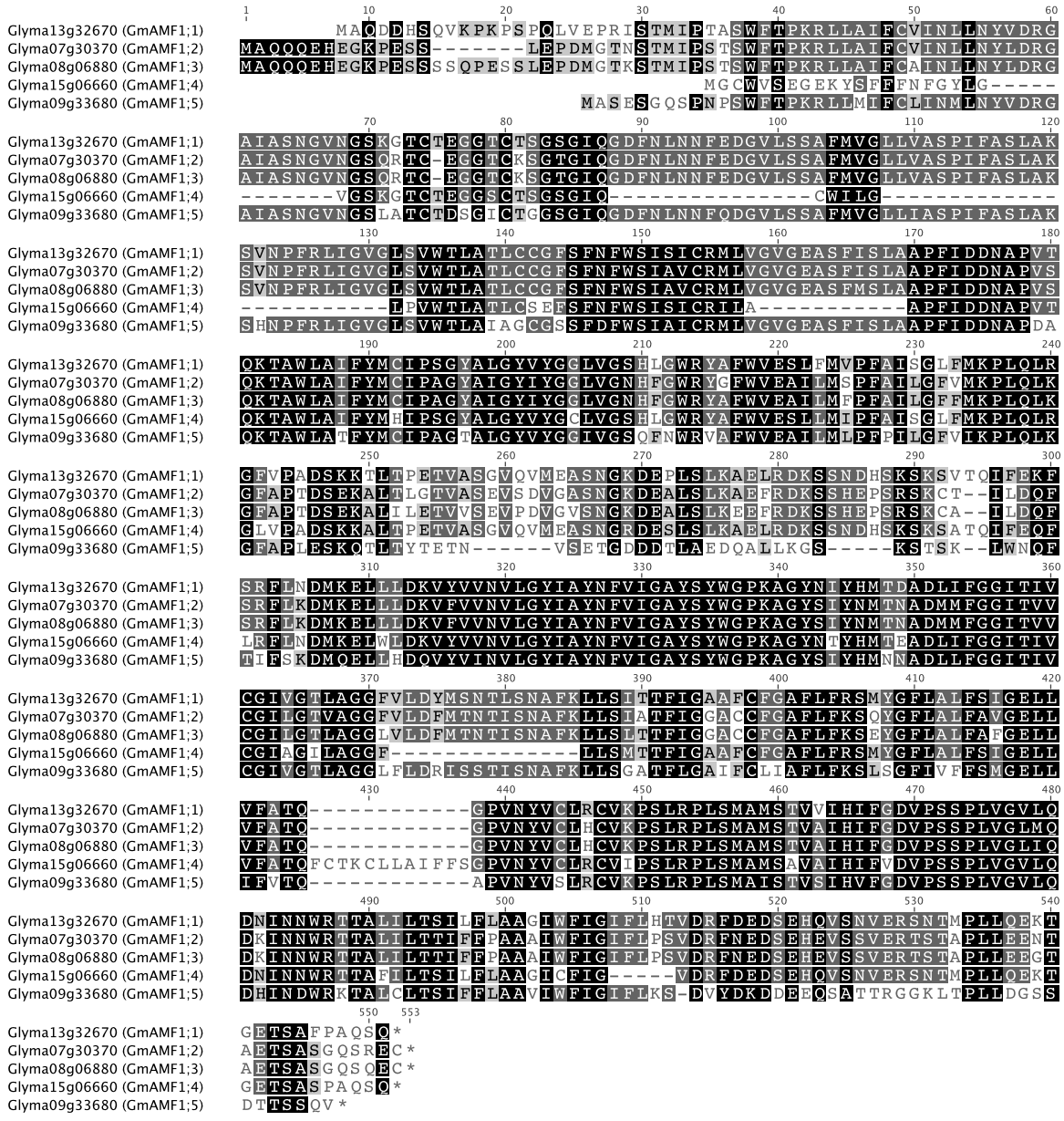

Figure 4.2: Alignment of identified soybean major facilitator subfamily members

Multiple MUSCLE alignment of the soybean AMF1 amino acid sequences as generated with Geneious® V 5.6 software. The cloned soybean *AMF1*, *GmAMF1;3* (*Glyma08g06880*) CDS was used in a BLAST search of the Phytozome predicted soybean gene database (http://www.phytozome.net). Previously uncharacterised MF proteins sequences with highest identity (50-90% similarity) with GmAMF1;3 were retrieved. Note: *GmAMF1;5* CDS was coned by David Chiasson (2012).

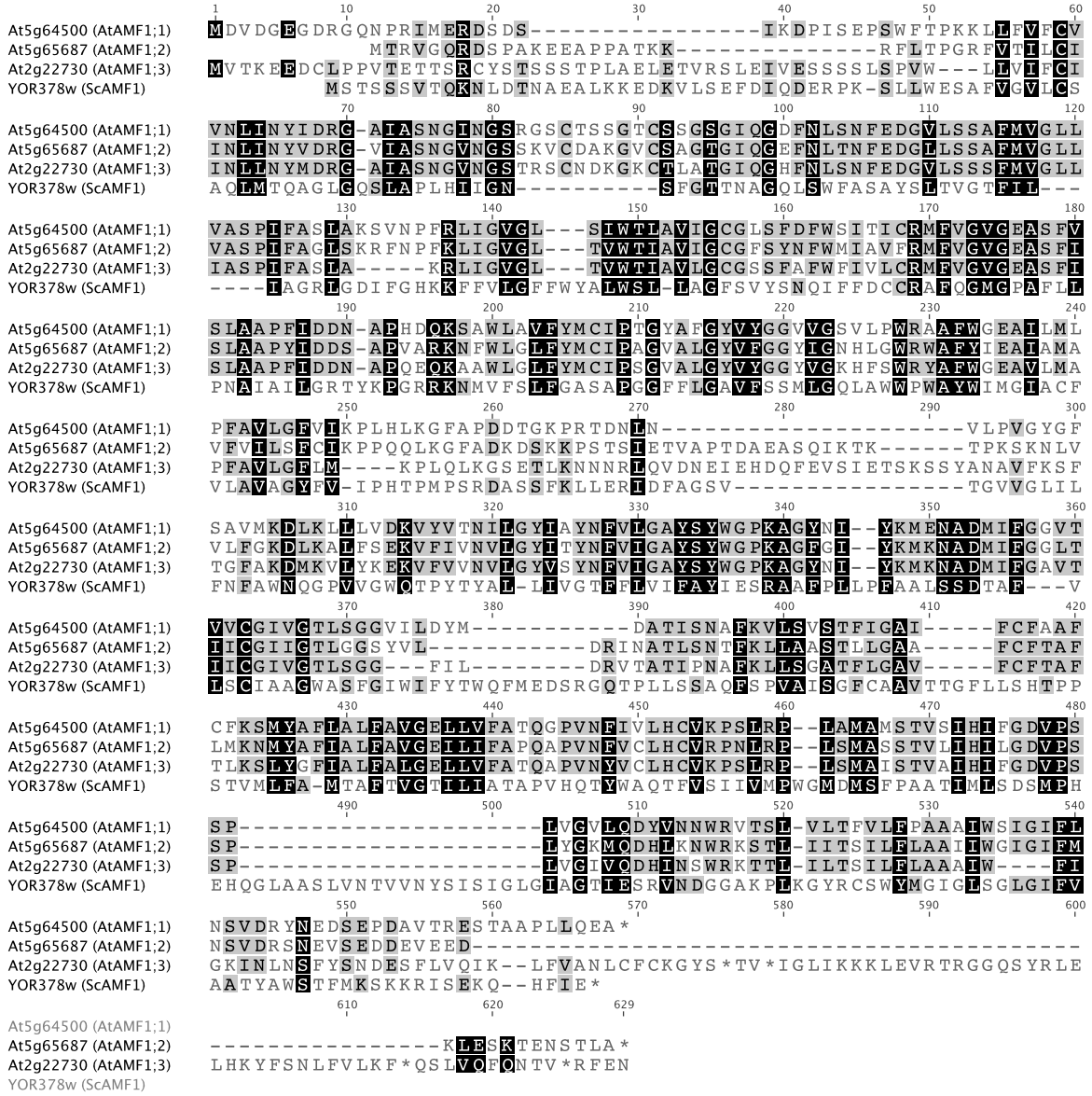

Figure 4.3: Alignment of the identified *Arabidopsis* MFS members with ScAMF1

Multiple MUSCLE alignment of ScAMF1 with the *Arabidopsis* AMF1 amino acid sequences as generated with Geneious® V 5.6 software. The *At5g64500* (*AtAMF1;1*) and *At5g65687* (*AtAMF1;2*) CDS were cloned from 4-week old *Arabidopsis* root cDNA, and were identical to the predicted amino acid sequences retrieved from the TAIR database (http://www.arabidopsis.org/cgi-bin/Blast/TAIRblast.pl).

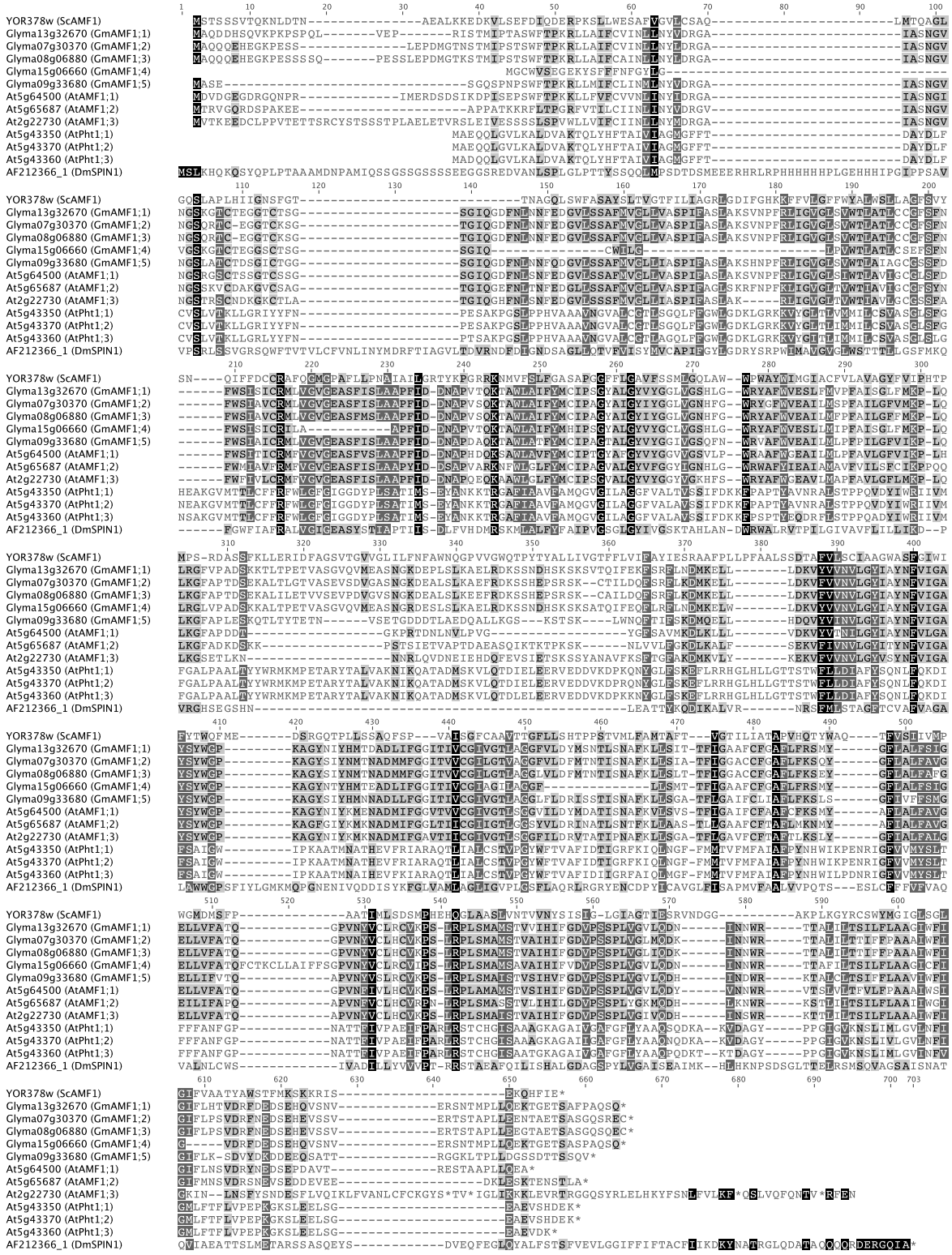

Figure 4.4: Alignment of the identified MFS members.

Multiple MUSCLE alignment of the MF amino acid sequences as generated with Geneious® V 5.6

software. The *GmAMF1;1* (*Glyma13g32670*) and *GmAMF1;2* (*Glyma07g30370*) sequences were retrieved from the Phytozome genome prediction database (http://www.phytozome.net), whilst the *GmAMF1;3* (*Glyma08g06880*) and *GmAMF1;5* (*Glyma09g33680*) sequences are verified clones. The soybean MF protein sequences are shown along with MF proteins identified in yeast (ScAMF1), *Arabidopsis* and *Drosophila* that present significant identity (11-16% similarity with GmAMF1;3).

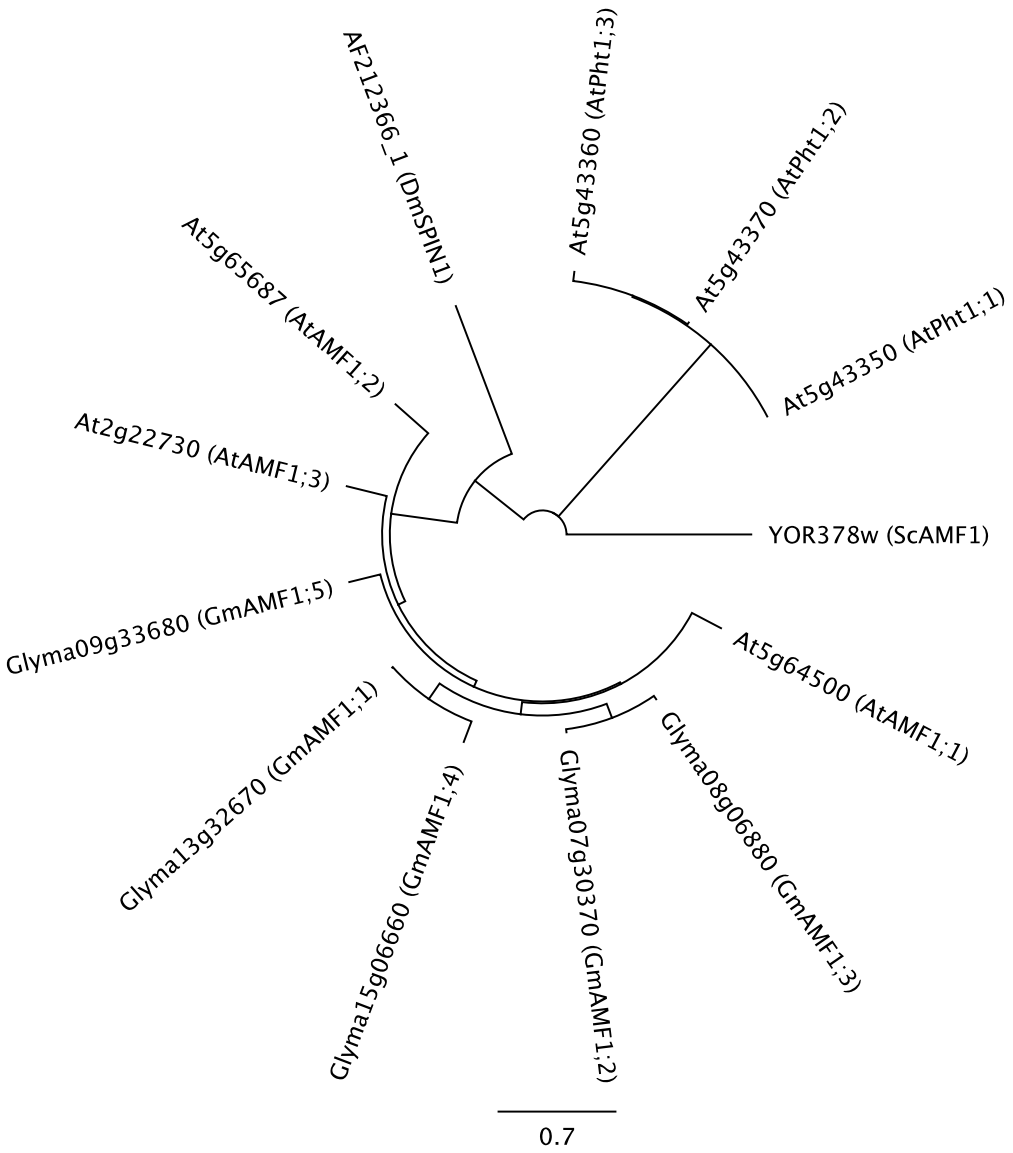

Figure 4.5: Circular phylogenetic tree of MFS transporters.

Phylogenetic analysis of yeast (Sc), *Drosophila melanogaster* (Dm), soybean (Gm) and *Arabidopsis* (At) MF transporter amino acid sequences. The neighbour-joining tree was generated using the program Geneious® V 5.6, using the Jukes-Cantor distance model. Scale represents the number of amino acid substitutions per site.

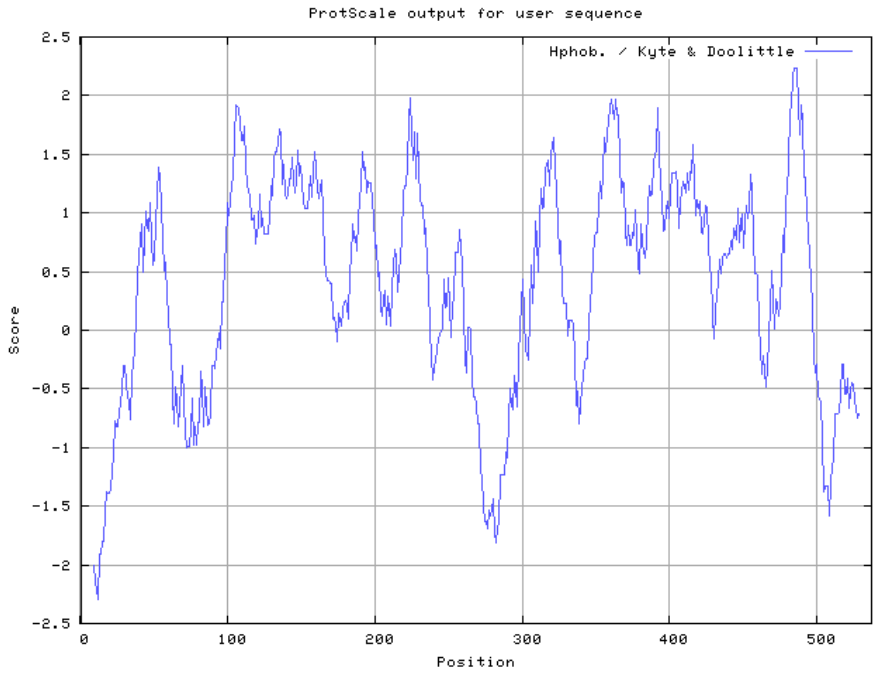

Figure 4.6: GmAMF1;3 predicted topology

The coding sequence (CDS) of *GmAMF1;3* was cloned from 28 day-old soybean root cDNA. Hydrophobic plots were generated for (**A**) AtAMF1;1 and (**B**) AtAMF1;2 with ExPASy Bioinformatics Resource Portal (web.expasy.org/protscale/) using the Kyte / Doolittle protocol with an amino acid window size of 19. The hydrophobic regions are indicated by positive hydrophilicity values.

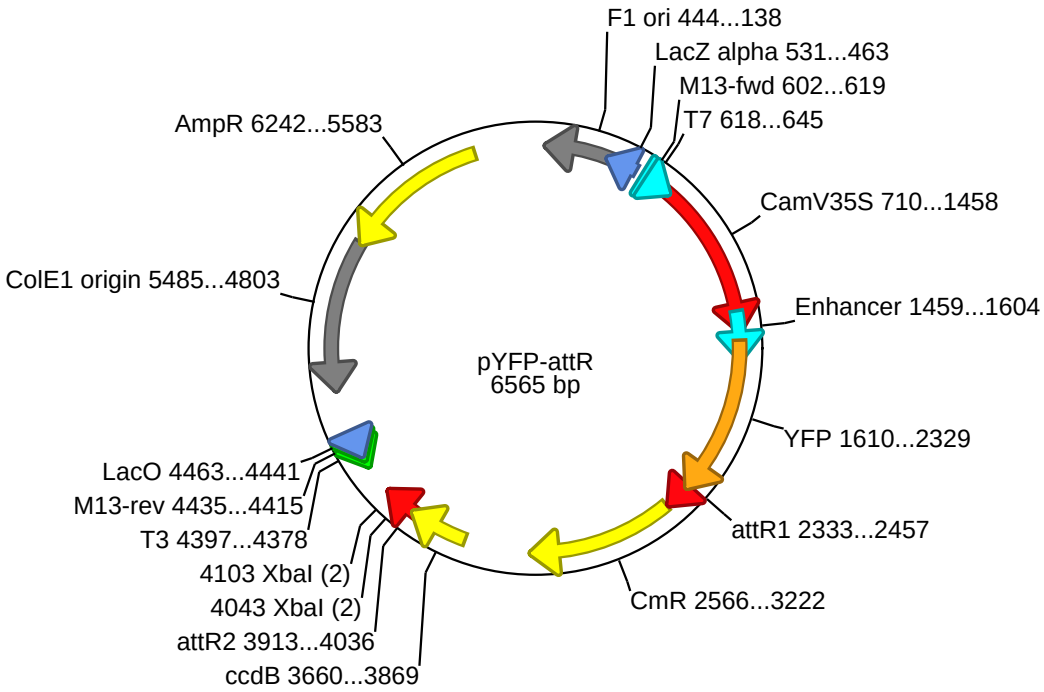

A

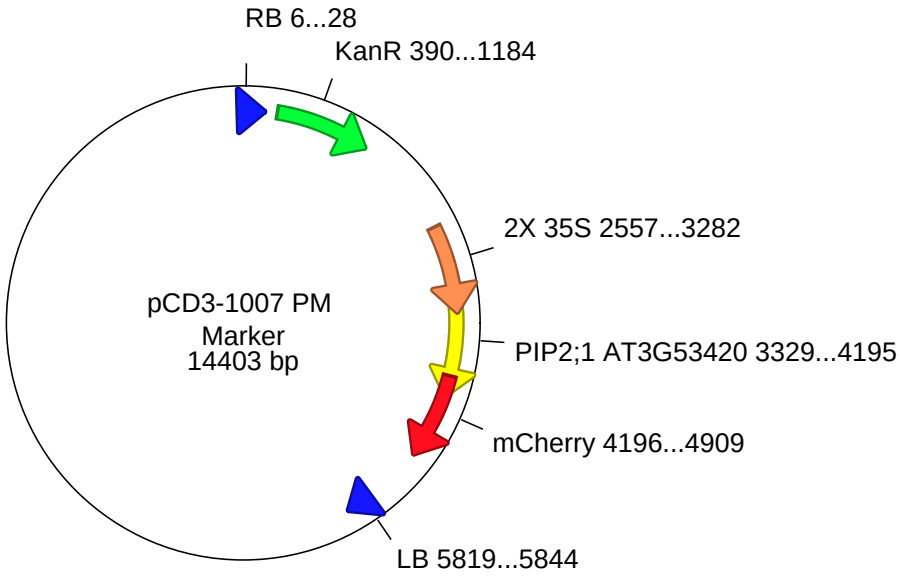

B

Figure 4.7: Vector maps of *pYFP-attR* and *pDC3-1007* for transient expression in onion epidermal cells

(A) *pYFP-attR* plasmid used for N-terminal YFP fusion protein driven by a *2x35S* promoter. (**B**)

The *pDC3-1007* plasmid was created by digesting the plasma membrane marker *PM-RK CD3-1007* (Nelson et al., 2007) with *Sac* I and *Eco* RI and inserting the fragment into *pBluescript* plasmid downstream of a *2x35S* promoter. The plasmid drives the expression of AtPIP2;1 with a C-terminal mCherry fusion, which serves as known plasma membrane marker. Note: David Chiasson subcloned *GmAMF1;3* into *pYFP-attR* (D. Chiasson, 2012).

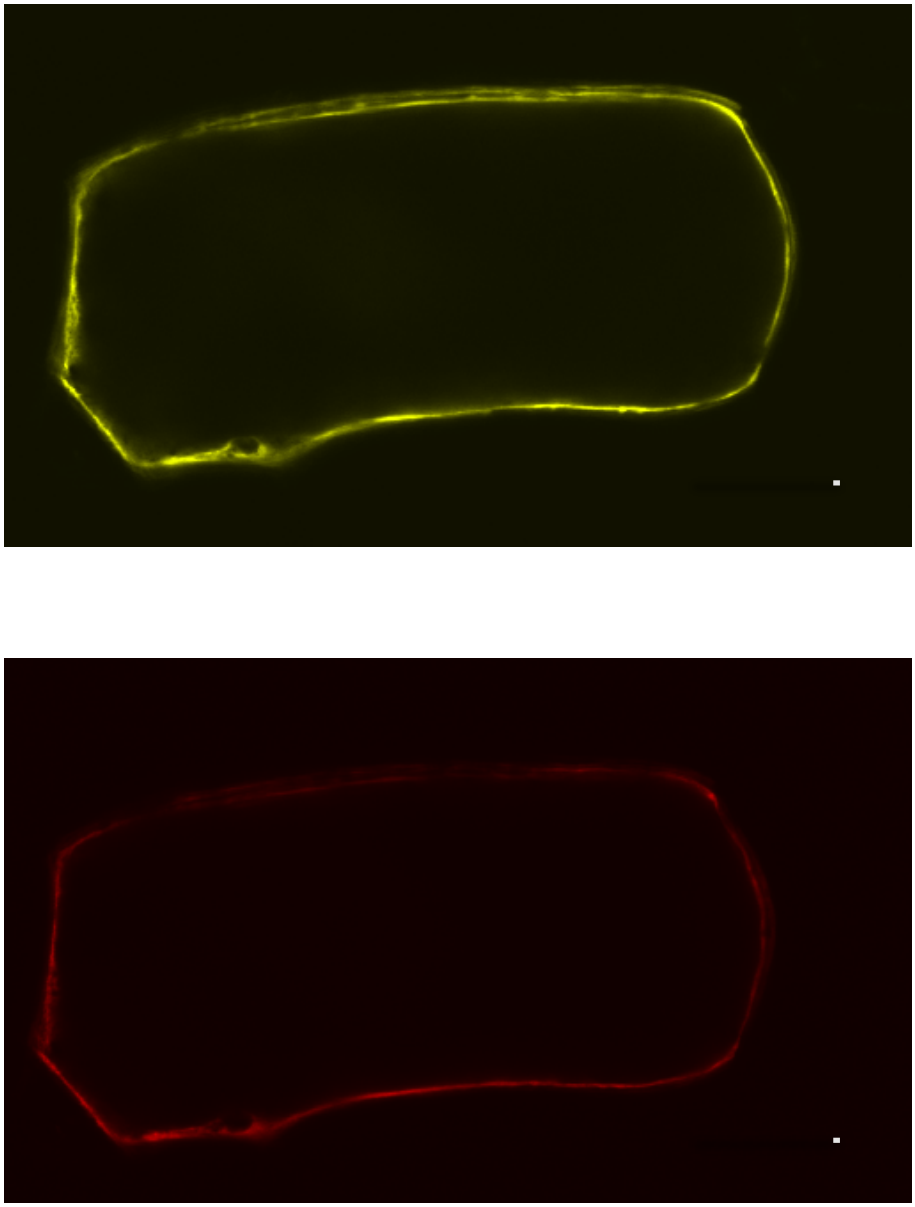

A

B

Figure 4.8: Subcellular localisation of N-terminally tagged YFP::GmAMF1;3 in onion epidermal cells.

(**A**) *2x35S::YFP::GmAMF1;3* and (**B**) *2x35S::PIP2;1::mCherry* expression in the same onion epidermal cell. Epidermal peels were co-bombarded with *pYFP::GmAMF1;3* and *pDC-1007* plasmids, incubated for 24 h, then sequentially viewed for (**A**) YFP and (**B**) mCherry signals by confocal microscopy. YFP was detected using an excitation 515 nm argon laser, and light emission

detected at 535-580, while the mCherry was detected using an excitation 543 nm helium/neon laser, and light emission detected at 615 nm, with a LSM 5 Pascal Laser Scanning microscope (Zeiss, Oberkochen, Germany). Both fusions were found associated with the plasma membrane. Bar = 40 μm. Note: David Chiasson performed the onion epidermal peel bombardments (D. Chiasson, 2012).

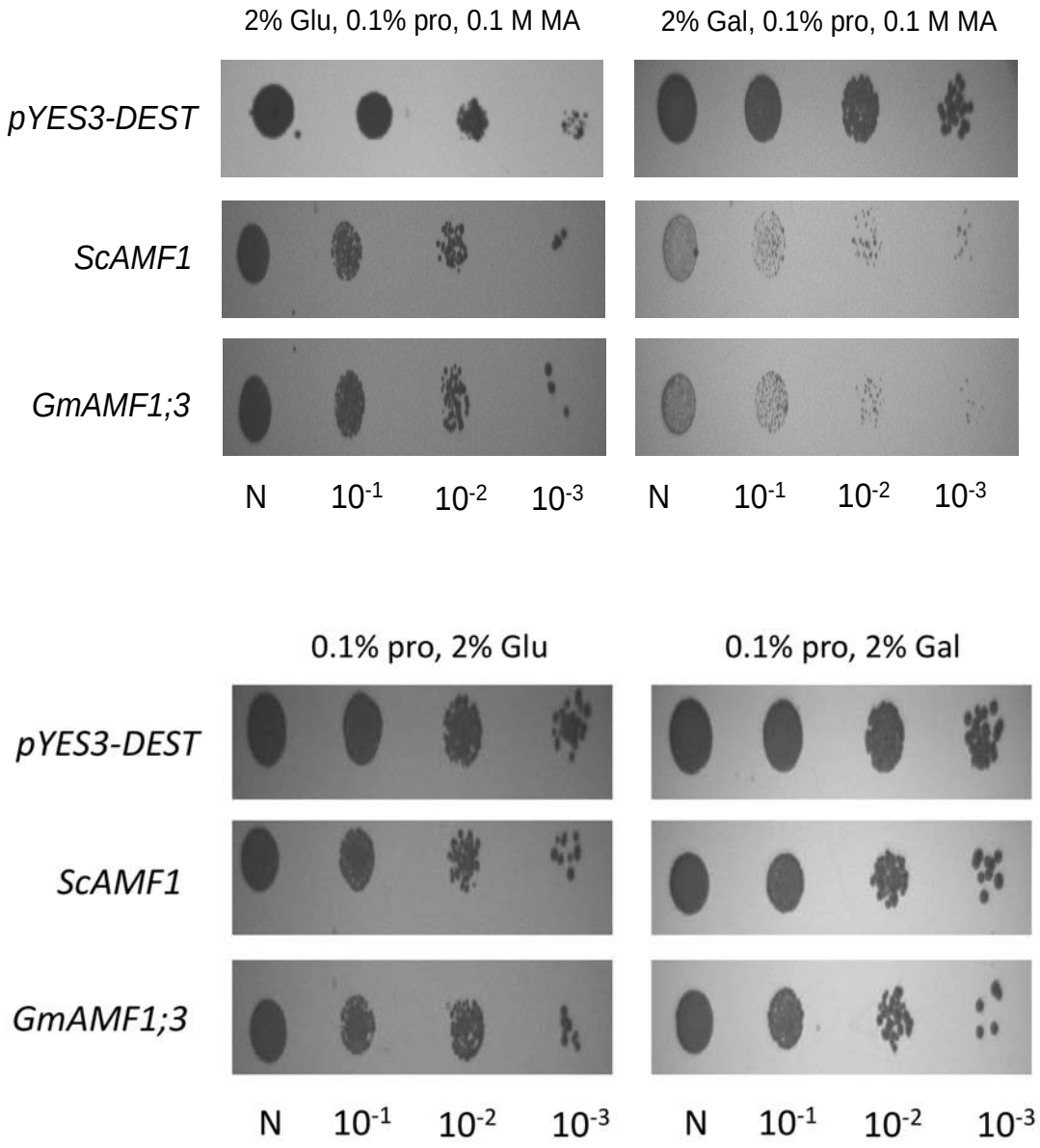

Figure 4.9: Growth of 26972c NH_4^+ transport deficient yeast strain expressing *GmAMF1;3* in the presence of methylammonium

The 26972c yeast strain was transformed with *pYES3-DEST* (control), *pYES3-ScAMF1* or *pYES3-GmAMF1;3* Cells were grown to mid-log phase and then serially diluted as described in Figure 2.9. Diluted cells were spotted onto yeast minimal media (Grenson, 1966) supplemented with 2% (w/v) glucose (Glu) or galactose (Gal), 0.1% proline (pro), 0.1 M methylammonium (MA) where indicated. The yeast plates were incubated for 6 days at 28°C.

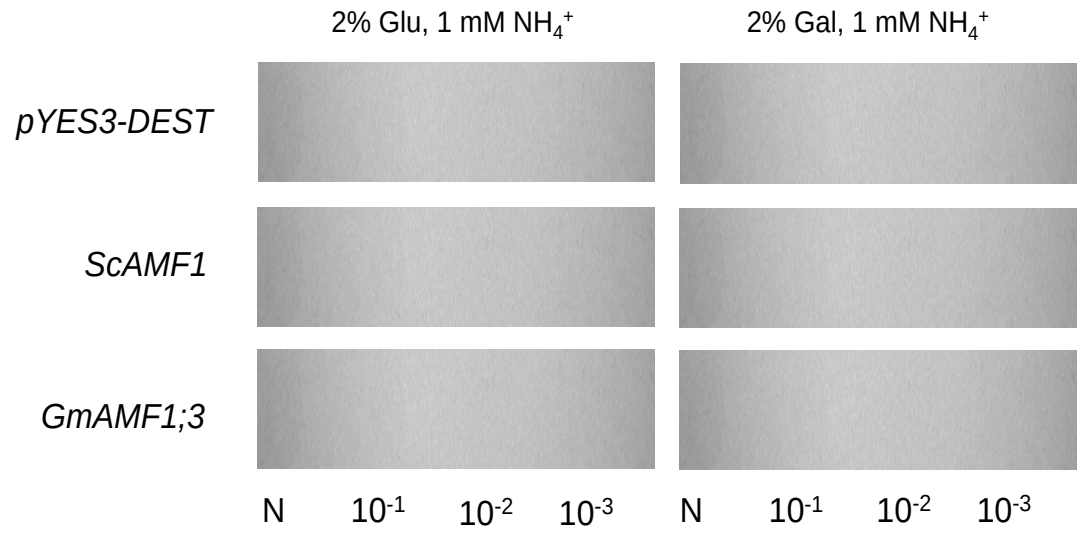

Figure 4.10: Growth of 26972c NH_4^+ transport deficient yeast strain expressing *GmAMF1;3* on NH_4^+ containing media

The 26972c yeast strain was transformed with *pYES3-DEST* (control), *pYES3-ScAMF1* or *pYES3-GmAMF1;3* Cells were grown to mid-log phase and then serially diluted as described in Figure 2.9. Diluted cells were spotted onto yeast minimal media (Grenson, 1966) supplemented with 2% (w/v) glucose (Glu) or galactose (Gal), 1 mM NH_4Cl where indicated. The yeast plates were incubated for 6 days at 28°C.

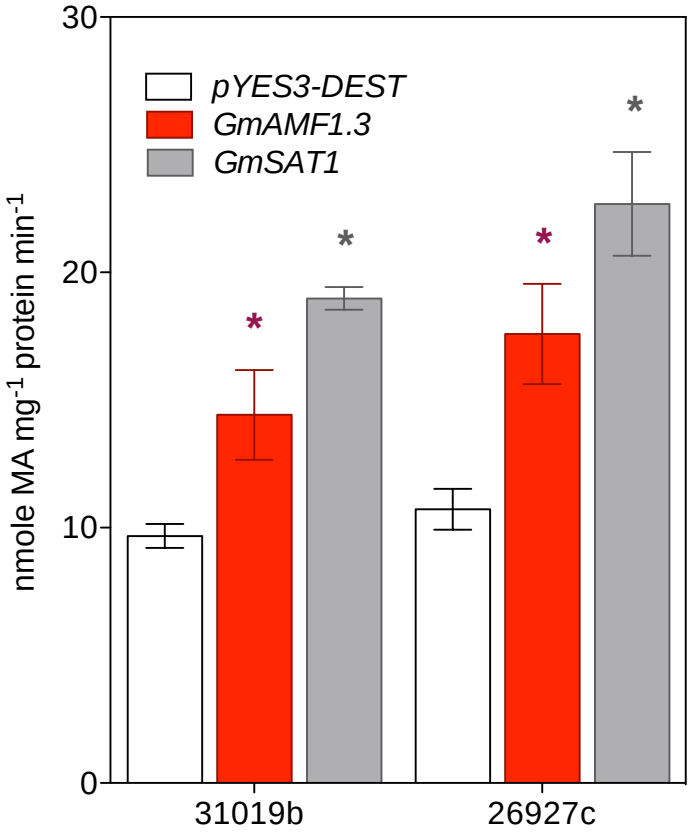

Figure 4.11: Rate of ^{14}C-MA influx into yeast cells over-expressing *GmSAT1* and *GmAMF1;3* relative to the empty *pYES3-DEST* vector.

Mutant NH_4^+ transport yeast strains were transformed with *pYES3-DEST* control (white), *pYES3-GmSAT1* (grey) or *pYES3-GmAMF1;3* (red) and grown for 16 h using liquid yeast minimal media without uracil (Grenson, 1966) supplemented with 2% (w/v) galactose and 1 mM NH_4Cl. Uptake of 1 mM ^{14}C-MA in a 2% (w/v) galactose KPO_4 buffer (pH 6.2) was measured over 5 min. Accumulated ^{14}C-MA was quantified by measuring the β-decay using a scintillation counter. Data presented are mean rate of MA uptake ± SE (n = 6). The data are representative of at least 5 independent biological experiments. Where indicated data are significant from the empty vector controls at * ($p<0.05$).

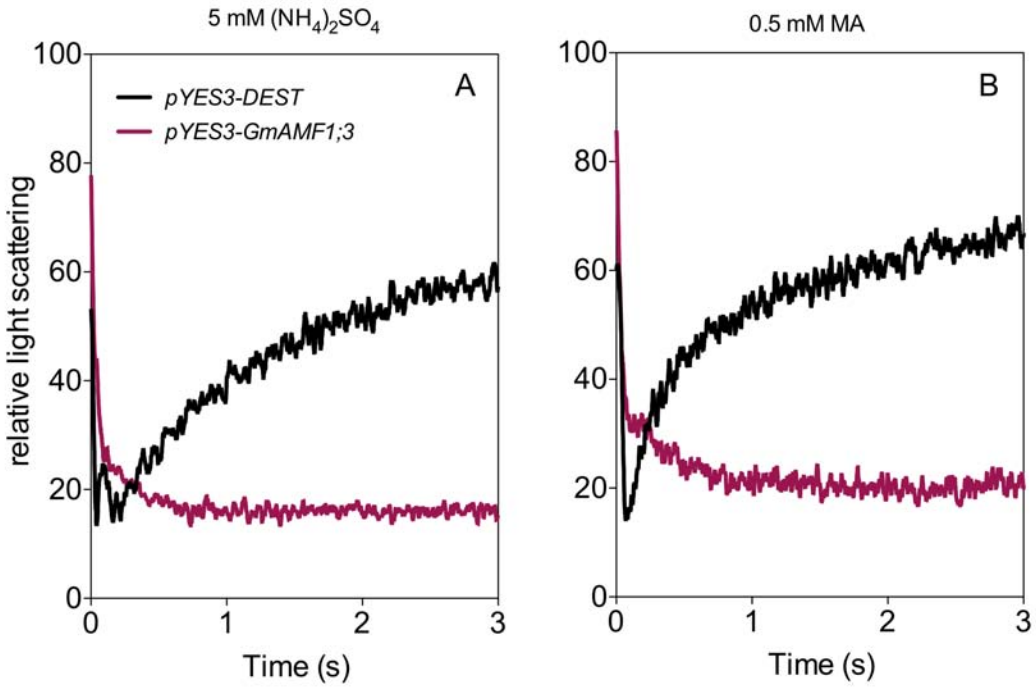

Figure 4.12: Swelling profile of 26972c spheroplasts expressing *GmAMF1;3* in response to MA and NH_4^+

Spheroplasts were made from 26972c yeast cells were resuspended to a uniform $OD_{475\ nm}$ of 1.0 and mixed with an equal volume of base solution supplemented with (**A**) 5 mM $(NH_4)_2SO_4$ or (**B**) 0.5 mM MA in a fast kinetics SFM-300, Biologic instrument. Volume changes of spheroplasts harbouring the *pYES3-DEST* (black), *pYES3-GmAMF1;3* (purple) were recorded at 16°C as light scattering at an angle 90° and light wavelength of 475 nm. The kinetics presented is the mean volume change recording (n = 6-9) each collected over a period of 6 s, and normalised with smoothing to 21 neighbours.

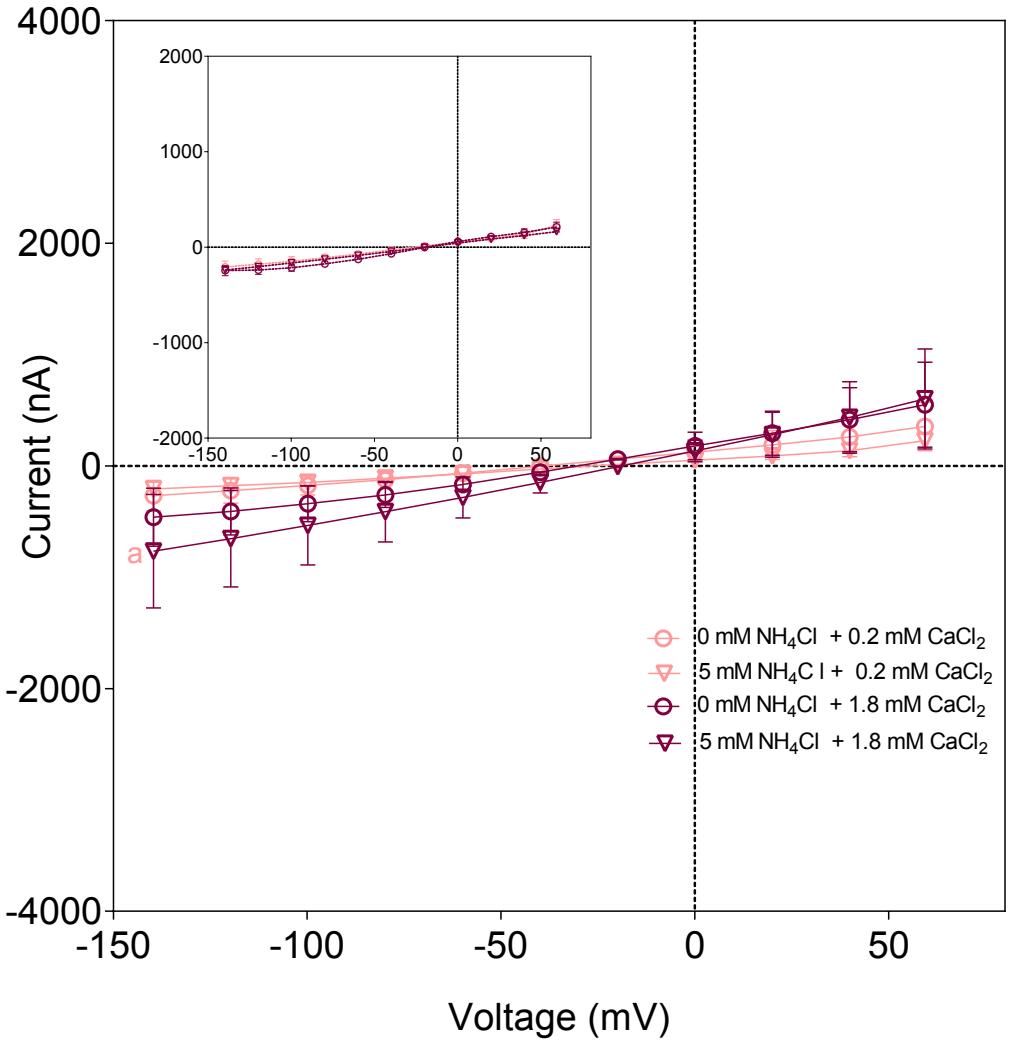

Figure 4.13: Effect of Ca^{2+} on GmAMF1;3 mediated currents carried by NH_4^+

X. laevis oocytes injected with *GmAMF1;3* cRNA or injected with an equal volume of RNase-free H_2O (inset) were preincubated ND10 buffer for 1-2 days prior to two-electrode voltage clamp analysis. Experiments were carried out at room temperature in modified ND10 base buffer (1 mM $MgCl_2$, 200 mM mannitol, 10 mM HEPES with pH adjusted to 7.5 with Trizma-base) supplemented with 0.2 mM $CaCl_2$ (light pink) or 1.8 mM $CaCl_2$ (dark pink) with 0 mM (open circles) or 5 mM NH_4Cl (open triangles). Data points in each experiment represent means of 3 (n = 3) oocytes ± SE, and asterisks denote significance (*P<0.05) using Two-way ANOVA statistical analysis.

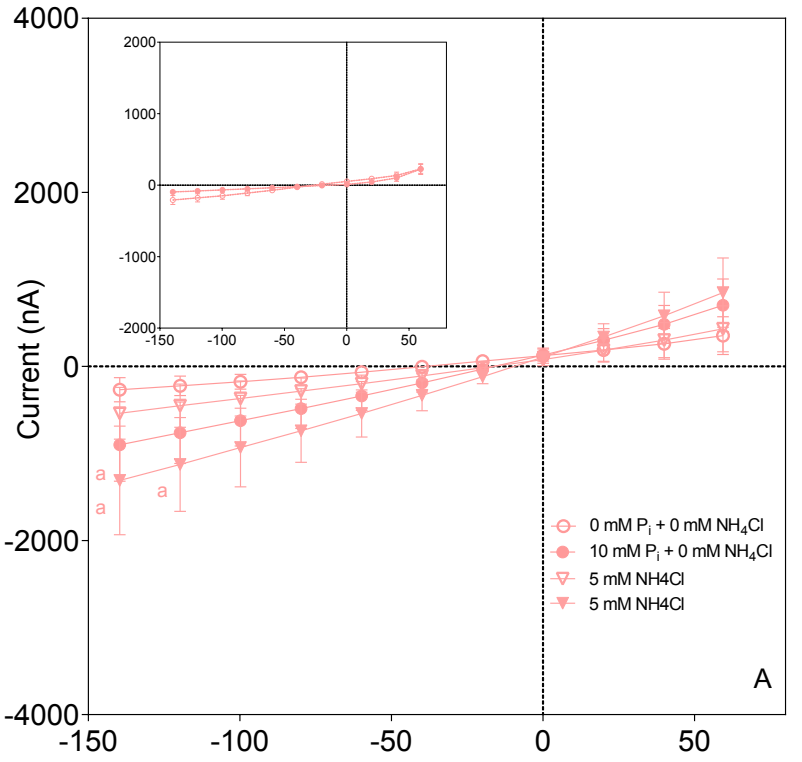
4000
2000
0
-2000
-4000
Current (nA)
-150
-100
-50
0
50
2000
1000
0
-1000
-2000
a
a
a
0 mM Pi + 0 mM NH4Cl
10 mM Pi + 0 mM NH4Cl
5 mM NH4Cl
5 mM NH4Cl
A

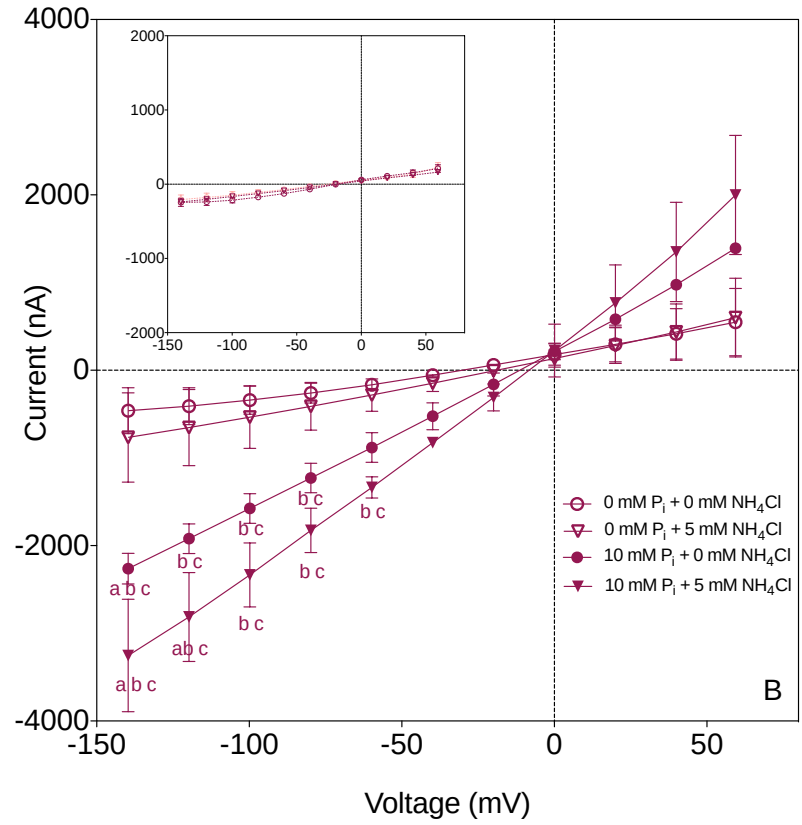
4000
2000
0
-2000
-4000
Current (nA)
-150
-100
-50
0
50
Voltage (mV)
2000
1000
0
-1000
-2000
a b c
a b c
a b c
b c
b c
b c
b c
b c
0 mM Pi + 0 mM NH4Cl
0 mM Pi + 5 mM NH4Cl
10 mM Pi + 0 mM NH4Cl
10 mM Pi + 5 mM NH4Cl
B

Figure 4.14: Amplitude of GmAMF1;3 facilitated NH_4^+ currents in *X. laevis* oocytes subjected to preincubation with P_i

X. laevis oocytes were prepared and two-electrode voltage clamp analysis was carried out as described in Figure 4.13. *GmAMF1;3* cRNA and H_2O-injected oocytes were preincubated with 0 mM or 10 mM NaH_2PO_4. Voltage clamping buffer contained (**A**) 0.2 mM $CaCl_2$ or (**B**) 1.8 mM $CaCl_2$ with no supplements (circles) or 5 mM NH_4Cl (triangles). Data points in each experiment represent means of 3 (n = 3) oocytes ± SE, and asterisks denote significance (*$P<0.05$) using the Two-way ANOVA statistical analysis.

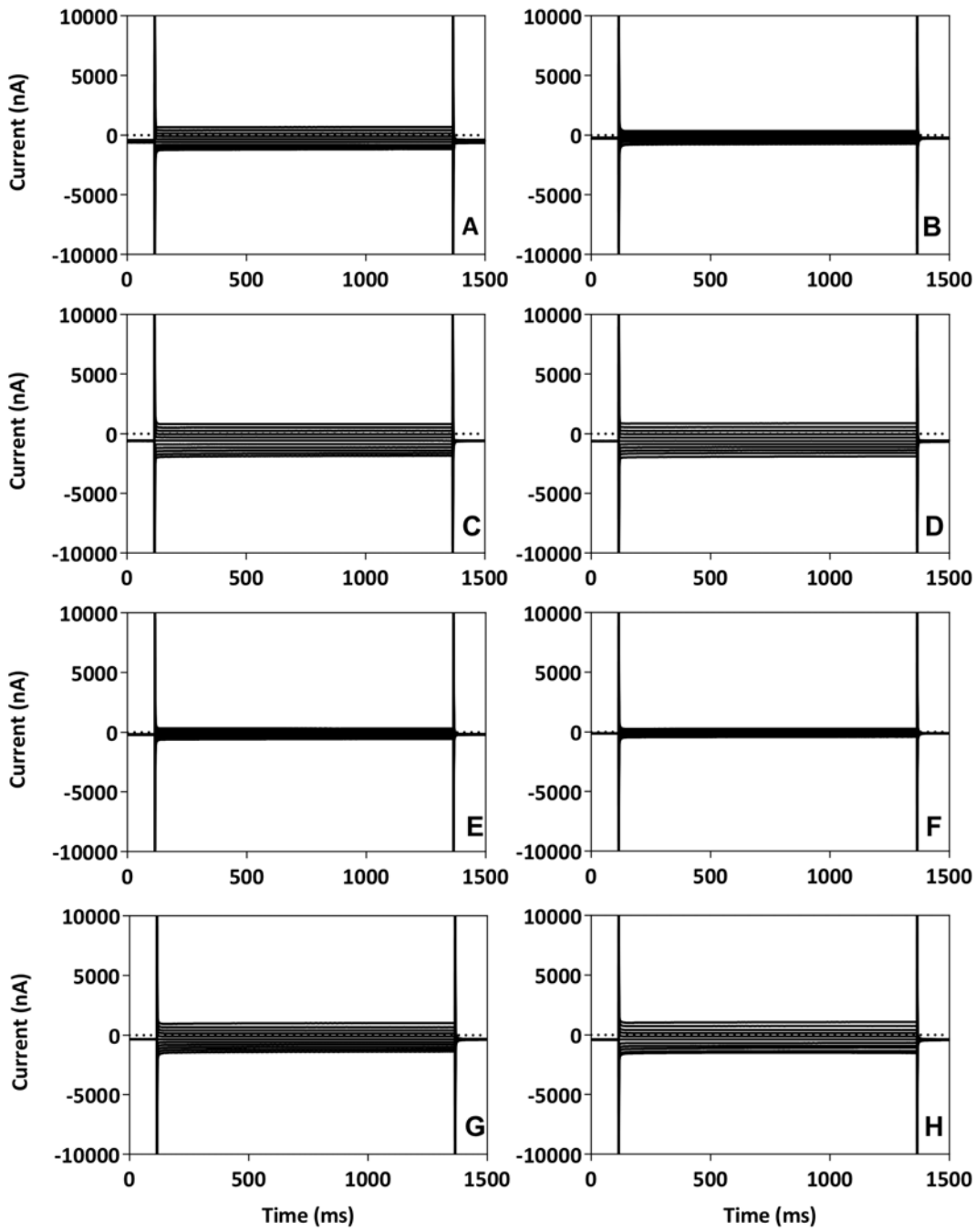

Figure 4.15: Representative currents elicited by *X. laevis* oocytes expressing *GmAMF1;3* or injected with H_2O in the presence of varied Ca^{2+} concentrations

Representative time dependant current profiles of oocytes (n = 1) injected with *GmAMF1;3* cRNA

(C, D, G, H) or H_2O (**A, B, E, F**). Oocytes were prepared as described in Figure 4.14 with 10 mM NaH_2PO_4 preincubation. Oocytes were voltage-clamped in modified ND10 buffer (minus NaCl or KCl) with 0.2 mM $CaCl_2$ (**A, B, E. F**) or 1.8 mM $CaCl_2$ (**C, D, G, H**) plus 0 mM NH_4Cl (**A, C, E, G**) or 5 mM NH_4Cl (**B, D, F, H**).

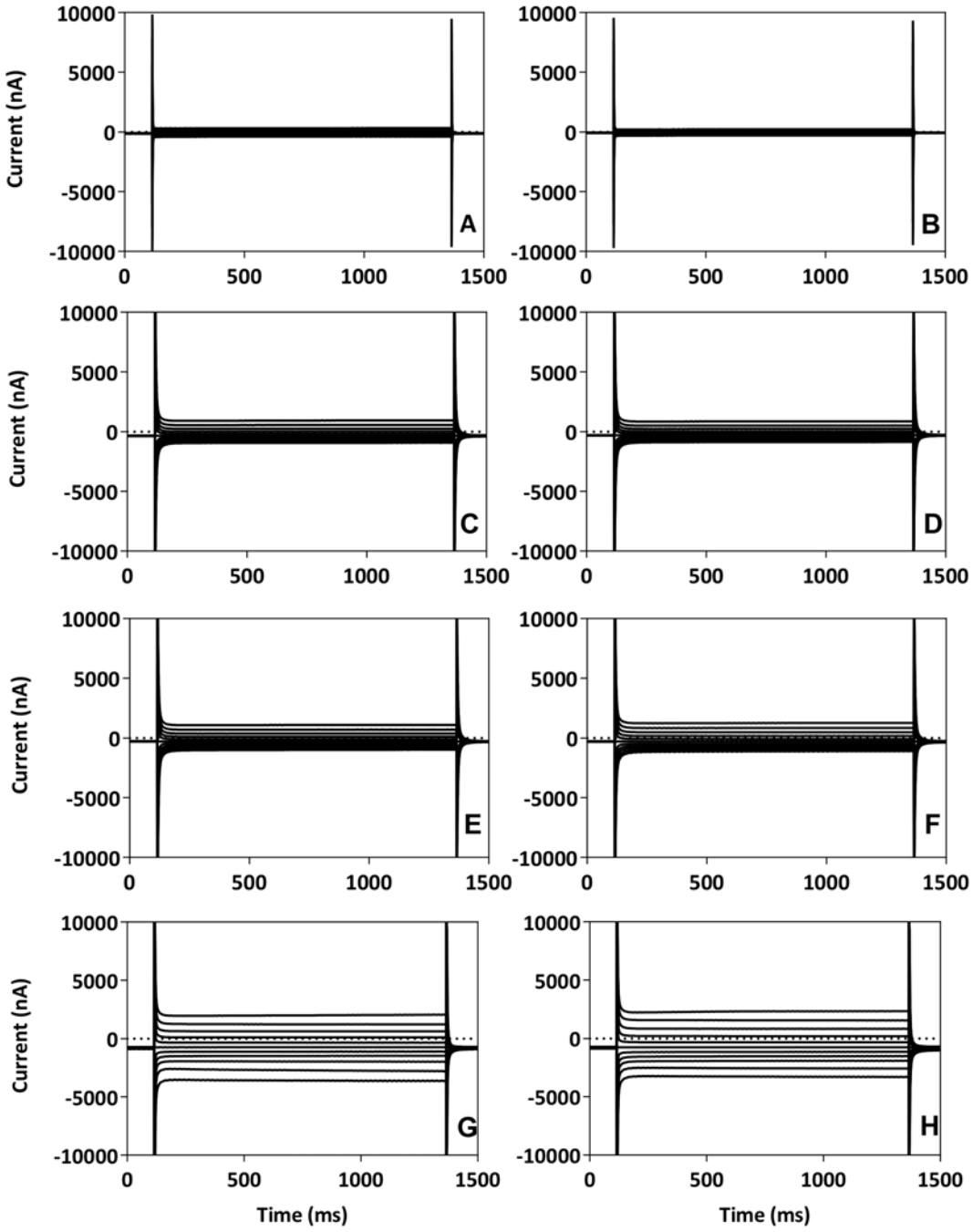

Figure 4.16: Representative currents elicited by *X. laevis* oocytes expressing *GmAMF1;3* or injected with H_2O in the presence of varied Ca^{2+} concentrations after P_i-preincubation

Representative time dependant current profiles of oocytes (n = 1) injected with *GmAMF1;3* cRNA (C, D, G, H) or H_2O (A, B, E, F). Oocytes were prepared as described in Figure 4.14 with 10 mM NaH_2PO_4 preincubation. Oocytes were voltage-clamped in modified ND10 buffer (minus NaCl or KCl) with 0.2 mM $CaCl_2$ (A, B, E. F) or 1.8 mM $CaCl_2$ (C, D, G, H) plus 0 mM NH_4^+ (A, C, E, G) or 5 mM NH_4^+ (B, D, F, H).

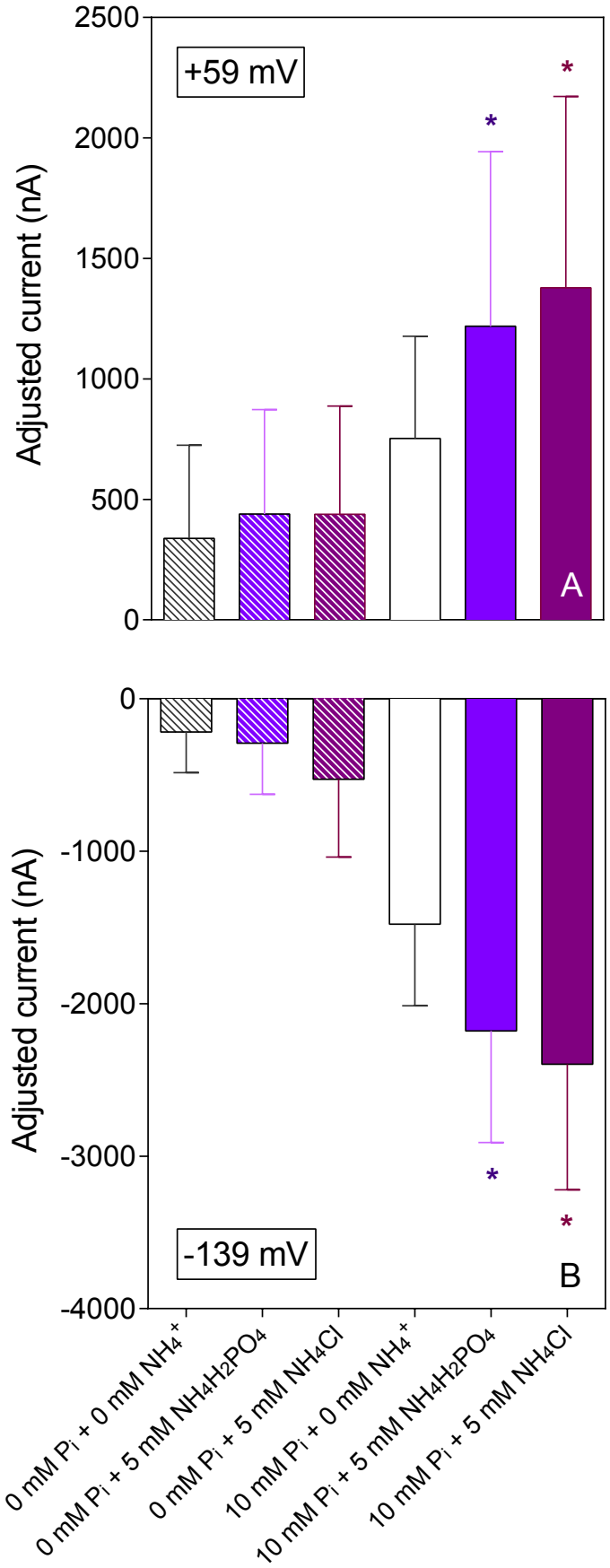
+59 mV
Adjusted current (nA)
2500
2000
1500
1000
500
0
A
-139 mV
B
-1000
-2000
-3000
-4000
0 mM Pi + 0 mM NH4+
0 mM Pi + 5 mM NH4H2PO4
0 mM Pi + 5 mM NH4Cl
10 mM Pi + 0 mM NH4+
10 mM Pi + 5 mM NH4H2PO4
10 mM Pi + 5 mM NH4Cl

Figure 4.17: Effect of P_i gradients across the oocyte plasma membrane on GmAMF1;3 mediated currents carried by NH_4^+

The *GmAMF1;3* induced current at (**A**) +59 mV or (**B**) -139 mV minus corresponding H_2O-injected controls. *X. laevis* oocytes were prepared and two-electrode voltage clamp analysis was carried out as described in Figure 4.13. Oocytes were preincubated with 0 mM or 10 mM NaH_2PO_4. Voltage clamping buffer without NH_4^+ supplements, 5 mM $NH_4H_2PO_4$ or 5 mM NH_4Cl. Data presented represent means of 3 (n = 3) oocytes ± SE, and asterisks denote significance (*P<0.05) using the Two-way ANOVA statistical analysis. Corresponding H_2O-injected oocyte controls showed no significant difference (data not shown).

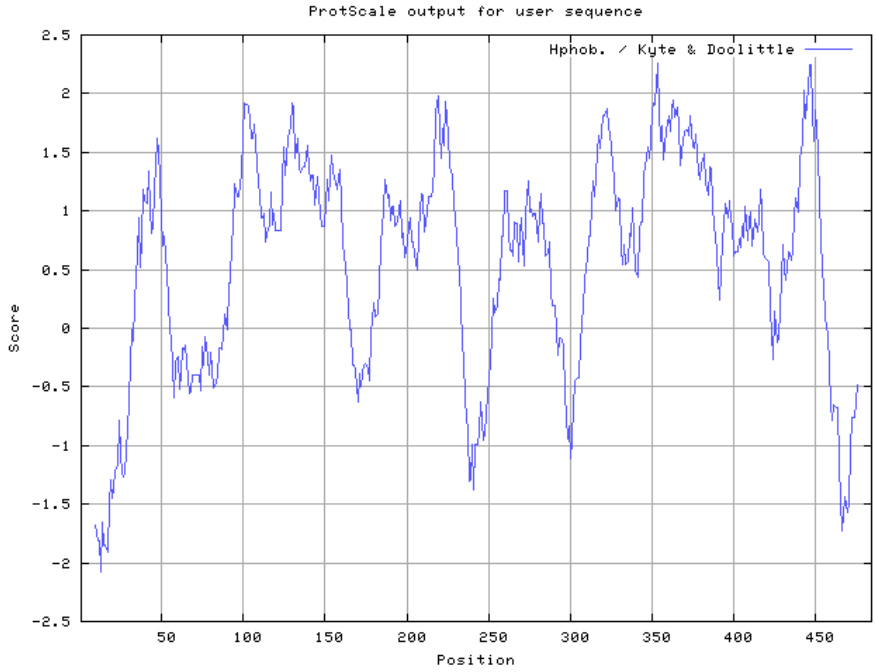

A

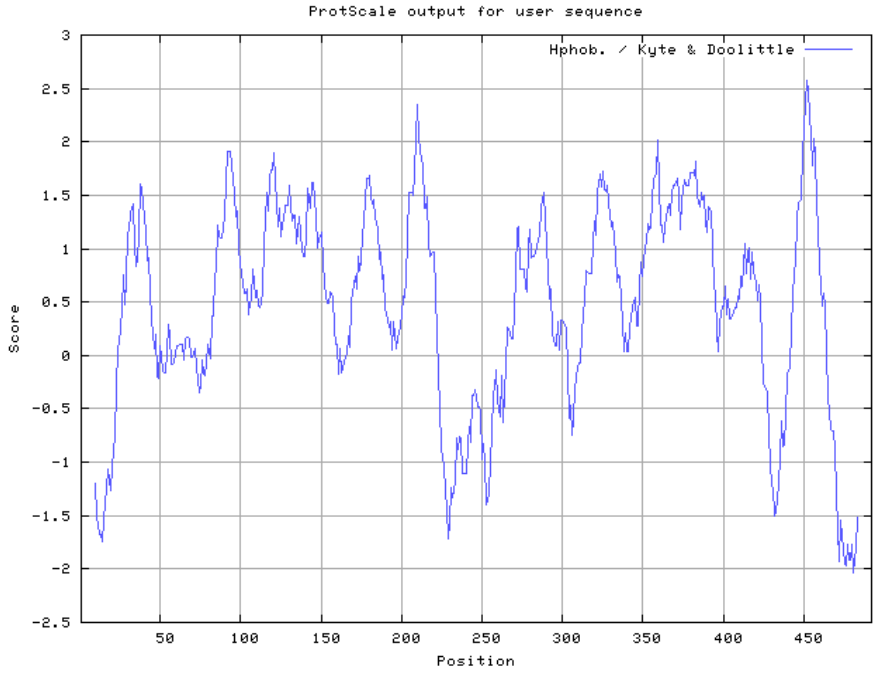

B

Figure 4.18: GmAMF1;3, AtAMF1;1 and AtAMF1;2 protein sequence and predicted topology

The coding sequence (CDS) *AtAMF1;1 and AtAMF1;2* were cloned from 4-week old *Arabidopsis*

root cDNA. Amino acid translations were identical to the predicted sequence retrieved from the TAIR *Arabidopsis* genome database (www.arabidopsis.org). Hydrophobic plots were generated for (**A**) AtAMF1;1 and (**B**) AtAMF1;2 with ExPASy Bioinformatics Resource Portal (web.expasy.org/protscale/) using the Kyte / Doolittle protocol with an amino acid window size of 19. The hydrophobic regions are indicated by negative hydrophilicity values.

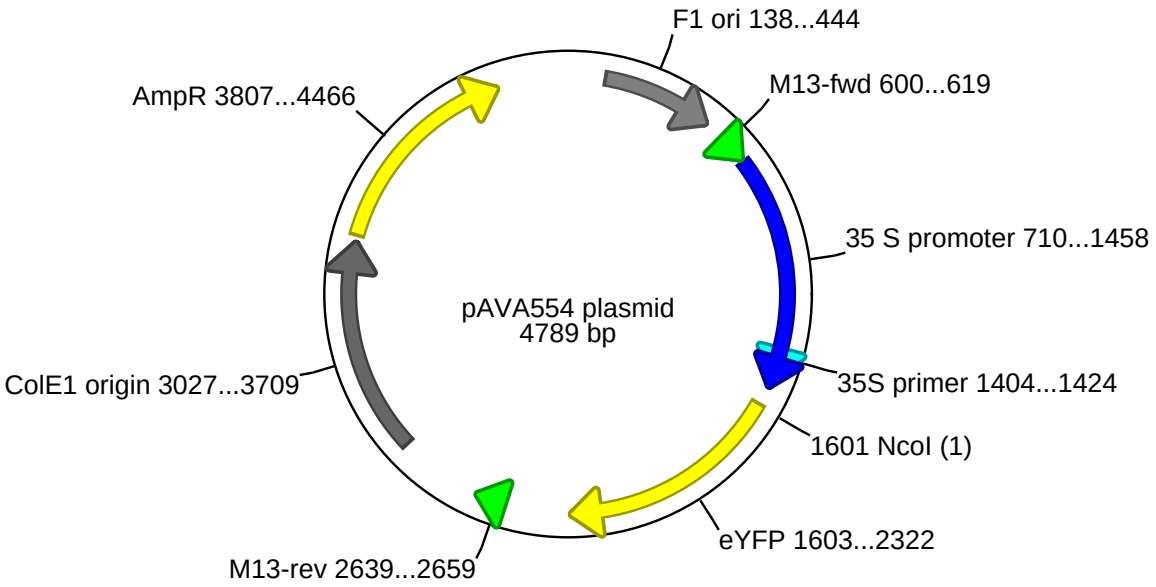

Figure 4.19: Vector map of *pAVA554* for transient expression in onion epidermal cells

The *pAVA554* plasmid used for C-terminal eYFP fusion protein driven by a *35S* promoter (Molendijk et al., 2008).

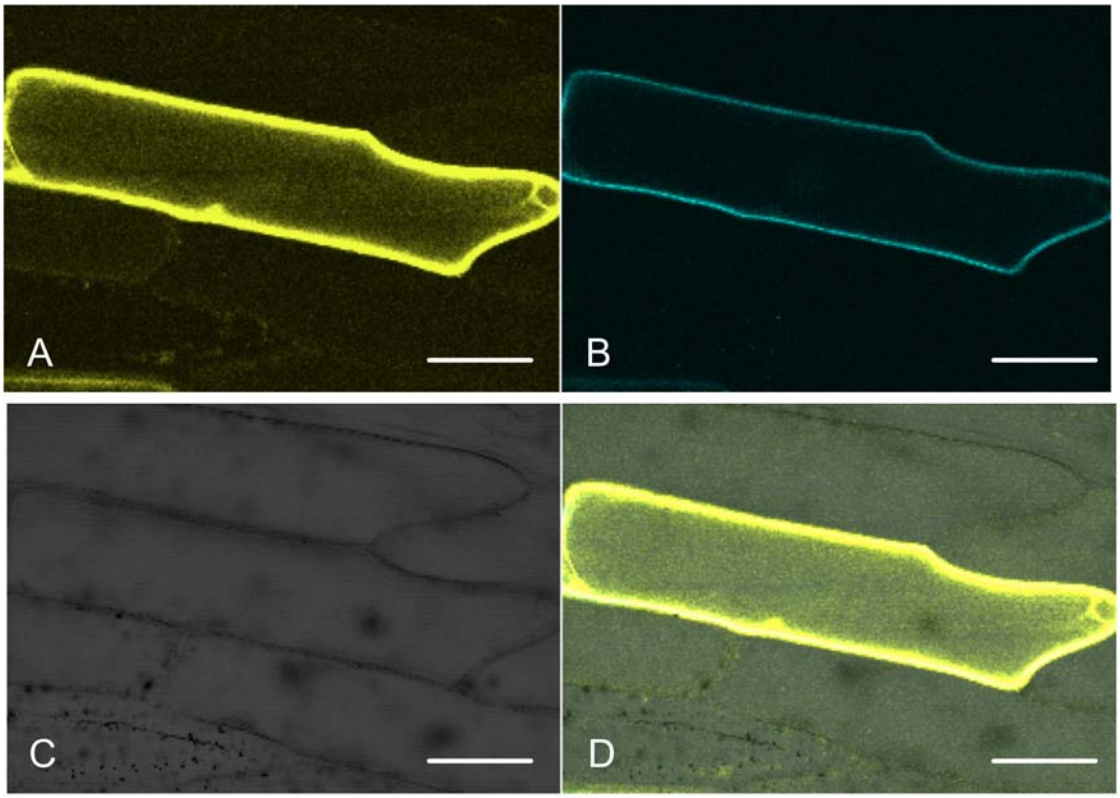

Figure 4.20: Subcellular localisation of C-terminal *Arabidopsis* AMF1;1::eYFP fusions in onion epidermal cells.

(**A**) *35S::AtAMF1;1::eYFP* (**B**) *35S::AtRop11::eCFP* expression in onion cells. Epidermal peels were co-bombarded with *pAVA554-AtAMF1;1* and *AtRop11::eCFP-marker* plasmids, and incubated for 24 h prior to confocal fluorescence microscopy. (**A**) Plasma membrane localisation of AtAMF1;1::eYFP (**B**) Localisation of AtRop11::eCFP plasma membrane marker. (**C**) Bright-field image of onion cell. (**D**) Overlay of AtAMF1;1::eYFP and AtRop11::eCFP expression. Bar = 40 µm.

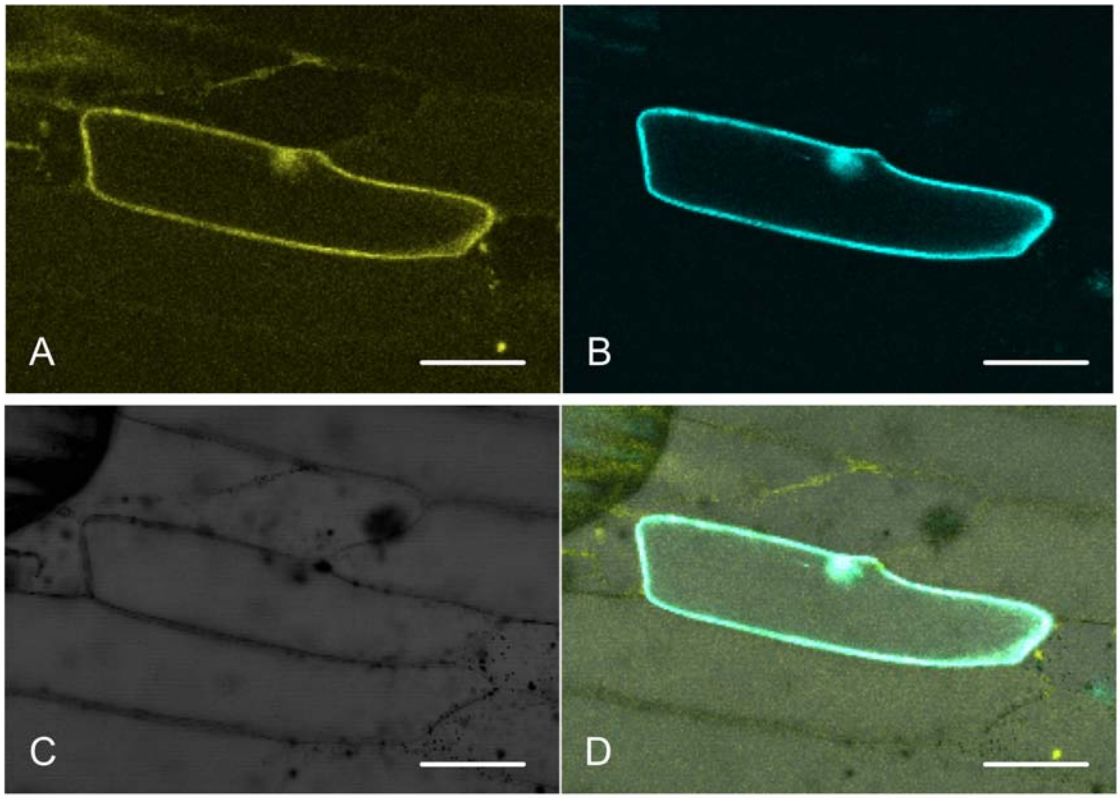

Figure 4.21: Subcellular localisation of C-terminal *Arabidopsis* AMF1;2::eYFP fusions in onion epidermal cells.

(**A**) *35S::AtAMF1;2::eYFP* and (**B**) *35S::AtRop11::eCFP* expression in onion cells. Epidermal peels were co-bombarded with *pAVA554-AtAMF1;2* and *AtRop11::eCFP-marker* plasmids, and incubated for 24 h prior to confocal fluorescence microscopy. (**A**) Plasma membrane localisation of AtAMF1;2::eYFP (**B**) Localisation of AtRop11::eCFP plasma membrane marker. (**C**) Bright-field image of onion cell. (**D**) Overlay of AtAMF1;2::eYFP and AtRop11::eCFP expression. Bar = 40 µm.

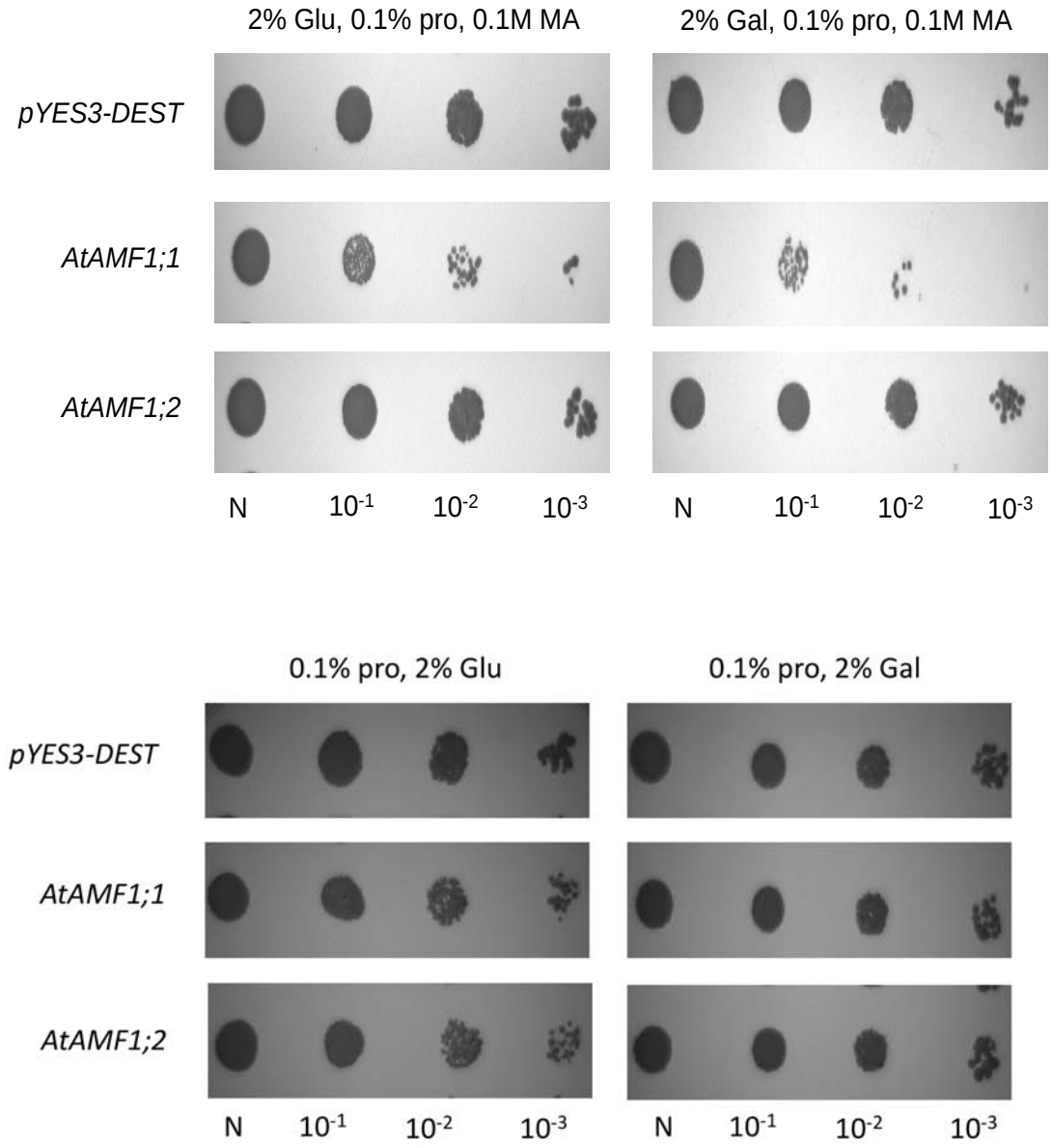

Figure 4.22: The growth of 26972c NH_4^+ transport deficient yeast strain expressing *AtAMF1;1* or *AtAMF1;2* in the presence of 0.1 M MA

The 26972c yeast strain was transformed with *pYES3-DEST* (control), *pYES3-AtAMF1;1* or *pYES3-AtAMF1;2*. Cells were grown to mid-log phase and then serially diluted as described in Figure 2.9. Diluted cells were spotted onto yeast minimal media (Grenson, 1966) supplemented with 2% (w/v) glucose (Glu) or galactose (Gal), 0.1% (w/v) L-proline (pro) and 0.1 M methylammonium (MA) where indicated. Yeast plates were incubated for 6 days at 28°C.

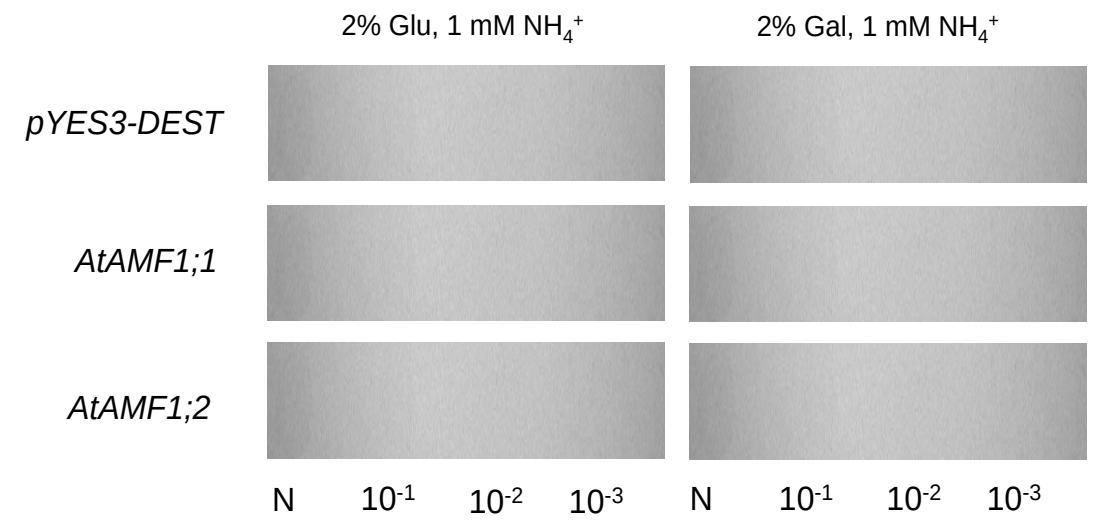

Figure 4.23: The growth of 26972c NH_4^+ transport deficient yeast strain expressing *AtAMF1;1* or *AtAMF1;2* in the presence of 1 mM NH_4^+

The 26972c yeast strain was transformed with *pYES3-DEST* (control), *pYES3-AtAMF1;1* or *pYES3-AtAMF1;2*. Cells were grown to mid-log phase and then serially diluted as described in Figure 2.9. Diluted cells were spotted onto yeast minimal media (Grenson, 1966) supplemented with 2% (w/v) glucose (Glu) or galactose (Gal), 1 mM NH_4Cl where indicated. Yeast plates were incubated for 6 days at 28°C.

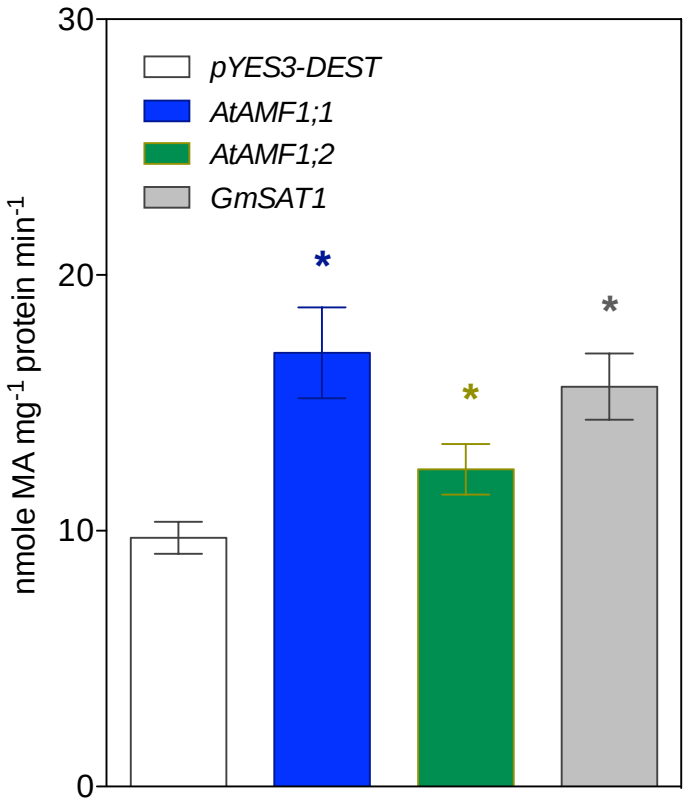

Figure 4.24: The rate of ^{14}C-MA influx into yeast cells over-expressing *GmSAT1*, *AtAMF1;1* or *AtAMF1;2* relative to the empty *pYES3-DEST* vector.

The 26972c NH_4^+ transport mutant yeast strain was transformed with *pYES3-DEST* (control), *pYES3-GmSAT1*, *pYES3-AtAMF1;1* or *pYES3-AtAMF1;2* and grown for 16 h using liquid yeast minimal media without uracil (Grenson, 1966) supplemented with 2% (w/v) galactose and 1 mM NH_4Cl. Uptake of 1 mM ^{14}C-MA in a 2% (w/v) galactose KPO_4 buffer (pH 6.2) was measured over 5 min. Accumulated ^{14}C-MA was quantified by measuring the β-decay using a scintillation counter. Data presented are mean rate of MA uptake ± SE (n = 6). The data are representative of at least 5 independent biological experiments. Where indicated data are significant from the empty vector controls at * ($p<0.05$).

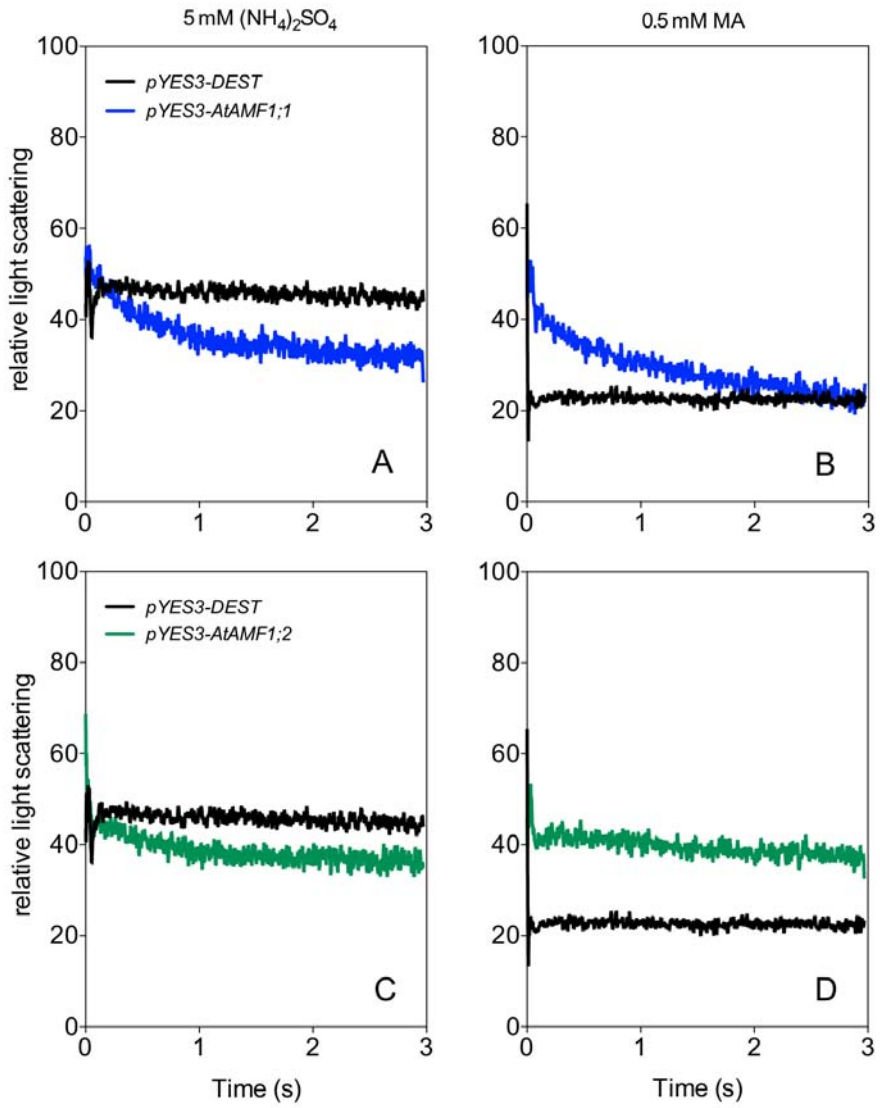

Figure 4.25: The swelling profiles of 26972c spheroplasts expressing *AtAMF1;1 or AtAMF1;2* in response to MA and NH_4^+

Spheroplasts were made from 26972c yeast were resuspended to a uniform $OD_{475\ nm}$ of 0.5 and mixed with an equal volume of base solution supplemented with (**A & C**) 5 mM $(NH_4)_2SO_4$ (**B & D**) 0.5 mM MA or in a fast kinetics SFM-300, Biologic instrument. Volume changes of spheroplasts with *pYES3-DEST* (black), *pYES3-AtAMF1;1* (blue) or *pYES3-AtAMF1;2* (green) were recorded at 16°C as light scattering at an angle 90° and light wavelength of 475 nm. The

kinetics is the mean volume change recording (n = 6 - 9) each collected over a period of 3 s, and normalised with smoothing to 21 neighbours.

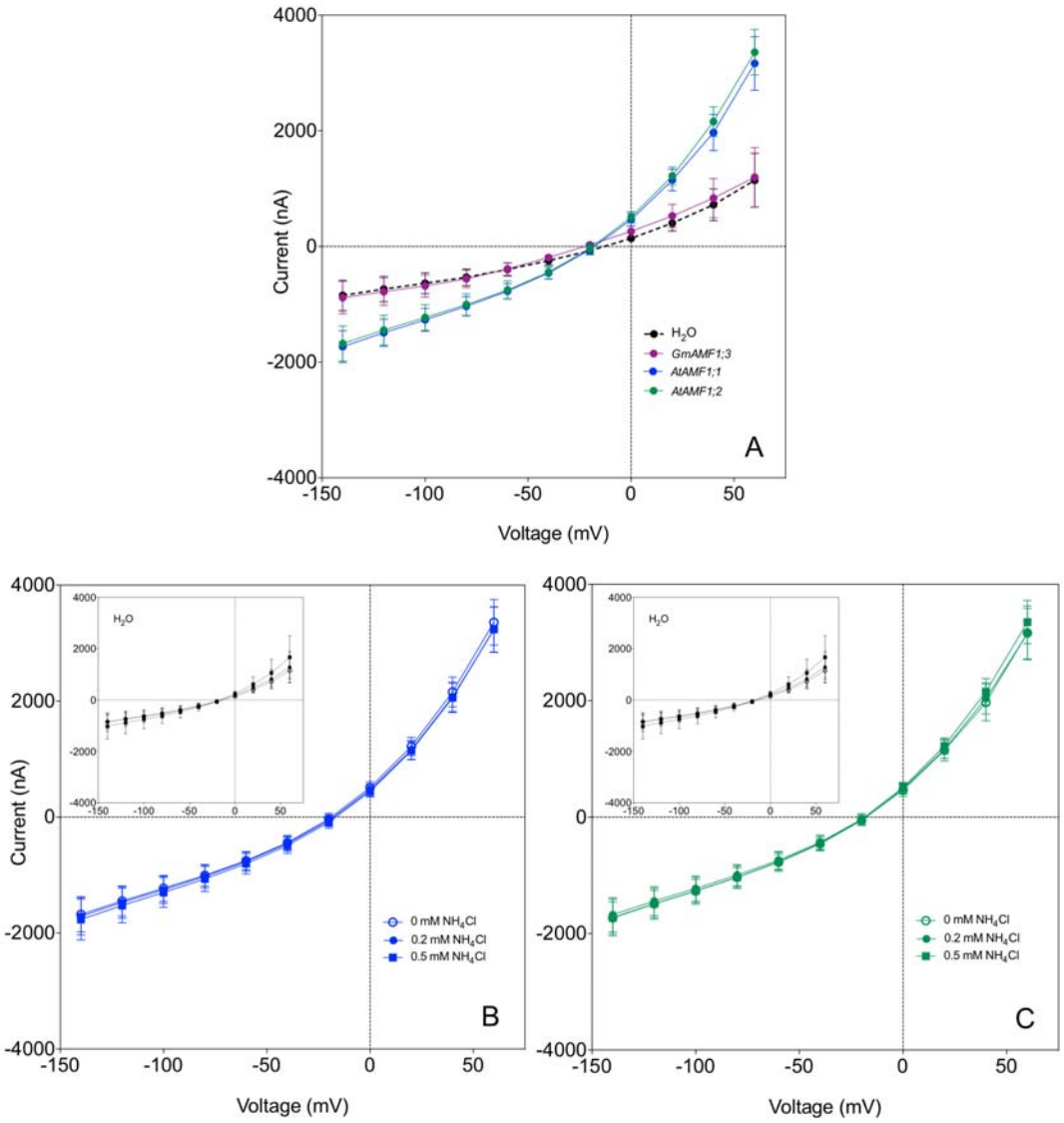

Figure 4.26: The current / voltage relationships of *X. laevis* oocytes expressing *GmAMF1;3, AtAMF1;1* or *AtAMF1;2* cRNA in the presence of monovalent cations

X. laevis oocytes were injected with *GmAMF1;3*, *AtAMF1;1*, *AtAMF1;2* cRNA or an equal volume of RNase-free H_2O (inset - same H_2O controls for each AMF1 homolog) were preincubated ND10 buffer for 24 h prior to two-electrode voltage clamp analysis. Experiments were carried out at room temperature in modified ND10 base buffer (10 mM NaCl, 2 mM KCl, 1.8 mM $CaCl_2$, 1 mM $MgCl_2$, 200 mM mannitol, 10 mM HEPES with pH adjusted to 7.5 with Trizma-base). The

current/voltage response of AMF1 plant homologs in comparison to H_2O-controls in base buffer (**A**) or AtAMF1;1 (**B**) & AtAMF1;2 (**C**) in response to 0, 0.2 mM or 0.5 mM NH_4Cl. Data points in each experiment represent means of 3 (n = 3) oocytes ± SE, and asterisks denote significance (*P<0.05) with respect to base buffer without NH_4Cl using Two-way ANOVA statistical analysis.

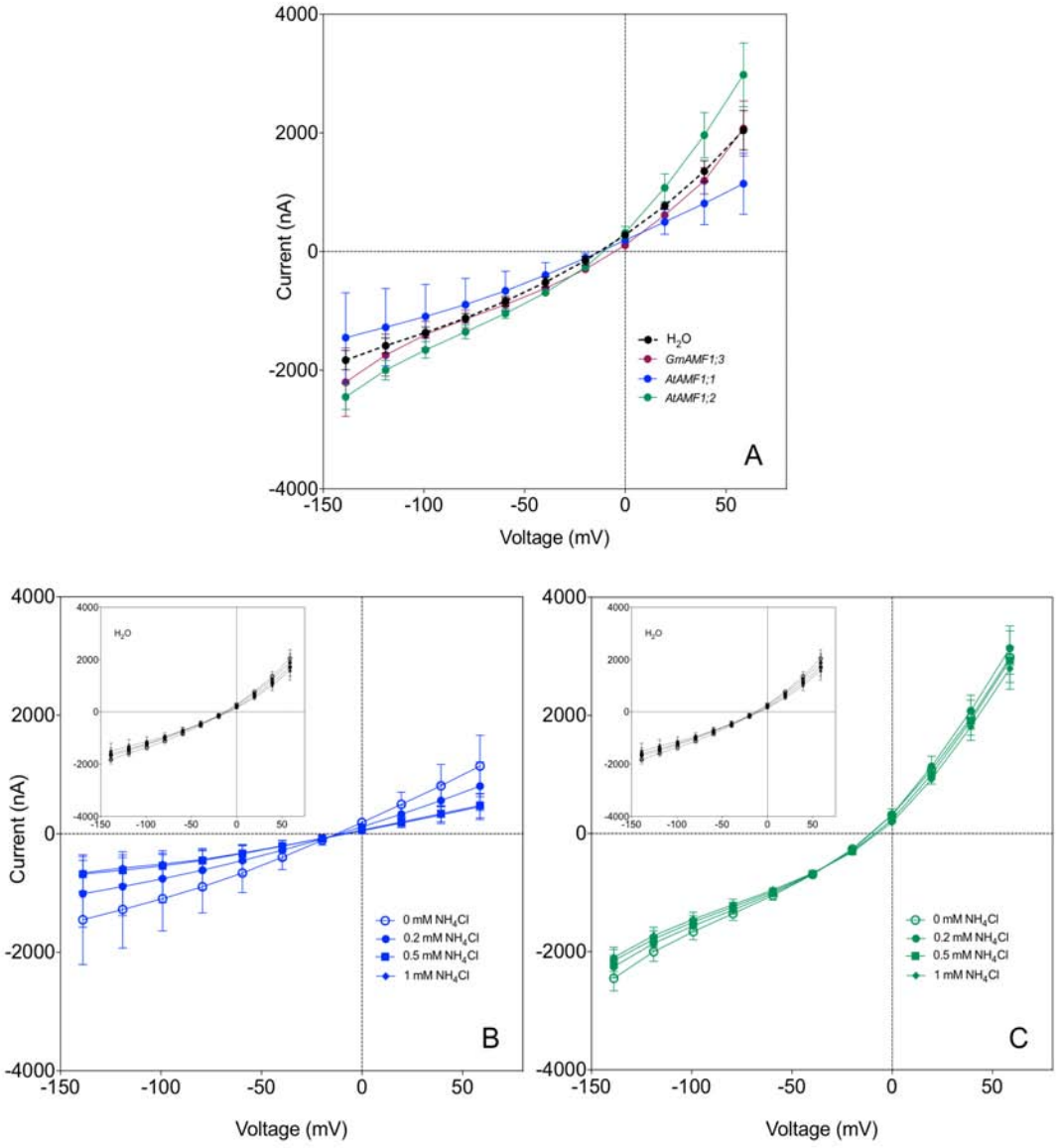

Figure 4.27: The current / voltage relationships of *X. laevis* oocytes expressing *GmAMF1;3, AtAMF1;1* or *AtAMF1;2* cRNA in the absence of Na^+

X. laevis oocytes were injected with *GmAMF1;3, AtAMF1;1, AtAMF1;2* cDNA or an equal volume of RNase-free H_2O (inset - same H_2O controls for each AMF1 homolog) were prepared and two-electrode voltage clamp analysis was carried out in ND10 buffer minus 10 mM NaCl as described in Figure 4.26. Oocytes were preincubated in ND10 buffer with 10 mM KH_2PO_4. The current/voltage response of AMF1 plant homologs in comparison to H_2O-controls in base buffer

(**A**) or AtAMF1;1 (**B**) & AtAMF1;2 (**C**) in response to 0, 0.2 mM, 0.5 mM or 1 mM NH_4Cl. Data points in each experiment represent means of 3 (n = 3) oocytes ± SE, and asterisks denote significance (*P<0.05) with respect to base buffer using Two-way ANOVA statistical analysis.

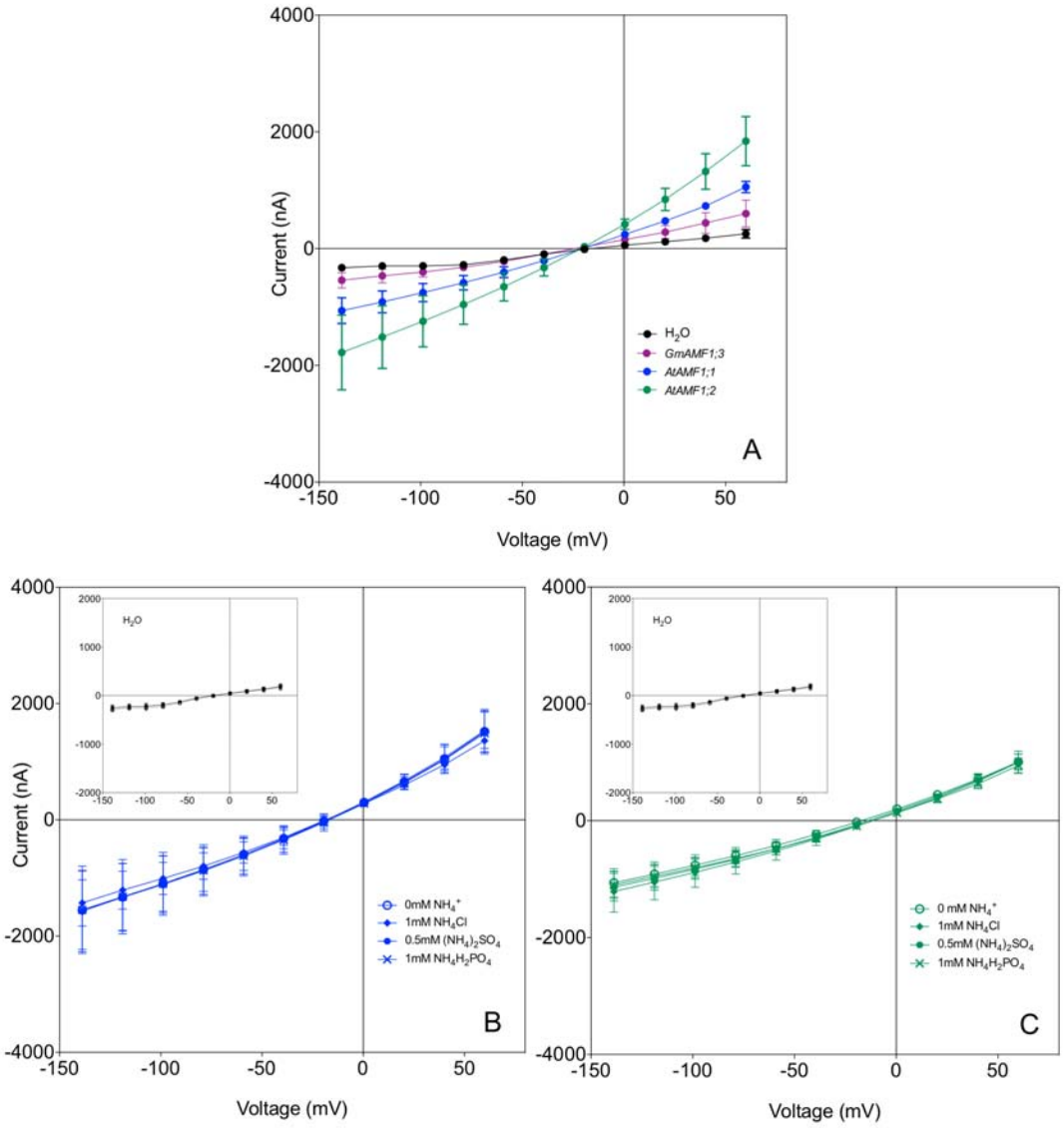

Figure 4.28: The current / voltage relationships of *X. laevis* oocytes expressing *GmAMF1;3, AtAMF1;1* or *AtAMF1;2* cRNA in the absence of Na^+ and K^+

X. laevis oocytes were injected with *GmAMF1;3, AtAMF1;1, AtAMF1;2* cRNA or an equal volume of RNase-free H_2O (inset - same H_2O controls for each AMF1 homolog) were prepared and two-electrode voltage clamp analysis was carried out in ND10 buffer minus 10 mM NaCl and 2 mM KCl as described in Figure 4.26. Oocytes were preincubated ND10 buffer with 10 mM KH_2PO_4. The current/voltage response of AMF1 plant homologs in comparison to H_2O-controls in base

buffer (**A**) or AtAMF1;1 (**B**) & AtAMF1;2 (**C**) in response to 1mM NH_4^+ coupled to various anions. Data points in each experiment represent means of 3 (n = 3) oocytes ± SE, and asterisks denote significance (*P<0.05) with respect to base buffer using Two-way ANOVA statistical analysis.

Table 4.1: List of primers used in Chapter 4.

All primers were ordered from GeneWorks (Adelaide, South Australia).

Primer Name	**Final primer sequence (5'-3')**
GmAMF1;3.cds.F	ATGGCACAACAACAAGAACATGA
GmAMF1;3.cds.R3	TCAGCATTCTTGGGATTGACC
GmAMF1;3.cds.R	TCATAATGACTTACCTATAAACCAT
Fw-At5g64500	ATGGATGTTGACGGAGAAGGTGATCGTGG
Rv-At5g64500	TCATGCTTCCTGGAGAAGAGGCGCAGC
Fw-At5g65687	ATGACGAGAGTTGGCCAGAG
Rv-At5g65687	TTAGGCGAGAGTAGAGTTCTCTG
Fw-At2g22730	ATGGTGACCAAAGAAGAAGATTGCC
Rv-At2g22730	TTATGAATATCCCTTGCAAAAGCAC
YFPAt5g64500 Fw	GCCATGGATGTTGACGGAGAAGGTGATCGT
YFPAt5g64500 Rv	ACCCATGGCTGCTTCCTGGAGAAGAGGCGCA
YFPAt5g65687 Fw	GCCATGGGTATGACGAGAGTTGGCCAGA
YFPAt5g65687 Rv	ACCCATGGCGGCGAGAGTAGAGTTCTCTG
35S promoter Fw	CTATCCTTCGCAAGACCCTTC
At5g64500promoter-Fw	CCTTGAGATCCACGCAATAG
At5g64500promoter-Rv	GCAAGCTCGGTTTTCTGAG
At5g65687promoter-Fw	CACTCTACAGTCTACATTGGC
At5g65687promoter-Rv	GCTGTCAGATTCAATAACAC
At2g27730promoter-Fw	CTTCCTCTAGCCAAGGCACT
At2g27730promoter-Rv	CTC AACGAATTTGTTTAGCC

4.3 Discussion

High-affinity transport of NH_4^+ in plants is mediated by the coordinated effort of AMT ortholog activity. Low-affinity NH_4^+ transport in plants is poorly understood but is purported mediated by non-selective cation channel(s) (Tyerman et al., 1995; Demidchik, 2002a). Unfortunately, the genetic identity of low-affinity NH_4^+ transport proteins in plants has been lacking. This includes the genetic identity of the monovalent cation channel previously identified on the symbiosome membrane, considered important in the transfer of high concentrations of NH_4^+ produced by N-fixing bacteroids (Tyerman et al., 1995; Obermeyer and Tyerman, 2005). ScAMF1 has broadened our knowledge of NH_4^+ transport systems in general. The studies conclude that ScAMF1 possesses transport properties reminiscent of non-selective cation channels. Homologous AMF1 proteins have been identified in most plant species by sequence comparisons including multiple members present in both soybean and *Arabidopsis*. However, the exact function of these proteins remains unclear. Our lab has recently found that a distantly related AMF1 in soybean (*GmAMF1;3*) is preferentially expressed in nodules compared to root tissues and specifically in the nodule parenchyma and vasculature tissues which encircle the N-fixing zone of legume nodules (D. Chiasson, 2012). The data presented here suggests GmAMF1;3 most likely operates as an NH_4^+ channel in legume nodules and thus may have a role in N redistribution in the nodule and possibly to the rest of the plant.

4.3.1 The NH_4^+ transport properties of GmAMF1;3

This study has provided a basis for the characterisation of GmAMF1;3 transport. The electrophysiological profile of GmAMF1;3 in *X. laevis* oocytes is intriguing as it has many parallels with the electrophysiological profile generated for ScAMF1 activity under similar conditions. Like ScAMF1, GmAMF1;3 has the ability to mediate the transport of NH_4^+ in the absence of competing monovalent cations. The amplitude of the NH_4^+ carried current is enhanced by elevated extracellular Ca^{2+} concentrations, indicative of potential divalent cation gating. This commonality between ScAMF1 and GmAMF1;3 gives weight to the AMF1 proteins as a novel subgroup of MFS proteins existing in different organisms. Based on the chemical and electrical signatures in yeast and *X. laevis* oocytes, we suggest AMF1 activity represents a previously uncharacterised major facilitator subfamily with the capacity to facilitate low-affinity NH_4^+ transport in both yeast and *X. laevis* oocytes.

4.3.2 The relationship between GmAMF1;3 mediated NH_4^+ and P_i transport

As for ScAMF1, it is apparent that external P_i has an effect on the apparent GmAMF1;3 facilitated movement of NH_4^+. Again, the mechanism by which this occurs is unclear. GmAMF1;3 may couple the influx of NH_4^+ with the efflux of P_i or a product of P metabolism. A coupled transport mechanism may reflect transport mechanisms occurring natively in soybean. *X. laevis* oocytes have been used for characterization of various P_i transporters including mammalian sodium (Na^+)-P_i co-transporters and low-affinity P_i MF transporters of the PHT1 subfamily from rice and barely (Bacconi et al., 2005; Ai et al., 2009; Preuss et al., 2010). Given the characterised transport properties of GmAMF1;3, it is a possibility that an ortholog of it in soybean may be responsible for the NH_4^+ transport activity identified on the symbiosome membrane. If this transport is linked to P_i export then this would be an efficient way of delivering P to the N-fixing bacteroids in exchange

for NH_4^+ to the plant. An adequate supply of P_i is essential for effective N-fixing symbiosis, presumably to supply the required amounts of P_i for the large amounts of plant and bacterial protein synthesis and metabolic activity in this organ. Accordingly, P_i levels have been shown to be at least three-times higher in nodules than in roots (Gaude et al., 2004). It is of note that plant PHT1 transport proteins are homologous to the PHS MF symporters in yeast (Paulsen et al., 1996; Nagy et al., 2005; Bucher, 2007). GmSAT1 activity in yeast, which resulted in the identification of ScAMF1 activity, was also shown to enhance the expression of yeast genes involved in maintaining P homeostasis (D. Mazurkiewicz, 2008).

4.3.3 Putative *in planta* function of AMF1 activity in soybean

GmAMF1;3 is expressed in roots without nodules but at a lower level (D. Chiasson, 2012). This observation suggests GmAMF1;3 may also have a non-symbiotic role. Closer inspection of the GmAMF1;3 protein sequence reveals that it belongs to the KOG subfamily of major facilitators, which are more closely related to the vertebrate SPINSTER proteins, involved in the transport of sugar species across cellular membranes (Rong et al., 2011). In the future, a comprehensive electrophysiological analysis of GmAMF1;3 specificity for monovalent cations and other substrates will serve to clarify the apparently non-selective cation transport properties that have been demonstrated in this study. Recently, D. Chiasson (2012) cloned a second soybean AMF1 homolog, *GmAMF1;5* from soybean nodules. It showed strong expression in N-fixing nodules compared to the other known AMF1 homologs. Interestingly, *GmAMF1;5* was identified as downregulated in nodules in response to knockdown of *GmSAT1* transcription by RNA interference (D. Chiasson, 2012). Unfortunately, the functional characterisation of its activity has yet to be completed. Determining the mechanism of transport and preferred substrates of

GmAMF1;5 and other soybean AMF1 transporters will help clarify the role of this family *in planta*.

4.3.4 The NH_4^+ transport properties of AMF1 proteins in *Arabidopsis*

AMF1 proteins represent a subfamily of MFS transport proteins capable of facilitating the low affinity flux of NH_4^+. Two *AMF1* homologs in *Arabidopsis* were cloned and analysed for their transport activities in both yeast and *X. laevis* oocytes. Analysis of AtAMF1;1 and AtAMF1;2 in *X. laevis* oocytes provided preliminary evidence that these proteins demonstrate poor discrimination between monovalent cations, which had to be eliminated from the voltage-clamping buffer before NH_4^+ currents could be detected. Both AtAMF1;1 and AtAMF1;2 induced similar physiology in yeast and *X. laevis* oocytes to that of the yeast and soybean homologs. At the very least, the electrophysiology profile of *Arabidopsis* AMF1 homologs provides the direction for the future analysis of these proteins in the oocyte expression system. The activity of AtAMF1;1 and AtAMF1;2 in oocytes needs to be investigated in further detail to explore the potential effect of P_i and Ca^{2+} on NH_4^+ elicited currents.

4.3.5 Putative *in planta* function of *Arabidopsis* AMF1 homologs and future prospects

Based on the limited expression data available in databases (Gene Investigator, accessed June 2013), the *Arabidopsis AMF1* homologs appear to be expressed throughout the whole plant with no clear tissue-specific expression. *AtAMF1;1* has the highest expression level (medium to high expression), followed by *AtAMF1;2*, which demonstrated low to medium expression, and *AtAMF1;3* with the lowest level of expression. The non-specific tissue expression suggests that these AMF1 proteins might have roles related to nutrient NH_4^+ remobilisation in tissues and not exclusively to low-affinity NH_4^+ uptake via roots. As part

of this study, *AtAMF1* genes were cloned into *pKGWFS7-DEST* (Karimi et al., 2002) via Gateway transformation for the tissue specific expression of *AtAMF1* genes. The constructs transformed by the *Agrobacterium* floral dip method (Clough and Bent, 1998) into *Arabidopsis*. However, time constraints prevented the appropriate growth analysis for the visualization of promoter driven *GUS*/*GFP* expression. *In planta* analysis of *Arabidopsis* AMF1 homologs are essential for defining endogenous function. Preliminary growth and flux analysis of knockout mutants have been initiated where single knockout lines have been identified to investigate putative low-affinity NH_4^+ transport mediated by AMF1 proteins. It is intended that loss of individual AMF1 homologs will have a significant impact on NH_4^+ uptake in roots, possibly indicating a degree of functional redundancy and a potential functional overlap with the high-affinity NH_4^+ AMT system (A. Situmorang, 2012). To elucidate the function of each individual AMF1 in plants, multiple AMF1 knockout mutant lines in conjunction with the single knockout mutants are required to resolve possible compensatory effects or redundancies between various members of the AMF1 family.

Chapter 5 General Discussion

In yeast and plants, two distinct mechanisms operate to facilitate NH_4^+ transport. In plants, high-affinity uptake of NH_4^+ is mediated by the coordinated effort of AMT proteins, which share significant homology with MEP transporters operating at low external NH_4^+ concentration in yeast. Low-affinity NH_4^+ transport is poorly understood but is purported mediated by non-selective cation channel(s) (Tyerman et al., 1995; Demidchik et al., 2002a). When yeast spheroplasts expressing *GmSAT1* were previously patch-clamped, a slow time-dependent NH_4^+ permeable current was observed across the yeast PM (Kaiser et al., 1998) that displayed striking similarity to that found on the SM (Tyerman et al., 1995). The genetic identity of the soybean symbiotic NH_4^+ transporter is key to understanding the molecular regulation of N exchange in the legume-*Rhizobium* symbiosis.

In this thesis, mutant yeast strains with defective NH_4^+ transport systems have been utilised to search for analogous mechanisms regulated by GmSAT1 activity, a TF important in the soybean N_2-fixing symbiosis. Here, it was reasoned that the genetic events controlled by GmSAT1 in yeast might reflect events occurring in soybean. GmSAT1 influences the expression of a number of yeast genes capable of NH_4^+ transport. Central to this thesis is the identification of ScAMF1, a novel NH_4^+ transport mechanism distinct from MEP activity, through a direct interaction with GmSAT1. Through sequence homology we observed that *AMF1* homologs are common in plants including, soybean and *Arabidopsis.* Based on the chemical and electrical signatures in yeast and *X. laevis* oocytes, we suggest AMF1 activity represents a previously uncharacterised mechanism involved in

low-affinity NH_4^+ transport in both yeast and plants.

This study has shown that ScAMF1 is yeast PM transport protein capable of low-affinity MA transport and establishing a related sensitivity phenotype at elevated MA concentrations, distinct in activity from known MEP transporters. We have verified its transport activity further in *X. laevis* oocytes using both chemical (MA uptake) and electrical (NH_4^+ induced ion currents) studies, which also provide preliminary evidence that ScAMF1 behaves as a non-selective monovalent cation transporter. In comparison to AMT/MEP/Rh proteins, ScAMF1 demonstrated limited ability to restore growth of 26972c or 31019b cells on low NH_4^+. However, it is clear that MEP high-affinity NH_4^+ transporters are required for yeast growth at low (1 mM) NH_4^+ concentrations. Here, GmSAT1 was shown to influence *MEP3* expression, an activity that most-likely contributed to its ability to restore growth on 1 mM NH_4^+, while also supporting a previous observation that GmSAT1 enhanced MEP3 in 26972c. The ScAMF1-enhanced permeability of NH_4^+ across the yeast PM may account for the enhanced *MEP3* transcription, although this to be remains to be clarified.

Based on the activity of ScAMF1 in yeast and oocytes, we were able to make predictions as to the functional activity of a representative soybean AMF1 protein, GmAMF1;3. Similarly, GmAMF1;3 enhanced MA transport and mediated NH_4^+ induced currents in yeast and *X. laevis* oocytes, respectively. It is intriguing that GmAMF1;3 demonstrated functional properties comparable to ScAMF1 activity in relation to NH_4^+ transport. This may reflect the relationship between the structural and functional commonalities of AMF1 proteins. As MF transporters are known to couple transport (as antiporters and symporters), AMF1 proteins may mediate the movement of an additional substrate, such as an anion or a metabolite. Chemical and electrical profiles suggests that

ScAMF1 and GmAMF1;3 operate as exchangers, potentially mediating the outward movement of P_i or a product of P metabolism to drive the inward movement of NH_4^+ into oocytes. Unfortunately, the precise mechanism and implications of this activity remains to be determined. The impact of P_i on the AMF1 movement of NH_4^+ cannot be ascertained from ion currents alone. Interestingly, an adequate supply of P_i is essential for effective N_2-fixing symbiosis, presumably to supply the required amounts of P_i for the large amounts of plant and bacterial protein synthesis and metabolic activity in this organ. The *Arabidopsis* AMF1 characterisation presented in this thesis suggests that AMF1 proteins possess common transport capabilities across plant species. In future studies, substrate profiles of AMF1 proteins need to be expanded through further electrophysiological analysis in oocytes coupled with functional analyses in *AMF1* overexpression and knockout plants. With this in mind, *in planta* analyses of soybean and *Arabidopsis* AMF1 homologs have been initiated.

In light of this study, I conclude that ScAMF1 activity shares some similarity with the apparent non-selective cation current detected by Kaiser et al., (1998) in spheroplasts expressing *GmSAT1*, whilst GmAMF1;3 may be involved in the poorly understood low-affinity transport of NH_4^+. The mechanism responsible for NH_4^+ transport across the SM is still unknown. Whether the SM channel activity involves AMF1 proteins remains to be shown. However, the expression pattern of *GmAMF1;3* is similar to that of *GmSAT1*, where both are preferentially expressed in nodules over that of root tissues. This relationship may suggest that GmAMF1;3 or potentially another AMF1 homolog that is expressed in the nodule may be responsible for SM NH_4^+ transport. However, the functionality of AMF1 proteins also remains to be determined but most likely operate as exchangers or co-transporters.

Future Directions

The identification and functional analysis of AMF1 proteins has opened the door to understanding low-affinity NH_4^+ transport in yeast and plants. As a result of this study, a number of *AMF1* homologs have been subsequently identified in soybean and other plants, such as Maize. Recently, an additional soybean *AMF1* homolog, *GmAMF1;5* from soybean nodules was identified as it showed downregulation in *GmSAT1* silenced nodules and strong expression in N-fixing nodules compared to the other known *AMF1* homologs (D. Chiasson, 2012). Unfortunately, the functional characterisation of its activity has yet to be completed.

Detailed electrophysiological characterisation in oocytes coupled with *in planta* functional analysis is required to expand on the preliminary functional analysis of *Arabidopsis* AMF1 homologs described in this study. Preliminary growth and flux analysis of knockout mutants have been initiated with single knockout lines to investigate putative low-affinity NH_4^+ transport mediated by AMF1 proteins. In addition, tissue specific *AtAMF1* expression constructs were created and transformed into *Arabidopsis* in anticipation but were unable to be analysed due to time constraints.

Chapter 6 Bibliography

Ai P, Sun S, Zhao J, Fan X, Xin W, Guo Q, Yu L, Shen Q, Wu P, Miller AJ, et al., (2009) Two rice phosphate transporters, OsPht1;2 and OsPht1;6, have different functions and kinetic properties in uptake and translocation. *Plant Journal* **57:** 798–809

Angus J (2001) Nitrogen supply and demand in Australian agriculture. *Australian Journal of Experimental Agriculture* **41:** 277-288.

Ardourel M, Demont N, Debelle F, Maillet F, de Billy F, Prome J, Denarie J, Truchet G (1994) *Rhizobium meliloti* Lipooligosaccharide nodulation factors: different structural requirements for bacterial entry into target root hair cells and induction of plant symbiotic development responses. *Plant Cell* **6:** 1357-1374

Atchley WR, Finch WM (1997) A natural classification of the basic Helix-Loop-Helix class of transcription factors. *Proceedings of the National Academy of Science USA* **94:** 5172-5176

Bacconi A, Virkki LV, Biber J, Murer H, Forster IC (2005) Renouncing electroneutrality is not free of charge: switching on electrogenicity in a Na^+-coupled phosphate cotransporter. *Proceedings of the National Academy of Science USA* **102:** 12606–12611

Bakouh N, Benjelloun F, Hulin P, Brouillard F, Edelman A, Cherif-Zahar B, Planelles G (2004) NH_3 is involved in the NH_4^+ transport induced by the functional expression of the human RhC glycoprotein. *Journal of Biological Chemistry* **279:** 15975-15983

Beman JM, Arrigo, Matson PA (2005) Agricultural runoff fuels large phytoplankton blooms in vulnerable areas of the ocean. *Nature* **434:** 211-214

Benito B, Rodriguez-Navarro A (2003) Molecular cloning and characterization of a sodium-pump ATPase of the moss *Physcomitrella patens*. *Plant Journal* **36:** 382-389

Bienert GP, Moller AL, Kristiansen KA, Schulz A, Moller IM, Schjoerring JK, Jahn TP (2007) Specific aquaporins facilitate the diffusion of hydrogen peroxide across membranes. *Journal of Biological Chemistry* **282:** 1183-1192.

Blumwald E, Fortin MG, Rea PA, Verma DPS, Poole RJ (1985) Presence of host-plasma membrane type H^+-ATPase in the membrane enveloping enclosing the bacteroids in soybean root nodules. *Plant Physiology* **78:** 665-672

Bozdag GO, Uluisik I, Gulculer GS, Karakaya HC, Koc A (2011) Role of ATR1 paralogs YMR279c and YOR378w in boron stress tolerance. *Biochemical and Biophysical Research Communications* **409:** 748-751

Bucher M (2007) Functional biology of plant phosphate uptake at root and mycorrhiza interfaces. *New Phytologist* **173:** 11-26

Burckhardt BD, Burckhardt G (1997) NH_4^+ conductance in *Xenopus laevis* oocytes. I. Basic observations. *Pflügers Arch* **434:** 306-312

Cardenas L, Holdaway-Clarke TL, Sanchez F, Quinto C, Feijo JA, Kunkel JG, Helper PK (2000) Ion changes in legume root hairs responding to Nod Factors. *Plant Physiology* **123:** 443-451

Chiasson D (2012) Characterisation of GmSAT1 and related proteins from legume nodules. Ph.D. Thesis. The University of Adelaide, Australia

Clough SJ, Bent AF (1998) Floral dip: a simplified method for Agrobacterium-mediated transformation of *Arabidopsis thaliana*. *Plant Journal* **16:** 735-743

Cohn J, Day RB, Stacey G (1998) Legume nodule organogenesis. *Trends in Plant Science* **3:** 105-110

Collart MA, Oliviero S (2001) Preparation of yeast RNA. *Current Protocols in Molecular Biology* **13:** 12

Coronado C, Zuanazzi J, Sallaud C, Quirion JC, Esnault R, Husson HP, Kondorosi A, Ratet P (1995) Alfalfa root flavonoid production is nitrogen regulated. *Plant Physiology* **108:** 533-542

Day DA, Poole PS, Tyerman SD, Rosendahl L (2001) Ammonia and amino acid transport across symbiotic membranes in nitrogen-fixing legume nodules. *Cellular and Molecular Life Sciences* **58:** 61-71

Demidchik V, Davenport, R. J, Tester M (2002a) Nonselective cation channels in plants. *Annual Review of Plant Biology* **53:** 67 – 107

Demidchik V, Bowen HC, Maathuis FJM, Shabala SN, Tester MA, White PJ, Davies JM (2002b) *Arabidopsis thaliana* root non-selective cation channels mediate calcium uptake and are involved in growth. *Plant Journal* **32:** 799-808

Denarie J, Debelle F, Promen JC (1996) Rhizobium lipochitooligosaccharide nodulation factors: Signaling molecules mediating recognition and morphogenesis. *Annual Reviews of Biochemistry* **65:** 503-535

Dubois E, Grenson M (1979) Methylamine/ammonium uptake systems in *Saccharomyces cerevisiae*: Multiplicity and regulation. *Molecular Gen. Genetics* **175:** 67-76

Edvardo PJ, Tate R, Maurizio I (2002) Key role of bacterial NH_4^+ metabolism in Rhizobium-plant symbiosis. *Microbiology and Molecular Biology Reviews* **66:** 203-222

Fedorova E, Thomson R, Whitehead LF, Maudoux O, Udvardi MK, Day DA (1999) Localisation of H^+-ATPases in soybean root nodules. *Planta* **209:** 25-32

Gage JD (2004) Infection and invasion of roots by symbiotic nitrogen-fixing Rhizobia during nodulation of temperate legumes. *Microbiology and Molecular Biology Reviews* **68:** 280-300

Gbelska Y, Krijger JJ, Breunig KD (2006) Evolution of gene families: The multidrug resistance transporter genes in five related yeast species. *FEMS Yeast Research* **6:** 345-355

Gietz RD, Schiestl RH, Willems AR, Woods RA (1995) Studies on the transformation of intact yeast cells by the LiAc/SS-DNA/PEG procedure. *Yeast* **11:** 355-360

Glass ADM, Brito DT, Kaiser BN, Kronzucker HJ, Kumar A, Okamoto M, Rawat S, Siddiqi MY, Silim SM, Vidmar JJ (2001) Nitrogen transport in plants, with an emphasis on the regulations of fluxes to match plant demand. *Journal of Plant Nutrition and Soil Science* **164:** 199-207

Grenson M (1966) Multiplicity of the amino acid permeases in *Saccharomyces cerevisiae*. *Biochimica et Biophysica ACTA* **127:** 339-346

Grewer C, Gameiro A, Mager T, Fendler K (2013) Electrophysiological characterisation of membrane transport proteins. *Annual Review of Biophysics* **42:** 95-120

Gurdon JB, Lane CD, Woodland HR, Marbaix G (1971) Use of frogs and oocytes for the study of messenger RNA and its translation in living cells. *Nature* **233:** 177-182

Herridge DF (1982) Relative abundance of ureides and nitrate in plant tissues of soybean as a quantitative assay of nitrogen fixation. *Plant Physiology* **70:** 1

Hess DC, Lu W, Rabinowitz JD, Botstein D (2006) Ammonium toxicity and potassium limitation in yeast. *PLoS Biology* **4:** e351

Hill WG, Southern NM, Maclver B, Potter E, Apodaca G, Smith CP, Zeidel ML (2005) Isolation and characterisation of the Xenopus oocyte plasma membrane: a new method for studying activity of water and solute transporters. *American Journal of Renal Physiology* **289:** 217-224

Holm LM, Jahn TP, Moller AL, Schjoerring JK, Ferri D, Klaerke DA, Zeuthen T (2005) NH_3 and NH_4^+ permeability in aquaporin-expressing Xenopus oocytes. *Pflugers Arch.* **450:** 415-428

Holman Z (2012) GmSAT1 and its interaction with AMF1 in the regulation of P homeostasis in yeast. Honours Thesis. The University of Adelaide, Australia

Howitt SM, Udvardi MK (2000) Structure, function and regulation of ammonium transporters in plants. *Biochimica et Biophysica ACTA-Biomembranes* **1465:** 152-170

Javelle A, Thomas G, Marini A.M, Kramer R, Merrick, M (2005). In vivo functional characterization of the Escherichia coli ammonium channel AmtB: Evidence for metabolic coupling of AmtB to glutamine synthetase. *Journal of Biochemistry* **390:** 215-222.

Kaiser BN, Finnegan PM, Tyerman SD, Whitehead LF, Bergersen FJ, Day DA, Udvardi MK (1998) Characterisation of an ammonium transport protein from the peribacteroid membrane of soybean nodules. *Science* **281:** 1202-6

Kaiser BN, Moreau S, Castelli J, Thomson R, Lambert A, Bogliolo S, Puppo A, Day DA (2003) The soybean NRAMP homologue, GmDMT1, is a symbiotic divalent metal transporter capable of ferrous iron transport. *The Plant Journal* **35:** 295-304

Karimi M, Inz D, Depicker A (2002) GATEWAY (TM) vectors for Agrobacterium-mediated plant transformation. *Trends in plant science* **7:** 193

Khademi S, O'Connell J, Remis J, Robles-Colmenares Y, Miercke LJ, Stroud R.M. (2004). Mechanism of ammonia transport by Amt/MEP/Rh: structure of AmtB at 1.35 A. *Science* **305:** 1587-1594

Krusell L, Krause K, Ott T, Desbrosses G, Krämer U, Sato S, Nakamura Y, Tabata S, James EK, Sandal N (2005) The sulfate transporter SST1 is crucial for symbiotic nitrogen fixation in Lotus japonicus root nodules. *The Plant Cell Online* **17:** 1625- 1636

Kaya A, Karakaya HC, Fomenko DE, Gladyshev VN, Koc A (2009) Identification of a novel system for boron transport: Atr1 is a main boron exporter in yeast. *Molecular and Cellular Biology* **29:** 3665-3674

Klepek YS, Geiger D, Stadler R, Klebl F, Landouar-Arsivaud L, Lemoine R, Hedrich R, Sauer N (2005) *Arabidopsis* polyol transporters, a new member of the monosaccharide

transport-like superfamily, mediates H^+-Symport of numerous substrates including myo-inositol, glycerol, and ribose. *Plant Cell* **17:** 204-218

Lawlor DW, Lemaire G, Gastal F (2001) Nitrogen, plant growth and crop yield. Lea PJ, Morot-Gaudry JF (eds.) *Plant Nitrogen*. Berlin: Springer-Verlag. pp 343-367

Lerouge P, Roche P, Faucher C, Maillet F, Truchet G, Prome JC, Denarie J (1990) Symbiotic host-specificity of *Rhizobium meliloti* is determined by sulphated and acylated glucosamine oligosaccharide signals. *Nature* **344:** 781-784

Livak KJ, Schmittgen TD (2001) Analysis of relative gene expression data using real-time quantitative PCR and the 2-[Delta][Delta] CT method. *Methods* **25:** 402

Loughlin PC (2007) Elucidation of a peribacteroid membrane-bound bHLH transcription factor required for legume nitrogen fixation. Ph.D. Thesis. The University of Adelaide, Australia

Ludwig U, von Wirén N, Frommer WB (2002) Uniport of NH_4^+ by the root hair plasma membrane ammonium transporter LeAMT1;1. *Journal of Biological Chemistry* **277:** 13548-13555

Ludwig U, Wirén S, Wu B, Jost W, Obrdlik P, El Bakkoury M, Marini AM, Andre B, Hamacher T, Boles E (2003) Homo- and hetero-oligomerisation of ammonium transporters-1 NH_4^+ uniporters. *Journal of Biological Chemistry* **278:** 45603-45610

Marini AM, Vissers S, Urrestarazu A, André B. (1994) Cloning and expression of the *MEP1* gene encoding an ammonium transporter in *Saccharomyces cerevisiae*. *EMBO Journal*. **13:** 3456 -3463

Marini AM, Soussi-Boudekou S, Vissers S, Andre B (1997) A family of ammonium transporters in *Saccharomyces cerevisiae*. *Molecular and Cell Biology* **17:** 4282-4293

Marini AM, Raynal V, André B, Cartron J, Chérif-Zahar B (2000a) The human Rhesus-associated RhAG protein and a kidney homologue promote ammonium transport in yeast. *Nature Genetics* **26:** 341-344

Marini AM, Springael JY, Frommer WB, Andre B (2000b) Cross-talk between ammonium transporters in yeast and interference by the soybean SAT1 protein. *Molecular Microbiology* **35:** 378-385

Massari ME, Murre C (2000) Helix-Loop-Helix proteins: Regulators of transcription in eukaryotic organisms. *Molecular and Cellular Biology* **20:** 429-440

Masson-Boivin C, Giraud E, Perret X, Batut J (2009) Establishing nitrogen-fixing symbiosis with legumes: how many rhizobium recipes? *Trends Microbiol* **17:** 458- 466

Mazurkiewicz D (2008) Functional analysis of the legume PBM bHLH transcription factor GmSAT1. Honours Thesis. The University of Adelaide, Australia

Miller A, Cramer M (2005) Root nitrogen acquisition and assimilation. Root physiology: from gene to function. *Plant and Soil* **274:**1-36

Molendijk AJ, Ruperti B, Singh MK, Dovzhenko A, Ditengou FA, Milia M, Westphal L, Rosahl S, Soellick TR, Uhrig J, Weingarten L, Huber M, Palme K (2008) A cysteine-rich receptor-like kinase NCRK and a pathogen-induced protein kinase RBK1 are Rop GTPase interactors. *Plant Journal* **53:** 909-923

Moreau S, Thomson RM, Kaiser BN, Trevaskis B, Guerinot ML, Udvardi MK, Puppo A, Day DA (2002) GmZIP1 encodes a symbiosis-specific zinc transporter in soybean. *Journal of Biological Chemistry* **277:** 4738-4746

Mouritzen P, Rosendahl L (1997) Identification of a transport mechanism for NH_4^+ in the symbiosome membrane of pea root nodules. *Plant Physiology* **115:** 519–526

Nagy R, Karandashov V, Chague W, Kalinkevich K, Tamasloukht M, Xu GH, Jakobsen I, Levy AA, Amrhein N, Bucher M (2005) The characterization of novel mycorrhiza-specific phosphate transporters from *Lycopersicon esculentum* and *Solanum tuberosum* uncovers functional redundancy in symbiotic phosphate transport in solanaceous species. *Plant Journal* **42:** 236-250

Nakhoul NL and Hamm LL (2004) Non-erythroid Rh Glycoproteins: A putative new family of mammalian ammonium transporters. *European Journal of Physiology* **447:** 807-812

Näsholm T, Kielland K, Ganeteg U (2009) Uptake of nitrogen by plants. *New Phytology* **182:** 31-48

Ninnemann O, Jauniaux JC, Frommer WB (1994) Identification of a high affinity NH_4^+ transporter from plants. *EMBO Journal* **13:** 3464-3471

Obermeyer G, Tyerman SD (2005) Ammonium currents across the peribacteroid membrane of soybean. Macroscopic and microscopic properties, inhibition by Mg^{2+}, and temperature dependence indicate a subpicosiemens channel finely regulated by divalent cations. *Plant Physiology* **139:** 1015-1029

Oldroyd GE, Downie JA (2004) Calcium, kinases and nodulation signalling in legumes. *Nature Reviews Molecular Cell Biology* **5:** 566-576

Pao S, Paulsen IT, Saier MH (1998) Major facilitator superfamily. *Microbiology and Molecular Biology* **62:** 1-34

Paulsen IT, Brown MH, Skurray RA (1996) Proton-dependent multidrug efflux systems. *Microbiology Review* **60:** 575-608

Peirson SN, Butler JN, Foster RG (2003) Experimental validation of novel and conventional approaches to quantitative real-time PCR data analysis. *Nucleic Acids* **31:** 73

Peterson GL (1977) A simplification of the protein assay method of Lowry et al, which is more generally applicable. *Analytical biochemistry* **83**: 346

Preuss CP, Huang CY, Gilliham M, Tyerman SD (2010) Channel-like characteristics of the low-affinity barley phosphate Transporter PHT1;6 when expressed in Xenopus oocytes. *Plant Physiology* **152:** 1431

Ramos C (1996) Effect of agricultural practices on the nitrogen losses in the environment. Rodriguez-Barrueco C (ed). *Fertilizers and environment*. The Netherlands: *Kluwer Academic Publishers*. pp. 355-361

Reinders A, Panshyshyn JA, Ward JM (2005) Analysis of transport activity of *Arabidopsis* sugar alcohol permease homolog AtPLT5 **280:** 1594-1602

Riely BK, Mun JH, Ane JM (2006) Unravelling the molecular basis for symbiotic signal transduction in legumes. *Molecular Plant Pathology* **7:** 197-207

Roberts DM, Tyerman SD (2002) Voltage-dependent cation channels permaeble to NH_4^+, K^+ and Ca^{2+} in the symbiosome membrane of the model legume *Lotus japonicus*. *Plant Physiology* **128:** 370-378

Rong Y, McPhee CK, Deng S, Huang L, Chen L, Liu M, Tracy K, Baehrecke EH, Yu L, Lenardo MJ (2011) Spinster is required for autophagic lysosome reformation and mTOR reactivation following starvation. *Proceedings of the National Academy of Science USA* **108**, 7826

Sa-Correia I, dos Santos SC, Teixeira MC, Cabrito TR, Mira NP (2009) Drug:H^+

antiporters in chemical stress response in yeast. *Trends in Microbiology* **17:** 22–31

Saier MH Jr, Beatty JT, Goffeau A, Harley KT, Heijne WH, Huang SC, Jack DL, Jähn PS, Lew K, Liu J, Pao SS, Paulsen IT, Tseng TT, Virk PS (1999) The major facilitator superfamily. *Journal of Molecular Microbiology and Biotechnology* **1:** 257-279

Sambrook J, Russell D (2001) Molecular Cloning: A Laboratory Manual. Volume 2. Cold Spring Harbor Laboratory Press, Cold Spring Harbor, NY

Sauer N, Friedländer K, Gräml-Wicke U (1990) Primary structure, genomic organisation and heterologous expression of a glucose transporter from *Arabidopsis thaliana*. *EMBO Journal* **9:** 3045-3050

Shelden MC, Howitt SM, Kaiser BN, Tyerman SD (2009) Identification and functional characterisation of aquaporins in the grapevine, Vitis vinifera. *Functional Plant Biology* **36**: 1065

Situmorang A (2012) Characterisation of *Arabidopsis* T-DNA knock-out *AMF1* mutant lines. Masters Thesis. The University of Adelaide, Australia

Sobczak K, Bangel-Ruland N, Leier G, Weber WM (2010) Endogenous transport systems in the *Xenopus laevis* oocyte plasma membrane. *Methods* 51: 183-189

Srivastava AC, Ganesan S, Ismail IO, Ayre BG (2008) Functional characterisation of the *Arabidopsis* AtSUC2 Sucrose/H^+ symporter by tissue-specific complementation

reveals an essential role in phloem loading but not in long-distance transport. *Plant Physiology* **148:** 200-211

Stougaard J (2001) Genetics and genomics of root symbiosis. *Current Opinion in Plant Biology* **4:** 328-335

Stulen I, Perez-Soba M, De Kok LJ, Van Der Eerden L (1998) Impact of gaseous nitrogen deposition on plant functioning. *New Phytologist* **139:** 61-70

Subramanian C, Woo JC, Cai X, Xu X, Servick S, Johnson CH, A Nebenführ, von Arnim AG (2006) A suite of tools and application notes for in vivo protein interaction assays using bioluminescence resonance energy Transfer (BRET) *Plant Journal* **48:** 138-152

Szczyglowski K, Kapranov P, Hamburger D, deBruijn FJ (1998) The *Lotus japonicus LjNOD70* nodulin gene encodes a protein with similarities to transporters. *Plant Molecular Biology* **37:** 651-661

Teixeira MC, Monterio P, Jain P, Tenreiro S, Fernandes AR, Mira NP, Alenquer M, Freitas AT, Oliveria AL, Sá-Correia I (2006) The YEASTRACT database: A tool for the analysis of transcriptional regulatory associations in *Saccharomyces cerevisiae. Nucleic Acids Research* **34:** 446-451

Teste MA, Duquenne M, François JM, Parrou JL (2009) Validation of reference genes for quantitative expression analysis by real-time RT-PCR in *Saccharomyces cerevisiae*. *BMC Molecular Biology* **10:** 99

Tyerman SD, Whitehead LF, Day DA (1995) A Channel-like transporter for NH_4^+ on the symbiotic interfacing of N_2-fixing plant. *Nature* **378:** 629-632

Udvardi MK, Lister DL, Day DA (1991) ATPase activity and anion transport across the peribacteroid membrane of isolated soybean symbiosomes. *Archives of Molecular Biology* **156:** 362-366

Udvardi MK, Day DA (1997) Metabolite transport across symbiotic membranes of legume nodules. *Review of Plant Physiology and Plant Molecular Biology* **48:** 493-523

Vargas RC, García-Salcedo R, Tenreiro S, Teixeira MC, Fernandes AR, Ramos J, Sá-Correia I (2007) *Saccharomyces cerevisiae* multidrug resistance transporter Qdr2 is implicated in potassium uptake, providing a physiological advantage to quinidine-stressed cells. *Eukaryotic Cell* **6:** 134-142

Velasco I, Tenreiro S, Calderon IL, Andre B (2004) *Saccharomyces cerevisiae* Aqr1 is an internal-membrane transporter involved in excretion of amino acids. *Eukaryotic Cell* **3:** 1492–1503

Vincill ED, Szczyglowski K, Roberts DM (2005) GmN70 and LjN70: Anion transporters of the symbiosome membrane of nodules with a transport preference for nitrate. *Plant Physiology* **137:** 1435–1444

Wach A, Brachat A, Poehlmann R, Philippsen P (1994) New heterologous modules for classical or PCR-based gene disruptions in *Saccharomyces cerevisiae*, *Yeast* **10:**1793-1808

Wang MY, Siddiqi MY, Ruth TJ, Glass ADM (1993) Ammonium uptake by rice roots (Kinetics of $^{13}NH_4^+$ influx across the plasma membrane). *Plant Physiology* **103:** 1259-1267

Weaver CD, Crombie B, Stacey G, Roberts DM (1994) Nodulin 26, a nodule-specific symbiosome membrane protein from soybean, is an ion channel. *Journal of Biological Chemistry* **269:** 17858-17862

Whitehead FL, Day DA (1997) The peribacteroid membrane. *Physiologia Plantarum* **100:** 30-44

Whitehaed LF, Day A, Tyerman SD (1998) Divalent cation gating of an ammonium permeable channel in the symbiotic membrane from soybean nodules. *Plant Journal* **16:** 313-324

von Wirén N, Merrick M (2004) Regulation of ammonium carriers in bacteria, fungi and plants. *Topics in Current Genetics* **9:** 95-120

Wormit A, Trentmann O, Feifer I, Lohr C, Tjaden J, Meyer S, Schmidt U, Martinoia E, Neuhaus HE (2006) Molecular identification and physiological characterisation of a novel monosaccharide transporter from *Arabidopsis* involved in vacuolar sugar transport. *American Society of Plant Biologist* **18:** 3476-3490

Yuan L, Loque D, Kojima S, Rauch S, Ishiyama K, Inoue E, Takahashi H, von Wiren N (2007) The organization of high-affinity ammonium uptake in *Arabidopsis* roots depends on the spatial arrangement and biochemical properties of AMT1-type transporters. *Plant Cell* **19:** 2636-2652

Yui G, McCord A, Wise A, Jindal R, Hardee J, Kuo A, Shimogawa MY, Cahoon L, Wu M, Kloke J, Hardin J, Mays Hoopes LL (2008) Pathway change in expression during replicative aging in *Saccharomyces cerevisiae*. *J Gerontol A Bio Sci Med Sci* **63:** 21-34

Zheng L, Kostrewa D, Berneche S, Winkler K, Li X.D (2004). The mechanism of ammonia transport based on the crystal structure of AmtB of Escherichia coli. *Proceedings of the National Academy of Science USA* **101:** 17090–17095